Abstract

Scanning transmission X-ray microscopy (STXM) was used as the major tool to characterize microcapsule wall cross-sections. Two types of microcapsules were studied, composite polyurea microcapsules and base-triggerable aminoplast microcapsules. Composite polyurea microcapsules were prepared by sequential interfacial polymerization of different aromatic and aliphatic isocyanates with aqueous amines. Quantitative STXM mappings showed different wall morphologies depending on the choice of monomers, suggesting different wall formation mechanisms. The difference in wall formation mechanisms was attributed to the cross-linking ability and the polarity of the monomers. STXM studies on the base-triggerable aminoplast microcapsules revealed that the microcapsule wall formation followed a polymer phase separation mechanism and the condensation between methylol groups in the aminoplast resin and the cross-linker was primarily responsible for the wall formation.

The surface modifications on polyurea microcapsules using functional polyelectrolytes were performed to enrich microcapsule surface chemistry. Laser scanning confocal microscopy (CLSM) and fluorescence microscopy were utilized to confirm that the modifications were restricted to the outer surface of polyurea microcapsule walls. In the meantime, a simple microfluidic device based on commercially available MicroTEE was constructed to produce monodisperse xylene-in-water emulsions with tuneable sizes. Narrow-dispersed polyurea microcapsules were successfully made using this device, based on monodisperse emulsions.

A simple method for making Pickering emulsifiers by electrostatically modifying charged particle surfaces using oppositely charged both electrolytes and polyelectrolytes was demonstrated. The Pickering emulsions based on organic electrolyte modified particles were shown to be pH responsive, which was due to the reversible interaction between the particle surface and the modifier. Particle surface modification using polyelectrolytes rendered particles surface active and enabled anchoring of desirable functional groups on particle surfaces. The resulting Pickering emulsions were utilized to template the wall growth at oil-water interfaces for making microcapsules via either layer-by-layer assembly or atom transfer radical polymerization depending on the polyelectrolyte modifiers used. Compared to classical microencapsulation methods, these Pickering emulsion templated methods showed less dependence on the polarity of core materials and thus are applicable to the encapsulation of a wide range of hydrophobic materials.

Acknowledgements

First and foremost I would like to thank my primary advisor, Professor Harald Stöver for accepting me into his group, for encouraging me to explore what was interesting, for valuable guidance on scientific thinking and for the tremendous support throughout these years. I have been feeling extremely lucky to have him as my advisor.

I would like to thank my second advisor, Professor Adam Hitchcock for leading me into the world of STXM, for accommodating my own interests and for your understanding and patience for my research. His enthusiasm for science and a wide breadth of knowledge have been an constant inspiration to me.

Thank you to my committee member, Professor Robert Pelton, for his suggestions over the years and for allowing me to access the research instruments in his group. His wide range of knowledge in chemistry and colloid science is very much appreciated.

I am grateful to Dr. Ian Shirley from Syngenta for the collaboration and valuable suggestions and discussions. Mrs. Marcia West is acknowledged for her time and help on sample preparation and electron microscopy imaging. Sincere appreciation is also extended to Dr. Yang Chen, Dr. Wei Chen, Dr. Youguo Cui, Dan Zhang, Mr. Frank Gibbs, for their help on sample characterizations.

I am grateful to all the members in Stöver and Hitchcock's groups: Dr. Nick Burke, Dr. Jafar Mazumdar, Mohit, Janice, Casey, Rachelle, Padraic, Sara, Dr. Glen Cooper, Dr. Jian Wang, Dr. Daniel Hernandez Cruz, Dr. Zulima Martin, Dr. Bonnie Leung, Ebi,

Karen, Hua, Dr. Li Li, little Adam and Sam. I learnt so much from each of you and I really appreciate your help and friendship.

I would like to thank the staff in the Chemistry Department office, Carol Dada, Lynda Fraser, Connie Carrabs, Cathy Bottos, Christine Cosgrove, Tammy Feher. They have been a great help in keeping us focusing on our study and research.

I would like to thank my parents and my sister for their unfailing faith in me and for always being there for me. Your continuous support and caring help me succeed every step of the way. There are no words that can express my gratitude for you.

I am very much indebted to my wife, Yuli (Annie) Liu for your immeasurable love, unremitting support, tremendous encouragement, great understanding and patience, which are my greatest sources of strength to overcome obstacles in my life and to realize my dreams.

Financial supports from Natural Sciences and Engineering Research Council (NSERC) of Canada, Syngenta, Ontario government and McMaster University are acknowledged.

Table of Contents

List of Figures

List of Tables

List of Schemes

List of Abbreviations

A100f	Fluorescein Labeled Poly(methacrylic acid)
A70bf	Poly(methacrylic acid-co-butyl methacrylate)
A70f	poly(sodium methacrylate-co-2-(methacryloyloxy) ethyl acetoacetate)
AFM	Atomic force microscopy
AIBN	2, 2'–Azobis(isobutyronitrile)
ALS	Advanced light source
ATRP	Atom transfer radical polymerizations
BIEM	2-(2-Bromoisobutyryloxy)ethyl methacrylate
CLSM	Laser scanning confocal microscopy
CT-LbL	Colloid templated Layer-by-Layer
DCM	Dichloromethane
DETA	Diethylenetriamine
DMF	Dimethylformamide
DMSO	Dimethyl sulfoxide
DRP	Dispersion radical polymerizations
ETRP	Emulsion-templated radical polymerization
FITC	Fluorescein isothiocyanate
FTIR	Fourier transform infrared
GPC	Gel permeation chromatography
HDPP	High density polyproplyene

HEMA	2-Hydroxyethyl methacrylate
HMDI	Hexamethylene diisocyanate
HMTETA	1,1,4,7,10,10-Hexamethyltriethylenetetramine
HPLC	High pressure liquid chromatography
IEP	Isoelectric point
IPDI	Isophorone diisocyanate,
IRP	Interfacial radical polymerization
KHP	Potassium hydrogen phthalate
LbL	Layer-by-Layer
MA	Methacrylic acid
MBAAm	N,N'-Methylene bisacrylamide
MAPTAC	3-(Methacrylamino)propyl]trimethylammonium chloride
MBMCA	4,4′-Methylenebis(2-methylcyclohexylamine)
MC	Microcapsule
MDI	Methylene diphenyl diisocyanate
NEXAFS	Near edge X-ray absorption fine structure
NIPAM	N-Isopropylacrylamide
NMR	Nuclear magnetic resonance
PAPM	Poly (N-(3-aminopropyl) Methacrylamide)
PAPM*r*	Rhodamine Labeled Poly(N-(3-aminopropyl) methacrylamide)
PDADMAC	Poly(diallyldimethylammonium chloride)
PDI	Polydisperse index

PETI-ATRP	Pickering emulsion templated interfacial atom transfer radical polymerization
PMOETAC	Poly(2-Methacryloyloxyethyl trimethyl ammonium chloride)
PMPPI	Polymethylenepolyphenyl polyisocyanate
PSB	Poly (sodium styrenesulfonate-*co*-2- (2-bromoisobutyryloxy)-ethyl methacrylate)
PSS	Poly(sodium styrenesulfonate)
PUMC	Polyurea microcapsule
PVA	Polyvinyl alcohol
RAFT	Reversible addition-fragmentation chain transfer
SaPSeP	Self-assembly of phase-separated polymer
SEC	Size exclusion chromatography
SEM	Scanning electron microscope
SM	Sodium methacrylate
SS	Sodium styrenesulfonate
STXM	Scanning transmission X-ray microscopy
TEA	Triethylamine
TEM	Transmission electron microscopy
THF	Tetrahydrofuran
TTE	Trimethylolpropane triglycidyl ether

PREFACE-THESIS OUTLINE

This thesis has been prepared in a "sandwich" style. Charter 1 gives a brief introduction to microcapsules (MCs), their applications and classical microencapsulation methods and outlines the objectives of this thesis. Each subsequent chapter represents a manuscript or published journal article. Chapters 2 and 3 focus, respectively, on characterization of composite polyurea and base-triggerable aminoplast MCs using scanning transmission X-ray microscopy (STXM), along with other techniques. Chapter 4 deals with surface modification of polyurea MCs and with the development of a simple microfluidic device for making monodisperse MCs. Chapter 5 introduces a new nanoparticle surface modification method for preparing Pickering emulsifiers, and discusses the pH response of the resulting Pickering emulsions. Chapters 6 and 7 focus on using Pickering emulsions as templates for making MCs via layer-by-layer assembly and atom transfer radical polymerization, respectively, based on the nanoparticle surface modification method introduced in Chapter 5. Proposed future work is discussed in Chapter 8. The aims of research and a brief description of the thesis chapters follow below.

Chapter 1 - Introduction to Microcapsules: Applications and Microencapsulation Methods

A brief introduction to traditional and emerging applications of MCs is presented, followed by a discussion of classical microencapsulation methods. Some challenges in current MC research are identified and the research objectives of this thesis are outlined.

Chapter 2 - A New Approach to Studying Microcapsule Wall Growth Mechanisms

Research Objective

The goal of this chapter was to explore the use of scanning transmission X-ray microscopy (STXM) as an analytical tool to study the wall growth mechanisms of composite polyurea MCs.

Synopsis

This chapter describes the preparation of polyurea MCs by sequential interfacial reaction of different aromatic and aliphatic isocyanates. The resulting composite MC walls were studied using STXM, in order to quantitatively map the distributions of the resulting aromatic and aliphatic polyureas across the capsule wall. Application of this method to both cross-linked and non-cross-linked polyurea capsules resulted in observation of different capsule wall growth mechanisms, depending mainly on the choice of monomers.

Associated Publication

"A New Approach to Studying Microcapsule Wall Growth Mechanisms" Jian Li, Adam P. Hitchcock, Harald D. H. Stöver, Ian Shirley, *Macromolecules* **2009**, *42,* 2428-2432

Chapter 3 - Probing Wall Chemistries of Base-triggerable Aminoplast Microcapsules via Scanning Transmission X-ray Microscopy

Research Objective

The goal of this research is to use STXM as the major tool to investigate the morphologies and chemical compositions of commercial base-triggerable aminoplast MCs in order to understand the properties of these MCs and their formation mechanisms.

Synopsis

STXM was applied to study base-triggerable aminoplast MCs developed by Syngenta for crop protection. These MCs were formed at Syngenta by the condensation reaction between an aminoplast resin (U80) and pentaerythritol tetrakis(3-mercaptopropionate) (thioester). The sample preparation for STXM, carried out at McMaster, involved MC embedding in polystyrene using in-situ polymerization and subsequent microtoming to produce thin films containing MC wall cross-sections. The examination of the wall cross-sections of native (unhydrolyzed) MCs using STXM revealed: 1. a dense and single-layer MC wall; 2. the formation of internal compartments having chemical compositions similar to those of the primary MCs. These observations

indicate that the microencapsulation proceeded at least in part by an internal polymer phase separation mechanism in addition to the interfacial polycondensation pathway that is widely assumed for aminoplast MC formation. Chemical mapping studies suggest that the condensation reaction between pendant methylol groups in U80 and thioester may be primarily responsible for the wall formation, while the reaction between the pendant butoxymethyl groups and thioester may only play a minor role in the process. Studies on base-hydrolyzed MCs using rhodamine 6G labelling and fluorescence microscopy indicate presence of anionic carboxylate groups on the outer MC surfaces generated by the hydrolysis of thioester. Experiments carried out to use potassium and calcium ions as markers to map the distributions of these carboxylate groups in the hydrolyzed MC walls by STXM proved inconclusive due to the weak binding of these metal ions to the carboxylate groups in MC walls.

Associated Publication

"Probing Wall Chemistries of Base-triggerable Aminoplast Microcapsules via Scanning Transmission X-ray Microscopy" Jian Li, Ann Waller, Ian M. Shirley, Adam P. Hitchcock, Harald D. H. Stöver*, To be sumbitted*

Chapter 4 - Studies on Polyurea Microcapsules: Surface Modifications and Capsule Size Control

Research Objective

The goal of this research is to develop a post-modification method to modify polyurea MC surfaces using functional polyelectrolytes and to make monodisperse polyurea MCs via a simple microfluidic device.

Synopsis

A post-modification method for polyurea MC surfaces using functional polyelectrolytes is reported in this chapter. Fluorescein isothiocyanate (FITC) was utilized to probe the chemistry on polyurea MC surface and label nucleophilic groups on the surface, in particular amines. As well, a fluorescently labeled polyanion containing electrophilic acetoacetate groups was used to covalently react with these nucleophilic groups on the polyurea MC surfaces. This modification causes charge reversion of the originally cationic polyurea MC and enables subsequent layer-by-layer (LbL) coating using other polyelectrolytes, allowing for covalent or non-covalent modification of the capsule surface. All modification steps were monitored using either laser scanning confocal microscopy (CLSM) or fluorescence microscopy. Optical and fluorescence microscopy of polyurea MC wall cross-sections embedded in resin confirmed that the modifications were restricted to the outer surface of polyurea MCs, offering minimum interference of this modification method with other capsule wall prosperities.

A simple T-junction type microfluidic device based on a commercially available MicroTee was assembled to produce monodisperse oil-in-water emulsions with tunable

sizes. This device was easy to set up and operate and was proved to be an useful tool for making narrow-disperse polyurea MCs.

Associated Publication

"Studies on Polyurea Microcapsules: Surface Modifications and Capsule Size Control", Jian Li, M.A. Jafar Mazumder, Ian M. Shirley, Adam P. Hitchcock, Harald D.H. Stöver *To be submitted.*

Chapter 5 - Doubly pH-Responsive Pickering Emulsion

Research Objective

The goal of this research was to develop a simple method for making Pickering emulsifiers based on electrostatic modification of hydrophilic particle surfaces and to study the pH-response of the resulting emulsions.

Synopsis

This chapter describes a pH-responsive Pickering emulsion that were designed on the basis of commercially available alumina-coated silica nanoparticles (Ludox CL silica particles) and potassium hydrogen phthalate (KHP). KHP was found to bind to cationic particle surfaces at pH values between 3.5 and 5.5, enabling the resulting surface-active particles to stabilize emulsions of xylenes in water. Above and below this pH range, the

system demulsifies, resulting in a reversible Pickering emulsifier having two pH-controlled, reversible transitions.

Associated Publication

"Doubly pH-Responsive Pickering Emulsion" Jian Li, Harald D. H. Stöver, *Langmuir* **2008**, *24*, 13237-13240.

Chapter 6 - Pickering Emulsion Templated Layer-by-layer Assembly for Making Microcapsules

Research Objective

The goal of this research was to develop a microencapsulation method that used Pickering emulsions as templates to direct the layer-by-layer assembly of polyelectrolytes and charged nanoparticles at oil-water interfaces for making composite MCs.

Synopsis

Pickering emulsions stabilized by poly(sodium styrenesulfonate) (PSS) surface-modified Ludox CL particles were used as templates for the layer-by-layer (LbL) deposition of polyelectrolytes and charged nanoparticles to form composite shells. The MCs resulting from repeated LbL coating with poly(diallyldimethylammonium chloride) (PDADMAC) and PSS had porous walls due to the loose arrangement of the original nanoparticle aggregates at the oil-water interface, leading to significant microcapsule

rupture and low encapsulation efficiency. MCs formed by coating with PDADMAC and anionic Ludox HS nanoparticles led to dense walls and stronger MCs, suitable for microencapsulation of hydrophobic materials with a wide range of polarities.

Associated Publication

"Pickering Emulsion Templated Layer-by-layer Assembly for Making Microcapsules", Jian Li, Harald D. H. Stöver, *Langmuir* **2010**, *26*, 15554–15560.

Chapter 7 - Pickering Emulsions Templated Interfacial Atom Transfer Radical Polymerization for Microencapsulation

Research Objective

The goal of this research was to develop a microencapsulation method that used Pickering emulsions as templates to confine the atom transfer radical polymerizations (ATRPs) of different monomers at interface for making composite MCs.

Synopsis

This chapter describes a new microencapsulation method based on a Pickering emulsion templated interfacial atom transfer radical polymerization (PETI-ATRP). Cationic Ludox CL nanoparticles were coated electrostatically with an anionic polymeric ATRP initiator, poly (sodium styrenesulfonate-*co*-2- (2-bromoisobutyryloxy)-ethyl methacrylate) (PSB) prepared by radical copolymerization of sodium styrenesulfonate

and 2-(2-bromoisobutyryloxy)ethyl methacrylate (BIEM). The resulting PSB-modified CL particles were surface active and could be used to stabilize oil-in-water Pickering emulsions. ATRP of water-soluble cross-linking monomers, confined to the oil-water interface by the surface-bound PSB, then led to nanoparticle/polymer composite shells. This method allowed encapsulation of core solvents (xylene, hexadecane, perfluoroheptane) with different solubility parameters. The MC wall chemistry could accommodate different monomers, demonstrating the versatility of this method. Double-walled MCs were formed by sequentially carrying out PETI-ATRP and in-situ polymerization of encapsulated monomers. The double-walled structure was verified by both transmission electron microscopy (TEM) and STXM.

Associated Publication

"Pickering Emulsions Templated Interfacial Atom Transfer Radical Polymerization for Microencapsulation", Jian Li, Adam P. Hitchcock, Harald D. H. Stöver, *Langmuir*, **2010**, *26*), 17926–17935

Chapter 8 – Summary and Future work

The contributions of this thesis to microcapsule studies are summarized and the future directions are proposed.

Contribution Declaration

Under the guidance of Professors Harald Stöver and Adam Hitchcock, the author generated key ideas for this thesis and performed all the synthetic and analytical work with the exception follows:

a. In Chapter 2, the synthesis and STXM data analysis of PMPPI/IPDI-DETA double-layered polyurea microcapsules were carried out by Sander Reijerkerk and Padraic Foley, respectively;

b. In Chapter 3, both native and hydrolyzed aminoplast microcapsules were synthesized by Ann Waller (Syngenta);

c. In Chapter 4, A70f and PAPM were synthesized by Jafar Mazumdar;

d. All sample sectioning was done by Marcia West (Electron Microscopy Facility, McMaster University) ;

e. In Chapter 7, the thermogravimetric analyse on composite CL/MBAAm microcapsules were performed by Frank Gibbs (BIMR, McMaster University);

f. Some STXM data was acquired by Professor Adam Hitchcock, Dr. Daniel Hernandez Cruz, Dr. Jian Wang, Dr. Martin Obst, Dr. Chithra Karunakaran;

d. Professor Adam Hitchcock helped with some STXM analysis.

CHAPTER 1- INTRODUCTION TO MICROCAPSULES: APPLICATIONS AND MICROENCAPSULATION METHODS

1.1 Microcapsules and Microencapsulation

Microcapsules (MCs) are micron-sized particles in which core materials are enclosed by a shell. Depending on the number of cores in a MC, MCs can be categorized as single-core MCs and multi-core MCs. Comparing to multi-core MCs, single-core MCs tend to attract more attention as they have a better defined internal structure and thus provide more uniform release profiles of core materials. The core material can be a solid, liquid or gas and the wall is normally a solid composed of inorganic materials, organic polymers or composite materials. MCs are generally applied to protect the core materials from harsh environments, to confine their movements, to control their release profiles, to mask their unpleasant odors and to transform liquids into easily handled solid materials. Microencapsulation is the process to create a shell that encases the core using either chemical or physical or physicochemical methods.

The first report on the application of MCs dated back to late 1950s[1] when MCs were designed to encapsulate photosensitized materials for a photochemical printing process, which later led to the invention of carbonless copy paper, one of the most widespread applications of MCs. Since then, microencapsulation technology has been evolving

rapidly, fuelled by ever-increasing MC applications. According to a survey conducted using Scifinder, there are 21,483 reports* on MCs to date and the number of reports increased exponentially over the last 60 years, manifesting an increasing interest on this subject.

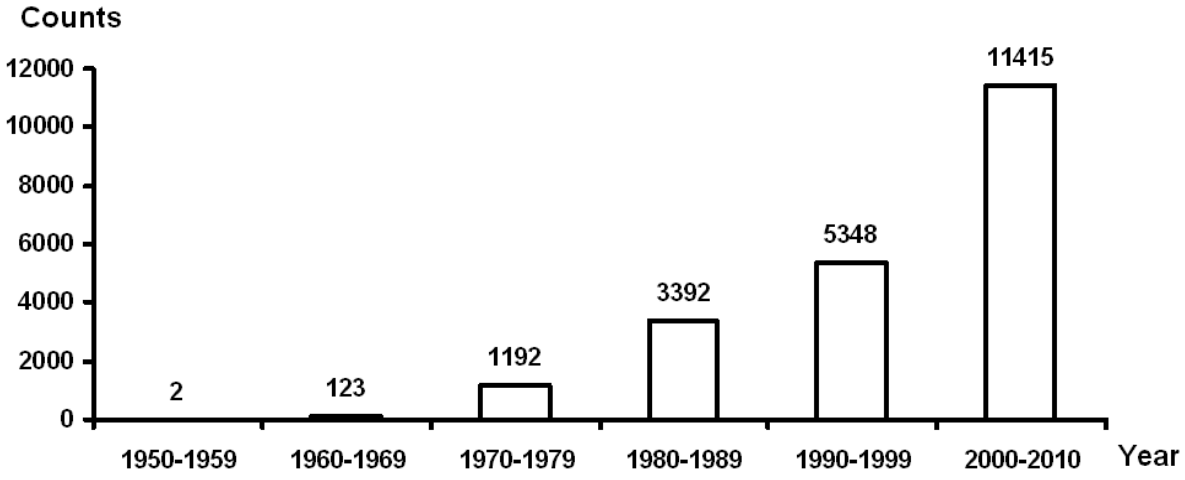

Figure 1.1 The number of report on microcapsules of each decade

1.2 Classical Applications of Microcapsules

Traditional applications of MCs include paper industry, agriculture, cosmetics, food industry and drug delivery. Carbonless copy paper has been, by far, the largest application of MCs as some 100,000 metric tons of MCs are used annually to make carbonless copy paper[2]. The principle of carbonless copy paper is illustrated in Figure 2[3]. In this

* Based on the Scifinder search using the keyword "microcapsules" at 17:00pm February 21, 2010 (eastern time)

application, MCs enables physical separation of encapsulated a dye precursor from a developing reagent. The dye precursor-containing MCs are coated on the back of the top page, while the developing reagent is evenly pre-coated on the front of the underlying page. When writing on the top page, the pressure ruptures MCs to release the dye precursor, which triggers an immediate reaction between dye precursor and developing reagent, causing the appearance of a coloured replica of pen trails on the second page.

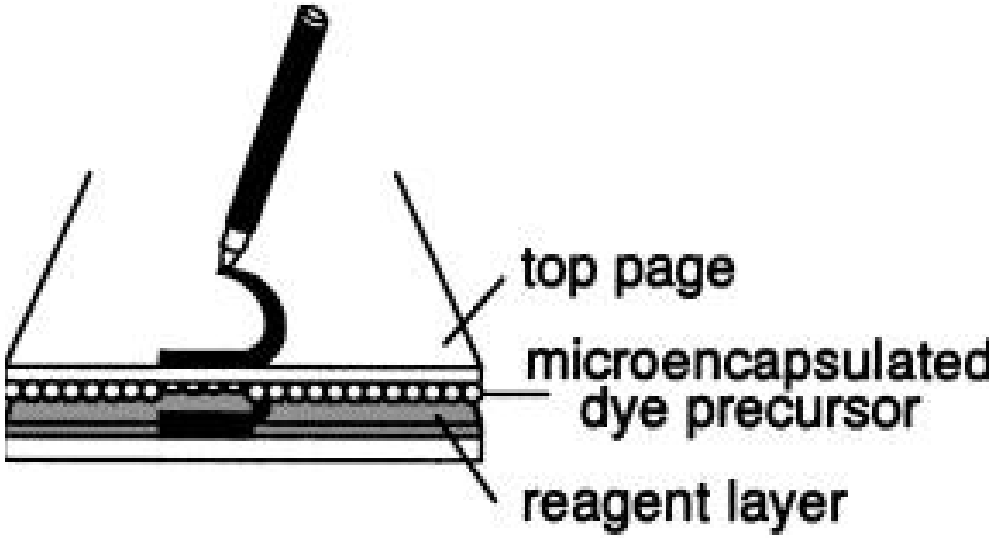

Figure 1.2 Schematic of the principle of carbonless copy paper. Reproduced from reference 3.

Another important application of MCs is the controlled delivery of pesticides and pheromones for crop protection.**Error! Bookmark not defined.** In most cases, encapsulated pesticides and pheromones are dispersible in aqueous phase, which eliminates the need of using organic solvents, making the process less costly and more environmentally friendly. The release profile of encapsulated pesticides and pheromones is normally dictated by the properties of MC walls, and various release mechanisms have

been established to meet the requirements of different applications, which enhances pesticides' efficacy and increases their functioning time.

In pharmaceutical industry, MCs are used to encapsulate drugs, enzymes, cells and genetically modified microorganisms[4] in order to realize sustainable drug release or immuno-isolation. In food industry, microencapsulation has been widely applied to mask or preserve flavours and aromas, to protect sensitive food ingredients, to retain nutrients and to increase the shelf life of food products[5]. MCs are also important for formulating one-pot adhesives where either resins or hardening agents are encased within MCs, which allows adhesive formulators to remix them without substantial reactions and to make adhesives with a longer shelf life.

1.3 Emerging Applications of Microcapsules

Recent years have witnessed an accelerating pace of applying microencapsulation technology to emerging areas, fostering the development of new materials and devices with amazing properties that may not be attainable using other technologies. Several new applications of MCs are presented below:

Electrophoretic Inks

MCs have been playing a pivotal role in the development of electrophoretic paper-like display, a concept that was introduced by Jacobson and others in the late 90s[6]. The idea involves confining electrophoretic pigments within MCs and placing these MCs

between micro-electrodes. When an electrical field is applied across these MCs, the encapsulated pigments with different charges and colours migrate accordingly, to show different colours at different locations, as shown in Figure 1.3a. Because electrophoretic displays rely on ambient light reflection and do not need backlight, they provide a more pleasant paper-reading experience with less stress on eyes than traditional backlit displays. These displays are ideal candidates for making electronic papers that promise to replace paper and to revolutionize the way people read.

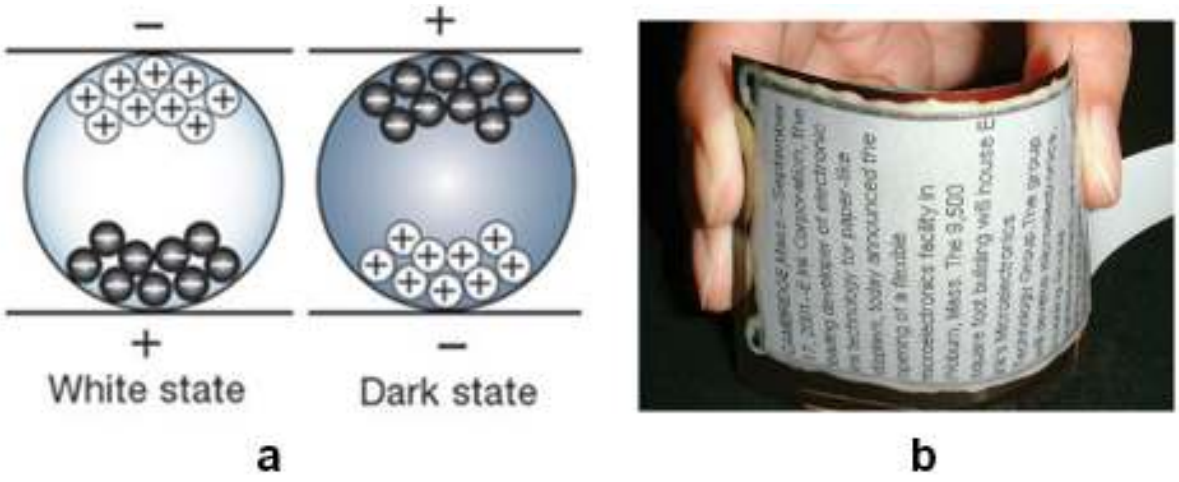

Figure 1.3 (a) Schematic illustration of electrical field directed alignments of electrophoretic pigments within microcapsules. (b) Photograph of a flexible display based on electrophoretic inks. Reproduced from reference 7.

Microcapsules Based Self-healing Materials

Another emerging field involving MCs is the development of self-healing materials. Self-healing materials are one type of smart materials that can automatically

repair mechanical damage to prevent their further spread. Self-healing materials enable early repair of damages on a microscopic level, which is almost impossible by other means and is essential for preventing a large scale of failure of materials. MC based self-healing materials are typically formulated by embedding MCs containing healing agents in a composite matrix. MCs separate the healing agent from a catalyst that has been evenly distributed in the matrix, which prevents its polymerization during normal usage. Upon damaging, MCs on the crack propagation trails rupture to release the liquid healing agent, which will fill the crack planes by capillary action and then polymerize by its contact with the pre-dispersed catalysts, repairing the cracks. Comparing to other self-healing systems[7], MC based approach features simplicity, robustness and ease of scale up, and shows great potential for practical applications.

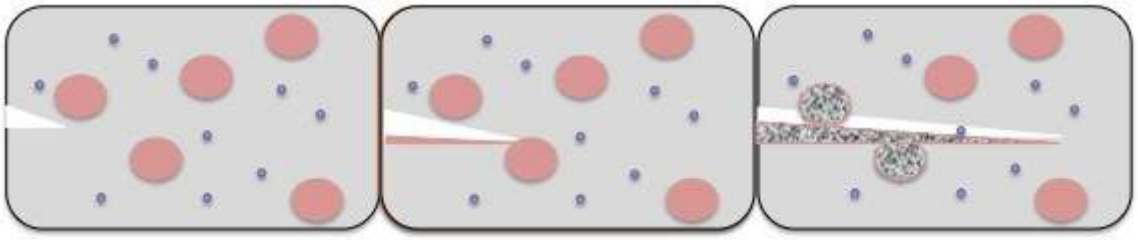

Figure 1.4 Illustration of the crack propagation and the self-healing process. Red circles stand for microcapsules and the catalyst is shown in blue dots. Reproduced from reference 8.

Catalysts Encapsulation

MCs play an important role in designing novel catalysts for organic transformations. Many catalysts have been encapsulated within MCs in order to achieve

easy separation after the reaction. These catalysts normally maintain high reactivity due to the solvent-like environments in MC interiors.[9] Different microencapsulated catalysts can mix with minimum interferences, which is essential for designing multi-step one-pot reactions.[10] In addition, MCs can be used to control the on/off state of reactions to produce chemicals and materials on demand. Recently, Frechet's group [11] has demonstrated that Grubbs catalyst could be encapsulated in MCs along with carbon nanotubes. These catalyst-containing MCs could mix with monomers for weeks with negligible reactions. When the mixture was irradiated with a near-IR laser, the carbon nanotubes inside MCs absorbed the light that was then converted into heat owing to the carbon nanotube's optothermal property. The heating caused an abrupt temperature and pressure increase within MCs, which eventually led to the rupture of MCs to release the catalyst to facilitate subsequent polymerization, as illustrated in Figure 1.5b.

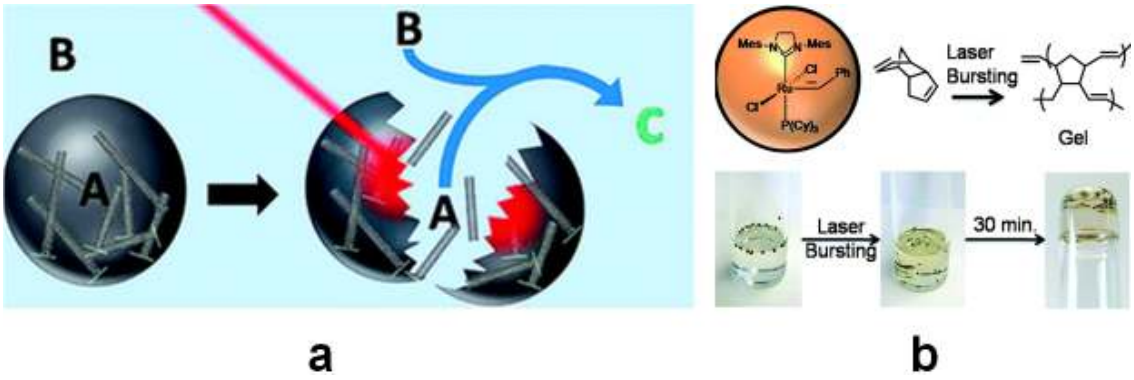

Figure 1.5 (a) Schematic illustration of a phototriggerable microcapsule. (b) Ring opening polymerization of dicyclopentadiene. Images of catalyst-containing microcapsules in dicyclopentadiene (left), after microcapsules bursting (center), and finally after gelling (right). Reproduced from reference 12.

1.4 Microencapsulation Methods

Microencapsulation technology has evolved for over 60 years and many methods have been developed to make MCs with various properties. In this section, several classical microencapsulation methods are introduced, including interfacial polycondensation, coacervation, in *situ* polymerization, solvency-change triggered phase separation, and colloid templated layer-by-layer (CT-LbL) assembly. Most these methods use emulsions as templates and involve a chemical or physicochemical or both processes. Purely mechanical process based microencapsulation methods, though interesting and very useful, are not the focus of this thesis and interested readers are referred to related references[12].

1.4.1 Interfacial Polycondensation

Interfacial polycondensation is an emulsion templated microencapsulation method that involves the condensation reaction between two very reactive monomers at the emulsion interface to form polymeric MC shells. Usually, these two monomers have very different polarities so that one monomer resides in the oil phase and the other one is primarily located in the aqueous phase. As a consequence, the polymerization is largely restricted to the oil-water interface. Monomer pairs for interfacial polycondensation include isocyanate/polyamine, isocyanate/polyol, acid halide(anhydride)/polyamine, and polyurea, polyurethane and polyamide MCs can be synthesized accordingly. Due to the high reactivity of these monomer pairs, fast polymerization happens at the interface

leading to the formation of an initial thin membrane in a short time. This thin membrane separates the two monomers at the interface and acts as a barrier to impede further reaction. This can normally be overcome by raising the temperature to encourage the diffusion of monomers through the interfacial membrane to form thicker MC walls. The MCs made by interfacial polymerization are usually mechanically strong due to rigid backbones and extensive hydrogen bonding in wall-forming polymers. MC wall properties can be tuned to some extent by varying the monomer loading, polarity of core materials, monomers and encapsulation process parameters. Both aqueous core and oil core MCs have been synthesized using interfacial polycondensation, with oil core MCs being more important for industrial applications such as pesticide and pheromone delivery, catalyst encapsulation, making carbonless copy paper and phase change materials, and for fragrance packaging. One inherent limitation of interfacial polycondensation for microencapsulation is its poor chemical compatibility with core materials bearing nucleophilic groups, excluding the encapsulation of these materials.

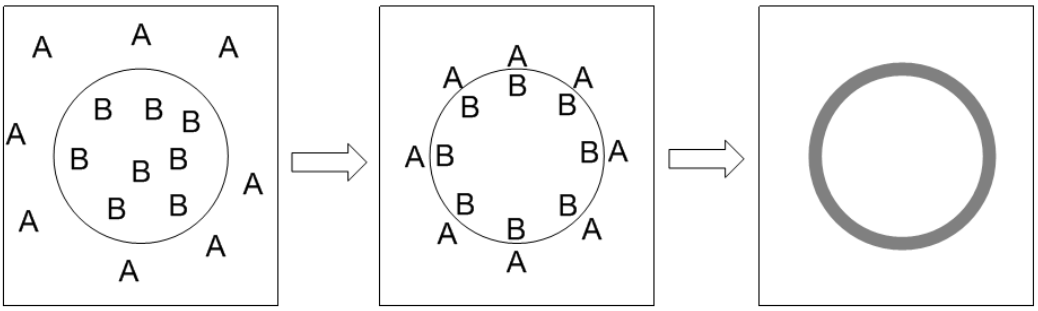

Figure 1.6 Schematic illustration of interfacial polycondensation for making a microcapsule. A stands for an aqueous soluble monomer and B means an oil soluble monomer.

1.4.2 Coacervation

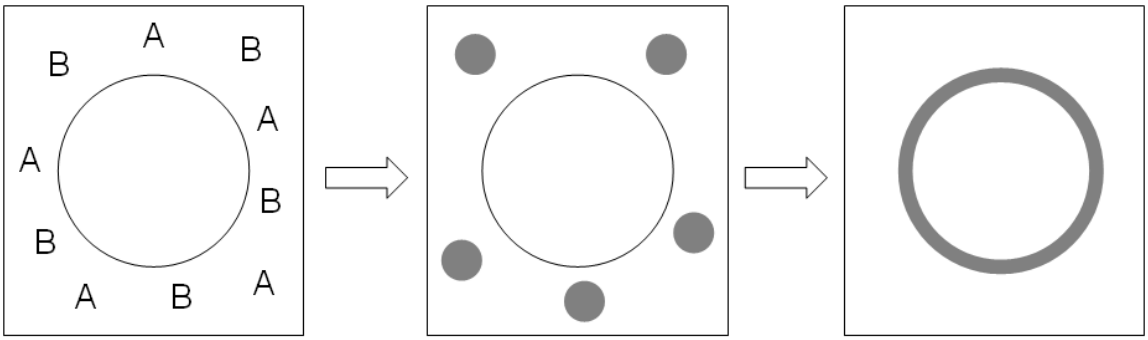

Figure 1.7 Schematic illustration of complex coacervation for making a microcapsule. A stands for a polycation and B refers to a polyanion.

Coacervation is a polymer phase separation process that causes the formation of two immiscible liquid phases. The polymer rich liquid phase is called coacervate and comprises a mixture of polymer and solvent. Coacervations can be classified as simple coacervations and complex coacervations. In a simple coacervation, only one polymer is involved and the coacervate formation is usually induced by means like temperature change, variation of ionic strength, change of solvency, etc. In contrast, complex coacervation is caused by the complexation between two or more polymers to form less soluble complexes. In heterogeneous systems such as particle suspensions or emulsions, both simple coacervates and complex coacervates would coat the particle or emulsion surfaces to form MCs, driven by minimization of interfacial tensions. Further strengthening of MC walls can be realized by chemical cross-linking of coacervates in subsequent steps. Coacervation is one of the most commonly applied methods for microencapsulation. As coacervation usually happens in the continuous phase, this

method shows little interference with core materials. However, coacervation is sometimes difficult to achieve due to specific conditions required. This method requires good polarity match between the core and coacervates, limiting it to the encapsulation of relatively hydrophobic core materials. As well, the use of toxic cross-linkers sometimes raises concerns about the safety of the MCs produced.

1.4.3 In-*situ* Polymerization

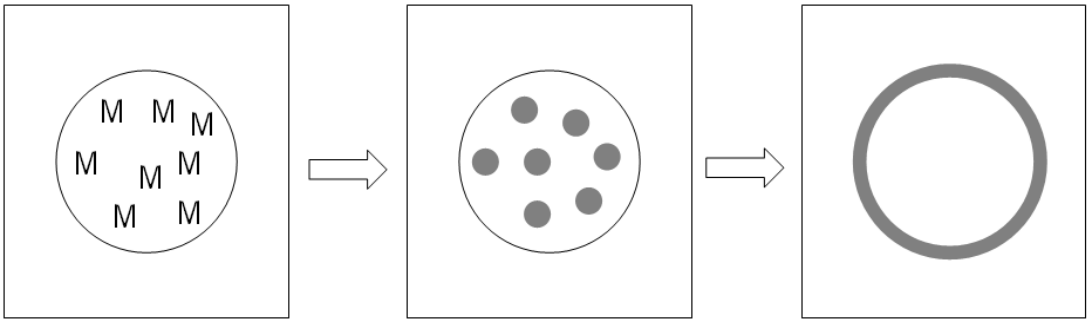

Figure 1.8 A schematic illustration of in-*situ* polymerization for making a microcapsule. M stands for monomers.

An in-situ polymerization for microencapsulation usually refers to a radical polymerization process that takes place within a dispersed phase. The polymerization causes the phase separation of the formed polymer due to the polymer's limited solubility in the dispersed phase. Given the intermediate polarity, the polymer precipitates at the oil-water interface to form MC walls. This method features simplicity and robustness. However, it has a strong dependence on the polarities of wall-forming polymers and core materials, which makes it only applicable to the encapsulation of certain types of core materials.

1.4.4 Solvency Change Triggered Polymer Phase Separation

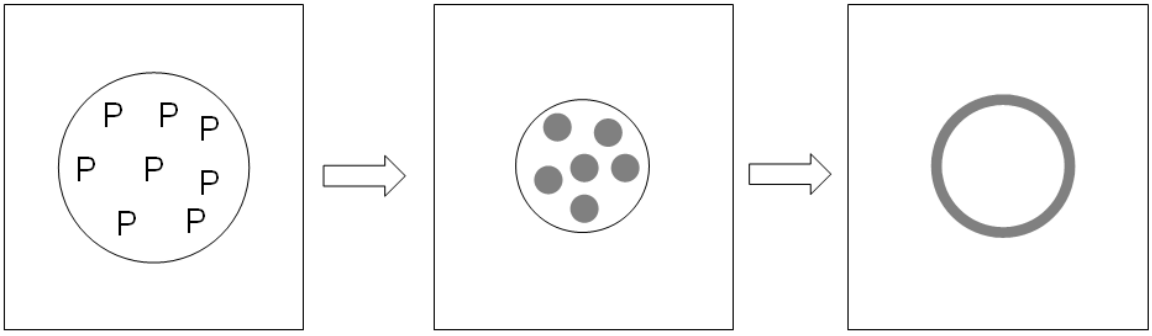

Figure 1.9 Schematic illustration of polymer phase separation method for making a microcapsule. P stands for a polymer.

This method starts with dissolving a polymer in a mixture of a good solvent and a non-solvent and the resulting solution is dispersed in another phase to form a stable emulsion. The good solvent is chosen to be volatile or extractable into the continuous phase. With the loss of the good solvent from the dispersed phase, the concentration of the good solvent decreases, inducing the phase separation of the polymer within the dispersed phase. If the polymer possesses an intermediate polarity between the dispersed phase and the continuous phase, the polymer phase-separation may happen at the interface to reduce interfacial tension and to form MC walls. Since this method uses pre-formed polymers as wall-forming materials with no reactions involved, it shows excellent chemical compatibility with a wide range of materials. Also this method does not necessarily require heating and thus is useful for the encapsulation of thermo-sensitive materials. However, it is important to find a good polarity match between the polymer and the core materials in order to achieve capsular structures. Any mismatch would lead

to the formation of undesirable morphologies. As a result, only a small fraction of materials can be encapsulated using this method and the choice of wall-forming polymers is often limited.

1.4.5 Double Emulsion

Double emulsions are usually made by dispersing a primary emulsion into a continuous phase and they can be divided into water-in-oil-in-water (W/O/W) emulsions and oil-in-water-in-oil (O/W/O) emulsions. For making MCs, the wall-forming materials are usually present in the middle phase and are solidified by either polymerization or polymer precipitation due to the loss of good solvent, resulting in the formation of MC walls. Since the wall formation process is completely separated from core materials, the interference between them is minimized, showing great chemical compatibility of this method with core materials. Also this method is less dependent on the polarity of core materials and the wall forming polymers, making it possible to encapsulate a wide range of materials. However, this method tends to produce multi-core MCs with different core size, which often exhibit complicated release profiles. Recent development of microfluidic devices enables the preparation of well-defined MCs. Weitz's group at Harvard University developed both a coaxial microcapillary and a T-junction device to generate double emulsions with a precise control over the number and size of cores.[13] They also demonstrated making single-core MCs using double emulsions via different means, indicating the diversity of this method. Further development of this method looks

into making the devices more practical so that it could meet the scale requirements of industrial applications.

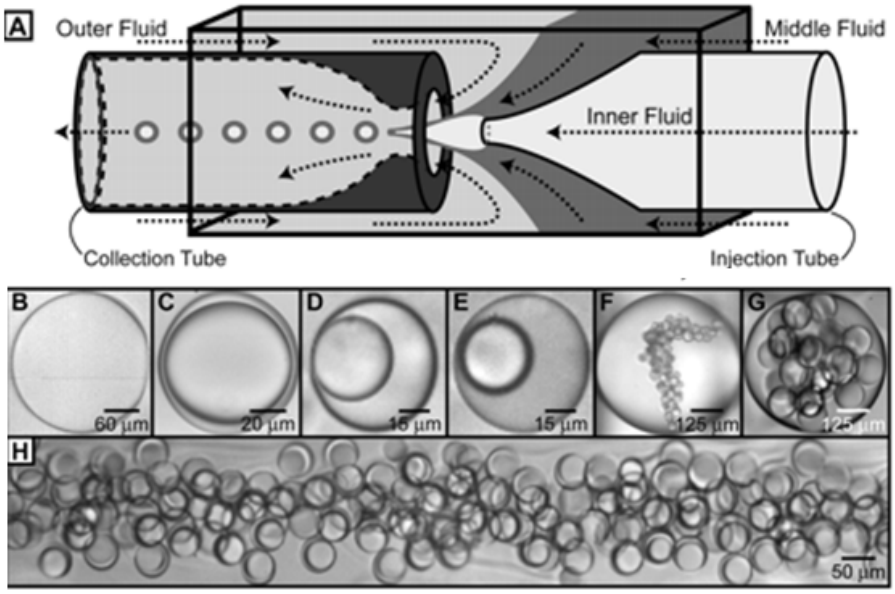

Figure 1.10 (A) Schematic of the coaxial microcapillary fluidic device. (B)-(E) single-core double emulsions with different core size. (F)-(G) multi-core double emulsions. (H) Single-core double emulsion droplets flowing in a collection tube. Reproduced from Reference 14.

1.4.6 Colloid Templated Layer-by-Layer (CT-LbL) Assembly

Lay-by-layer assembly is a thin film fabrication method. Common driving forces utilized in LbL assembly include electrostatic interaction, hydrogen bonding[14], covalent attachment[15], halogen bonding[16] and so on. Among them, electrostatic interactions are the most frequently used means to assemble polyelectrolytes and other charged materials to form multilayer films. To make MCs, solid templates are firstly used to confine LbL

assembly on particle surface and are subsequently removed via either chemical or physical treatments to generate capsular structures.[17] This method has advantages in the control of wall thickness, composition, functionality and mild fabrication process. However, it suffers from a tedious coating process and the difficulty of loading active ingredients, which make this method less practical.

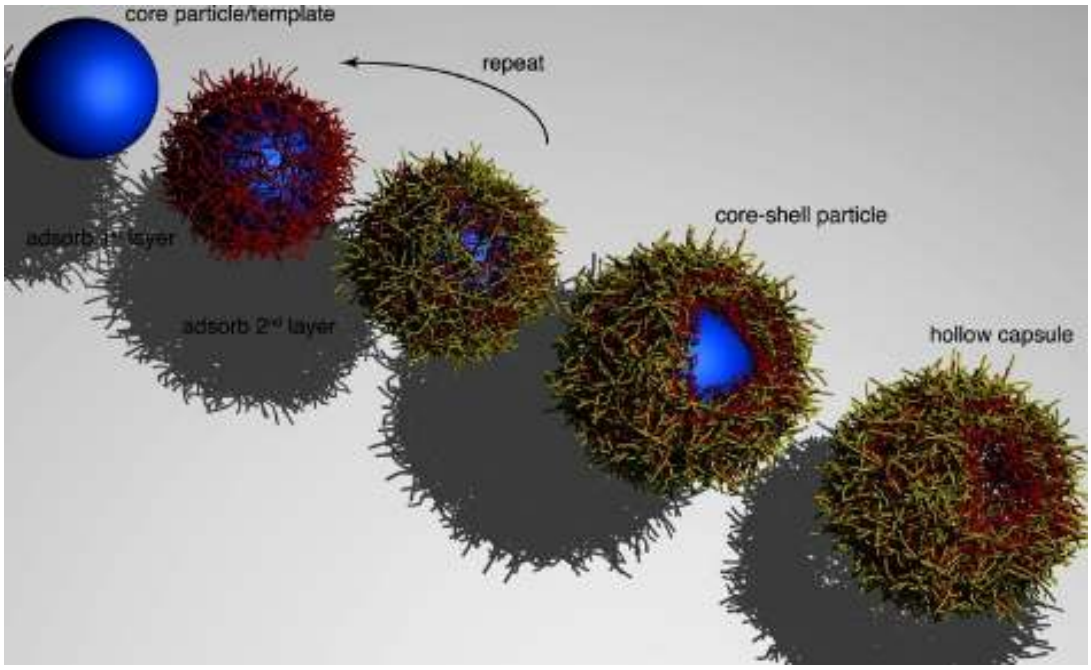

Figure 1.11 Schematic depiction of colloid template layer-by-layer for making a microcapsule. Reproduced from Reference 15.

1.5 Thesis Objectives

Over 60 years of development of microencapsulation, many methods have been invented to produce MCs with various properties and a wide range of core materials have been encapsulated using these methods for different applications. However, there are still

many challenges facing MC studies and addressing some of these challenges is the focus of this thesis.

1.5.1 Microcapsule Characterization

MC characterization is important for understanding MC formation, morphology, properties and for MC optimization. MC characterization has been routinely carried out using traditional analytical techniques such as nuclear magnetic resonance (NMR) spectrometry, Fourier transform infrared (FTIR) spectrometry, optical microscopy, atomic force microscopy (AFM), laser scanning confocal microscopy (CLSM), electron microscopy. These techniques enable direct imaging of MCs and provide information about MC bulk compositions. An important part of MC characterization is to study MC wall cross-sections to reveal the wall morphology and the chemical distributions of different components across MC walls, which contain rich information about MC formation and properties. However, due to either poor spatial resolution or the lack of chemical sensitivity, the aforementioned techniques are not sufficient to investigate sub-micron thick MC wall cross-sections, which has rendered current MC characterization rather empirical. Therefore, advanced analytical techniques that have the ability to provide chemical information with a high resolution are needed for characterizing MC wall cross-sections, which would allow a quantitative understanding of the formation and properties of MCs and provide guidance for MC optimization. Scanning transmission X-ray microscopy (STXM) is a near edge X-ray absorption fine structure (NEXAFS)

spectrum based spectromicroscopy. It has emerged as an excellent tool for analyzing composite materials as it provides both good chemical sensitivity and a high resolution. Previous studies have shown the feasibility of applying STXM to MC wall cross-section studies.[18] One of the goals of this thesis is to extend the utility of STXM for MC studies to investigate wall morphologies and chemistries of some industry relevant MCs, which would lead to better understanding of these MCs and provide guidance to optimize them in order to better meet the requirements of different applications.

1.5.2 Microcapsule Modification

MCs are useful micro-structures that have been widely applied in industry. Different applications call for different MC properties. However, the properties of MCs are normally determined by core materials, wall formers and microencapsulation processes. In order to meet the requirements of different applications, MCs needs to be modified in some way to render MCs some new functions or properties.

One objective of this thesis is to develop novel methods for the modifications of polyurea MCs. Polyurea MCs are commonly synthesized by interfacial polycondensation and have been extensively applied in industry for over 50 years due to their excellent mechanical strength and ease of synthesis. However, due to fast reaction rates and the relatively inert nature of polyurea, modifications of polyurea MCs have been largely unexplored. Chapter 4 aims to develop a post-modification method to improve the surface properties of polyurea MCs and also to develop a simplified microfluidic device that is

capable of producing monodisperse polyurea MCs. These modifications would allow the modulation of polyurea MC adhesion to substrate surfaces and studies of size-dependent MC properties.

1.5.3 Microcapsule Synthesis

Although the development of microencapsulation has enabled the encapsulation of a wide range of core materials for different applications, situations still exist where the properties of MCs made by existing microencapsulation methods cannot completely satisfy the requirements of ever-increasing applications. Therefore, in addition to MC modifications, there is a strong need to develop new microencapsulation methods that bear new features and can solve some inherent problems associated with current methods.

The formation of MC walls in most microencapsulation methods are driven by the minimization of interfacial tensions, which imposes requirements on the polarity balance between core materials, wall formers and dispersing media. This strong polarity dependence limits most microencapsulation methods to specific core materials with narrow selections of the wall materials and properties. Therefore, to develop more general microencapsulation methods, one needs to research approaches where the confinement of wall growth at the interface is achieved by other mechanisms than interfacial tension reduction. Such methods are desirable as they can be applied to a wider range of core materials and can produce walls with diverse properties. One possible solution to alleviate the polarity dependence is to use initiator-bearing surface-active agents that can firmly

anchor at oil-water interfaces. These initiators at interfaces can then be utilized to initiate the growth of materials to generate MC walls. In this way, the interfacial anchoring and wall growth can be well separated and the method's dependence on the polarity match of different components can be lessened.

Chapters 5, 6 and 7 aim to develop general microencapsulation methods that could encapsulate hydrophobic materials with a wide range of polarities and produce MCs with different properties. Specifically, Pickering emulsion templated microencapsulation methods are considered, as Pickering emulsions generally have high stability, which makes them ideal MC precursors. Our strategy is to synthesize initiator-bearing Pickering emulsifiers that could firmly anchor at oil-water interfaces. MC walls could be generated by subsequent material growth confined at the interface by these Pickering emulsifiers. Chapter 5 aims to explore a new surface modification method to make Pickering emulsifiers via electrostatic interaction and to study the pH response of the resulting Pickering emulsions. Based on this electrostatic modification method, modifiers bearing different initiators are tested to make Pickering emulsifiers and to direct the growth of various materials at interface driven by either layer-by-layer assembly (Chapter 6) or atom transfer radical polymerization (Chapter 7).

1.6 Methods and Techniques

1.6.1 Scanning transmission X-ray microscopy

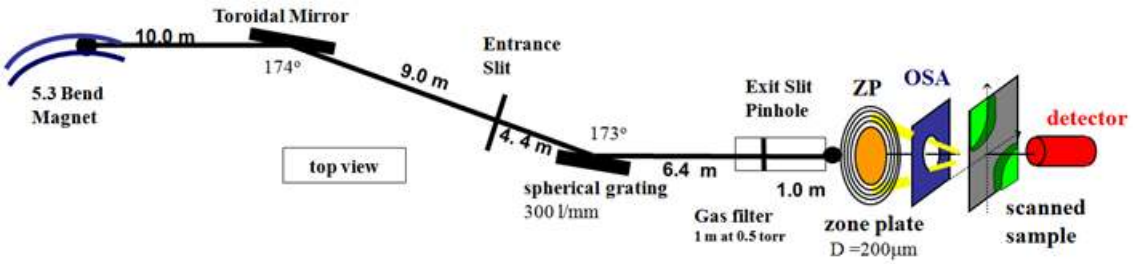

Figure 1.12 Bend magnet STXM beamline 5.3.2 in Advanced Light Source (ALS)

It is well known that X-ray irradiation can be absorbed by substances and the absorbed photons can either promote inner shell electons to unoccupied energy levels or remove them from substances to form an ionization state. Because every element has an unique absorption edge in the soft X-ray range (100-1200 eV), X-ray absorption spectroscopy has been widely used for elemental analysis. The applicaton of synchrotron light in X-ray absorption spectroscopy enables obtaining absorption spectra with fine scale details at each edge and such spectra are called near edge X-ray absorption fine structure (NEXAFS) spectra. NEXAFS spectra reflect the electronic states and geometries of samples and are useful for material identification and quantification.

Scanning transmission X-ray microscopy (STXM) is a synchrotron-based X-ray absorption spectromicroscopy. It is a unique analytical tool that can provide high resolution images with a good chemical sensitivity, ideal for MC wall studies. The typical setup of STXM is illustrated in Figure 1.12. For measuring a STXM image, a sample section is raster-scanned by a focused monochromatic X-ray beam and the transmited signals are then recorded by a detector. Currently, STXM has a spatial resolution ~20 nm and the contrast of STXM images arises from different X-ray absorption coefficients of

different components in samples. For quantitative analysis, a series of STXM images are normally taken with different photon energies to obtain a so-called image sequence or image stack. The image sequence is then fitted with reference NEXAFS spectra pixel-by-pixel using singular value decomposition to generate quantitative component maps. The spatial arrangement of different components in the sample can be illustrated by creating a colour-coded composite chemical map with arbitrary colour assignment.

1.6.2 Pickering emulsions

Pickering emulsions are solid particle stabilized emulsions. In Pickering emulsions, particles at oil/water interface exerts steric hindrance and sometimes electrostatic repulsion in case with charged particles to prevent emulsion droplets from coalescence. In general, Pickering emulsions are much more stable than surfactants stabilized emulsions. The stability of Pickering emulsions can often be estimated by calculating the energy needed to remove one particle from corresponding oil-water interface, which is given by equation 1[19]:

$$E = \pi r^2 \gamma \ (1 \pm \cos\theta)^2 \qquad (1)$$

Where E is the attachment energy of one particle to the interface, r is the radius of particle, γ is the interfacial tension between oil and water, θ is the three phase contact angle made by the particle with an oil-water interface (Scheme 8.1). The negative sign in the bracket is for removing the particle to the aqueous phase, while the positive sign is used when the particle is transferred from the interface to the oil phase. According to the

equation, though the particle radius r and oil-water interfacial tension γ play some roles, the particle's tendency to stay at the interface is largely dependent on the contact angle θ, which reflects the wettability of the particle surface by both phases. It has been reported in literature[20] that the optimum contact angles for stabilizing oil-in-water emulsions are between 70 °C and 86 °C, while for water-in-oil emulsions, the optimum contact angles are between 94 °C and 110 °C. With suitable contact angles, the particle attachment energy could be much higher than the thermal energy, making particles' absorption at interface irreversible under normal conditions, That accounts for extremely high stability of some Pickering emulsions, making Pickering emulsions ideal candidates for templating material growth at oil/water interface for making composite MCs.

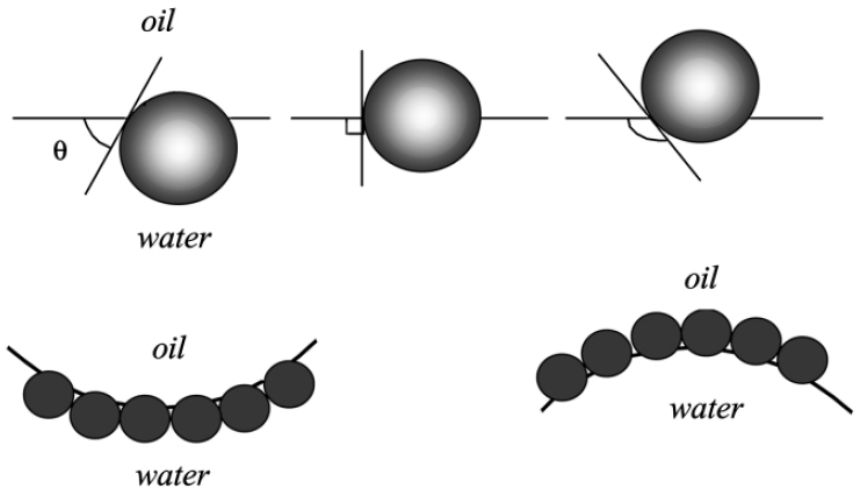

Figure 1.13 (Upper) Positions of a spherical particle at oil-water interface with different contact angles. (Lower) Different types of emulsions stabilized by particles with different contact angles. Taken from reference 19 with minor modifications.

1.6.3 Atom transfer radical polymerization

Atom transfer radical polymerization (ATRP) is a controlled radical polymerization technique. Alkyl halides are often used as radical initiators in ATRP that can react with transition metal complexes to produce alkyl radicals and oxidized metal complexes. The formed radicals can propagate in the presence of monomers to form polymer chains, termed as propagating or active chains. The active chain can then react with the oxidized metal complex to regenerate halide-terminated polymer, so-called dormant chain. Because the redox equilibrium often favours the formation of dormant chains, the radical concentrations in the reaction media are very low, which prevents radical polymerization from termination caused by both radical-radical coupling and disproportionation. The basic ATRP mechanism is illustrated in Scheme 1.1. Due to its relatively simple procedures, mild conditions, good compatibility with a wide range of monomers, ATRP has been widely applied for the syntheses of narrowdisperse polymers, block copolymers and polymer brushes.

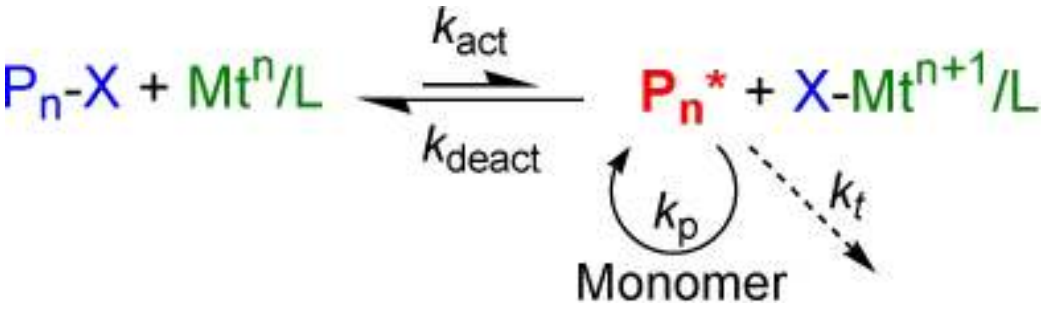

Scheme 1.1 Basic mechanism of atom transfer radical polymerization. Taken from Reference 21.

1.7 References

[1] Green B. K.; Schleicher L. US Patent 2,800,457, **1957**

[2] Arshady, R. *Microspheres, Microcapsules & Liposomes*, Plenum, New York **1998.**

[3] White, M. A. *Journal of Chemical Education* **1998**, *75*, 1119-1120.

[4] Chang, T. M. S.; Prakash, S. *Molecular Biotechnology* **2001**, *17*, 249-260.

[5] Desai, K. G. H.; Park, H. J. *Drying Technology* **2005**, *23*, 1361-1394.

[6] Chen, Y.; Au, J.; Kazlas, P.; Ritenour, A.; Gates, H.; McCreary, M. *Nature* **2003**, *423*, 136-136.

[7] Murphy, E. B.; Wudl, F. *Progress in Polymer Science*, *35*, 223-251.

[8] http://en.wikipedia.org/wiki/File:Polymerization_in_situ.jpg

[9] Price, K. E.; Mason, B. P.; Bogdan, A. R.; Broadwater, S. J.; Steinbacher, J. L.; McQuade, D. T. *Journal of the American Chemical Society* **2006**, *128*, 10376-10377.

[10] Poe, S. L.; Kobaslija, M.; McQuade, D. T. *Journal of the American Chemical Society* **2006**, *128*, 15586-15587.

[11] Pastine, S. J.; Okawa, D.; Zettl, A.; Frechet, J. M. J. *Journal of the American Chemical Society* **2009**, *131*, 13586-+.

[12] (a) Gharsallaoui, A.; Roudaut, G.; Chambin, O.; Voilley, A.; Saurel, R. *Food Research International* **2007**, *40*, 1107-1121. (b) Senuma, Y.; Lowe, C.; Zweifel, Y.; Hilborn, J. G.; Marison, I. *Biotechnology and Bioengineering* **2000**, *67*, 616-622. (c)Aebischer, P.; Wahlberg, L.; Tresco, P. A.; Winn, S. R. *Biomaterials* **1991**, *12*, 50-56.

[13] Utada, A. S.; Lorenceau, E.; Link, D. R.; Kaplan, P. D.; Stone, H. A.; Weitz, D. A. *Science* **2005**, *308*, 537-541.

[14] Lutkenhaus, J. L.; Hrabak, K. D.; McEnnis, K.; Hammond, P. T. *Journal of the American Chemical Society* **2005**, *127*, 17228-17234.

[15] Huang, C. J.; Chang, F. C. *Macromolecules* **2009**, *42*, 5155-5166

[16] Wang, F.; Ma, N.; Chen, Q. X.; Wang, W. B.; Wang, L. Y. *Langmuir* **2007**, *23*, 9540-9542.

[17] Johnston, A. P. R.; Cortez, C.; Angelatos, A. S.; Caruso, F. *Current Opinion in Colloid & Interface Science* **2006**, *11*, 203-209.

[18] Hitchcock, A. P.; Stöver, H. D. H.; Croll, L. M.; Childs, R. F. *Australian Journal of Chemistry* **2005**, *58*, 423-432.

[19] B. P. *Current Opinion in Colloid & Interface Science* **2002**, *7*, 21-41.

[20] Kaptay, G. *Colloids and Surfaces a-Physicochemical and Engineering Aspects* **2006**, *282*, 387-401.

[21] http://www.cmu.edu/maty/development-atrp/index.html

CHAPTER 2 - A NEW APPROCH TO STUDYING MICRO-CAPSULE WALL GROWTH MECHANISMS

2.1 Introduction

Microcapsules are small, hollow devices designed to protect their contents from environmental degradation and to control the rate of release. Most microcapsules are prepared by interfacial polyaddition of oil-soluble polyisocyanates dispersed in water, with aqueous polyamines, though analogous approaches are used to form polyurethane and polyamide capsules. The resulting spherical polymer capsules typically contain an organic active or fill, such as insect pesticides or pheromones, inks, and fragrances, and are mainly used in agriculture, carbonless papers applications, and personal care products. Recent applications involve capsules as catalyst supports[1,2] and in display devices.[3,4]

Understanding the mechanisms of capsule wall formation and growth is key to controlling wall strength and permeability and hence to improving capsule performance, especially in terms of variable release[3] and release triggered by acid[4] or base[5]. The two major wall growth mechanisms are the moving boundary mechanism[6] and the stationary boundary mechanism, both illustrated in Figure 2.1. Pearson and Williams[7] determined that the reaction zone in interfacial encapsulations often moves during the reaction, with the water-soluble monomer diffusing through the initially formed polymer film to reach and react with the oil-soluble monomer, building up successive layers on the interior

capsule wall. This model has been used by many researchers to interpret the encapsulation processes for polyurethane, polyurea, and polyamide microcapsules.[7] In contrast, the stationary boundary mechanism invokes the presence of a stable, stationary reaction zone during the encapsulation process (Figure 2.1b). Under this mechanism, capsule wall thickness does not increase with time once the initial polymer film has been formed, though its density may change.

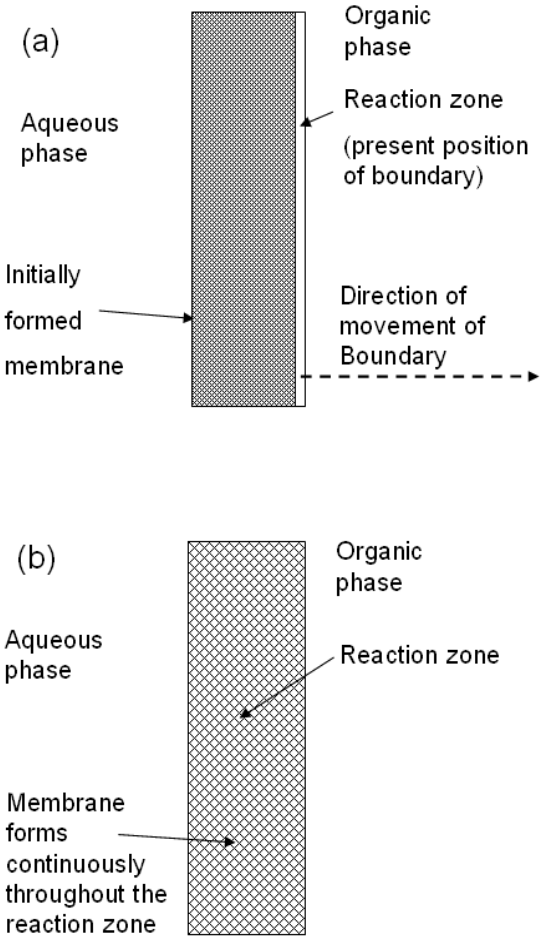

Figure 2.1 Illustration of two different mechanisms proposed for capsule wall formation: (a) moving boundary mechanism; (b) stationary boundary mechanism.

Encapsulation processes can be affected by many factors, including the polarity, diffusion coefficients and reactivities of monomers, the polarity and permeability of the forming polymers, solvent polarity, solution pH, and temperature. While a better understanding of the encapsulation process could lead to improved capsule design, experimental studies of the encapsulation process have been complicated by the high rate of interfacial polymerizations and the typically submicron thickness of the wall.

Janssen and co-worker[7d] used narrow-disperse capsules prepared from 2,4-toluene diisocyanate (TDC) and diethylenetriamine (DETA) with diameters varying from 3 to 5 mm to study the wall formation process experimentally. They found that the capsule wall thickness increased with reaction time, in agreement with the moving boundary mechanism. In contrast, Jabbari,[8] studying smaller microcapsules prepared from hexamethylene diisocyanate (HMDI) and hexamethylenediamine (HMDA), found that capsule wall thickness did not increase with time once the initial polymer film had been formed, implying that the boundary is stationary in this system.

We aim to design an effective approach to studying polyurea capsule wall composition and wall formation mechanism. Our strategy involves using mixed isocyanate monomers of different reactivity in the organic or fill phase and studying their sequential interfacial polyaddition with aqueous amines to form composite polyurea capsules. The spatial distribution of the different isocyanate residues across the capsule wall should then reflect the capsule wall formation process.[9] We are using scanning transmission X-ray microscopy (STXM) to map the distribution of these different monomers across the capsule wall with submicron spatial resolution.

We demonstrate here a strategy to study interfacial encapsulation processes and determine the growth processes in two types of polyurea capsules as a function of cross-linking and polymerization temperature. Our approach involves using mixtures of aromatic and aliphatic isocyanates in an oil phase consisting mainly of *p*-xylene. Aromatic isocyanates are known to be significantly more reactive than their aliphatic counterparts.[10] Sato reported the rates of reaction of phenyl isocyanate with methanol to be 50 times higher than the rate of reaction of ethyl isocyanate with methanol.[11] Kuck et al. reported the reaction of HMDI with secondary amines to be about an order of magnitude lower than the corresponding reaction of TDI.[12] Competitive interfacial polyaddition of a mixture of aromatic and aliphatic isocyanates should thus lead to sequential incorporation of these two isocyanates. If the rate-limiting step is diffusion of the aqueous amine into the oil phase, then the polyurea formed early should be rich in aromatic residues, while polyurea formed later should be rich in aliphatic groups. Hence, observation of an aromatic/aliphatic composition gradient across the capsule walls would indicate that wall formation involves a moving reaction zone or boundary (Figure 2.1a), as the wall grows toward the interior of the capsule. Conversely, absence of such a compositional gradient would imply wall formation with a fixed though broad reaction zone, leading to an interpenetrating network (IPN) of sequentially formed aromatic and aliphatic polyureas, as illustrated in Figure 2.1b.

We compared two types of polyurea microcapsules, both based on mixtures of aromatic and aliphatic isocyanates, but with different degrees of cross-linking. **PID** capsules (**P**MPPI + **I**PDI/**D**ETA) are formed by reaction of mixtures of polymethylene

polyphenylene isocyanate (PMPPI) and isophorone diisocyanate (IPDI), with diethylenetriamine (DETA) as aqueous amine. **MHH** capsules (**M**DI + **H**MDI/**H**MDA) are formed by reaction of methylene diphenyl 4,4′-diisocyanate (MDI) and hexamethylene diisocyanate (HMDI), with aqueous hexamethylenediamine (HMDA). PMPPI and MDI are two aromatic isocyanates commonly used for preparing microcapsules. They have similar reactivities toward polyamines, but only PMPPI acts as a cross-linker. IPDI and HMDI are aliphatic isocyanates commonly used for their UV resistance and serve as aliphatic markers in this study. DETA and HMDA are widely used polyamines, with DETA being more polar and also acting as a cross-linker.

2.2 Experimental Section

2.2.1 Sample Preparation

The interfacial polymerizations were carried out in a jacketed glass reactor fitted with an overhead stirrer. A mixture of 1 g of aromatic and 1 g of aliphatic isocyanate dissolved in a total of 10 mL of *p*-xylene was dispersed into 35 mL of 1 wt % aqueous PVA solution at about 800 rpm for 15 min. Then 1.5 equiv of polyamine, on an amino group per isocyanate group basis, in 5 mL of 1 wt % PVA solution was added to the emulsion. Different polymerization temperatures were employed as described below. The obtained capsules were washed on a Buchner vacuum filter with water and tetrahydrofuran to remove residual aqueous amine and extract the oil phase, respectively. They were subsequently dried under vacuum to constant weight. For TEM and STXM

analysis, dried capsules were embedded in an epoxy resin prepared by mixing trimethylolpropane triglycidyl ether (TTE) and 4,4′-methylenebis(2-methylcyclohexylamine) (MBMCA) in a 1:1 weight ratio and cured at 70 °C for 3 days. This epoxy showed superior radiation resistance compared to the commonly used Spur epoxy and does not contain carbonyl and phenyl groups that might interfere with the spectral analysis. The embedded samples were ultramicrotomed to about 100 nm thickness.

2.2.2 Scanning Transmission X-ray Microscopy

Scanning transmission X-ray microscopy (STXM) at the dedicated polymer STXM beamline 5.3.2 of the Advanced Light Source (ALS) was used to map the distribution of aromatic and aliphatic polyureas across the capsule wall. STXM is a microscopy-based version of near-edge X-ray absorption fine structure (NEXAFS) spectroscopy,[13] combining good energy resolution of about 0.1 eV with spatial resolution of about 50 nm. Our previous results have shown that STXM is a powerful tool for microcapsule studies.[14] For measurement, a 100 nm thick microtomed section of capsules embedded in epoxy resin is imaged with a monochromatic X-ray beam, and a sequence of images are taken over a range of X-ray energies covering the C 1s spectral region. The data analysis is carried out using the program aXis2000.[15] It involves a pixel-by-pixel fit of the image sequence to quantitative C 1s reference spectra for the pure aromatic and aliphatic polyureas as well as the epoxy resin. The fit coefficients are then assembled into

individual component maps, and color-coded composite maps are further constructed by mapping each component to one of the three primary colors (in this work we assign red to epoxy, green to aromatic, and blue to aliphatic). STXM can easily distinguish between aromatic and aliphatic polyurea, based on the strong C 1s → π* absorption band present only in the aromatic urea 285 eV. Both ureas have strong C 1s → π* absorption bands near 289.4 eV (carbonyl bands), while the epoxy resin was designed to not have any aromatic and carbonyl groups so as not to interfere with the urea analysis.[10b]

2.3 Results and Discussion

2.3.1 Cross-linked Polyurea Microcapsule System

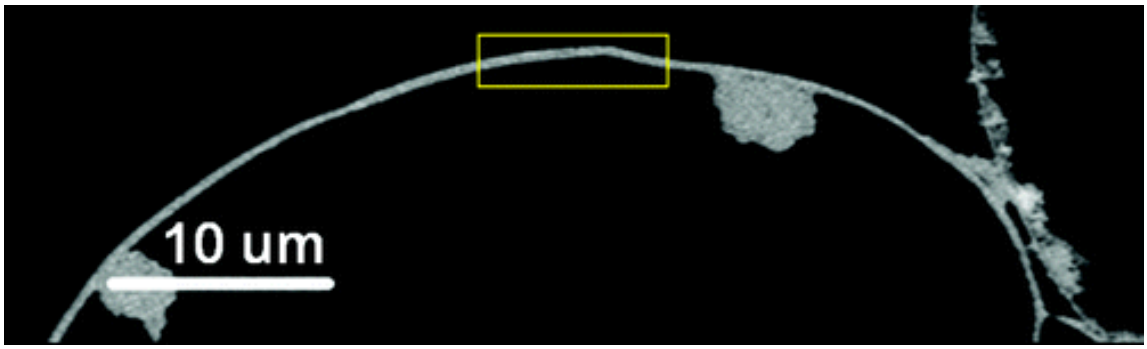

Figure 2.2 STXM overview image (optical density) at 285.2 eV, of PID capsule wall prepared at 50 °C. The yellow rectangle indicates the area where the image sequence for Figure 2.4 was recorded.

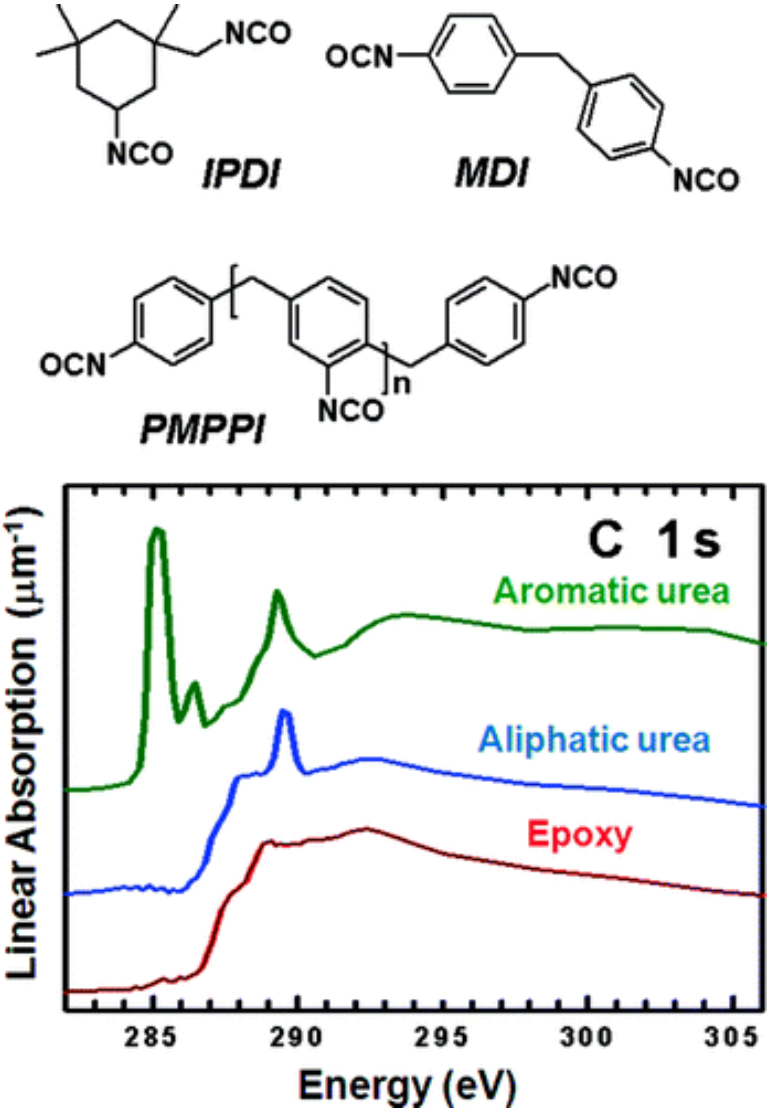

Figure 2.3 Chemical structures of IPDI, MDI, and PMPPI and reference spectra for the three chemical components of the samples: embedding epoxy, aliphatic polyurea, and aromatic polyurea. The spectra were placed on absolute intensity scales by scaling to match the elemental response outside of the near-edge region and vertically offset for clarity.

First we examined the **PID** capsules prepared from PMPPI + IPDI//DETA at constant temperature of 50 °C for 24 h. Figure 2.2 shows a STXM image of a partial wall cross section taken at 285.2 eV, the energy of maximum contrast of capsules to the epoxy resin.

Figure 2.3 shows the chemical structures for IPDI, MDI, and PMPPI as well as reference spectra for the three components present in the microtomed capsule wall sections: aromatic polyurea (green), aliphatic polyurea (blue), and epoxy (red).[16]

The reference spectrum for the epoxy resin was obtained directly from each sample to account for minor differences in curing between samples, while the spectra for the two types of polyurea were obtained from model polyureas and capsules.[16] These three reference spectra were used to analyze the image sequence obtained for the boxed area indicated in Figure 2.2. Singular value decomposition (SVD)[16] resulted in the component maps and the color-coded composite map shown in Figure 2.4. Integrations across the boxed area in Figure 2.4b resulted in composition profiles across the capsule wall shown in Figure 2.4c. STXM provides quantitative composition information, with good spatial resolution. The capsules shown here have thin and dense walls due to use of the poor solvent *p*-xylene and the high cross-linking ability of the PMPPI used as major wall former.

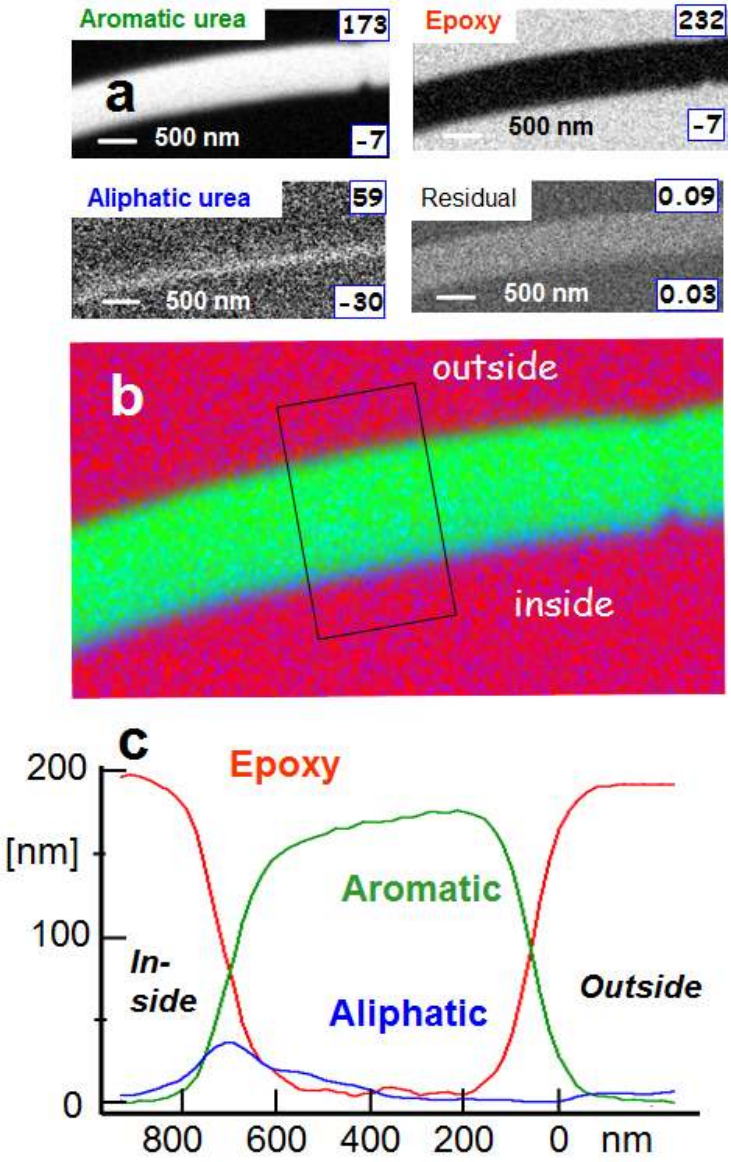

Figure 2.4 (a) Individual component maps of aromatic urea, aliphatic urea, and epoxy resin, for the wall section of the PID capsule shown in Figure 2.2, prepared at 50 °C. (b) Color-coded composite map of the same three components. (c) Component profiles (in nanometer thickness) across the capsule wall (orange box).

There is a slight compositional gradient across the capsule wall, with aromatic polyurea more prevalent in the outer layer and aliphatic polyurea enriched in the inner layer, in accordance with their expected sequential incorporation into the wall, as described earlier.[16] Here we are interested in exploring the mechanistic implications of this compositional gradient in terms of wall formation and cross-linking. The presence of this gradient indicates that the reaction zone moves during the encapsulation process. It starts with the formation of mainly aromatic polyurea in the outer shell layer and moves inward as conversion shifts to the less reactive aliphatic isocyanate. The line-out across the capsule wall (Figure 2.4c) shows these gradients. The wall segment studied further reveals low conversion of IPDI, with a ratio of aromatic/aliphatic urea of 10:1. We attribute this low conversion of IPDI to the low permeability to amine of the cross-linked aromatic polyurea formed at 50 °C in *p*-xylene, a poor solvent for polyurea, as well as to the lower reactivity of the IPDI compared to the aromatic isocyanate, PMPPI.

Subsequently, we carried out polymerizations using the same protocol but at room temperature, designed to lead to less dense aromatic polyurea walls and hence increase the in-diffusion of DETA. Figure 2.5a−c shows the STXM results obtained for **PID** capsules formed at room temperature after 24 h.

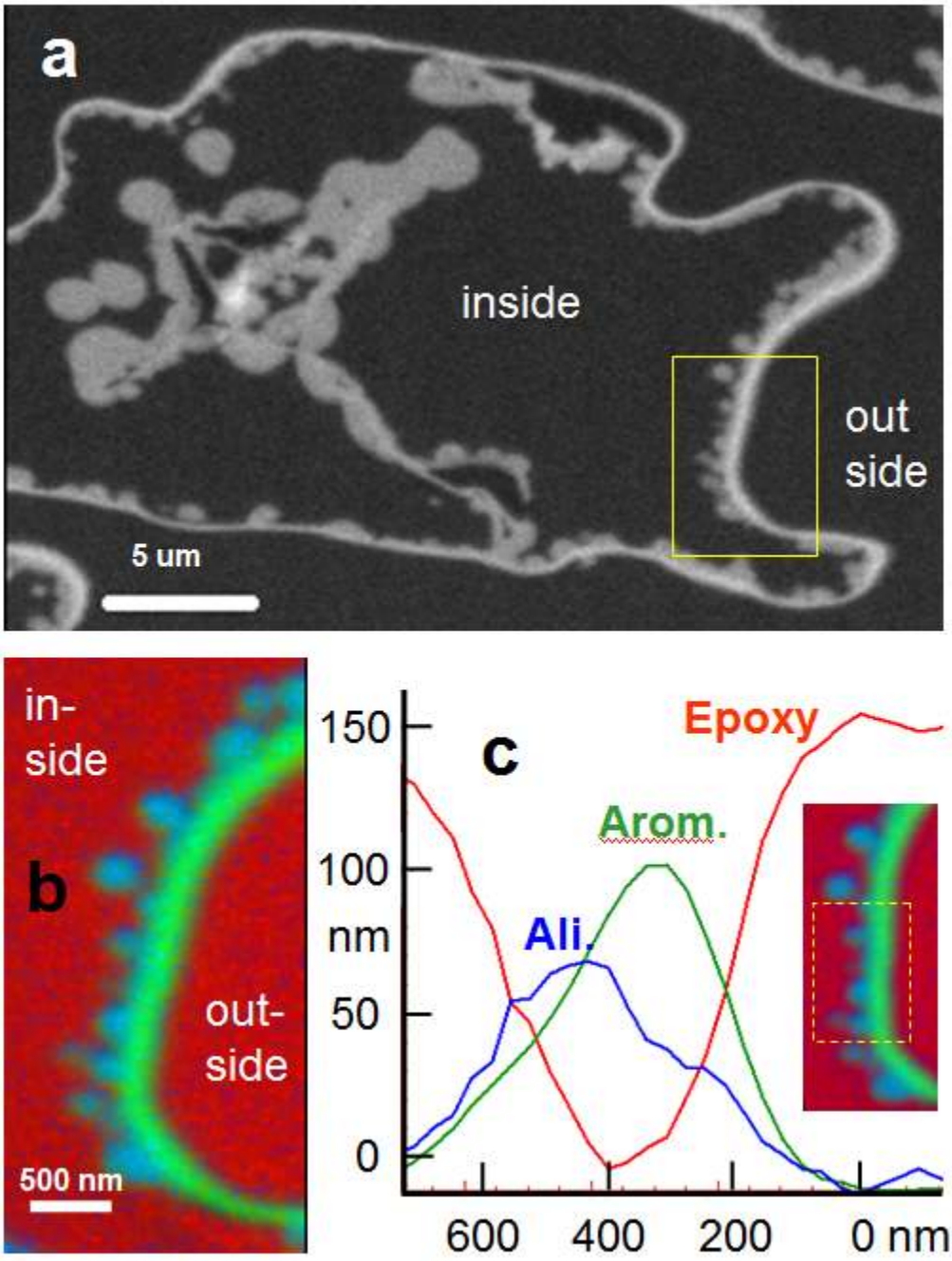

Figure 2.5 Chemical mapping of PID capsule wall prepared at room temperature: (a) STXM image taken at 285.2 eV; (b) chemical mapping the wall of PID capsule; (c) plot of averaged component profiles across the component maps.

The STXM image taken at 285.2 eV (Figure 2.5a) shows an overall image of a capsule embedded in epoxy. Typical for such capsules, the outside surface templated by the oil−water interface is much smoother than the inside surface. The color-coded compositional map is shown in Figure 2.5b while component across-wall profiles are shown in Figure 2.5c. The latter were obtained by rotating the component maps and summing multiple horizontal line profiles (yellow box in the inset to Figure 2.5c) to improve statistics. This analysis confirms that the outer layers are rich in aromatic polyurea while the inner bulbous features are deposits or growths that are rich in aliphatic polyurea. These aliphatic bulbs may reflect the presence of pores in the aromatic outer shell that admit amine. The large aggregates seen in the center of the capsule in Figure 2.5a are attributed to aggregates of mainly aliphatic polyurea formed in the interior of the capsule. The wall segment studied shows comparable levels of aromatic and aliphatic polyurea being produced at this stage of the encapsulation.

To try to further enhance the conversion of IPDI in these **PID** capsules, we used a two-stage thermal profile consisting of 24 h at room temperature followed by another 24 h at 70 °C (Figure 2.6a). This polymerization protocol had been shown earlier to lead to two-layer walls.[16]

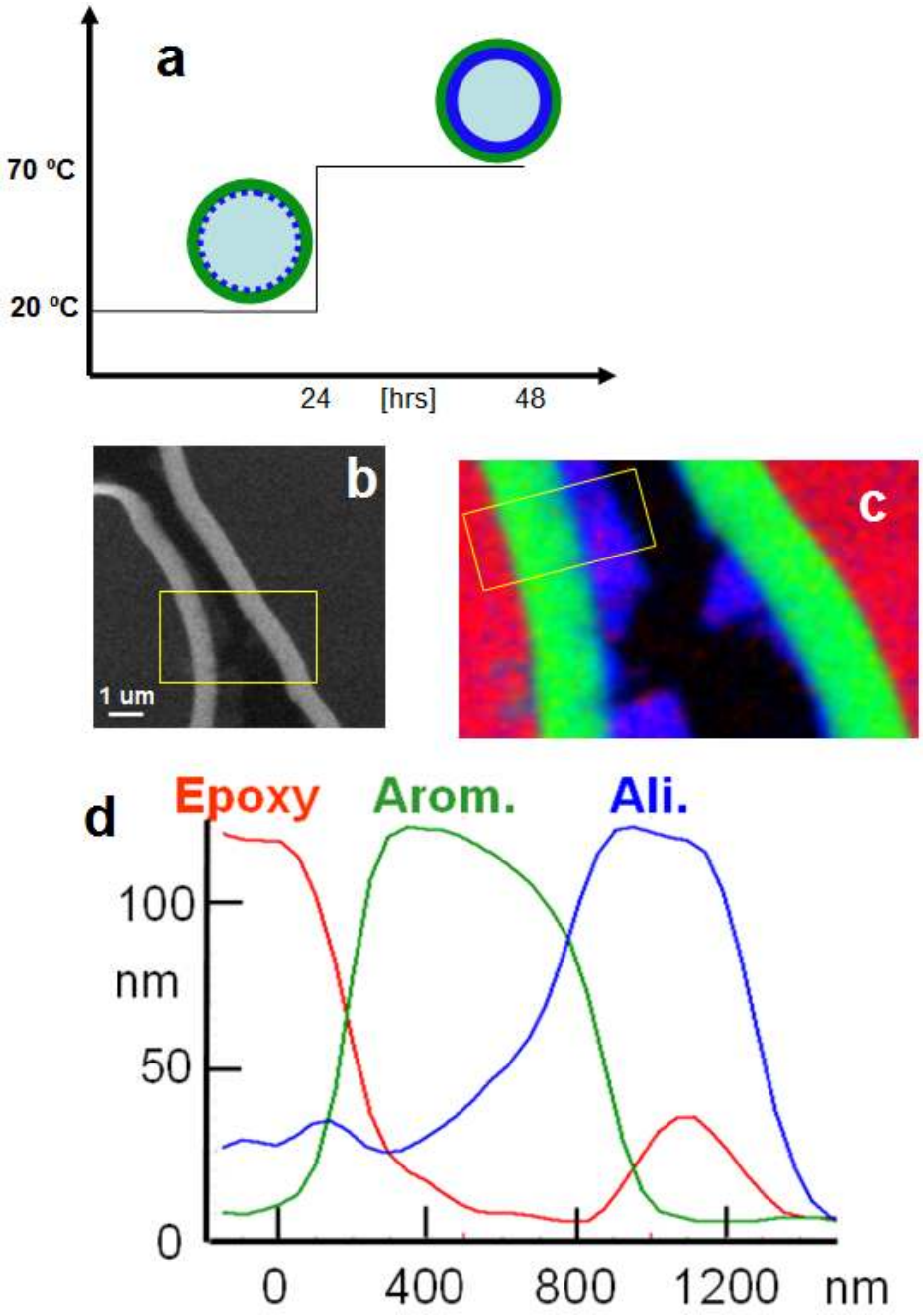

Figure 2.6 Chemical mapping of PID capsule wall prepared using the two-stage temperature process: (a) STXM image taken at 285.2 eV; (b) chemical mapping the wall of PID capsule; (c) plot of averaged profiles across the component maps.

The high conversion of aliphatic isocyanate in that case indicated that the aromatic polyurea formed at room temperature during the first 24 h is more permeable, allowing continued diffusion of DETA into the reaction zone. The subsequent temperature increase to 70 °C should also facilitate diffusion of DETA through the capsule wall and ensure high conversion of the less reactive isocyanate, IPDI. Figure 2.6b shows a STXM image taken at 285.2 eV, at the end of the 48 h reaction. At this energy only the aromatic polyurea is seen since it is the only species with significant absorption (see Figure 2.3). The STXM compositional maps and across-wall profiles (Figure 2.6c and 2.6d) for the **PID** system prepared by this two-stage polymerization confirm the overall aromatic/aliphatic wall gradient, indicating a moving boundary mechanism. The wall segment studied shows high conversion of IPDI, comparable to that of PMPPI, suggesting that the aromatic polyurea walls formed at room temperature are less dense and permit subsequent aliphatic polyurea wall growth.

Both at 25 and 50 °C, all **PID** capsules show compositional gradients across the capsule walls, which indicates that the overall wall formation mechanism does not change over this temperature regime. Changing the temperature does appear to change the density of the initially formed aromatic polyurea capsule wall, which affects the subsequent rate of growth of aliphatic polyurea capsule wall.

2.3.2 Non-cross-linked Polyurea Microcapsule System

To explore the effect of different levels of cross-linking on the wall structure and on the wall formation mechanism, we studied **MHH** capsules composed of MDI + HMDI//HMDA, both using the two-stage temperature process, and at constant 50 °C. Both processes produce **MHH** capsules with very porous walls (Figures 2.7 and 2.8) and without large-scale aromatic/aliphatic compositional gradients across the walls. In both cases aromatic and aliphatic polyurea densities decrease in parallel from the outer to the inner wall surface, suggesting formation of an interpenetrating network (IPN) structure. This is attributed to wall growth according to the stationary boundary mechanism, where the HMDA keeps diffusing into the organic phase to react with MDI and HMDI subsequently in a broad but static reaction zone. From wall segment studies we also observed that the **MHH** capsules formed with the two-stage temperature process show a higher aromatic to aliphatic ratio compared to that of **MHH** capsules made from constant 50 °C. We again attribute this difference to the formation of a denser polyurea skin at 50 °C which slows the diffusion of HMDA and affects conversion of especially HMDI.

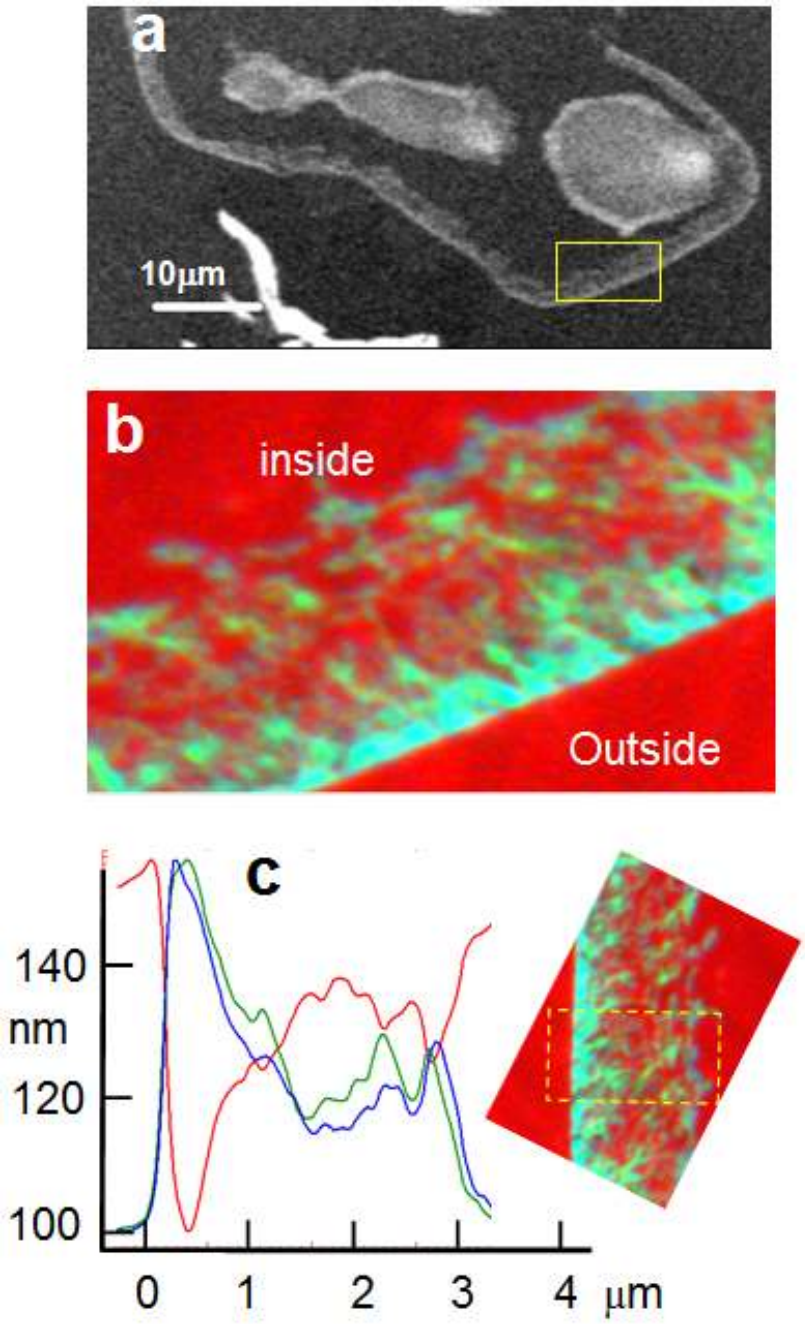

Figure 2.7 Chemical mapping of MHH capsule wall prepared using the two-stage temperature process: (a) STXM image taken at 285.2 eV; (b) chemical mapping the MHH capsule wall; (c) plot of averaged profiles across the component maps.

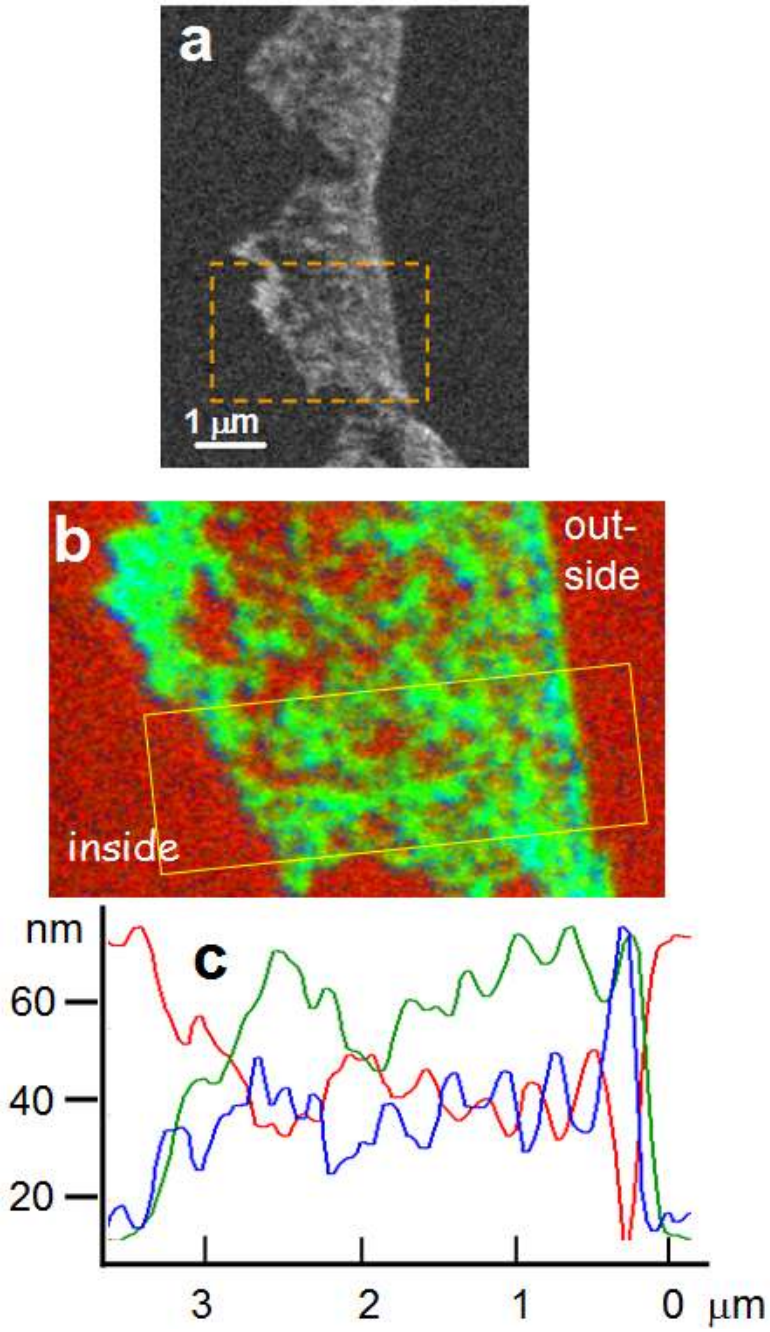

Figure 2.8 Chemical mapping of MHH capsule wall made from constant temperature of 50 °C: (a) STXM image taken at 285.2 eV; (b) chemical mapping the wall of MHH capsule; (c) plot of averaged profiles across the component maps.

Comparison of these two systems indicates that the capsule wall formation can change dramatically with the cross-linking ability and the polarity of the monomers used. Changing the temperature does not fundamentally change the wall formation mechanism but affects the densities of the capsule walls. Dense capsule walls would limit the diffusion of either isocyanates or polyamines, leading to lower conversion of the less reactive isocyanates. Similarly, wall density would affect release of the active fill material.

2.4 Conclusions

Capsule wall morphologies and growth mechanisms in polyurea capsules prepared using mixtures of isocyanates have been studied by STXM. Highly cross-linked, dense PMPPI + IPDI//DETA (**PID**) capsules are shown to grow by the moving boundary mechanism, while their less cross-linked and less dense MDI + HMDI//HMDA (**MHH**) analogues are shown to grow by a stationary boundary process. This approach of studying interfacial polymerization is not limited to polyurea capsules but may be useful in mechanistic studies of other interfacial systems.

This information can help guide the design of new capsules, depending on release and strength properties required. Capsule walls formed from highly cross-linking monomers, resulting in moving boundary mechanism, would tend to result in slowly releasing walls. If higher mechanical wall strength is required for such capsules, one answer could be to use a combination of highly cross-linking aromatic isocyanates to form the release-controlling outer skin by the moving boundary mechanism, with less

reactive and aliphatic isocyanates to form a permeable inner support membrane by the stationary boundary mechanism.

2.5 References

[1] (a) Ramarao, C.; Ley, S. V.; Smith, S. C.; Shirley, I. M.; DeAlmeida, N. *Chemical Communications* **2002**, 1132-1133. (b) Price, K. E.; Mason, B. P.; Bogdan, A. R.; Broadwater, S. J.; Steinbacher, J. L.; McQuade, D. T. *Journal of the American Chemical Society* **2006**, *128*, 10376-10377.

[2] (a) Comiskey, B.; Albert, J. D.; Yoshizawa, H.; Jacobson, J. *Nature* **1998**, *394*, 253-255.(b) Yoshizawa, H. *KONA* **2004**, *22*, 23

[3] Scher, H. B.; Van Koppenhagen, J. E.; Shirley, I. M.; Follows, R.; Wade, P.; Earley, F. G. P.; Shirley, D. B. *WO 2001019509 A1*.

[4] Van Koppenhagen, J. E.; Scher, H. B.; Lee, K.-S.; Shirley, I. M.; Wade, P.; Follows, R. *WO 0005952*, **2000**.

[5] Van Koppenhagen, J. E.; Scher, H. B.; Lee, K.-S.; Lee, C. C.; Shirley, I. M.; Wade, P.; Follows, R. *US Patent 2002037306 A1*.

[6] Stadelhofer, J. W.; Zellerhoff, R. B. *Chemistry & Industry* **1989**, 208-211.

[7] (a) Pearson, R. G.; Williams, E. L. J. Polym. Sci., Polym. Chem. Ed. **1985**, 23, 19. (b) Sirdesai, M.; Khilar, K. C. *Canadian Journal of Chemical Engineering* **1988**, *66*, 509-513. (c) Yadav, S. K.; Suresh, A. K.; Khilar, K. C. *Aiche Journal* **1990**, *36*, 431-438. (d) Janssen, L.; Tenijenhuis, K. *Journal of Membrane Science* **1992**, *65*, 59-68. (e) Yadav, S.

K.; Khilar, K. C.; Suresh, A. K. *Aiche Journal* **1996**, *42*, 2616-2626. (f) Kubo, M.; Harada, Y.; Kawakatsu, T.; Yonemoto, T. *Journal of Chemical Engineering of Japan* **2001**, *34*, 1506-1515.

[8] Jabbari, E. *Journal of Microencapsulation* **2001**, *18*, 801-809.

[9] Croll, L. M.; Morin, C.; Koprinarov, I.; Hitchcock, A. P.; Stöver, H. D. H. *Journal De Physique Iv* **2003**, *104*, 507-507.

[10] 10. (a) Hong, K.; Park, S. *Materials Science and Engineering a-Structural Materials Properties Microstructure and Processing* **1999**, *272*, 418-421. (b) Sultan, W.; Busnel, J. P. *Journal of Thermal Analysis and Calorimetry* **2006**, *83*, 355-359.

[11] Sato, M. J. Org. Chem. **1962**, 27, 819

[12] Kuck, M.; Balle, G.; Slawyk, W. *Analyst* **1999**, *124*, 933-939.

[13] Stohr, J. NEXAFS Spectroscopy; Springer Tracts in Surface Science 25; Springer: Berlin, **1992**.

[14] (a) Croll, L. M.; Stöver, H. D. H.; Hitchcock, A. P. *Macromolecules* **2005**, *38*, 2903-2910. (b) Hitchcock, A. P.; Morin, C.; Zhang, X. R.; Araki, T.; Dynes, J.; Stöver, H.; Brash, J.; Lawrence, J. R.; Leppard, G. G. *Journal of Electron Spectroscopy and Related Phenomena* **2005**, *144*, 259-269. (c) Hitchcock, A. P.; Stöver, H. D. H.; Croll, L. M.; Childs, R. F. *Australian Journal of Chemistry* **2005**, *58*, 423-432.

[15] aXis2000 is written in Interactive Data Language (IDL). It is available free for non-commercial use from http://unicorn.mcmaster.ca/aXis2000.html.

[16] Hitchcock, A. P.; Li, J.; Reijerkerk, S. R.; Foley, P.; Stöver, H. D. H.; Shirley, I. *Journal of Electron Spectroscopy and Related Phenomena* **2007**, *156*, 467-471.

Chapter 3 - Probing Wall Chemistries of Base-triggerable Aminoplast Microcapsules via Scanning Transmission X-ray Microscopy

3.1 Introduction

Microcapsules (MCs) are important microcontainers used for making carbonless copy papers[1], delivering agrochemicals[2], protecting sensitive food ingredients[3] and encapsulating phase change materials[4]. Characterization of MC structure and chemistry is becoming increasingly important in this field as it embraces a wider range of fills, increasingly sophisticated wall compositions and active release mechanisms involving a range of chemical reactions. Traditional analytical techniques used for MC characterization include NMR[5], FTIR[6], AFM[7], electron microscopy (EM)[8] and optical microscopy, which can provide information about composition and morphology of MCs. Unfortunately, compositional information of MCs with sub-micron spatial resolution, which is key to understanding both microencapsulation processes and the structure-property correlation of MCs, has been difficult to access using traditional techniques due to either poor spatial resolution or insufficient chemical sensitivity.

Scanning transmission X-ray microscopy (STXM) is a synchrotron based spectromicroscopy technique combining good chemical sensitivity and spatial resolution.[9] STXM relies on near edge X-ray absorption fine structure (NEXAFS) spectra for

chemical speciation, and achieves high spatial resolution by focusing the energy-resolved X-ray beam through precisely fabricated zone-plates onto 20 – 30 nm diameter focal points through which the thin samples can be scanned.[10] STXM has become a mature technique that is capable of analysing composite materials on a sub-micron scale,[11] making it an ideal tool for MC studies.

Tzvetkov et al. used STXM to study phase change MCs[12] and air-filled poly(vinyl alcohol) microbubbles[13] in aqueous suspensions that were sandwiched between two Si_3N_4 windows. In both cases, the prolonged irradiation with soft X-rays resulted in morphological and compositional changes of these MCs, which were characterized using NEXAFS spectra. However, Tzvetkov's approach was limited to imaging the shape of MCs, and obtaining composite NEXAFS spectra of MC wall and core materials. Detailed studies on the morphology and composition of MC walls were not attempted, though such information is of great importance for understanding microencapsulation process and MC properties.

We recently developed methods to investigate MC cross-sections in order to study both MC wall morphology and composition in greater detail using STXM.[14] These studies have given insights on wall morphology[15], composition distribution in the radial direction[16] and wall formation mechanisms[17], which have advanced our understanding of MCs and microencapsulation processes. To measure MC cross-sections by STXM, MCs need to be embedded in a polymer matrix and microtomed to yield ~100 nm thin sections. Wall cross-sections of composite polyurea MCs[15,17,18] and sodium acrylate- and N-vinylpyrrolidone-enhanced alginate MCs[16] have been studied by us using this method. In

this paper, the same approach is applied to investigate the wall cross-sections of base-triggerable aminoplast MCs[19] that were developed by Syngenta for pesticide delivery. Base-triggerable MCs are useful for releasing pesticides selectively within the alkaline intestinal tract of certain insect pests. With these MCs, only pests that feed on MCs containing pesticides will be affected, reducing the pesticides' impact on beneficial insects.

The chemistry of forming these base-triggerable aminoplast MC walls is illustrated in Scheme 3.1. The wall is believed to form by a condensation reaction between an aminoplast resin (U80 component) and pentaerythritol tetrakis(3-mercaptopropionate) (thioester component) with the loss of water and butanol, catalyzed by sulfuric acid. U80 is a highly butylated urea formaldehyde prepolymer, soluble in many organic solvents and with a lower tendency for self-condensation compared to methylated analogs.[20] Co-condensation of U80 and thioester hence leads to cross-linking and phase separation to form cross-linked MC walls. The microencapsulation process is carried out in aqueous emulsion where the two wall formers, U80 and thioester, reside in the dispersed organic phase with the active ingredients. After forming an oil-in-water emulsion, sulfuric acid is added and the temperature is raised to 55 ˚C to induce the reaction. It was believed that the microencapsulation followed an interfacial polycondensation mechanism in which the condensation of U80 and thioester was restricted to the oil side of oil-water interface, limited by the slow diffusion of protons into the oil phase.

The ester groups in the thioester are labile under alkaline conditions. Hydrolysis of these ester groups may happen at high pHs, resulting in degradation of the MC wall

and enhanced out-diffusion of core materials. The release behaviors of these MCs have been studied by Dale and Unwin[21] who found that fast release could be triggered at pHs of 9.7 and 10.05 with rates that were dependent on both pH and capsule size, exhibiting sensitivity of the MC walls to pH changes.

This paper aims to use STXM as the major tool to study the wall cross-sections of these base-triggerable aminoplast MCs in order to understand the morphologies of MC walls, to gain insights on the microencapsulation process and to evaluate the composition variations imposed by pH changes.

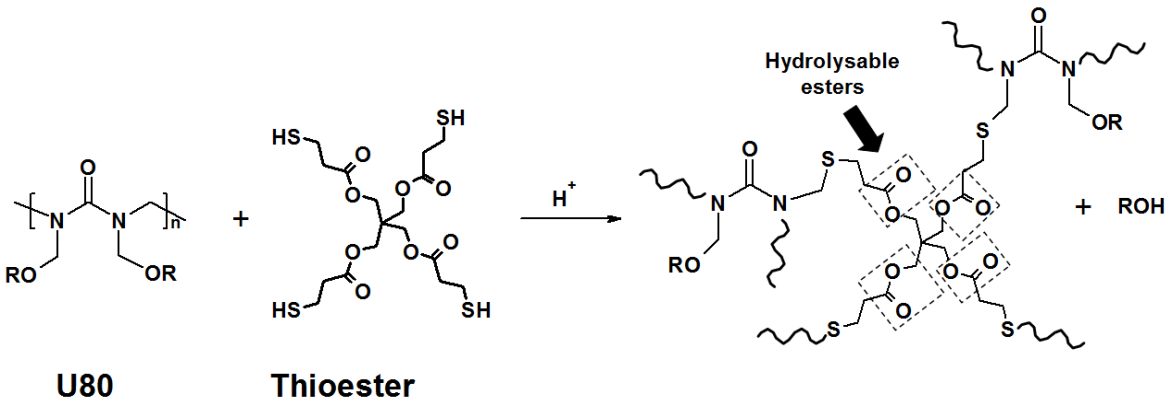

Scheme 3.1 Condensation reaction between U80 and pentaerythritol tetrakis(3-mercaptopropionate) (thioester) to form a cross-linked network. R is mostly a butyl group with some methyl and hydrogen.

3.2 Experimental Section

3.2.1 Materials

Styrene, tetrahydroforan (THF),dimethylformamide (DMF), rhodamine 6G, pentaerythritol tetrakis(3-mercaptopropionate) were purchased from Aldrich and were used as received. azobisisobutyronitrile (AIBN) is a product of Bayer, U80 resin is a gift from Cytec Industries. Both native (unhydrolyzed) MCs and hydrolyzed MCs were provided by Syngenta.

3.2.2 Methods

Microcapsule Treatments

MC hydrolysis involved treating native MCs with KOH at pH 12.4 for 48 hours to afford potassium hydrolyzed (PH) MCs. Ammonia hydrolyzed (AH) MCs were prepared by first hydrolyzing native MCs in a 25 wt% NH_4OH solution at pH 11.9 for 48 hours and then replacing ammonium ion with calcium by exposing the hydrolyzed MCs to a $CaCl_2$ solution. Centrifugation and washing with 50 mL DI water were performed for three times to ensure complete removal of unbound ions in the hydrolyzed MC suspensions.

Microcapsule Embedding and Wall Section Preparation

MCs were filtered and dried in air to afford powders that were then manually crushed between glass slides. Crushed MCs were washed three times using 150 mL THF on a filter paper and then dried in a vacuum oven at room temperature for 24 hours. A small amount of dried MC fragments was transferred into a BEEM® embedding mold, which was then filled with a styrene solution containing 1.18 wt% AIBN. The mold was

then sealed and placed in a 70 ° C oven for 24 hours to cure. Thin sections of the resulting PS embedding blocks were cut with a Leica Ultracut UCT ultramicrotome, and picked up onto Formvar-coated Cu TEM grids.

Fluorescence Dye Labelling

MCs were first treated with 0.1 M EDTA for 10 min and then washed on a filter paper using 50 mL DI water five times. A 0.5 mL 0.23 wt% Rhodamine 6G aqueous solution was added to a 10 mL MC suspension and the resulting suspension was gently rotated (30 rpm) for 10 min. Sufficient DI water was then used to wash the rhodamine 6G coated MCs until a rhodamine-free supernatant was obtained (verified by UV/Vis spectrometry).

Determination of Potassium and Calcium in the Micricapsule Walls

2 mL MC suspension was filtered using filter paper and the MCs dried under vacuum without any further washing. The dried MCs were then crushed and the MC fragments washed three times using 150 mL THF to remove residual fill materials. The resulting wall fragments were dried under vacuum for about 24 hours at room temperature. 10% nitric acid was used to rinse 30 mL screw cap glass vials that were used to contain sample solutions. 30 mg dry MC fragments were weighed into each vial. 10 mL 10% nitric acid was added to each vial and the resulting suspensions were shaken on a multi-wrist shaker for 20 min at setting 10. After filtration through a filter paper, filtrates were measured by atomic absorption spectrometry at the McMaster Occupational and Environmental Health Laboratory.

STXM Measurements and Data Analyses

The reference spectra acquisition, the C 1s absorption edge studies on native MC walls and the Ca 2p and K 2p absorption edge investigations on all MC walls were carried out at the Advanced Light Source (ALS, Berkeley, CA, USA) using the STXM microscope[22] at beamline 5.3.2[23]. The C 1s spectromicroscopy studies were performed on three different MCs: native MCs, native MCs hydrolysed using 1M potassium hydroxide (PH MCs) and native MCs hydrolyzed using ammonium hydroxide (AH MCs). The PH and AH MCs were performed on the STXM at BL 10ID1, the soft X-ray spectromicroscopy (SM) beamline of the Canadian Light Source (CLS, Saskatoon, Canada). Image sequences (stacks) were measured in transmission mode by recording images of suitable sample areas at a series of X-ray energies. The transmission signals were then converted into optical densities [absorbance, OD = -ln (I/I_0)] using incident flux (I_0) measured through open areas devoid of film samples. The processing and analyses of image stacks including alignment of image stacks, extraction of NEXAFS spectra, components mapping, line profile plotting, etc. were carried out using aXis2000[24].

Instruments

The optical and fluorescence micrographs of MCs were obtained using an Olympus BX51 optical microscope fitted with a Q-Imaging Retiga EXi digital camera, ImagePro software and fluorescence optics for fluorescein. The atomic absorption of MC samples were measured on a Perkin Elmer 5100 Atomic Absorption Spectrophotometer with a quoted accuracy at detection limits of 3-5% for K and Ca. UV measurements were carried out on a Cary 50 UV/Vis spectrophotometer.

3.3 Results and Discussion

3.3.1 Studies on Native Aminoplast Microcapsules

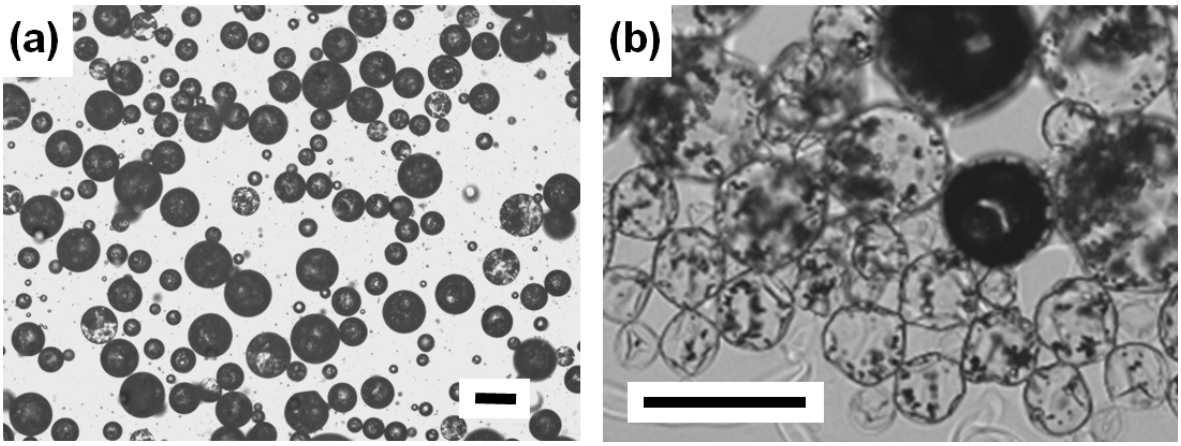

Figure 3.1 Optical micrographs of native aminoplast microcapsules in a (a) water suspension (reflection mode) and (b) DMF suspensions (transmission mode). The scale bars are 100 μm.

Figure 3.1a shows a typical optical micrograph of native (unhydrolyzed) aminoplast MCs in an aqueous suspension. These MCs appear to be spherical with some indentations on the surface. These MCs are mechanically strong and can survive dehydration on a microscope slide without rupturing. Dried MCs were treated with DMF that swelled the MC walls. As seen in Figure 3.1b, the swelling makes the MC walls transparent and the MC internal structure can now be seen by optical microscopy in transmission mode. This reveals the presence of small particles within the interior of the MCs. The morphology and chemical composition of these internal structures needed to be elucidated, which would provide useful information about the microencapsulation process

and capsule wall formation mechanism. It is noted that there is no apparent difference between native and hydrolyzed aminoplast MCs by optical microscopy.

To study the wall cross-sections of these MCs, it is necessary to embed them in a polymer matrix that can be microtomed to produce thin sections. Epoxy based materials have been generally used as embedding matrix for studying MC wall morphologies and properties. We reported on several occasions[17, 25] use of an epoxy system consisting of trimethylolpropane triglycidyl ether (TTE) and 4,4'-methylenebis(2-methylcyclohexylamine) (MBMCA) to embed MC samples for STXM measurements, as it shows low radiation damage by STXM. In this study, the TTE/MBMCA combination was not chosen due to its potential reactivity with the wall materials and due to its lack of distinctive spectroscopic features. We turned to a more inert embedding process that involves an in-*situ* radical polymerization of styrene at 70 ° C in the presence of MC fragments. Polystyrene (PS) has been used previously as an embedding material[26] due to its good cutting properties and resistance to radiation damage.[27] Radical polymerization of styrene is believed to be compatible with the functional groups in the aminoplast MC walls and PS, has a characteristic peak at 285.2 eV in its C1s NEXAFS spectrum, making it easily distinguishable from the wall materials. Being a small molecule with an intermediate polarity and low viscosity, styrene can partially penetrate into MC walls. Therefore, curing of styrene can render good adhesion between MC walls and the embedding matrix, which benefits subsequent microtoming to make nice sections.

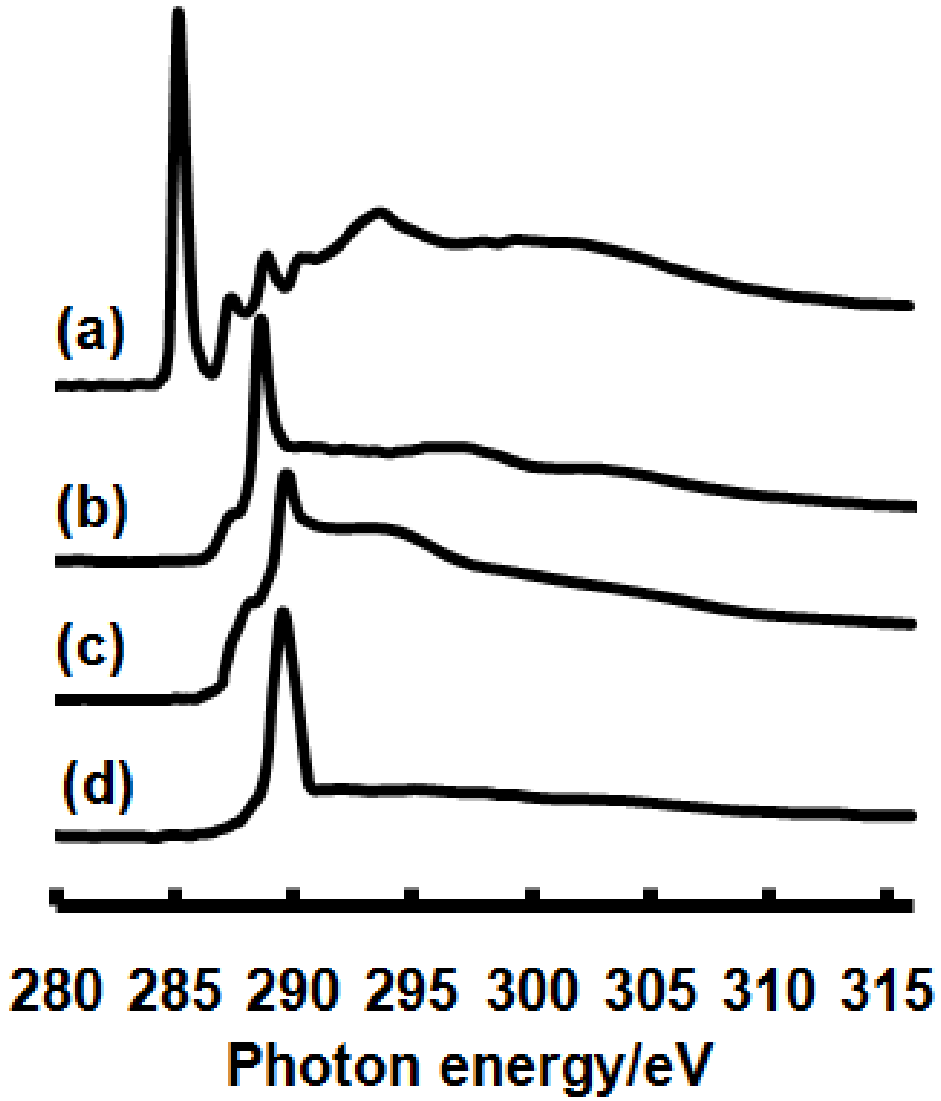

Figure 3. 2 Reference NEXAFS spectra of (a) PS, (b) thioester, (c) U80 and (d) U80F

STXM is an X-ray absorption spectroscopy based microscope technique with sub-micron resolution, which relies on near edge X-ray absorption fine structure (NEXAFS) spectra of reference materials to quantify the composition. In order to understand the composition of MC walls, it is essential to have accurate reference spectra of wall formers. The reference NEXAFS spectra of U80 and thioester were measured by

sandwiching a small amount each sample between two X-ray transparent Si_3N_4 windows and the spectra were recorded by measuring the transmitted signals through sample areas over X-ray energies ranging from 280 - 316 eV with selected energy steps. The NEXAFS spectrum of embedding PS was measured from the microtomed sample sections in areas free from any MC walls. As shown in Figure 3.2, the NEXAFS spectrum of U80 shows a distinctive peak at 289.5 eV, corresponding to the C1s$\rightarrow\pi_{C=O}$* transition of urea groups in U80. For thioester, there is a strong absorption at 288.6 eV, due to the C1s$\rightarrow\pi_{C=O}$* of the ester group. Since these characteristic peaks for U80 and thioester are 0.9 eV apart, STXM instruments with ~0.1 eV energy resolution can easily distinguish between these two components in MC walls. The major absorption of PS at 285.2 eV is far from those of U80 and thioester, ensuring minimum interference of PS with the wall components in STXM analyses.

Figure 3.3a and 3.3b show STXM optical density images of cross-sections of native aminoplast MC walls, taken at 285.2 eV where PS has strongest absorption. In both images, PS appears to be off-white while other materials are dark due to their low absorption at this energy. In contrast, a magnified image of the MC wall recorded at 289.5 eV (Figure 3.4c), where the urea groups in U80 have the most absorption, shows highlighted MC walls in white. It is evident from these images that there exist some small internal MCs inside the primary MCs. In Figure 3.3c, there are some small bright areas, indicating more absorption. We believe those are thick sample areas caused by folding of the film during sample preparation. Both primary and internal MCs show dense and

relatively uniform walls. For primary MCs, there is an equal intensity of PS inside and outside the MCs. This is because these primary MCs were ruptured by grinding before embedding, which allowed styrene to reach both sides of the MC walls. Compared to primary MCs, many internal MCs preserve a hollow interior with much higher shell-to-core volume ratios. It appears that these internal MCs largely survived grinding due to their much smaller capsule sizes and their relatively thick walls, which prevented penetration of styrene during embedding. By sequentially recording images in the same sample area using different photon energies, an image stack was obtained that was subject to a series of analyses to retrieve compositional information about the native MC walls. First, the spectra of the primary and internal MC walls were extracted from designated areas shown in Figure 3.3c. Both spectra show similar features. The peak at 285.2 eV is assigned to the embedding PS, suggesting styrene penetrated both walls to some extent and polymerized in situ during embedding to render PS formation in the walls. The fact that the walls of both primary and internal MCs have similar spectra indicates they have similar chemical composition and were formed by the condensation reaction between thioester and U80 during the microencapsulation process.

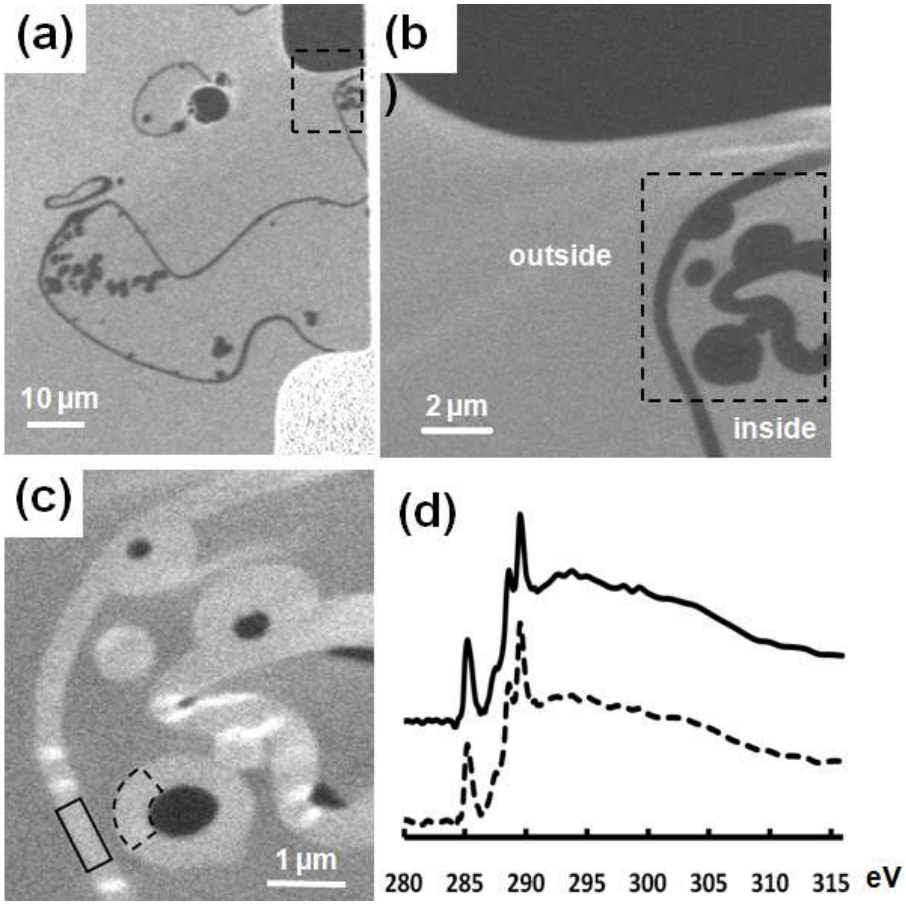

Figure 3.3 STXM optical density images of the wall cross-sections of native microcapsules taken at 285.2 eV. (b) is an enlarged STXM optical density image measured in the boxed area in (a); (c) is an enlarged STXM optical density image of the boxed area in (b) and was recorded at 289.5 eV; (d) shows the extracted NEXAFS spectra of both primary (solid line) and internal (dashed line) microcapsule walls from the boxed areas in (c).

It has been suggested in the literature that the formation of aminoplast MCs generally follows an interfacial polycondensation mechanism where the condensation of

wall forming material is restricted to the oil-water interface.[28] MCs formed by interfacial polycondensation normally show asymmetrical wall morphology with a two-layer structure. The outer wall is usually tight and its formation is templated by the oil-water interface with a fast reaction. The underlying layer is often porous, caused by the slow diffusion of the aqueous reactant or catalyst across the interface and into the oil phase. This porous layer is thus called a diffusion layer. However, the aminoplast MCs in this study show dense and uniform wall cross sections with no indication of a diffusion layer, for both primary and internal MCs. This one layer wall morphology implies that the wall formation may follow another mechanism rather than a classical interfacial polycondensation. Meanwhile, the formation of internal MCs that have similar wall composition to the primary MCs is also incongruent with an acid-catalyzed interfacial polycondensation mechanism. It is reasonable to assume that the internal MCs are templated by internal water-in-oil-in-water (w/o/w) emulsions formed during the emulsification stage. At this emulsification stage, both continuous and dispersed aqueous phases should be about neutral in pH as no sulfuric acid had been added. The subsequent addition of sulfuric acid to the continuous aqueous phase instantly decreased the external pH, while the pH of the dispersed aqueous phase should remain neutral and unaffected because it was isolated from the continuous aqueous phase by the intermediate oil phase, Therefore, an interfacial polycondensation mechanism can not account for the formation of internal MCs due to the fact there was likely no acid catalyst present in the dispersed aqueous phase to facilitate the condensation between U80 and thioester. We thus speculate that most of the condensation reaction happened in the dispersed organic phase

instead of at the interface. In this scenario, U80 was activated by its association with protons at the oil-water interface. Because of the low reaction rate and the relatively hydrophobic nature of U80, the protonated U80 left the interface and diffused to the dispersed phase to react with thioester. Hence the cross-linking and phase separation took place in the dispersed phase and the precipitating polymer then migrates to all available interfaces to form both primary and internal MC walls, driven by interfacial tensions and cohesive forces, shown in Scheme 3.2. The fact that the internal MCs have higher wall-to-core ratios than primary MCs could be explained by the relatively high mobility of the internal MCs, which allowed them to catch more precipitated polymers within the dispersed oil phase. It can be seen in Figure 3.3c that some small internal MCs have fused into each other, which suggests that these internal MCs did not have sufficient colloidal stability due to the lack of surfactants in the dispersed oil phase. As a result, these internal MCs aggregated and fused when the wall forming polymer went through a viscoelastic stage during the microencapsulation process. This polymer phase separation mechanism has accounted for various microencapsulation processes with different inducing methods for polymer phase separation.[29] Most MCs formed via this mechanism tend to have a dense and uniform wall, due to close packing of precipitated polymers driven by a cohesive forces. The formation of aminoplast MCs involving such a polymer phase separation mechanism has not been reported in the literature to the best of our knowledge. The reason for this different mechanistic path is unclear and may involve the polarities of both the aminoplast resin and the cross-linker.

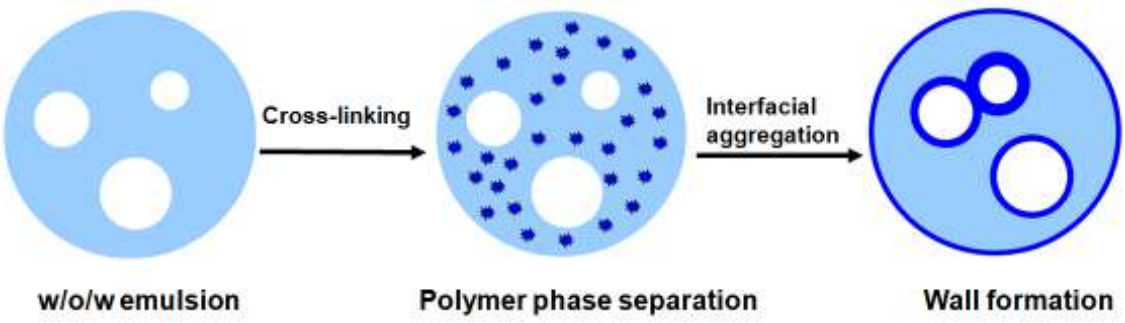

Scheme 3.2 Schematic illustration of the formation of an aminoplast microcapsule by polymer phase separation mechanism

To study the distribution of different components across the MC wall, the image stack was fit with the reference spectrum of each component via singular value decomposition (SVD) to produce component maps. As the PS reference spectrum was extracted directly from the image stack, the mapping for PS in the stack should be accurate. According to the Scheme 3.1, there is a minor structural change for thioester (loss of hydrogens) after the reaction. We believe that this change is small enough that the reference spectrum of the thioester starting material is still valid to represent the spectrum of the thioester component in the MC walls. On the contrary, the structural change for U80 could be significant due to the loss of butanol and thus the reference spectrum of U80 is no longer adequate to map the reacted U80 in the MC walls. This problem can be overcome by adding another reference spectrum of fully reacted U80, termed U80F, whose chemical structure is shown in Scheme 3.3. As a result, U80 with any extent structural change in MC walls can be represented by the average of U80 and U80F and the distribution of U80F in MC walls would indicate the extent of reaction during the microencapsulation process. Due to the unavailability of U80F, we had to construct a

U80F spectrum based on U80. Because U80F has the same urea group as U80 but much fewer atoms in its structure, relative to U80, the spectrum of U80F is expected to have an enhanced urea peak at 289.5 eV. Therefore, the construction of U80F spectrum was done by firstly raising the height of the urea peak of U80 to match the composition of U80F and then normalizing the resulting spectrum by the elemental composition and atomic absorption coefficients of U80F to correct the scale. The constructed reference spectrum for U80F is shown in Figure 3.2d.

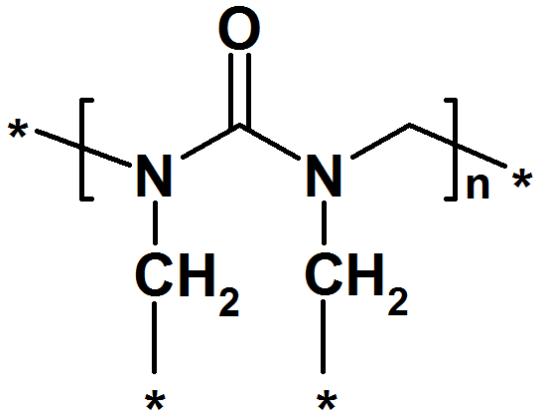

Scheme 3.3 Proposed chemical structure of U80F

The results of the chemical mapping of the image stack using reference spectra of PS, thioester, U80 and U80F are shown in Figure 3.4.

Due to the excellent spectroscopic differentiation between the PS matrix and the aliphatic wall components, mapping the occurrence of PS across the capsule walls should give an indication of the ability of styrene to penetrate the walls. The aliphatic polyurea walls are not expected to be easily swellable by nonpolar styrene, and hence any presence of PS within the walls, presuming the wall sections are in a vertical orientation to the

sectioning plane, would indicate porosity on the nanometer scale conducive to styrene in-penetration.

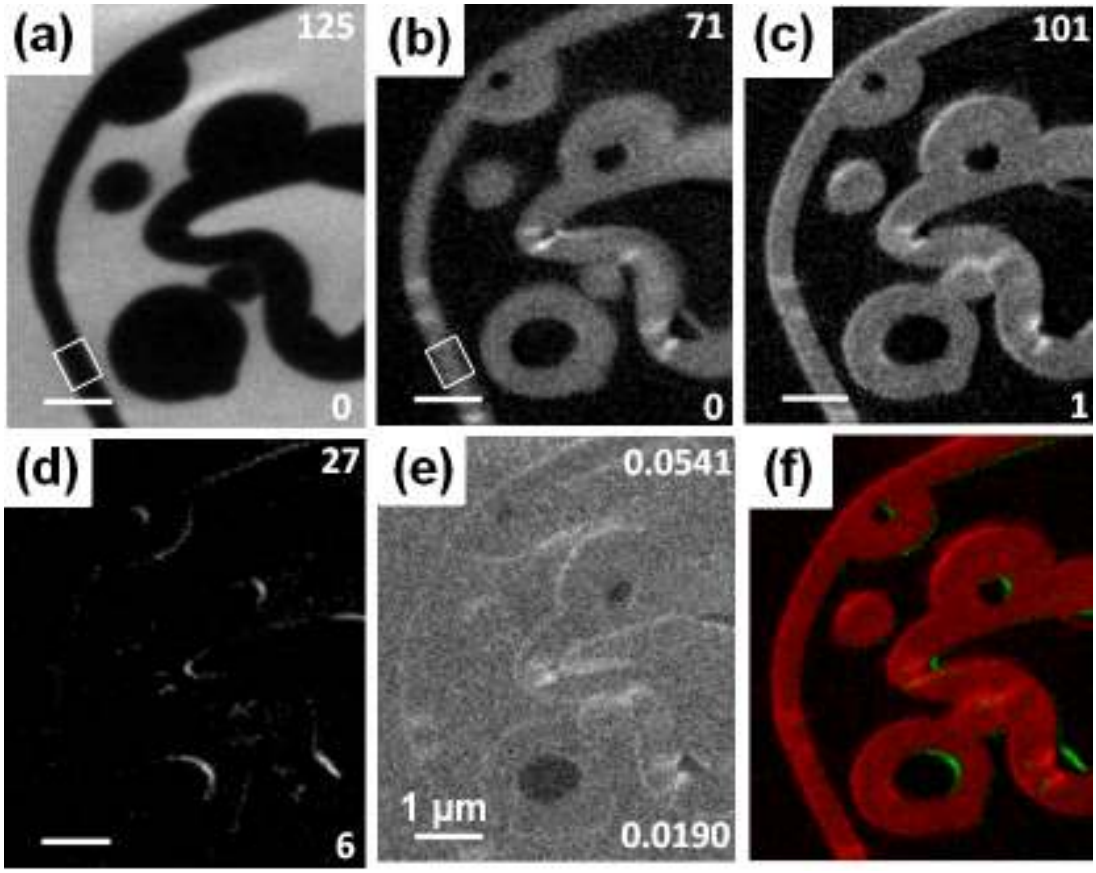

Figure 3.4 Component maps of (a) PS, (b) thioester,(c) U80, (d) U80F and (e) residue in the native microcapsule wall. The numbers on the right corners of each image indicate the range of thickness of each component in a grayscale. (f) is a color-coded composite map of U80 (red) and U80F (green).

The PS profile (Figure 3.5) across the native MC wall was extracted from the boxed area in Figure 3.4a. The width of the wall is defined by the inflection points of the PS profile, which is shown in the dashed box in Figure 3.5. Figure 3.5 shows that the in-

penetration of the walls by styrene is very limited, pointing to a dense, homogeneous wall not swollen by styrene. We did notice however an apparently lower PS content on the outer side of wall section, implying less porosity of the outer wall. However, when the same analysis was applied to other stacks, it was found that, in most cases, lower PS content appeared on the left side of wall sections, irrespective of actual wall alignment. This observation may be due to an off-vertical wall alignment or could be due to a systematic (not necessarily physical) instrument 'drift'. Comparing to the PS profile, no apparent gradient is observed for thioester, shown in the dashed line in Figure 3.5, indicating an even distribution of thioester across the primary MC wall.

The structural change of U80 across the wall was investigated by studying the component maps of U80 and U80F in Figure 3.4. Surprisingly, the fitting program detected weak signals of U80F, most of which are located inside MCs and close to the capsule walls. Since these signals are not in the capsule walls, we believe most of them are false signals and were probably caused by the mis-alignment of the image stack (the stack was carefully aligned but subtle mis-alignments are inevitable). This indicates that there was little structural change of U80 after the reaction, meaning no substantial loss of butyl groups from U80. This finding suggests that no or only a small amount condensation reaction between butoxymethyl groups in U80 and thioester happened during the process, implying its minor role in the wall formation. As a result, we believe that the wall formation is mainly the result of the condensation reaction between the methylol groups in U80 and thioester. This is reasonable because the methylol groups are more reactive than the butoxylmethyl groups in U80 and their condensation reaction with

thioester only produces water, which renders much less structural change of U80. Further reaction between the butoxymethyl groups in the wall with thioesters was possible but seemed not favored probably due to the slow reaction between two phases.

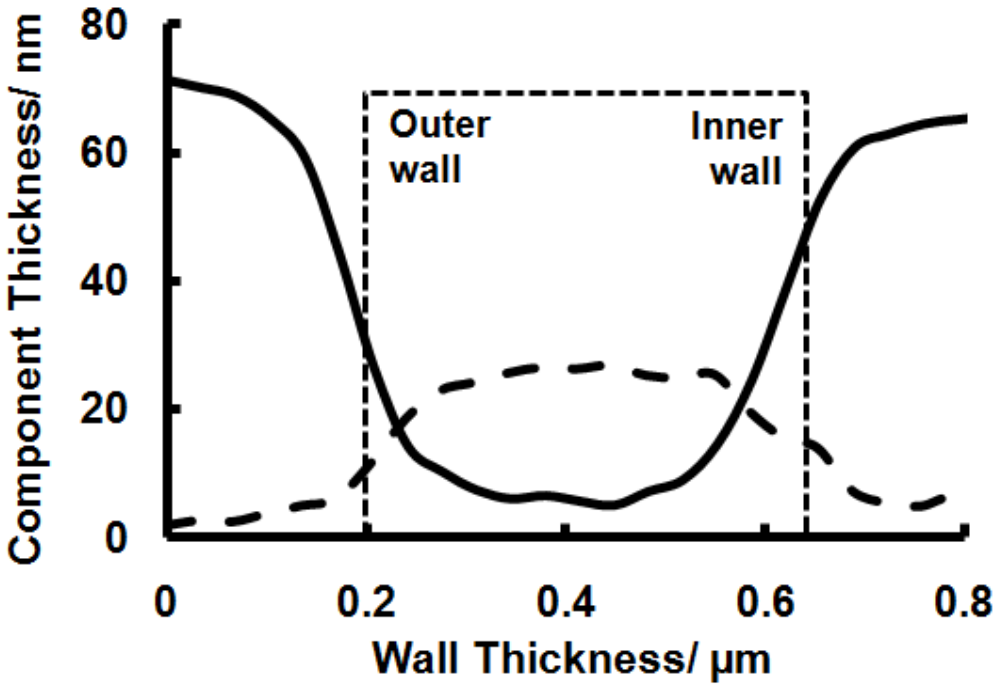

Figure 3.5 Wall profiles of PS (solide line) and thioester (dashed line), extracted from boxed areas in Figure 3.4a and 3.4b, respectively. The dotted box indicates the boundary of the primary microcapsule wall.

3.3.2 Comparing Native and Hydrolyzed Microcapsules

It has been experimentally established that these aminoplast MCs can be partly degraded by raising the pH to give enhanced release rates of the core materials.[19] The hypothesis is that the cross-linker, thioester, can undergo hydrolysis under alkaline

conditions, which increases the porosity of the MC walls and thus their release rates. The hydrolysis of thioester leads to the formation of carboxylate groups in the MC walls. Hence, mapping the loss of thioesters, or appearance of carboxylate following hydrolysis might indicate where and to what extent hydrolysis occurred in the wall.

Several approaches were taken to explore mapping the chemical changes in the MC walls upon hydrolysis. Fluorescence imaging was first used to evaluate the effects of the hydrolysis on these MC walls. Native MCs, native MVs hydrolyzed using potassium hydroxide (PH MCs) and native MCs hydrolyzed using ammonium hydroxide (AH MCs) were treated with an aqueous solution of rhodamine 6G, a cationic fluorescent dye, and then washed with DI water until rhodamine 6G could no longer be detected in the supernatant. It is believed that the positively charged rhodamine 6G can bind electrostatically to any anionic charges in the MC surfaces. Thus the observed intensity of fluorescence signal can qualitatively indicate the relative amounts of carboxylate groups on MC surfaces, inferring the extent of hydrolysis.

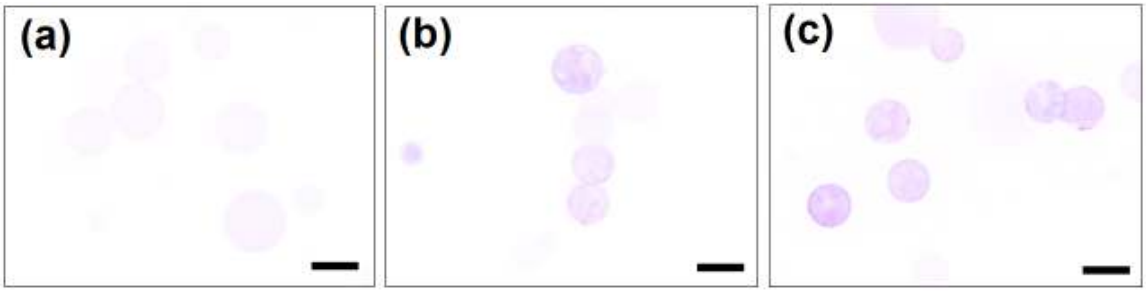

Figure 3.6 Fluorescence micrographs of rhodamine 6G coated (a) native microcapsules, (b) PH microcapsules and (c) AH microcapsules. The scale bars denote 100 μm and the color of the images was inverted to give better contrast.

As shown in Figure 3.6a, the native MCs, after rhodamine 6G treatment, show a very weak fluorescence signal, possibly due to leakage of a small amount of ambient light during image acquisition. Under the same acquisition conditions, both PH and AH MCs give stronger fluorescence signals (Figure 3.6b and 3.6c), suggesting more rhodamine 6G is binding to these MC surfaces. This indicates that hydrolyzed MCs may possess more anionic carboxylate groups on the surface caused by the alkaline hydrolysis. It is noteworthy that the fluorescence signals from AH MCs are slightly stronger than that of PH MCs. This suggests higher extent of hydrolysis of MCs with the more amphiphilic ammonium hydroxide, which is in good agreement with previous findings.[30]

Determination of the distribution of carboxylate groups in both native and hydrolyzed MC walls was also attempted using STXM. It is known that carboxylate groups bind strongly to alkali and alkaline earth cations. These bound metal ions could serve as markers for mapping carboxylate groups using STXM, taking advantage of STXM's good sensitivity and selectivity for some metal ions such as K^+ and Ca^{2+}. K^+ mapping was done using the potassium hydroxide hydrolyzed capsules (PH MCs). Ca^{2+} mapping was carried out using ammonium hydroxide hydrolyzed MCs that were subsequently exposed to calcium chloride, and washed to remove excess calcium. STXM measurements did not show detectible amounts of K^+ and Ca^{2+}. The absence of these metal ions was confirmed by atomic absorption spectrophotometry (Table 3.1). These results indicate that metal ions failed to bind these MCs. It is likely that the extensive water washing after metals loading during sample preparation removed most metal ions, given the relatively weak binding of these ions with carboxylate groups.

Table 3. 1 Quantification of Potassium and Calcium in the Microcapsules by Atomic Absorption Photospectrometry

	K concentration /wt %	Ca concentration /wt %
Native MCs	0.0050	0.0070
PH MCs	0.0076	0.0076
AH MCs	0.0037	0.0270

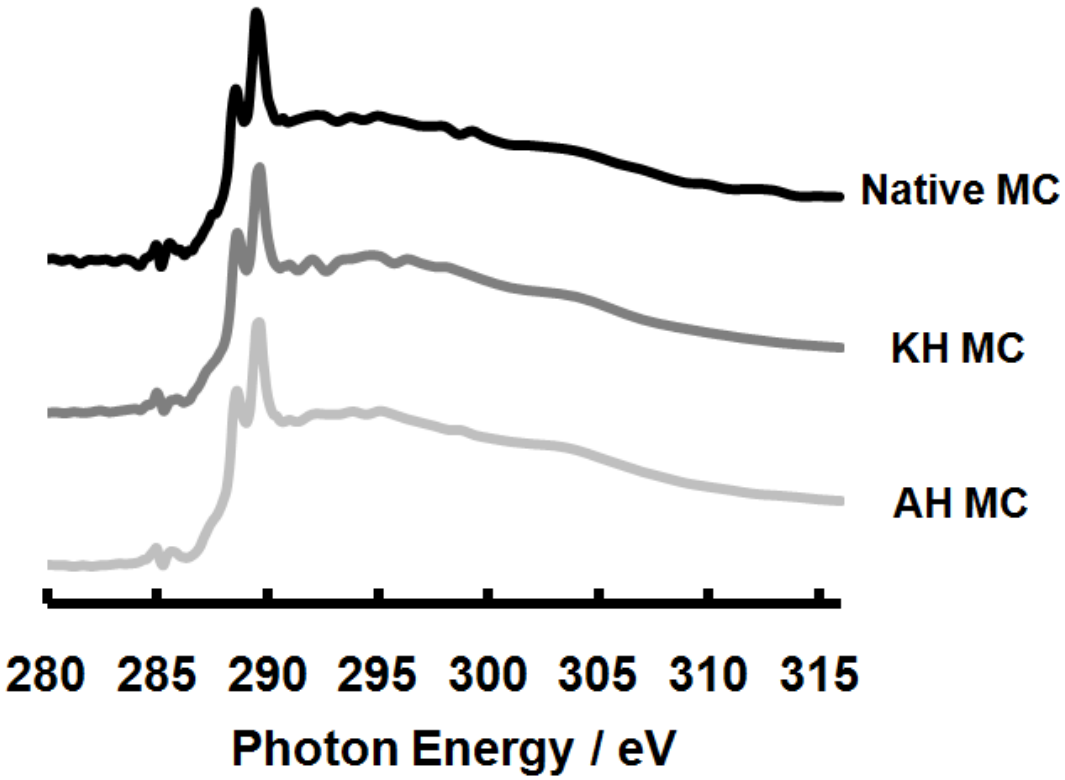

Figure 3.7 Extracted NEXAFS spectra (rescaled) of native microcapsule, PH microcapsule and AH microcapsule walls after PS subtraction

The hydrolyzed MC walls were also studied using C 1s NEXAFS. The wall spectra of both PH and AH MCs were obtained by subtracting the polystyrene contributions from corresponding wall spectra, as described above. The results (Figure 3.7) show that the NEXAFS spectra of hydrolyzed MC walls (both PH and AH) are very similar to that of the native MC walls, showing little impact of the hydrolysis on the overall NEXAFS spectra of MC walls. This spectral similarity is likely due to the similar absorption energies and absorption coefficients of carboxylate and ester carbonyl groups in the NEXAFS spectra.

3.4 Conclusions

The wall chemistry of base-triggerable aminoplast MCs was studied by STXM and other techniques. In *situ* polymerization of styrene was utilized to embed these MCs. This process is advantageous over traditional epoxy embedding due to its good compatibility with the wall functionalities and negligible spectral interference between PS and the other MC wall components. Wall cross-sections obtained by microtoming embedded MCs were examined by STXM. For native MCs, STXM revealed dense and uniform MC walls and confirmed the presence of internal MCs. NEXAFS spectra show that both primary and internal MC walls have the same chemical composition, which suggests that the microencapsulation happened by a polymer phase separation mechanism rather than the interfacial polycondensation that is generally accepted for aminoplast MC formation. To map the possible structural changes of U80 in the microencapsulation

process, a structure of a fully reacted U80 was proposed and its reference spectrum was constructed based on that of U80. The mapping results suggest that there was negligible structural change of U80 in the walls, implying no or a small extent of condensation between butoxymethyl groups in U80 and thioester. This finding led us to believe the condensation of pendant methylol groups in U80 and thioester was primarily responsible for the wall formation.

Fluorescence microscopy studies on both native and hydrolyzed MCs show that hydrolysis indeed happened to generate anionic carboxylate groups on MC surfaces. The attempts to map the distribution of these carboxylates across the walls using STXM were hampered by the weak binding between the metal markers and the carboxylates.

3.5 References

[1] White, M. A. *Journal of Chemical Education* **1998**, *75*, 1119-1120.

[2] Arshady, R. *Microspheres, Microcapsules & Liposomes*, Plenum, New York **1998**.

[3] Desai, K. G. H.; Park, H. J. *Drying Technology* **2005**, *23*, 1361-1394.

[4] Cho, J. S.; Kwon, A.; Cho, C. G. *Colloid and Polymer Science* **2002**, *280*, 260-266.

[5] Torini, L.; Argillier, J. F.; Zydowicz, N. *Macromolecules* **2005**, *38*, 3225-3236.

[6] Zhang, X. X.; Tao, X. M.; Yick, K. L.; Wang, X. C. *Colloid and Polymer Science* **2004**, *282*, 330-336.

[7] Mendelsohn, J. D.; Barrett, C. J.; Chan, V. V.; Pal, A. J.; Mayes, A. M.; Rubner, M. F. *Langmuir* **2000**, *16*, 5017-5023.

[8] (a) Hong, K.; Park, S. *Journal of Materials Science* **1999**, *34*, 3161-3164. (b) E. Jabbari, *Journal of Microencapsulation*, **2001**, *18*(6), 801-809

[9] J. Stöhr, *NEXAFS Spectroscopy* Springer Tracts in Surface Science, 25 (Berlin, **1992**).

[10] Sarkar, S. S.; Solak, H. H.; Raabe, J.; David, C.; van der Veen, J. F. *Microelectronic Engineering*, *87*, 854-858.

[11] Yoon, T. H. *Applied Spectroscopy Reviews* **2009**, *44*, 91-122.

[12] (a) Tzvetkov, G.; Fink, R. H. *Scripta Materialia* **2008**, *59*, 348-351. (b) Tzvetkov, G.; Graf, B.; Wiegner, R.; Raabe, J.; Quitmann, C.; Fink, R. *Micron* **2008**, *39*, 275-279.

[13] (a) Tzvetkov, G.; Fernandes, P.; Wenzel, S.; Fery, A.; Paradossi, G.; Fink, R. H. *Physical Chemistry Chemical Physics* **2009**, *11*, 1098-1104. (b) Fernandes, P. A. L.; Tzvetkov, G.; Fink, R. H.; Paradossi, G.; Fery, A. *Langmuir* **2008**, *24*, 13677-13682. (c) Tzvetkov, G.; Paradossi, G.; Tortora, M.; Fernandes, P.; Fery, A.; Graf-Zeiler, B.; Fink, R. H. *Materials Science & Engineering C-Materials for Biological Applications*, **2010**, *30*, 412-416.

[14] Hitchcock, A. P. *Journal of Synchrotron Radiation* **2001**, *8*, 66-71.

[15] L.M. Croll, H.D.H. Stöver and A. P. Hitchcock, *Macromolecules,* **2005**, *38*, 2903-2910.

[16] Araki, T.; Hitchcock, A. P.; Shen, F.; Chang, P. L.; Wang, M.; Childs, R. F. *Journal of Biomaterials Science-Polymer Edition* **2005**, *16*, 611-627.

[17] Li, J.; Hitchcock, A. P.; Stöver, H. D. H.; Shirley, I. *Macromolecules* **2009**, *42*, 2428-2432.

[18] Croll, L. M.; Morin, C.; Koprinarov, I.; Hitchcock, A. P.; Stöver, H. D. H. *Journal De Physique Iv* **2003**, *104*, 507-507.

[19] Van Koppenhagen, J. E.; Scher, H. B.; Lee, K.; Lee, C. C.; Shirley, I. M.; Wade, P.; Follows, R. *US 2002037306* A1

[20] http://www.uvacure.biz/Liquids/Downloads/CymelResins.pdf

[21] S. E. C. Dale and P. R. Unwin, *ACS meeting in Chicago* Mat **2007**

[22] Kilcoyne, A. L. D.; Tyliszczak, T.; Steele, W. F.; Fakra, S.; Hitchcock, P.; Franck, K.; Anderson, E.; Harteneck, B.; Rightor, E. G.; Mitchell, G. E.; Hitchcock, A. P.; Yang, L.; Warwick, T.; Ade, H. *Journal of Synchrotron Radiation* **2003**, *10*, 125-136.

[23] Warwick, T.; Ade, H.; Kilcoyne, D.; Kritscher, M.; Tylisczcak, T.; Fakra, S.; Hitchcock, A.; Hitchcock, P.; Padmore, H. *Journal of Synchrotron Radiation* **2002**, *9*, 254-257.

[24] aXis2000 is written in Interactive Data Language (IDL). It is available free for non-commercial use from http://unicorn.mcmaster.ca/aXis2000.html).

[25] Hitchcock, A. P.; Li, J.; Reijerkerk, S. R.; Foley, P.; Stöver, H. D. H.; Shirley, I. *Journal of Electron Spectroscopy and Related Phenomena* **2007**, *156*, 467-471.

[26] Frangioni, G.; Borgioli, G. *Stain Technology* **1979**, *54*, 167-172.

[27] Wang, J.; Morin, C.; Li, L.; Hitchcock, A. P.; Scholl, A.; Doran, A. *Journal of Electron Spectroscopy and Related Phenomena* **2009**, *170*, 25-36.

[28] Scher, H. B.; Rodson, M.; Lee, K. S. *Pesticide Science* **1998**, *54*, 394-400.

[29] (a) Okubo, M.; Minami, H.; Yamashita, T. *Macromolecular Symposia* **1996**, *101*, 509-516. (b) Loxley, A.; Vincent, B. *Journal of Colloid and Interface Science* **1998**, *208*, 49-62.

[30] Internal communication from Syngenta

CHAPTER 4 - STUDIES ON POLYUREA MICROCAPSULES: SURFACE MODIFICATIONS AND CAPSULE SIZE CONTROL

4.1 Introduction

Polyurea microcapsules (PUMCs) are micron-sized particles with a central cavity and a polyurea shell. They are typically used to protect the encapsulated materials from harsh environments and to control their release rate or mechanism. Because of their high chemical and mechanical stability, PUMCs are used in applications ranging from carbonless copy paper[1], thermal printing paper[2], textile[3] to agriculture[4]. Recent studies have explored the use of PUMCs in catalysis[5], self-healing materials[6], and flexible displays[7].

Since their inception, studies on PUMCs have focused on capsule properties[8], new applications[5, 6, 7], wall formation mechanisms[9], creating composite capsule walls[10], making functional capsules and imaging capsule morphologies[11]. These studies have greatly advanced the understanding of both PUMCs and encapsulation processes, making it possible to design structured PUMCs with multiple functions.

The outer PUMC surface mediates the capsule's interaction with the targeted substrates or surfaces, and is responsible for the capsule's dispersability, their adhesion to surfaces and their responses to environmental changes. It would thus be desirable to be

able to modify PUMC surface chemistries independent of the wall formation, to meet the requirements of different applications and fills. So far, most studies on PUMC surface modification have been focused on in-*situ* methods in which surface modifiers are utilized during encapsulation processes and, in most cases, modifiers are incorporated evenly throughout the capsule wall. Yan et al.[12] reported using lysine as comonomer to enhance capsule surface charge density and the resulting capsules showed improved dispersability in aqueous phases. Syngenta Ltd. has used polyEPS-520 as one of the aqueous phase wall formers to react with polyisocyanates, since the incorporation of this material provides a negatively charged capsule surface, which improved the capsules' dispersability in water as well as adhesion to foliage[13]. El-Gibaly and Anwar used 4,4-diaminostilbene-2,2-disulfonic acid as comonomer to introduce sulfonic groups onto capsule surfaces in order to improve oxygen-binding ability[14]. These *in-situ* approaches modified not only the capsule surfaces but also the bulk capsule walls, which, in some cases, had adverse effects on capsule wall properties and can necessitate re-optimization of capsule formulations for each new fill. Therefore, it is desirable to develop post-modifications that target the outermost surface of capsule walls to impart desirable surface properties without affecting bulk wall properties.

We describe surface modifications for PUMCs based on attaching low molecular weight and polymeric modifiers onto preformed PUMC surfaces. Because of diffusion limits of high molecular weight modifiers in dense PUMC walls, the modification is confined to the capsule surfaces, showing minimum interference with PUMC wall properties.

A common challenge in preparing capsules with controlled adhesion and release properties lies in the wide size distribution of PUMCs prepared by classical suspension interfacial polycondensation. Such PUMCs typically have a broad distribution of diameters and wall thickness, given their wide range of surface to volume ratios. Studies of capsule properties based on such polydisperse systems can only reflect statistical averages. While broad release ranges can be beneficial in certain applications requiring long release periods, access to monodisperse or narrow-disperse PUMCs could facilitate correlations between capsule size and properties. The formation of monodisperse or narrow-disperse PUMCs is often based on monodisperse emulsions prepared using microfluidic devices. Contrary to traditional top-down methods, the microfluidic approach produces emulsion droplets individually under identical conditions to ensure their uniformity. By varying flow rates and device geometry, the droplet size can be controlled, making microfluidic devices desirable tools for fabricating monodisperse emulsions[15], microspheres[16] and MCs[17]. However, microfluidic devices are most often fabricated by photolithography[18] and soft lithography[19], and thus not commonly accessible by chemists. In addition, isocyanates used for making PUMCs tend to hydrolyze and polymerize when in contact with water, which tends to lead to undesirable build-up in micro-channel devices. To address these challenges, McQuade et al. recently designed a simple version of a microfluidic device that uses a needle inserted into poly(vinyl chloride) tubing to form an inexpensive yet functional T-junction device capable of forming narrow-disperse polyamide MCs.[20] The only drawbacks are the requirement for careful positioning of the needle within the tubing, and a typical capsule

diameter of several hundreds of micrometers owing to the relatively large internal diameters of the needle and tubing, making it less practical for mimicking industrial products. We describe here a structurally robust microfluidic device built from commercially available T-junctions that is capable of producing monodisperse emulsions and microcapsules with diameters below 100 μm. Clogging problems can be resolved by replacing the relatively inexpensive T-junctions. We believe these studies will lead to preparation of well defined PUMCs with desirable functionalities on the surface, facilitating capsule property studies and wider applications of PUMCs.

4.2 Experimental Section

4.2.1 Materials

N-(3-aminopropyl) methacrylamide hydrochloride was purchased from Polysciences Inc. 2, 2'–Azobis(isobutyronitrile) (AIBN) was purchased from Dupont (Mississauga, ON). All other reagents were purchased from Sigma-Aldrich and used as received. The preparation of poly(sodium methacrylate-co-2-(methacryloyloxy) ethyl acetoacetate) (A70f) and its labelling with fluorescein isothiocyanate (FITC) was described previously[18]. All reagents were used as received. The #00 BEEM embedding capsules were purchased from Canemco Inc.

4.2.2 Methods

Synthesis of Aliphatic Polyurea Microcapsules

Aqueous polyvinyl alcohol solution (35 mL, 1 wt % polyvinyl alcohol (PVA), MW 9,000-10,000, 80% hydrolyzed) was first charged into a thermostatted Buchi suspension reactor, with an overhead three-blade stirrer driven at 1000 rpm. Isocyanate solution (2 g isophorone diisocyanate, IPDI, dissolved in 10 mL xylene) was added into the reactor and the mixture was stirred for 15 min at room temperature. The stirring rate was reduced to 500 rpm before adding diethylenetriamine (DETA) solution (1 g DETA dissolved in 5 mL 1 wt % aqueous PVA solution) within one minute. The temperature was then raised to 70°C and maintained for 65 hrs. The resulting capsules were washed on filter paper with deionized water until pH 6.7.

Preparation of Narrow-disperse Aromatic Polyurea Microcapsules Using a Microfluidic Device

A microfluidic device was built based on a MicroTEE (P-890, Upchurch) to prepare mono-disperse or narrow-disperse emulsions and PUMCs. The MicroTEE was placed vertically as shown in **Scheme 4.1**. The oil phase flow containing xylene and isocyanates was pumped into the side arm of the MicroTEE using a N-1600 Multiple syringe pump (New Era Pump Systems, Inc.), while the aqueous phase flow (1.0 wt % PVA in water) was introduced to the top arm of the MicroTEE by a Waters 590 programmable HPLC pump. The formed emulsion came out of the bottom arm and was directed into a reservoir solution in a centrifuge tube containing 1.0 wt % PVA solution that was placed directly underneath the MicroTEE. The connections between the MicroTEE and the pumps and the reservoir solution were made using Teflon FEP tubings

(1476, Upchurch). In the case of emulsion visualization, the emulsion formed was directly deposited onto a microscope slide and then imaged using an optical microscope. For making PUMCs, the oil phase containing 10.0 wt % PMPPI in xylene was pumped into the MicroTEE at a flow rate of 0.020 mL/min, while the flow rate of aqueous phase was set to 0.463 mL/min. The formed emulsion was then directed into a 10 mL reservoir solution containing 5.0 wt % DETA and 1.0 wt % PVA to facilitate the interfacial polymerization. The emulsion was collected for 5 min and then the tube was capped and placed on a rotator (Glas-Col) and rotated at a rate of 30 rpm for various lengths of time. The resulting MCs were washed 4 times with deionized water in the centrifuge tube to remove unreacted DETA and PVA. To avoid clogging by hydrolysis and polymerization of the isocyanate inside the MicroTEE, the system was flushed with neat xylene immediately after use.

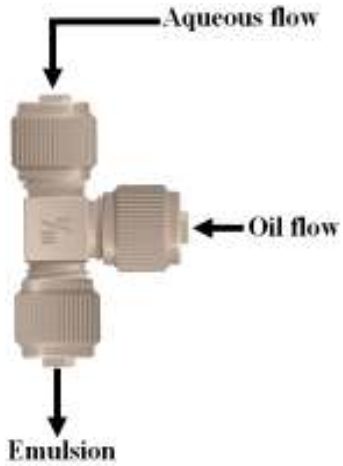

Scheme 4.1 MicroTEE (P-890, Upchurch)

Synthesis of Fluorescein Labeled Poly(methacrylic acid) (A100f)

Methacrylic acid 1.91 g (22.19 mmol), O-fluorescein methacrylate 89.7 mg (0.22 mmol) and AIBN 73.6 mg (0.45 mmol) were dissolved in 18 mL ethanol in a HDPE bottle. The solution was gently bubbled with dry N_2 for 10 min, placed in an HB-1000 hybridizer at 60℃ for 21 hrs and rotated at ~10 rpm. After reaction, the formed polymer was precipitated in 200 mL diethyl ether and washed 3 times with 50 mL diethyl ether. The solid product was dried under vacuum at 60℃ until constant weight. Yield: 1.69g (84.5%). M_n was determined using GPC to be 35,100 Da, with a PDI of 2.65. The fluorescence label content was measured using UV-Vis to be 0.05 mol % of total monomer units.

Synthesis of Fluorescein-labeled Poly(methacrylic acid-co-butyl methacrylate) (A70bf)

Methacrylic acid 0.5 g (5.8 mmol), butyl methacrylate 0.33 g (2.32 mmol), O-fluorescein methacrylate 65 mg (0.162 mmol) and 14 mg AIBN (0.085 mmol) were dissolved in 9 mL of ethanol in a 20 mL glass vial. The solution was gently bubbled with dry N_2 for 10 min and then heated to 70℃ for 30 hrs in a HB-1000 hybridizer at 15 rpm rotation. After reaction, the solution was precipitated twice into 100 mL cold diethyl ether, and dried under vacuum at 60℃ until constant weight. Yield: 0.634g (70%). The ratio of methacrylic acid to butyl methacrylate in the polymer was determined by NMR to be 70:30. M_n was determined using GPC to be 29,700 Da with a PDI of 2.45. The fluorescence label content was measured using UV-Vis to be 0.2 mol % of total monomer unites.

Synthesis of Poly (N-(3-aminopropyl) methacrylamide) (PAPM)

In a typical free radical polymerization, N-(3-aminopropyl) methacrylamide hydrochloride (5.24 g, 29.3 mmol) and 2,2'–azobis (2-methyl propionamidine) dihydrochloride (0.159 g, 0.59 mmol, 2 mol % relative to monomer) were dissolved in 50 mL water in a 60 mL HDPE bottle. The solution was bubbled with N_2 for 10 min. The sealed bottle was placed in an HB-1000 Hybridizer and heated at 60 °C for 24 hrs while being rotated at 15 rpm. After reaction, the polymer was purified by dialysis in cellulose tubing (12 kDa MW cut-off, Spectrum Laboratories, USA) against deionized water for 5 days, with daily changes of water, followed by freeze-drying. Yield: 4.29 g (82 %). Molecular weight of PAPM was determined using viscometry and found to be 260 kDa.

Synthesis of Rhodamine Labeled Poly(N-(3-aminopropyl) methacrylamide) (PAPMr)

Rhodamine isothiocyanate (12 mg, 0.224 mmol) was dissolved in 2 mL DMF and added over 1 min to a solution of PAPM (0.2 g, 1.12 mmol) in 10mL 0.1 M $NaHCO_3$ buffer (Ph=9), and the mixture stirred at room temperature for 2.5 hrs. Dialysis and freeze drying yielded a reddish solid in 83 % yield. The degree of rhodamine labeling was determined using UV-Vis to be 0.6 mol % of total monomer unites.

Fluorescein Isothiocyanate (FITC) Treatment on Polyurea Microcapsules

1 mL of a 1 mg/mL solution of FITC in DMF was added to 10 mL $NaHCO_3$ buffered (pH=9) PUMC suspension in a glass vial. The vial was rotated at ~15 rpm at room temperature for 20 hrs. The resulting capsules were washed using 10 % DMF water solution twice to remove unreacted FITC.

Polyurea Microcapsule Surface Modification Using A70f, A100f and A70bf

5 mg A70f was added to 10 mL PUMC suspension and the pH adjusted to 8.6. After 30 min of gentle stirring, the resulting capsules were washed on a filter paper until no fluorescence could be detected in the supernatant by UV-Vis. Surface modifications using A100f and A70bf were similar to that of A70f.

Layer-by-Layer Coating on Polyurea Microcapsule Surfaces

A70f-coated PUMCs were treated in sequence with PAPM*r,* A70f and PAPM*r* to form (A70f/PAPM*r*)$_2$ modified capsules. For each coating step, 5 mg PAPM*r* or A70f was added to 10 mL capsule suspension and the pH was adjusted to 7. The suspension was then gentled rotated at room temperature for 30 min and the resulting capsules washed on a filter paper to remove unattached polyelectrolyte, and redispersed in 10 mL distilled water for the next coating step.

Microcapsule Embedding

(A70*f*/PAPM*r*)$_2$ modified PUMCs were washed on a filter paper with THF three times to extract xylene from the core. A small amount of capsules (2-3 mg) was then added to a BEEM embedding capsule and mixed with ~2 mL of styrene containing 10 wt % benzoyl peroxide. The capsule was sealed and heated at 70 °C for 24 hrs to complete the embedding.

Characterization

The composition of A70B*f* was determined by proton NMR using a Bruker AV 200 spectrometer for samples dissolved in DMSO-*d6*. Size exclusion chromatography

(SEC) was conducted using a system consisting of a Waters 515 HPLC pump, Waters 717 plus Autosampler, three columns (Waters Ultrahydrogel-120, -250, -500; 30 cm 3 7.8 mm; 6-lm particles) and a Waters 2414 refractive index detector, calibrated with narrow molecular weight poly(ethylene glycol) standards (Waters). Samples were eluted at a flow rate of 0.80 mL/min with a mobile phase consisting of 0.3 M sodium nitrate in phosphate buffer (pH=7) prepared by dissolving 27.6 g monosodium phosphate, 101.98 g sodium nitrate, and 4.66 g sodium hydroxide in 4.0 L of HPLC grade water. The pH was adjusted to 7 with 1M NaOH. 1 % A100*f* or A70B*f* solutions for injection were prepared by adding a stoichiometric amount of 1 M NaOH to the corresponding copolymer dissolved in the mobile phase. The degree of labelling with FITC was measured by UV-Vis spectrophotometry, using a Varian Cary 50 BIO UV-Vis Spectrophotometer. Optical microscope images of capsules were taken using an Olympus BX51 optical microscope fitted with a Q-Imaging Retiga EXi digital camera and ImagePro software. A Confocal laser scanning imaging system equipped with an Argon-ion laser and a Nikon microscope using EZ-C1 software, version 1.50, was used to investigate the coatings on PUMC surfaces and all the confocal images were acquired using the same parameter settings.

4.3 Results and Discussion

4.3.1 Surface Modifications of Aliphatic Polyurea Microcapsules

Capsules used for surface modification study were prepared by interfacial polycondensation between IPDI and DETA at 70℃ for 65 hrs in order to form walls

thick enough for subsequent cross-sectional analysis[9(a)]. Most capsules turned out to be spherical with some dimples, characteristic for long reaction times, as shown in Figure 4.1.

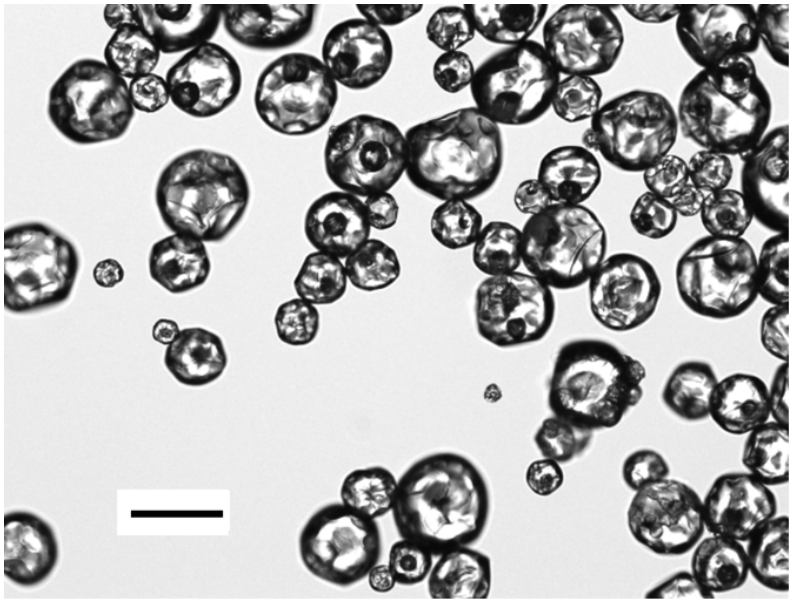

Figure 4.1 Optical micrograph of polyurea microcapsules made of IPDI and DETA. The scale bar is 100 um.

Understanding the surface chemistry of PUMCs is the first step in designing surface post-modification methods. PUMCs are synthesized by interfacial polycondensation between polyisocyanates and polyamines. Due to the high reactivity of these comonomers, the capsule surface and wall chemistries are dominated by urea groups though one would expect some residual amine groups on the outer surface of the capsule wall, due both to the use of aqueous polyamines as a wallformer, and due to hydrolysis of residual isocyanate groups by way of the amic acid intermediate. The interfacial nature of the wall forming reaction might further be expected to lead to the

formation of concentration gradients of both polyisocyanates and polyamines across the capsule wall during encapsulation, with more polyamines on the aqueous side and more polyisocyanates on the oil side of the interface. Both situations would lead to some residual amine groups attached to PUMC surfaces.

To probe the PUMC surface chemistry we treated PUMCs with fluorescein isothiocyanate (FITC) in a DMF/water mixture at pH 9. The isothiocyanate group in FITC is quite reactive towards nucleophilic groups such as amines on the capsule surface. Capsules before and after FITC treatment were subjected to confocal fluorescent microscopy. Optical sections from the capsule equator before and after FITC labeling are shown in Figure 4.2a and 4.2b. Without FITC treatment, PUMC capsule walls did not show fluorescence in the FITC channel of the confocal microscope, indicating absence of PUMC auto-fluorescence. After FITC treatment, fluorescence signals were observed in the FITC channel, indicating the incorporation of FITC into PUMC walls. The attachment of FITC to the capsule wall indicates that there are nucleophilic groups, most likely amine groups in PUMC walls that can react with FITC to form a covalent linkage.

Further evidence of amino group presence in the capsule wall came from capsules exposed to fluorescein-labeled poly(sodium methacrylate) (A100*f*) solution at pH 6.5. Figure 4.2c shows weak fluorescence on the capsule surface after A100*f* exposure, suggesting the attachment of A100*f* to the PUMC walls. This attachment could be attributed to the presence of amine groups in PUMC walls. At pH 6.5, most amino groups would be protonated and hence able to electrostatically bind negatively charged A100*f*. Compared to FITC treated PUMCs, A100*f* coated PUMCs showed much weaker

fluorescence probably due to both the low level of fluorescein labeling in A100*f* and inability of this polymer to penetrate into the PUMC wall. A100*f* coating was also attempted at pH 8.6 and no attachment was observed, reflecting the lower degree of ionization of amines at this pH. These observations support the presence of amine groups on PUMC surfaces, that could be used for capsule surface modifications.

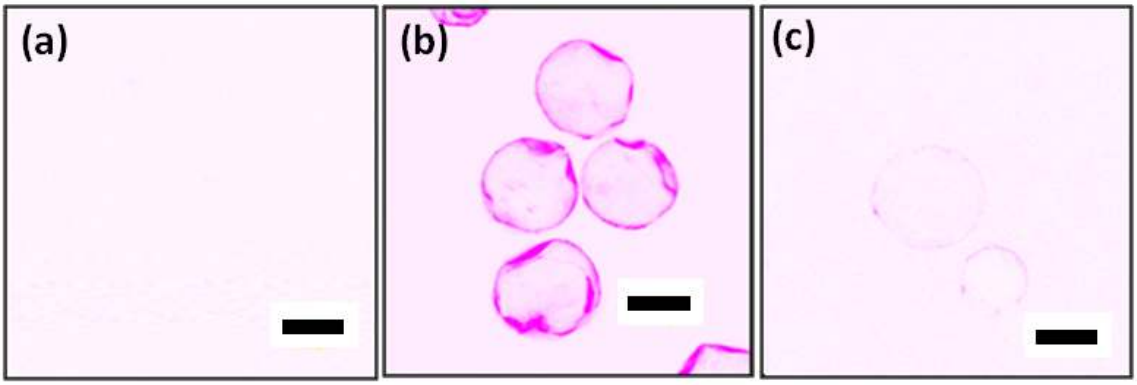

Figure 4.2 Equatorial confocal fluorescent microscope images (colour inverted) of polyurea microcapsules (a) without treatment. (b) after treatment with FITC. (c) after treatment with A100*f* . All scale bars are 50 μm.

4.3.2 Polyurea Microcapsule Surface Modifications

Several criteria need to be considered for designing surface modifiers for PUMCs: 1. the modifiers need to be soluble in aqueous PUMC suspensions; 2. the modifiers need to contain amine reactive groups that can help anchor modifiers to PUMC walls under mild conditions; 3. the modifiers need to carry the functional groups that needed for modification of the PUMC surfaces; 4. the modifiers need to have relatively high molecular weights to minimize their diffusion into the PUMC walls and their effect on

release and other wall properties; 5. the modifiers should contain a reporter group to allow assessing coating efficiency.

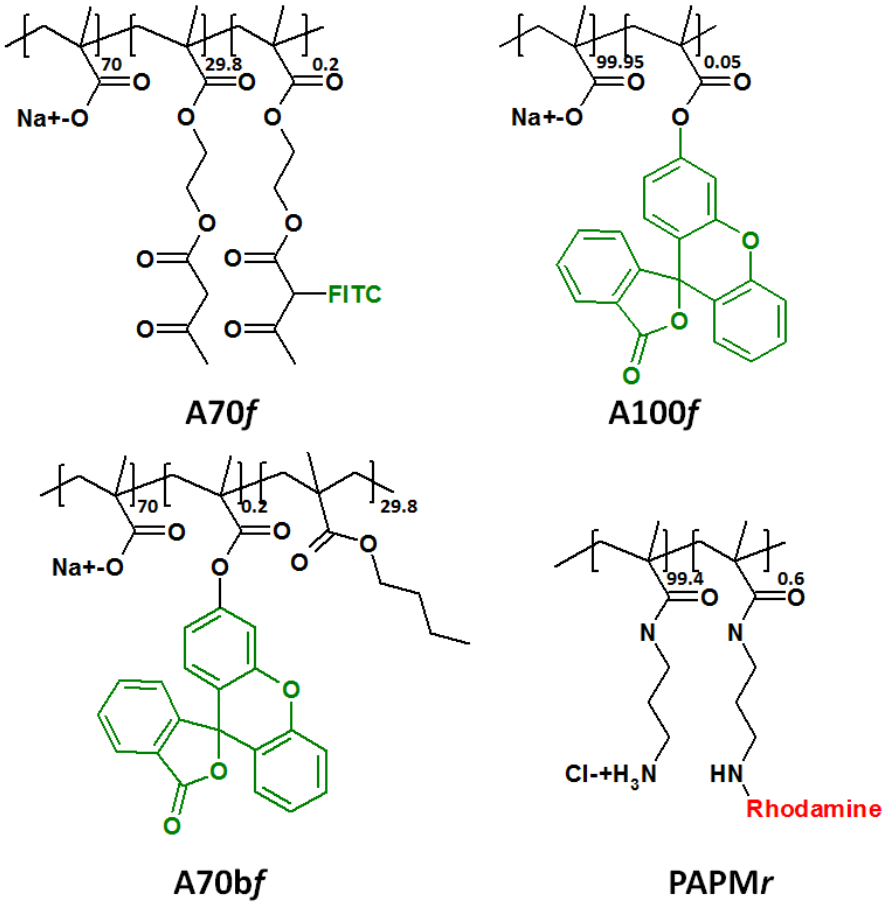

Scheme 4. 2 Chemical structures of A70*f*, A100*f*, A70b*f* and PAPM*r*

In order to meet these criteria, we used a fluorescein-labeled functional polyanion, poly(sodium methacrylate-*co*-2-(methacryloyloxy) ethyl acetoacetate) (**A70*f***) as a PUMC surface modifier. A70*f* was prepared by free radical copolymerization of methacrylic acid and methacryloyloxy ethyl acetoacetate. The presence of 70 mol % methacrylic acid provides solubility in water above pH 4.5 and provide electrostatic preconcentration of

the modifier on the capsule surface, while the 30 mol % acetoacetyl groups were designed to react with amine groups in PUMC walls to effect covalent attachment at room temperature. 0.67 mol % of the acetoacetyl groups were labelled with FITC, to enable mapping of the polymeric modifier using conventional and confocal fluorescence microscopy. The proposed modification mechanism is shown in **Scheme 4.2**.

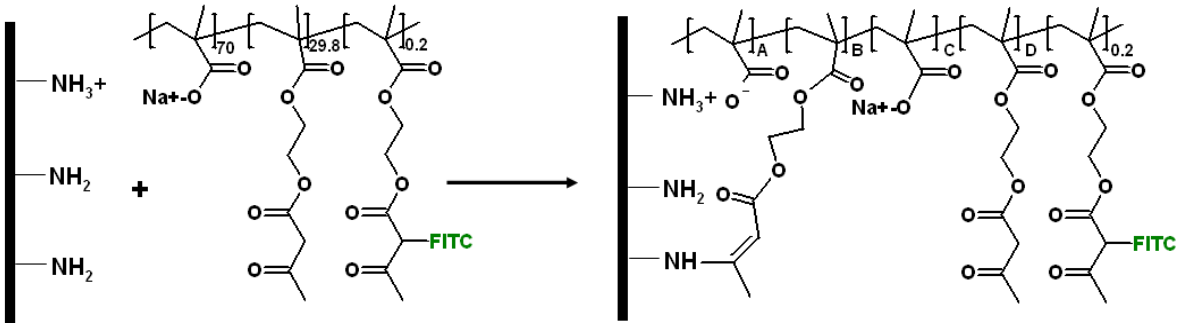

Scheme 4.3 The proposed mechanism for PUMC surface grafting by A70*f*. A+C=70; B+D=29.8

The PUMC surface modification was carried out at room temperature at pH 8.6. At this pH, sufficient amine groups in PUMC walls are in their free form and hence able to covalently react with acetoacetyl groups in A70*f*. The confocal image of capsules after A70*f* coating, observed through the FITC channel (Figure 4.3b), clearly shows substantial A70*f* binding, in comparison to uncoated capsules (Figure 4.3a). The fluorescence distribution seems heterogeneous, which is believed to reflect the irregular capsule shape (dimples) more than any inherent heterogeneity of PUMC walls.

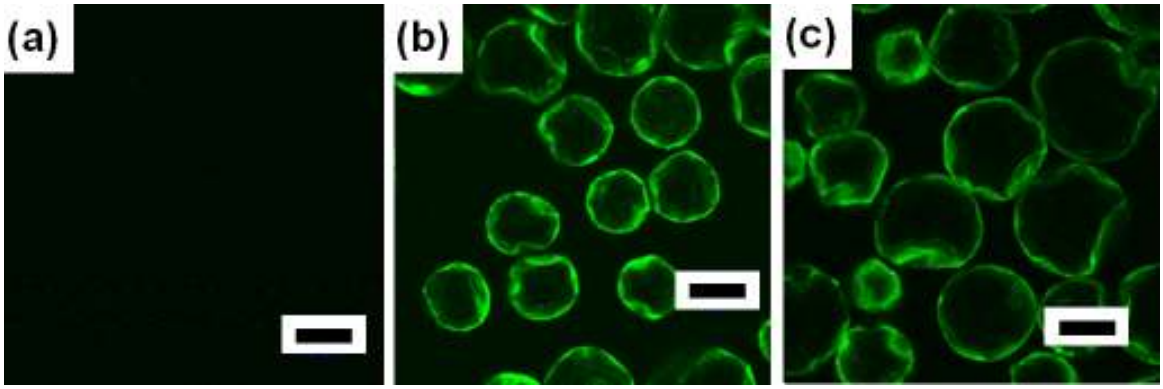

Figure 4.3 Confocal microscopy images of PUMCs (a) without modification; (b) modified by A70*f*; (c) first modified by A70*f* and then treated with 2M NaCl solution. All scale bars stand for 50 μm.

To further explore the interactions between PUMC walls and A70f, we carried out two controlled experiments. In the first experiment, A70*f* modified PUMCs were treated with 2M NaCl solution. It is known that purely electrostatic interactions between weak polyelectrolytes can be shielded using high concentrations of small electrolytes, leading to dissociation of the polyelectrolyte complex. The dissociation of A70 from its complexes with poly(2-methacryloyloxyethyl trimethyl ammonium chloride) (PMOETAC) has been studied earlier[21], showing that 2M NaCl was sufficient to dissolve those complexes. In this study, we observed that A70*f* modified PUMCs retained strong fluorescence **(**Figure 4.3c) after 2M NaCl treatment. This indicates that 2M NaCl could not dissociate A70*f* from PUMCs walls and thus electrostatic interaction was not primarily responsible for the attachment of A70*f*. In the second experiment, the possibility of hydrophobic-hydrophobic interactions between PUMC walls and A70*f* was explored with the attempt to use A70b*f* as a non-covalent polyanionic PUMC modifier. The butyl

groups in A70B*f* were designed as hydrophobic analogs of the acetoacetyloxy ethyl groups in A70*f,* with butyl groups being slightly more hydrophobic but not reactive towards electrophiles. Studies using confocal microscope revealed that no fluorescence signal was detected after A70b*f* treatment, suggesting no A70b*f* was attached to PUMC walls due to relatively hydrophilic PUMC surfaces. This helps rule out hydrophobic-hydrophobic interactions between PUMC walls and A70*f* and led us to conclude that covalent reaction between amine groups on PUMC surfaces and acetoacetyl groups in A70*f* were primarily responsible for the PUMC wall modification. The covalent modification is advantageous over either electrostatic or hydrophobic-hydrophobic interaction as it is non-reversible and thus has better stability.

The successful attachment of A70*f* on PUMC walls enables further capsule surface modifications. The negative charge in PUMC walls provided by the A70*f* attachment can attract polycations while the unreacted acetoacetyl groups in A70*f* enables reactions between walls and nucleophile-containing modifiers, which provide both electrostatic and covalent modifications. To demonstrate this, we used rhodamine-labelled poly(3-aminopropyl methacrylamide) (PAPM*r*) to further modify A70*f*-coated PUMCs. The resulting PUMCs showed fluorescence signals in both FITC and rhodamine channels shown in Figure 4.4. This indicates that both dyes were present in the PUMC walls, which can be attributed to the successful attachment of A70*f* and PAPM*r* to PUMC walls in two separate coating steps. It is evident that the fluorescence signal in the FITC channel became weaker upon PAPM*r* coating, which is attributed to partial quenching of the fluorescein by rhodamine groups present in close proximity[22]. Modified PUMCs were

further coated using A70*f* and PAPM*r* in a layer-by-layer fashion to prepare (A70*f*/PAPM*r*)$_2$ modified capsules. The overall fluorescence intensity increased with increasing number of layers, as shown in Figure 4.5, confirming the successful coating of each layer.

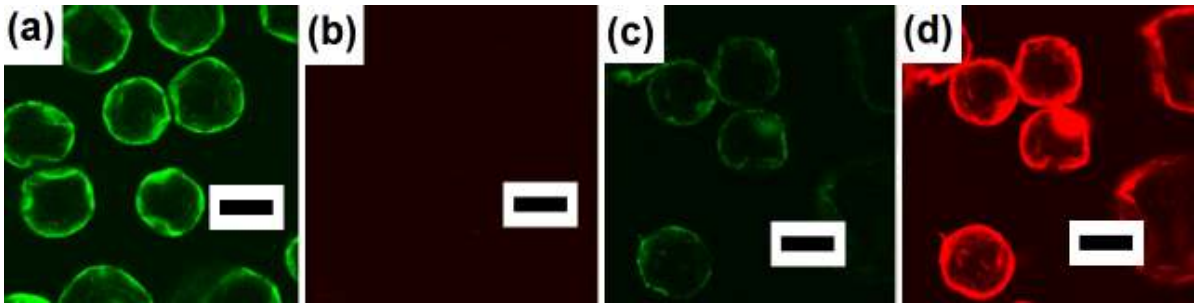

Figure 4.4 Confocal images of A70*f*-coated polyurea microcapsules in (a) FITC channel (b) rhodamine channel; and A70*f*/PAPM*r* bilayer polyurea microcapsules in (c) FITC channel (d) rhodamine channel. All scale bars denote 50 μm.

To determine if these fluorescently labelled polymers could penetrate the polyurea walls or were restricted to the wall surface, we examined the wall cross-sections of (A70*f*/PAPM*r*)$_2$ modified PUMCs using transmission electron microscopy, fluorescence and optical microscopy. This was done by embedding dried capsule samples in polystyrene and ultramicrotoming the embedded samples to about 100nm thickness. The resulting thin sections were subjected to microscopy imaging. Figure 4.6a shows the TEM micrographs of a PUMC wall cross-section. The PUMC wall appeared delaminated into a layered structure, which could be attributed to both low cross-linking density of the polyurea wall chemistry and the swelling effect of styrene during embedding. Optical and fluorescence microscopes were then used to examine the same sample area, shown in

Figure 4.6b and 4.6c. By comparing these two images, it is evident that the fluorescence came primarily from the outer edge of capsule wall, while the rest of wall showed very little fluorescence signal. This indicates that the modification occurred almost exclusively on the PUMC surfaces and the capsule walls were not modified due to limited diffusion of the macromolecular modifiers into the relatively dense PUMC walls. The confinement of modifications to the PUMC surface is beneficial as the modification steps did not interfere with the rest of the capsule wall and thus other wall properties would remain intact.

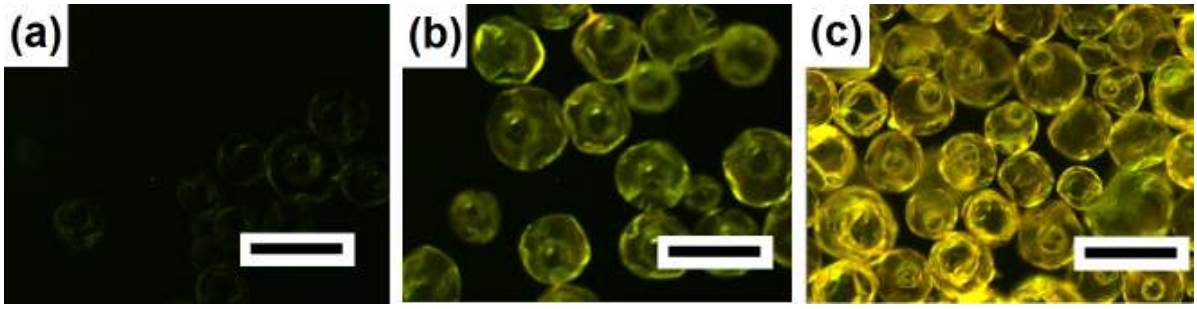

Figure 4.5 Conventional fluorescence microscope images of polyurea microcapsules using an FITC filter set (a) native capsules (b) (A70*f*/PAPM*r*) modified capsules (c) $(A70f/PAPMr)_2$ modified capsules.

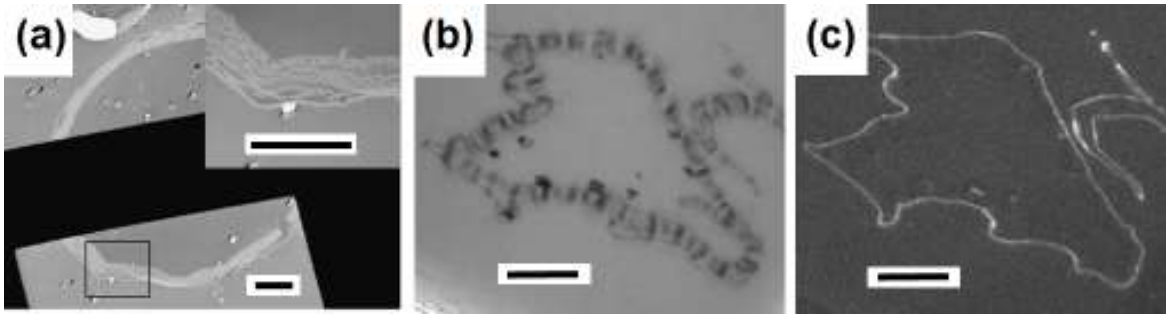

Figure 4.6 Wall cross-section of a (A70*f*/PAPM*r*)$_2$ modified polyurea microcapsule (a) a TEM micrograph showing a capsule cross-section (the insert in the upper right hand corner is the enlarged image of the boxed area) (b) an optical microscope image (c) a fluorescence microscope image (grey scale). (b) and (c) were taken in the same sample area. Scale bars denote 10 μm.

4.3.3 Preparing Narrow-disperse Polyurea Microcapsules Using a Microfluidic Device

In order to make monodisperse or narrow-disperse PUMCs, we designed a T-junction type microfluidic device that is capable of producing monodisperse emulsions. The key part of this device is a commercial T-junction machined from polyether ether ketone (MicroTEE, P-890, Upchurch) with 152.4 μm diameter thru-holes, ideal for making micro-sized emulsions. This MicroTEE can easily be connected using standard tubing to the two pumps delivering the aqueous continuous phase (1% PVA) from the top, and the organic dispersed phase (xylene) through the sidearm, with the formed emulsion being collected through the bottom fitting in a collection reservoir. This setup results in a

robust microfluidic devices based on shearing organic phase droplets into a high flow aqueous phase flow.

Before making PUMCs, the formation of xylene-in-water emulsions was examined using this microfluidic device. Figure 4.7 shows an optical microscope image of a xylene-in-water emulsion made using this device. Most emulsions are monodisperse with standard deviations less than 5%. Using this device, the size of the emulsion droplets can be easily tuned by varying the flow rates of either oil phase or aqueous phase (Figure 4.8). Within the flow rate regimes investigated, emulsion size increases with oil phase flow rate, and decreases with increasing aqueous phase flow. Accordingly, monodisperse emulsions with the size ranging from 50 μm to 160 μm were successfully made.

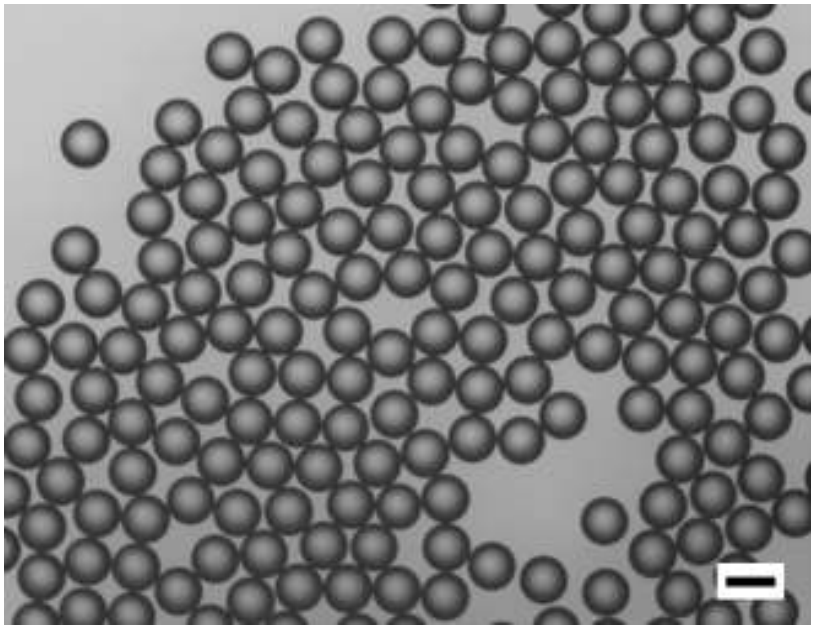

Figure 4.7 Optical micrograph of monodisperse xylene-in-water emulsion made using the microfluidic device. The scale bar is 100 μm.

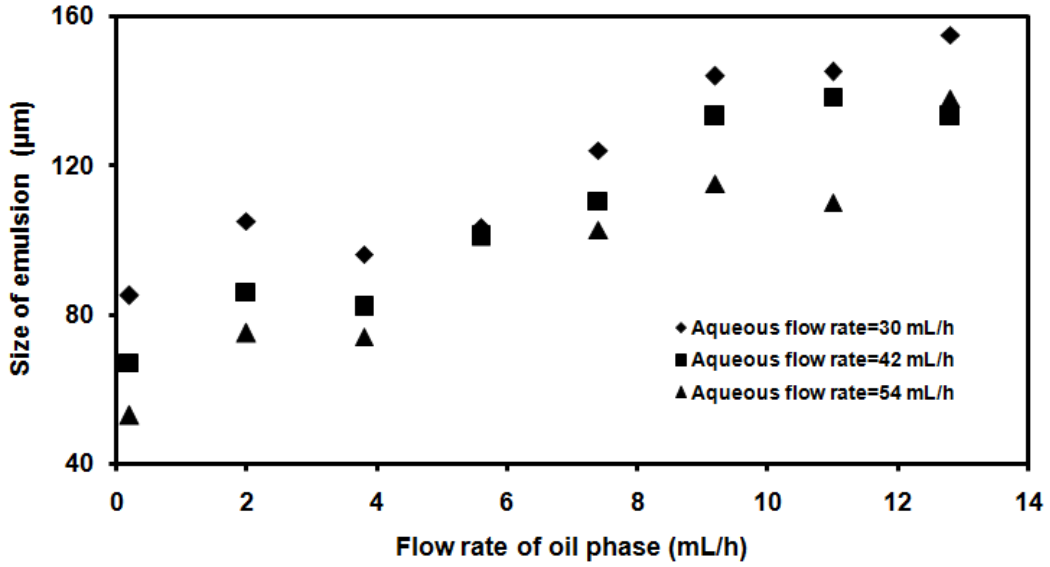

Figure 4.8 Dependence of emulsion size on the flow rates of both aqueous and oil phases.

The MicroTEE based microfluidic device was then utilized to prepare narrow-disperse aromatic PUMCs. 10 wt % PMPPI was dissolved in xylene to serve as oil phase, which was then pumped into the microfluidic device along with an aqueous flow (1.0 wt % PVA) to form an oil-in-water emulsion. The resulting PMPPI containing emulsion was subsequently directed into a reservoir solution containing DETA, to start the interfacial polycondensation between PMPPI and DETA. Due to the relatively fast rate of hydrolysis of PMPPI, clogging happens on occasion due to polyurea build-up in the MicroTEE. To mitigate this problem, the device was flushed with neat xylene immedeately after each use to remove PMPPI residues from the channels. When clogging does happen, the MicroTEE can be easily replaced and cleaned.

The narrow-disperse system allows us to precisely monitor the change of capsule size and morphology during the reaction, which is not apparent for polydisperse systems.

The morphology of the narrow-disperse PUMCs formed at room temperature with different reaction time was evaluated using optical microscopy and the results are shown in Figure 4.9. One hour reaction at room temperature led to the formation of dimpled PUMCs with smooth surfaces, as shown in Figure 4.9a. These capsules appear to be narrow-disperse with a mean diameter around 101 μm. The dimples on the surface were probably caused by collisions between capsules during the reaction. Extended reaction time (2 and 7 days) rendered rough surfaces and more deformation of those capsules, as shown in Figure 4.9b and 4.9c. This suggests that the polymerization at the later stage caused stresses in the initial PU membrane, leading to the morphological change on capsule surfaces, and internal phase separation of polyurea. The average diameter of these capsules did not change and stayed constant (~101 μm) during the extended reaction time.

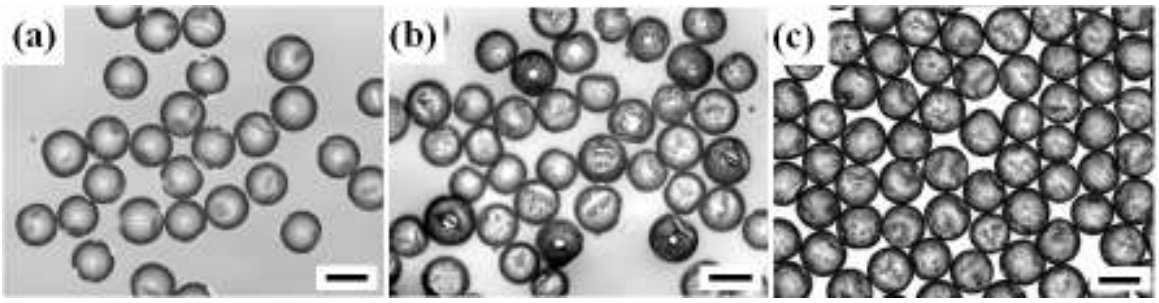

Figure 4.9 Optical micrographs of narrow-disperse aromatic polyurea microcapsules made using the microfluidic device at room temperature with different reaction time: (a) 1 hour; (b) 2 days; (c) 7 days. The scale bars are 100 μm.

The narrow-disperse aromatic PUMCs were then subjected to surface modification using A70*f* in order to test the generality of surface modification in terms of different types of PUMCs. After the surface modification, the resulting PUMCs were

imaged by fluorescence microscopy. As shown in Figure 4.10, all PUMCs fluoresce and the modification appears to be uniform, suggesting a fairly homogeneous chemical composition of these PUMC surfaces.

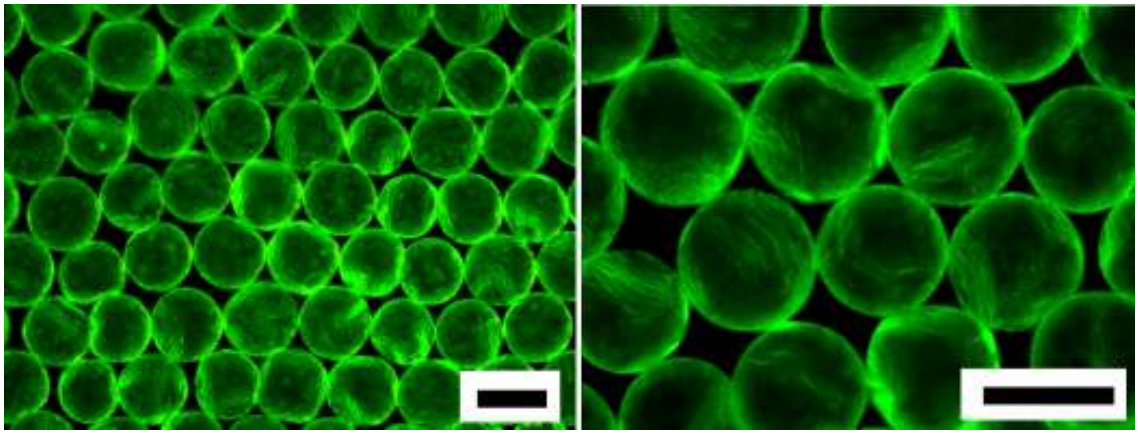

Figure 4.10 Fluorescence micrographs of narrow-disperse aromatic polyurea microcapsules surface modified with A70*f*. The scale bars are 100 μm.

4.4 Conclusions

In conclusion, a post-modification method was developed to change PUMC surface chemistry using an acetoacetyl functional polyanion. The acetoacetyl groups could react with amino groups on PUMC surfaces to achieve covalent tethering. Further modifications by layer-by-layer coating were performed to demonstrate the versatility of this method. Fluorescent labelling was utilized throughout to provide visual detection of modifications on the capsule surface. This method can be readily extended to introduce other desirable functional groups onto PUMC surfaces for different applications by designing corresponding polyelectrolyte modifiers. This method has several advantages

over *in-situ* modification methods as the wall formation and surface modification are well separated and other wall properties can be kept intact due to the confinement of modifications only to PUMC surfaces.

A T-junction type microfluidic device was constructed based on commercially available MicroTEEs. The device is easy to set up and operate. Monodisperse emulsions and narrow-disperse PUMCs can be made using this microfluidic device with their sizes easily tuned by the flow rates of either oil phase or aqueous phase.

4.5 References

[1] Horiike, T.; Kuroda, T.; Shiozaki, T. *French Patent* **1982**, Fr 2498474, CA **1983**, 98: 633639; *Japanese Patent* (examined) **1988**, 88-1347B

[2] Usami T, Tanaka T, Ishige S, *Electrophotography* **1987**, *26(1),* 115-119.

[3] (a) Giraud, S.; Bourbigot, S.; Rochery, M.; Vrornan, I.; Tighzert, L.; Delobel, R.; Poutch, F.; Elsevier Sci Ltd: 2005, p 106-113. (b) Sarier, N.; Onder, E. *Thermochimica Acta* **2007**, *452*, 149-160. (c) Zhong, Y.; Feng, J. H.; Chen, S. L. *Coloration Technology* **2005**, *121*, 76-80.

[4] (a) Hashemi, S. A.; Zandi, M. *Iranian Polymer Journal* **2001**, *10*, 265-270. (b) Schwartz, L.; Wolf, D.; Markus, A.; Wybraniec, S.; Wiesman, Z. *Journal of Agricultural and Food Chemistry* **2003**, *51*, 5972-5976. (c) Muro-Sune, N.; Gani, R.; Bell, G.; Shirley, I. *Computers & Chemical Engineering* **2005**, *30*, 28-41. (d) Paik, S.; Kim, H. S., Li, Y. B.,

Lee, S. W., Eds.; Trans Tech Publications Ltd: 2006, p 678-681. (e) Zhang, Q.; Zhang, P. P.; Jiao, Q. Z. *Chemical Research in Chinese Universities* **2006**, *22*, 379-382. (f) Scarfato, P.; Avallone, E.; Iannelli, P.; De Feo, V.; Acierno, D. *Journal of Applied Polymer Science* **2007**, *105*, 3568-3577.(g) Mihou, A. P.; Michaelakis, A.; Krokos, F. D.; Mazomenos, B. E.; Couladouros, E. A. *Journal of Applied Entomology* **2007**, *131*, 128-133.

[5] (a) Bremeyer, N.; Ley, S. V.; Ramarao, C.; Shirley, I. M.; Smith, S. C. *Synlett* **2002**, 1843-1844. (b) Ramarao, C.; Ley, S. V.; Smith, S. C.; Shirley, I. M.; DeAlmeida, N. *Chemical Communications* **2002**, 1132-1133. (c) Ley, S. V.; Ramarao, C.; Lee, A. L.; Ostergaard, N.; Smith, S. C.; Shirley, I. M. *Organic Letters* **2003**, *5*, 185-187. (d) Yu, J. Q.; Wu, H. C.; Ramarao, C.; Spencer, J. B.; Ley, S. V. *Chemical Communications* **2003**, 678-679. (e) Siu, J.; Baxendale, I. R.; Ley, S. V. *Organic & Biomolecular Chemistry* **2004**, *2*, 160-167. (f) Baxendale, I. R.; Griffiths-Jones, C. M.; Ley, S. V.; Tranmer, G. K. *Chemistry-a European Journal* **2006**, *12*, 4407-4416. (g) Broadwater, S. J.; McQuade, D. T. *Journal of Organic Chemistry* **2006**, *71*, 2131-2134. (h) Price, K. E.; Broadwater, S. J.; Bogdan, A. R.; Keresztes, I.; Steinbacher, J. L.; McQuade, D. T. *Macromolecules* **2006**, *39*, 7681-7685. (i) Screen, T.; Pears, D. *Chimica Oggi-Chemistry Today* **2006**, *24*, 33-34. (j) Mason, B. P.; Bogdan, A. R.; Goswami, A.; McQuade, D. T. *Organic Letters* **2007**, *9*, 3449-3451. (k) Ji, H. B.; Li, J. L.; Pei, L. X.; Gao, J. R. *Chinese Journal of Chemical Engineering* **2008**, *16*, 119-123.

[6] Yang, J. L.; Keller, M. W.; Moore, J. S.; White, S. R.; Sottos, N. R. *Macromolecules* **2008**, *41*, 9650-9655.

[7] (a) Chen, Y.; Au, J.; Kazlas, P.; Ritenour, A.; Gates, H.; McCreary, M. *Nature* **2003**, *423*, 136-136. (b) Li, G.; Feng, Y. Q.; Li, X. G.; Gao, P.; Wang, J.; Xie, J. Y. *Journal of Materials Science* **2007**, *42*, 4838-4844.

[8] (a) Hong, K.; Park, S. Journal of Materials Science **1999**, 34, 3161-3164. (b) Hong, K.; Park, S. Materials Science and Engineering a-Structural Materials Properties Microstructure and Processing **1999**, 272, 418-421.

[9] (a) Li, J.; Hitchcock, A. P.; Stöver, H. D. H.; Shirley, I. *Macromolecules* **2009**, *42*, 2428-2432. (b) Dhumal, S. S.; Wagh, S. J.; Suresh, A. K. *Journal of Membrane Science* **2008**, *325*, 758-771.

[10] (a) Croll, L. M.; Stöver, H. D. H.; Hitchcock, A. P. *Macromolecules* **2005**, *38*, 2903-2910. (b) Croll, L. M.; Stöver, H. D. H. *Pure and Applied Chemistry* **2004**, *76*, 1365-1374.

[11] (a) Hitchcock, A. P.; Li, J.; Reijerkerk, S. R.; Foley, P.; Stöver, H. D. H.; Shirley, I. *Journal of Electron Spectroscopy and Related Phenomena* **2007**, *156*, 467-471. (b) Hong, K. J.; Park, S. M. *Materials Research Bulletin* **1999**, *34*, 963-969. (c) Jabbari, E. *Iranian Polymer Journal* **2001**, *10*, 33-43. (d) Lan, X. Z.; Yang, C. G.; Tan, Z. C.; Sun, L. X.; Xu, F. *Acta Physico-Chimica Sinica* **2007**, *23*, 581-584.

[12] Ni, P. H.; Zhang, M. Z.; Yan, N. X. *Journal of Membrane Science* **1995**, *103*, 51-55.

[13] Scher, H. B.; Shirley, I. M.; Chen, J.; Mazeaud, I.; Kanne, D. B.; Padget, J. C.; Wade, P.; Waller, A. *WO 01/94001 A2* **2001**

[14] El-Gibaly, I.; Anwar, A. *International Journal of Pharmaceutics* **2004**, *278*, 25-40.

[15] J. H. Xu, S. W. Li, J. Tan, Y. J. Wang, G. S. Luo, *Langmuir*, **2000** 19 7943-7946

[16] Nisisako, T.; Torii, T.; Higuchi, T. *Chemical Engineering Journal* **2004**, *101*, 23-29.

[17] J. L. Steinbacher, D. T. Mcquade, *J. Polym. Sci.: Part A: Polym. Chem*., **2006** 44, 6505–6533

[18] D. Qin., Y. N. Xia, G. M. Whitesides, *Adv Mater* **1996**, 8, 917.

[19] Y. N. Xia, G. M. Whitesides, *Angew Chem Int Ed* **1998**, 37, 551.

[20] E. Quevedo, J. Steinbacher. D. T. McQuade, *JACS*, **2005** 127 10498-10499

[21] Burke, N. A. D.; Mazumder, M. A. J.; Hanna, M.; Stöver, H. D. H. *Journal of Polymer Science Part a-Polymer Chemistry* **2007**, *45*, 4129-4143.

[22] (a) Mossberg, K.; Ericsson, M. *Journal of Microscopy*. **1990**, *158*, 215–224. (b) Carlsson, K.; Mossberg, K., *Journal of Microscopy* **1992** *167*, 23–37

CHAPTER 5 – DOUBLEY PH-RESPONSIVE PICKERING EMULSION

5.1 Introduction

Emulsifiers with on/off properties have attracted attention recently because of their potential applications in heavy oil transportation,[1] oil recovery,[2] and emulsion polymerization.[3] The surface activity of these emulsifiers can be well controlled, resulting in on/off switchability in response to stimuli such as CO_2,[3] pH,[4] temperature,[5] magnetic fields,[6] metal ions,[7] and redox changes.[8] Currently, there is growing interest in developing stimulus-responsive particulate emulsifiers for Pickering emulsions because of their significant advantages over conventional surfactant systems, with special attention given to pH-responsive particulate emulsifiers. Hence, pH-responsive latexes,[9] silica particles,[10] hydroxyapatite particles,[11] cross-linked micelles,[12] layered double hydroxide particles,[13] and others colloids have been explored for use as reversible emulsifiers. However, these pH-responsive emulsifiers usually require significant synthesis effort. Furthermore, practical applications such as heavy oil transportation and oil recovery require sizable quantities of stable, affordable, and nonhazardous emulsifiers.

In Pickering emulsions, the particle's surface chemistry plays a key role in stabilizing emulsions.[14] Particles of intermediate wettability by both phases promise to be good emulsifiers. Different approaches have been used to modify particle surfaces to

improve their performance as emulsifiers. Covalent modifications have been used to introduce amphiphilic structures onto particle surfaces.[14] For example, pH-responsive polymers were successfully attached to particle surfaces, allowing the surface activity of the particles to be controlled using pH.[9, 10, 12] The simple modification of hydrophilic particles by electrostatic interaction is another effective way to improve their surface activity.[16] Such electrostatic modifications are appealing because they are usually reversible and can respond to many factors such as pH, salt concentration, and electrolyte type.

Herein, we describe a simple and reversible particulate emulsifier based on commercially available hydrophilic alumina-coated silica nanoparticles and the pH-responsive behavior of this emulsifier driven by the reversible binding of a small-molecule surface modifier, potassium hydrogen phthalate (KHP).

5.2 Experimental Section

5.2.1 Materials

Ludox CL silica particle dispersion (CL particle dispersion, 30 wt % in H_2O) and xylene (a mixture of *para*-, *meta*-, and *ortho*-xylene) were obtained from Aldrich, and potassium hydrogen phthalate (KHP) was obtained from BDH. CL particles are silica core nanoparticles with a thin layer of alumina on surface, rendering the surface positively charged at pH values below 8.5. The average diameters of CL particles were determined to be 15 ± 2 nm by Binks.[17] All chemicals were used as received.

5.2.2 Methods

Preparation of Particle Suspensions

CL particle suspensions (2 wt %) with and without 0.25 wt % KHP were prepared by diluting a commercial 30 wt % CL particle suspension with deionized water, followed by the addition of KHP where required. The pH of each suspension was adjusted using either 30 wt % aqueous HCl or 30 wt % aqueous NaOH solution to cover the pH range from 1.5 to 11.5. A semimicro Thermo Orion PerpHecT combination pH electrode combined with a Corning model 440 benchtop pH meter was used to determine solution pH values. Photographs of particle suspensions were taken using a Canon PowerShot S5 IS digital camera.

Particle Mobility Measurements

Electrophoretic mobilities of particles were measured on a ZetaPlus zeta potential analyzer (Brookhaven Instruments Corp.). For mobility measurements, suspensions with no apparent flocculation were measured directly, whereas the ones with flocculation were centrifuged at 2000 rpm for 15 min using a Hermle Z323 universal high-speed centrifuge and the supernatants used for mobility determinations. The error bars of the electrophoretic mobilities represent the standard error of the mean value of 6 runs (15 cycles/run). No additional electrolytes were added for these measurements. For particle suspensions at pH 1.5, measurements were performed within 15 min of pH adjustments, and other samples were measured within 3 h.

Determination of the Adsorption Isotherm of KHP on CL Particles

To measure the adsorption isotherm for KHP on particle surfaces, 2 wt % particle suspensions with 0.25 wt % KHP at different pH values were subjected to ultracentrifugation for 50 min at 50 000 rpm at 25 °C using a Beckman L7-55 preparative ultracentrifuge within 30 min of pH adjustments. Supernatants from all solutions were then diluted and adjusted with 30 wt % NaOH to pH values between 11.3 and 12.3. UV−vis spectra of the solutions were obtained using a Cary 50 UV/vis spectrophotometer. The height of the peak at ~272 nm in each spectrum was recorded and compared to the control, and the adsorption isotherms were calculated.

Preparation of Emulsions

To prepare emulsions, 0.78 mL of a freshly prepared dispersion, with pH adjusted within 30 min, was transferred to a 3 mL glass vial containing 0.78 mL of xylenes. The mixtures were homogenized using a Dremel Moto-Tool equipped with a tungsten carbide cutter (catalog no. 9905) at ~13 000 rpm for 2 min. The spin rate was determined using an Ametek model 1726 dual function digital tachometer. Micrographs of the emulsions were taken from a drop of the emulsions deposited on a glass slide without dilution using an Olympus BX51 optical microscope fitted with a Q-Imaging Retiga EXi digital camera and ImagePro software. Both conductivity measurements and drop tests were used to confirm the presence of normal (oil-in-water) emulsions. The volume average droplet diameter obtained using laser diffraction, after dilution, was found to be 93 μm (See Appendix 5.6.1 for details).

5.3 Results and Discussion

5.3.1 Synergistic Effect between Ludox CL Particles and Potassium Hydrogen Phthalate

Recently, we observed that a stable xylene-in-water emulsion was formed in the presence of a suspension of CL particles having an alumina coating on the surface and a small amount of KHP, as shown in Figure 5.1.

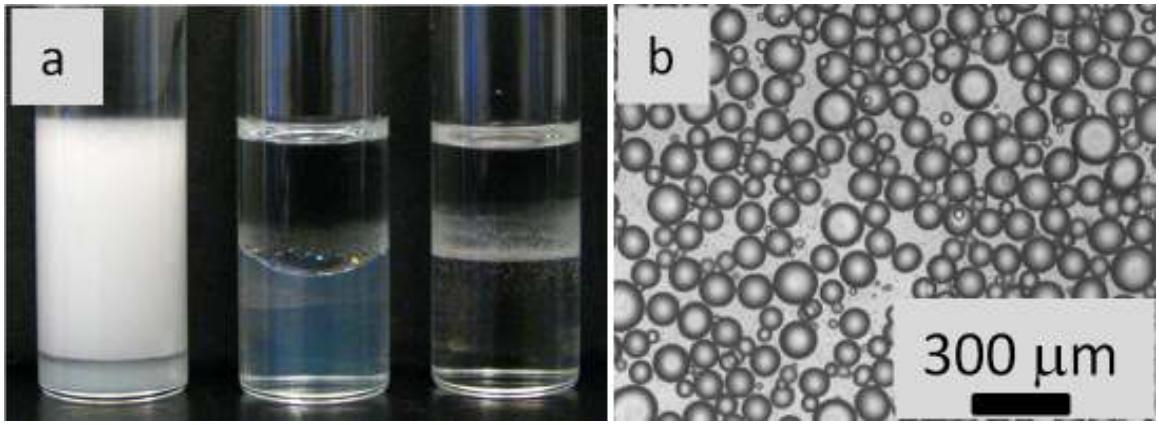

Figure 5.1 (a) Left vial: xylenes-in-water emulsion prepared using 2 wt % Ludox CL particles and 0.25 wt % KHP. Middle vial: attempt at forming an emulsion using 2 wt % Ludox CL only. Right vial: attempt at forming an emulsion using 0.25 wt % KHP only. The xylenes to aqueous phase ratio is 1:1, and the pH is 4.5 for each vial. (b) Optical microscope image of the stable emulsion from the left vial of (a).

Subsequent attempts to prepare emulsions using either CL particle suspensions or KHP solutions alone, at the same pH, proved unsuccessful, indicating synergy between the positively charged nanoparticles and KHP in the pH range used. This effect was attributed to the binding of phthalate anions to the positively charged particle surface,

increasing the particle hydrophobicity and enabling it to function as a Pickering emulsifier.

This electrostatic interaction between phthalate anions and CL particle surfaces offers an opportunity to design a pH-responsive emulsion system because both the ionization states of KHP (pK_a = 2.89 and 5.51)[18] and the charges on CL particle surfaces are pH-dependent. Accordingly, KHP binding to the particles would occur only within a certain pH range, with the resulting surface-active nanoparticles serving as Pickering emulsifiers. At more acidic pH values, neutral phthalic acid would predominate, and at more alkaline pH, the CL particles would gain a negative surface charge[18] and repel phthalate anions. Hence, at either extreme of the pH scale, electrostatic binding between KHP and CL nanoparticles would fail, and the particles would lose their ability to act as Pickering emulsifiers. Compared to other pH-responsive emulsion systems, this design is novel in that the emulsifier properties are driven by reversible pH-controlled binding between two inherently hydrophilic species.

A similar synergistic effect between particles and surfactants bearing opposite charges has been investigated in different systems by others.[16a-16d] The adsorption of surfactants onto hydrophilic particle surfaces was shown to increase the surface hydrophobicity, which led to particle flocculation and in turn enhances the particles' ability to stabilize emulsions. Although this synergy is probably also pH-tunable, it may be less favorable for designing pH-responsive systems because the surfactants alone would reduce the surface tension of the solution and stabilize the emulsion to some extent even in the absence of synergistic binding to particles.

In this study, the pH-dependent interaction between CL particles and KHP was investigated in detail with the aim of developing a pH-responsive Pickering emulsion system based on the reversible interaction between two simple components.

5.3.2 pH Dependence of the Interaction Between CL Particles and KHP

Electrophoretic mobilities of CL particles were measured to study particle suspensions with or without KHP at different pH values (Figure 5.2). The reversal point of the mobilities of CL particles has been reported to be around pH 8.5, reflecting the presence of a surface layer of aluminum hydroxide.[19]

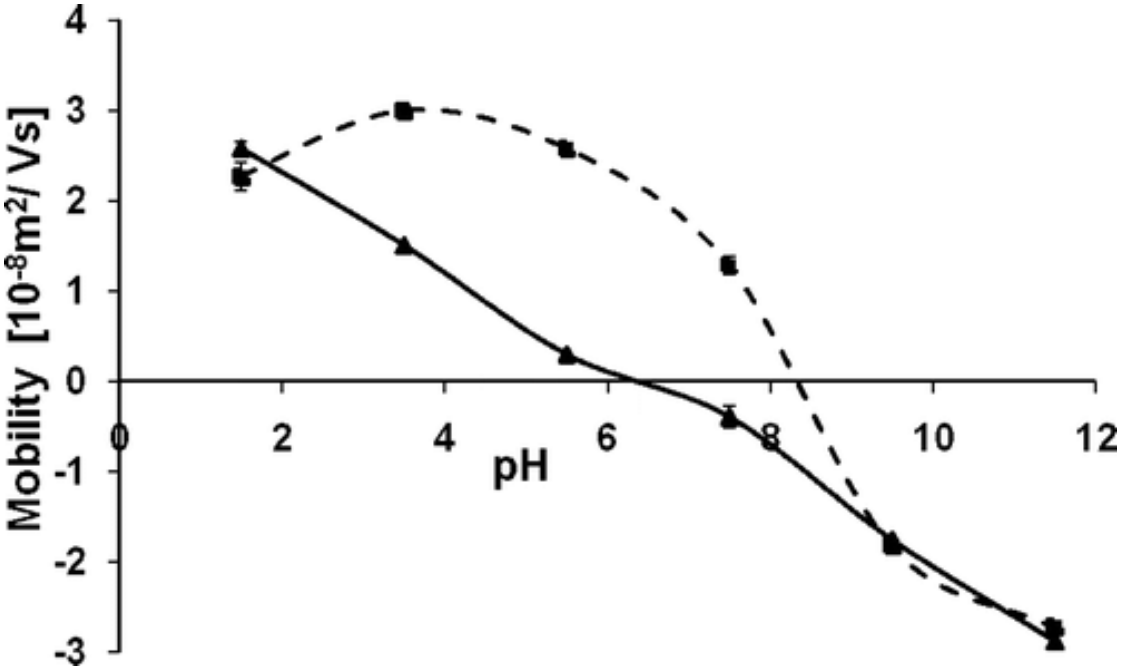

Figure 5.2 Electrophoretic mobility of CL particles in suspensions as a function of pH, both with (−) and without KHP (---). Lines are drawn to guide the eye.

A second reversal point is observed around pH 3 and attributed to the dissolution of the surface layer of alumina. Between pH 3.5 and 8.5, CL particles were positively charged because of the alumina layer on their surface. At pH 2.5, these particles showed a strongly negative surface charge, which was attributed to the slow desorption of aluminum from particle surfaces at low pH. This negative charge is more pronounced than the negative charge on pure silica nanoparticles (Ludox HS) at the same pH.[19] Our own results on Ludox CL nanoparticles showed only an IEP at about pH 8.5 and consistently positive charges down to pH 1.5 (Figure 5.2).

In the presence of KHP, the electrophoretic mobility of the particles decreases for pH values between 3.5 and 7.5. Within this pH range, the particles are positively charged and KHP is ionized, leading to the electrostatic adsorption of KHP on the particle surfaces, which lowers the positive charge density on the particle surfaces and in turn shifts the IEP from about pH 8.5 to roughly 6.3. A similar phenomenon was observed by Binks et al. in that when an anionic surfactant was absorbed on CL particle surfaces the particle zeta potential decreased in accordance with the amount of surfactant absorbed.[16c] At low pH (e.g., 1.5) and high pH (e.g., 9.5 and 11.5), the electrophoretic mobilities do not show any effect of KHP, implying no interaction between KHP and particles under these conditions, whereas in the intermediate pH range the electrophoretic mobility differences at the same pH reflect the extent of KHP binding to particle surfaces.

The adsorption of KHP on CL particles can also be studied by the depletion method using UV/vis spectroscopy. Figure 5.3 confirms that at both low (1.5) and high (9.5 and 10.5) pH KHP binding to particles is nearly zero, implying little interaction

between KHP and particles. At intermediate pH (3.5−7.5), binding takes place with a maximum of ~0.23 mg KHP/m^2 at about pH 5.5. This corresponds to ~40% of the total amount of KHP present in the system, with a surface density of ~0.56 KHP/nm^2.

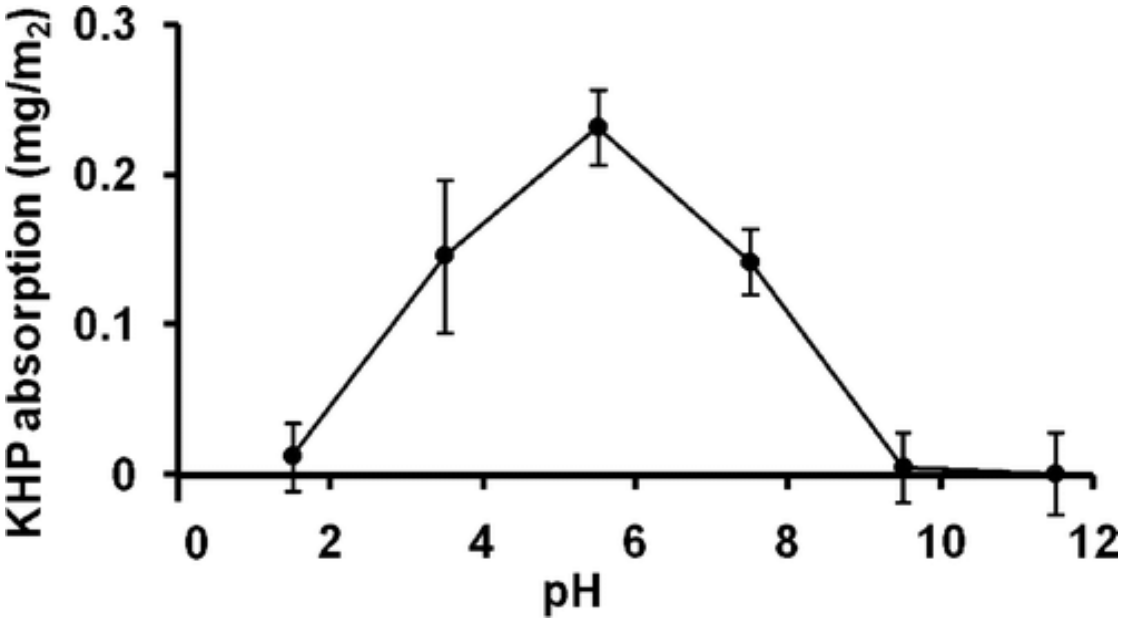

Figure 5.3 Absorption isotherm of KHP on CL particle surfaces at different pH values, measured by UV/vis spectroscopy. In all cases, suspensions contain 2 wt % CL particles and 0.25 wt % KHP.

Within the pH range of 3.5 to 7.5, the particles are positively charged, and hydrogen phthalate anions or phthalate dianions are bound to the particle surfaces. This result confirms our electrophoresis studies that indicate that the interaction between KHP and particles is limited to the pH range from 3.5 to 7.5.

To further evaluate the pH dependence of particle suspensions with or without KHP, photographs of particle suspensions in water at different pH values were taken (Figure 5.4). The upper row shows dispersions without KHP. Below pH 5.5, suspensions

are stable to flocculation and appear to be translucent, whereas above that pH particles flocculate, which turns the suspensions cloudy. In the presence of KHP, the suspension starts to turn cloudy at pH 3.5, and the cloudiness increases with pH. This shift of the cloud point to a lower pH can be attributed to the adsorption of KHP on the particle surfaces, which lowers the particle charge density and their colloidal stability, in accordance with the lowered IEP shown in Figure 5.2 for the presence of KHP. The proposed interactions between CL particles and KHP at different pH values are summarized in Scheme 5.1.

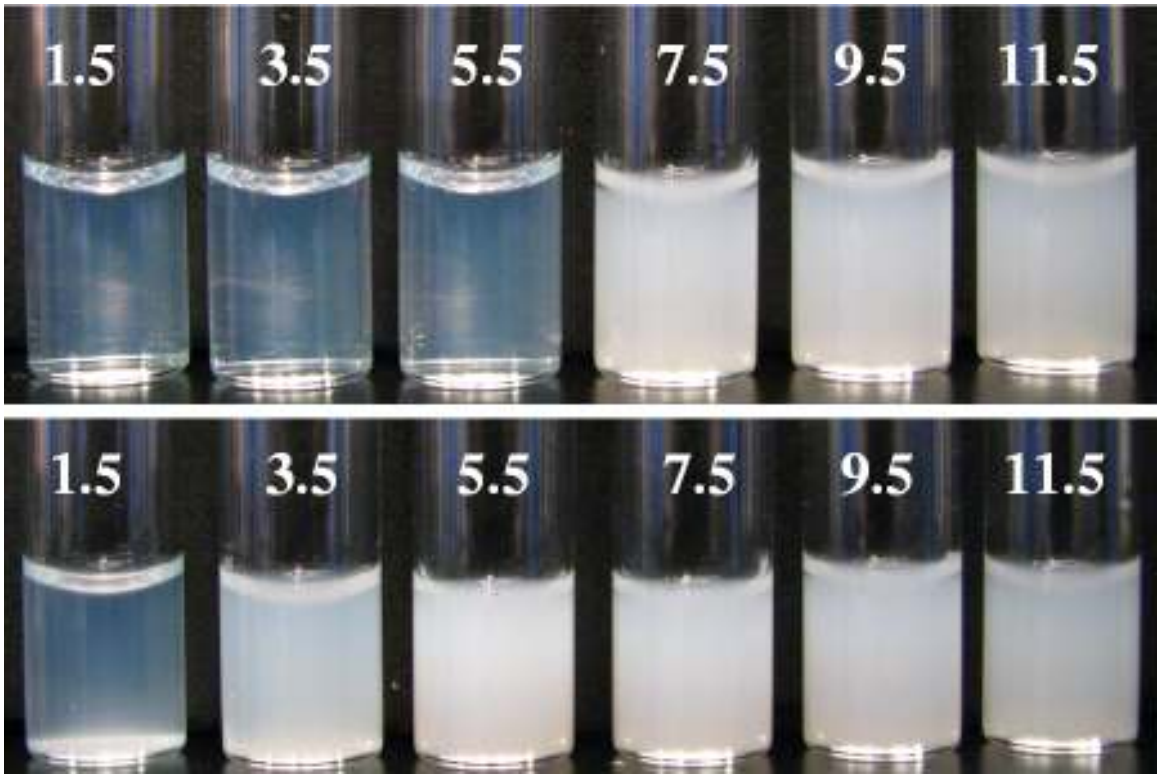

Figure 5.4 CL particle suspensions (2 wt %) at pH values ranging from 1.5 to 11.5, containing no KHP (upper row) and containing 0.25 wt % KHP (lower row). Images were taken within 30 min after the pH values were adjusted.

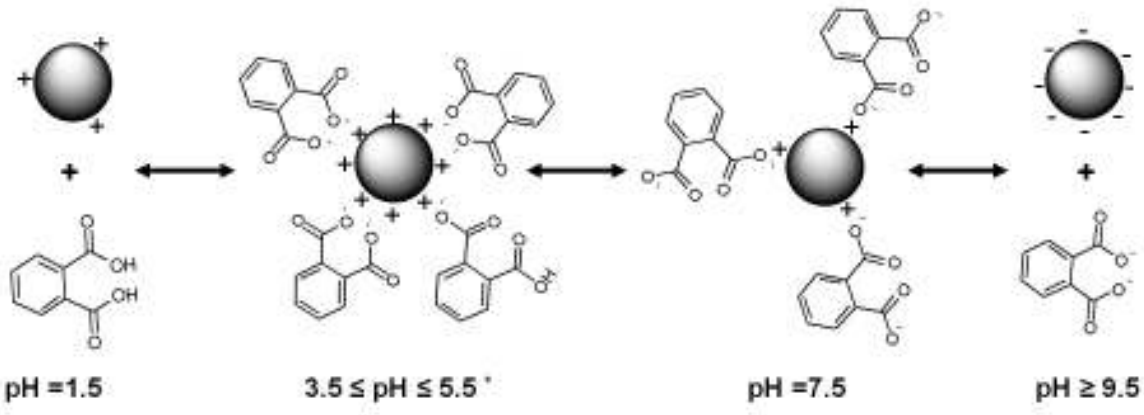

Scheme 5.1 Illustration of the pH-dependent interaction between CL particles and KHP. The asterisk (*) indicates that the ratio of hydrogen phthalate to the phthalate dianion absorbed on particle surfaces varies with pH.

5.3.3 pH Dependence of Emulsions

Knowing that the interaction between CL particles and KHP is pH-dependent, we started to examine the stability of xylene-in-water emulsions prepared at different pH values using CL particle suspensions with or without KHP in order to correlate the emulsion stability with particle−KHP interactions. In the absence of KHP (Figure 5.5, upper row), stable emulsions could not be formed within the pH range that we explored. Below pH 5.5, the hydrophilic CL particles are unable to stabilize the emulsions, and the two phases were resolved shortly after agitation ceased. As particles flocculate at higher pH, phase separation becomes sluggish, giving rise to relatively stable but coarse emulsions at both pH 7.5 and 9.5 with millimeter-sized emulsion droplets. This is probably due to low charge densities on the particle surfaces at these pH values, leading

to the formation of particle flocs that can stabilize emulsions to some extent,[20] resulting in incomplete gravity-driven coalescence. The further increase of pH to 11.5 expedites the separation due to particles regaining high charge densities on their surfaces, and two distinctive layers were formed soon after agitation ceased.

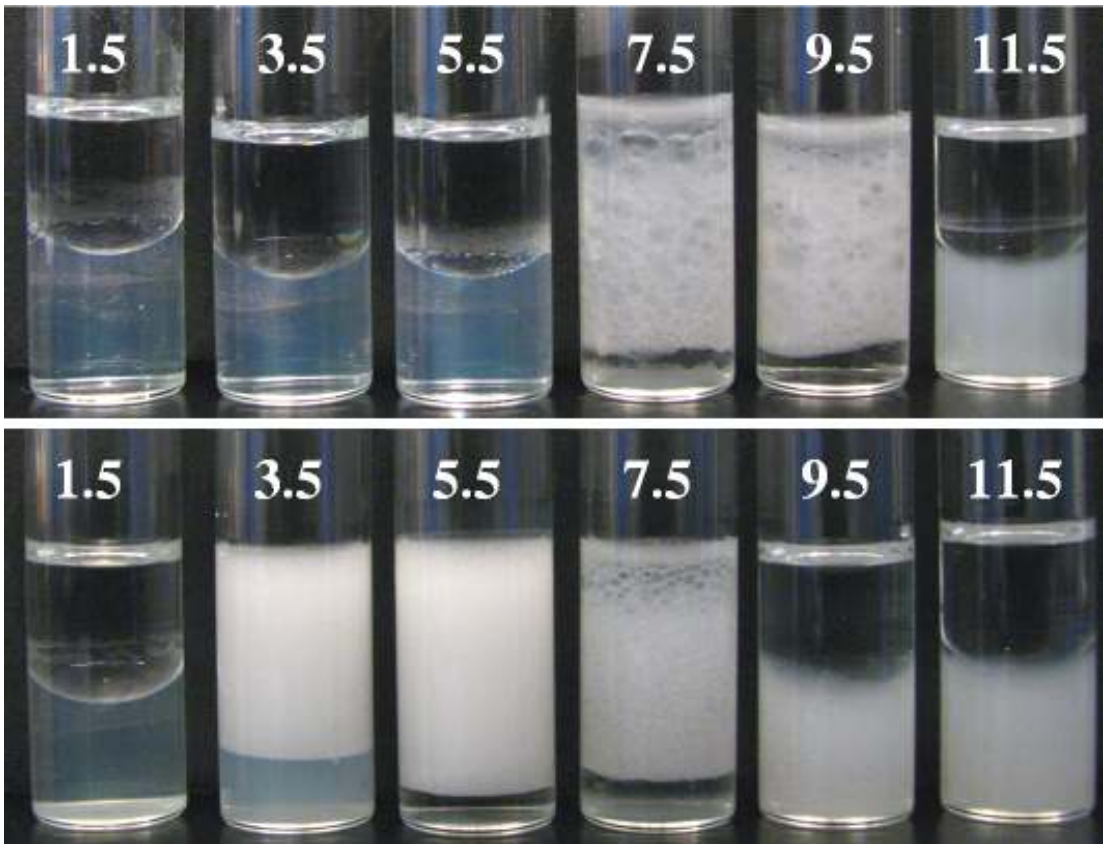

Figure 5.5 Xylene-in-water emulsions prepared at different pH values using 2 wt % CL particle suspensions in the absence of KHP (upper row) and in the presence of 0.25 wt % KHP (lower row). Volume ratio of xylenes to the aqueous phase is 1:1, and images were taken 48 h after emulsions were prepared.

When KHP is present, the emulsion stability is greatly improved at pH 3.5 and 5.5, as shown in the bottom row of Figure 5.5. This coincides with the pH range where the

extent of KHP adsorption on CL particle surfaces is high, which suggests that the emulsion stability is caused by the adsorption of KHP on CL particle surfaces. This adsorption lowers the particle charge density and increases its hydrophobicity, making the particle surfaces wettable by both phases. At pH 3.5, the emulsion is stable to coalescence but shows some creaming, whereas at pH 5.5 creaming decreases, which could be explained by the formation of a weak 3D network in the aqueous phase due to particle−particle interactions. Interestingly, at pH 7.5, fine emulsions cannot be prepared even though a significant amount of KHP has been absorbed on particle surfaces as proven by adsorption isotherm measurements. We attribute this to a complete ionization of KHP absorbed at this pH that renders the particle surfaces hydrophilic. At pH values where there are no particle−KHP interactions (e.g., 1.5, 9.5, and 11.5), quick phase separation is observed.

These results reflect a strong correlation between emulsion stability and KHP adsorption on particle surfaces. Emulsion stability increases with increasing amounts of absorbed KHP and can be tuned by pH changes.

5.3.4 Reversibility of Emulsification and Demulsification

To develop a pH-responsive emulsion system, it is vital that the emulsification/demulsification be reversible. To demonstrate this, a small amount of 1 M HCl was added to ~1.5 mL of an emulsion prepared at pH 4.5 in order to decrease the pH to 1.6. Demulsification took place quickly, resulting in the two separate layers shown in

Figure 5.6. Next, the same amount of 1 M NaOH was added to the solution to restore the pH to about 4.5, and subsequent homogenization for 2 min rendered a stable emulsion. This process was repeated five times without the loss of reversibility. It is known that the alumina layer on CL particle surfaces tends to dissolve at low pH values, leading to the loss of aluminum into solution. (See Appendix 5.6.2 for details.) To deal with this concern, we kept the emulsions at or below pH 1.5 for no more than 10 min per pH excursion to minimize aluminum loss. It has been suggested by Kuan et al. that the dissolved aluminum ions could precipitate again on particle surfaces upon increasing the pH,[21] which implies that the lost alumina could be restored on particle surfaces, making alumina loss a potentially reversible process.

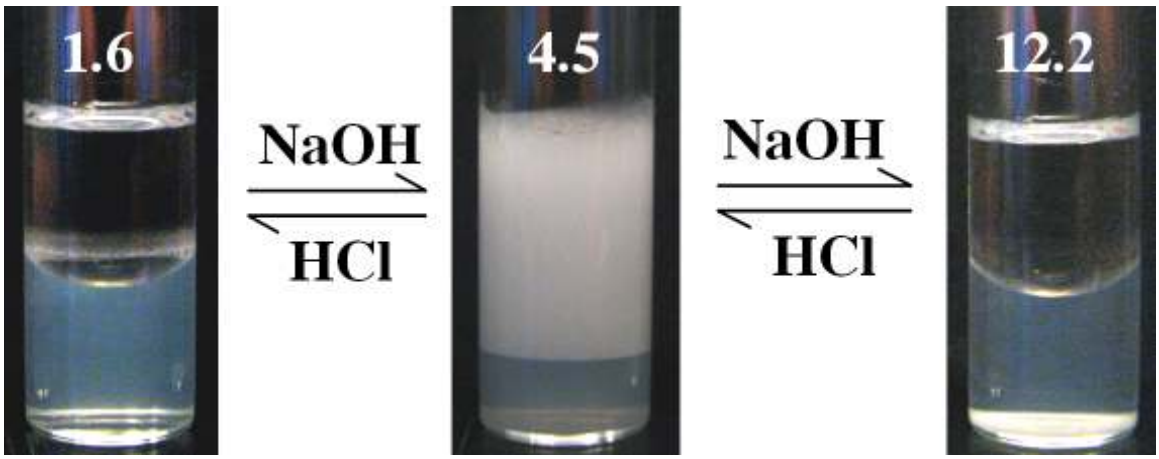

Figure 5.6 Demonstration of the reversibility of the emulsion system as a function of pH.

Similarly, demulsification can also happen at high pH. When 1 M NaOH was added to a stable emulsion prepared at pH 4.5 to increase the pH to 12.2, demulsification occurred. Adding the same amount of 1 M HCl brought the pH back to near the original

value and resulted in a stable emulsion upon agitation. This process was repeated five times without a noticeable change.

In summary, the stability of Pickering emulsions formed by combining cationic nanoparticles with KHP can be switched on and off reversibly by adding acid or base. To our knowledge, this is the first stimulus-responsive emulsion system that exhibits two reversible transitions with just one stimulus, pH change.

5.4 Conclusions

A pH-responsive Pickering emulsion system based on commercially available cationic silica particles has been described. The hydrophobicity of the particle surface can be increased by binding KHP at intermediate pH values. Dissociation of phthalate from the particle surface upon the addition of either base or acid leads to hydrophilic particles that are unable to stabilize the emulsions. Hence, at either high or low pH, emulsions are demulsified, whereas emulsions are stable in the pH range of 3.5−5.5. Thus, this system provides two reversible transitions using only one stimulus.

This synergy seems to be general and not limited to Ludox CL particles and KHP. We are currently investigating other combinations of colloids and non-surface-active organic ions having opposite charges.

5.5 References

[1] Langevin, D., Poteau, S., Henaut, I., and Argillier, J. F. *Oil Gas Sci. Technol.* **2004**, *59*, 511-521

[2] Masliyah, J., Zhou, Z. J., Xu, Z. H., Czarnecki, J., and Hamza, H. *Can. J. Chem. Eng***. 2004**, *82,* 628-654

[3] Liu, Y., Jessop, P. G., Cunningham, M., Eckert, C. A., and Liotta, C. L. *Science* **2006**, *313*, 958-60

[4] Mathur, A. M., Drescher, B., Scranton, A. B., and Klier, J. *Nature* **1998***, 392*, 367-370

[5] (a) Ngai, T., Behrens, S. H., and Auweter, H. *Chem. Commun*. **2005**, 331-333 (b) Ngai, T., Auweter, H., and Behrens, S. H. *Macromolecules* **2006**, *39*, 8171-8177 (c) Tsuji, S., and Kawaguchi, H. *Langmuir* **2008**, *24*, 3300-3305 (d) Brugger, B., and Richtering, W. *Langmuir* **2008**, *24*, 7769-7777 (e) Binks, B. P., Murakami, R., Armes, S. P., and Fujii, S. *Angew. Chem., Int. Ed*. **2005**, *44*, 4795-4798

[6] Melle, S., Lask, M., and Fuller, G. G. *Langmuir* **2005**, *21*, 2158-2162

[7] Dexter, A. F., and Middelberg, A. P. J. *J. Phys. Chem. C* **2007**, *111*, 10484-10492

[8] Schmittel, M., Lal, M., Graf, K., Jeschke, G., Suske, I., and Salbeck, J. *Chem. Commun*. **2005**, 5650-5652

[9] (a) Amalvy, J. I., Armes, S. P., Binks, B. P., Rodrigues, J. A., and Unali, G. F. *Chem. Commun*. **2003**, 1826-1827 (b) Amalvy, J. I., Unali, G. F., Li, Y., Granger-Bevan, S., Armes, S. P., Binks, B. P., Rodrigues, J. A., and Whitby, C. P. *Langmuir* **2004***, 20*, 4345-4354 (c) Read, E. S., Fujii, S., Amalvy, J. I., Randall, D. P., and Armes, S. P. *Langmuir* **2004**, *20*, 7422-7429 (d) He, X. D., Ge, X. W., Liu, H. R., Deng, M. G., and Zhang, Z. C. *J. Appl. Polym. Sci.* **2007**, *105*, 1018-1024

[10] (a) Fujii, S., Read, E. S., Binks, B. P., and Armes, S. P. *Adv. Mater*. **2005**, *17*, 1014−1018 (b) Motornov, M., Sheparovych, R., Lupitskyy, R., MacWilliams, E., Hoy, O., Luzinov, I., and Minko, S. *Adv. Funct.Mater.* **2007**, *17*, 2307-2314

[11] Fujii, S., Okada, M., and Furuzono, T. *J. Colloid Interface Sci.* **2007**, *315*, 287-296

[12] Fujii, S., Cai, Y., Weaver, J. V., and Armes, S. P. *J. Am. Chem. Soc.* **2005**, *127*, 7304-7305

[13] Yang, F., Niu, Q., Lan, Q., and Sun, D. J. *J. Colloid Interface Sci.* **2007***, 306*, 285-295

[14] Binks, B. P. *Curr. Opin. Colloid Interface Sci*. **2002**, *7*, 21-41

[15] (a) He, X. D., Ge, X. W., Wang, M. Z., and Zhang, Z. C. *J. Colloid Interface Sci.* **2006**, *299*, 791-796 (b) Binks, B. P., and Lumsdon, S. O. *Langmuir* **2000**, *16*, 8622-8631

[16] (a) Tambe, D. E., and Sharma, M. M. *J. Colloid Interface Sci*. **1993**, *157*, 244-253 (b) Binks, B. P., Desforges, A., and Duff, D. G. *Langmuir* **2007***, 23*, 1098-1106 (c) Binks, B. P., Rodrigues, J. A., and Frith, W. J. *Langmuir* **2007**, *23*, 3626-3636 (d) Binks, B. P., and Rodrigues, J. A. *Langmuir* **2007**, *23*, 7436-7439 (e) Binks, B. P., Liu, W., and Rodrigues, J. A. *Langmuir* **2008**, *24*, 4443-4446

[17] Binks, B. P.; Liu, W. H.; Rodrigues, J. A. *Langmuir* **2008**, *24*, 4443-4446

[18] CRC Handbook of Chemistry and Physics, 55th ed.; Weast, R. C., Ed.; *CRC Press*: Cleveland, OH, **1974−1975**; D130.

[19] Van der Meeren, P., Saveyn, H., Kassa, S. B., Doyen, W., and Leysen, R. *Phys. Chem. Chem. Phys*. **2004**, *6*, 1408-1412

[20] Tambe, D. E., and Sharma, M. M. *Adv. Colloid Interface Sci.* **1994**, *52,* 1-63

[21] Kuan, W. H., Lo, S. L., and Wang, M. K. *Water Sci. Technol*. **2000**, *42,* 441-446

5.6 Appendix

5.6.1 Emulsion Characterization

The type of emulsion was evaluated by both conductance measurement and the conductance was obtained using the conductance function in the ZetaPlus zeta potential analyzer. The emulsion made at pH 4.5 was tested directly and conductance was 1.628×10^3 μS under the applied voltage of 7.54, which shows that aqueous phase is the continuous phase and a xylene-in-water emulsion is established. Supporting evidence came from a "drop test". A drop of emulsion was added into 10mL water and a nice dispersion was formed immediately, indicating that water is the continuous phase in the emulsion.

Particle size distribution was determined using Malvern Mastersizer 2000 coupled with Hydro 2000G large volume wet sample dispersion unit. The refractive index of emulsion droplet was estimated to be 1.395. About 1.5 mL of xylene-in-water emulsion made by 2 wt % CL particle dispersion with 0.25 wt % KHP at pH 4.5 was added into 500 mL water with pH 4.5. Three sequential measurements were performed to get an average emulsion size of 93 μm.

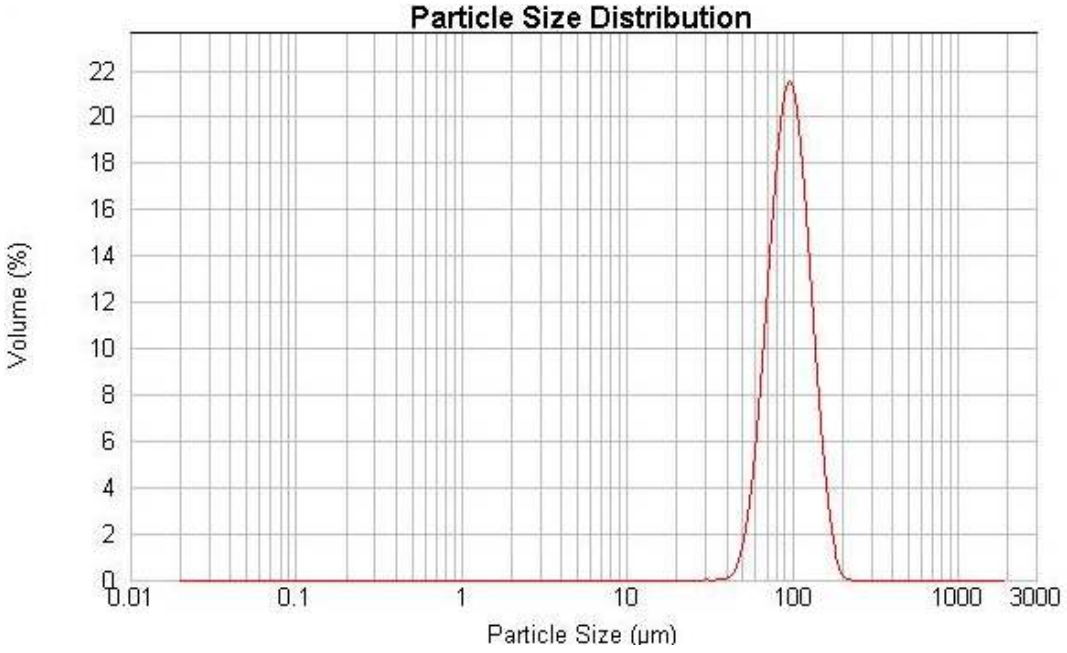

Figure 5A.1 Emulsion droplet size distribution plot obtained using Malvern Mastersizer 2000

5.6.2 Dissolution of Alumina Layer on CL Particle Surfaces at Low pH

To test the stability of alumina layer at low pH, we adjusted the pH of 2 wt % CL particle suspension to 1.5 and then observed the pH change vs. time.

As we can see in Figure 5A.2 that suspension pH increases with time and the increase rate decreases significantly with time. This is probably due to the dissolution of alumina layer on particle surfaces at low pH. The dissolution process consumes proton in solution, leading to pH increase. The dissolution happens fast during the first 10 hrs and then slows down at longer hours until it reaches the equilibrium between the alumina layer on particle surfaces and aluminum concentration in solution. Zeta potential of the suspension after 30 hrs still showed positive value, implying that there was still alumina

on particle surfaces. So in order to minimize alumina loss of particle surfaces, it is important to keep the particle suspension at low pH for a shorter time.

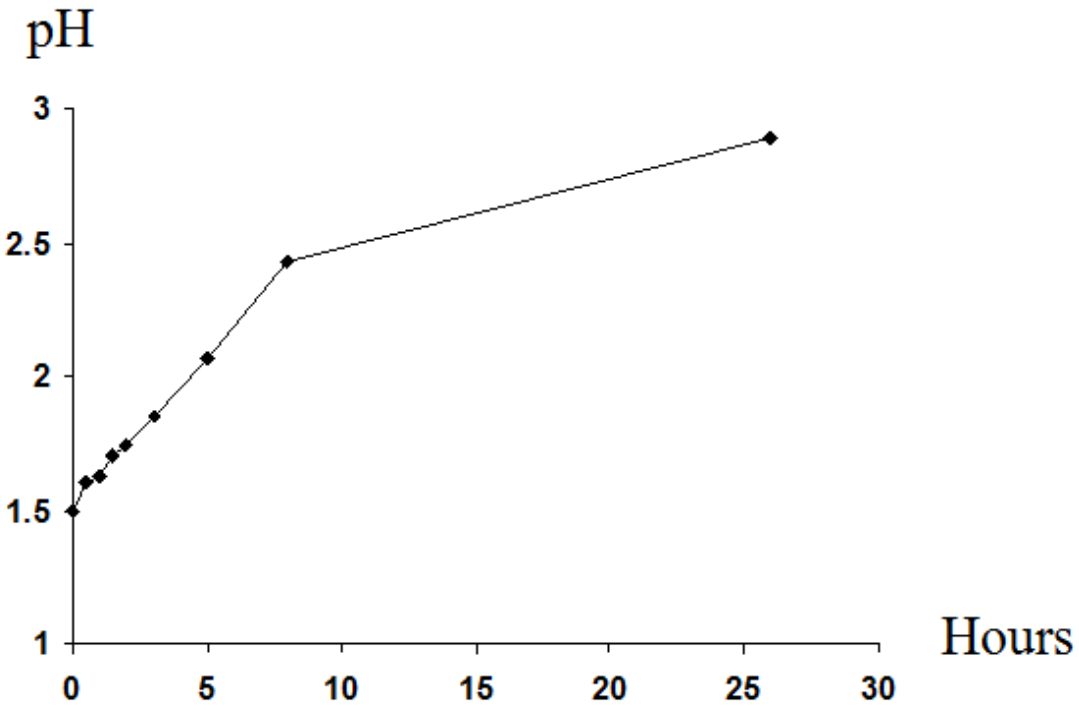

Figure 5A.2 The pH development of 2 wt % CL particle suspension starting at pH 1.5 with time

CHAPTER 6 - PICKERING EMULSION TEMPLATED LAYER-BY-LAYER ASSEMBLY FOR MAKING MICROCAPSULES

6.1 Introduction

Nano- and microcapsules are attracting much attention due to their potential applications in controlled drug delivery,[1] self-healing materials,[2] catalysis,[3] pests control,[4] and other areas.[5] Methods for making capsular structures include interfacial condensation polymerization,[6] in-situ radical polymerization,[7] internal phase separation,[8] coacervation,[9] and colloids-templated layer-by-layer (CT-LbL) assembly.[10] Among them, colloids-templated LbL assembly features mild fabrication conditions, a simple procedure, and precise control over wall composition and thickness, making it promising for a wide range of applications. The method involves LbL deposition of wall materials onto sacrificial colloidal templates that are subsequently removed by chemical or physical methods to afford hollow capsules. Since its inception in 1998,[11] a variety of templates,[12] wall materials,[13] and assembly methods[14] have been developed to make capsules with a wide spectrum of properties.[15] The often monodisperse solid templates allow precise control over capsule size and distribution but need to be removed before desired core materials can be loaded into the capsules. The core removal processes can affect capsule integrity and wall properties,[10b] while postloading is challenging in many cases. While

elegant attempts have been made to postload capsules,[16] general solutions are still needed that allow filling hollow LbL capsules efficiently with desired materials.

One route to improve the CT-LbL technique is to use gel particles[14d] and emulsions[17] that allow for the incorporation of encapsulants into the core prior to LbL assembly, eliminating the need for separate template removal and postloading. Although gel particle templates can provide high encapsulation efficiency and good stability for LbL assembies,[18] the gelled core can cause an undesirable decrease of mobility of the encapsulated materials within capsules and make the capsules more temperature sensitive. The use of emulsions as templates thus appears to be attractive, as core materials can be easily incorporated in the dispersed phase, and the emulsion droplets could be used directly as templates for LbL assemblies without further treatments, resulting in readily usable liquid-core capsules.

There have been numerous attempts to use emulsions as templates for LbL assemblies. One example used gas-in-water emulsions to template the formation of gas core microcapsules via LbL polyelectrolyte assembly, with the resultant microcapsules used as ultrasonic contrast agents.[19] Most efforts have been aimed at forming shells around surfactant-stabilized oil-in-water emulsions where the dispersed hydrophobic phase is or contains the key encapsulant. McClements and co-workers used oppositely charged biopolymers to coat lecithin-stabilized food emulsions in order to improve emulsion stability.[20] Caruso and co-workers coated sodium dodecyl sulfate stabilized emulsions of liquid crystals with LbL assemblies of polyelectrolytes and removed the liquid crystal core by dissolution in ethanol to obtain hollow capsules.[21] Grigoriev and co-

workers coated didodecyldimethylammonium bromide stabilized oil-in-water emulsions with polyelectrolytes to produce microcapsules.[22] Nanocapsules were also fabricated through LbL assembly using surfactant-stabilized emulsions as templates.[23] Although hollow capsules were successfully obtained in all cases, caution had to be exercised to prevent emulsions from coalescing in the early stage of LbL assemblies. The relative instability of these emulsions stems from the possibility for desorption of the surfactants from the oil−water interfaces, especially in the presence of added polyelectrolytes. It would hence be desirable to explore LbL capsule formation based on primary emulsions stabilized by more strongly held interfacial agents.

Pickering emulsions are emulsions stabilized by solid particles localized at the oil−water interface.[24] They are often more stable than conventional emulsions, as the particles at the oil−water interface exert steric hindrance and, in some cases, electrostatic repulsion to prevent emulsions from coalescing. In many cases, particle adsorption at the interface is deemed irreversible as the adsorption energy is much higher than the thermal energy, rendering extremely high emulsion stability.[25] The use of Pickering emulsions for making microcapsules has been explored extensively, involving interlocking interfacially anchored particles using various methods to afford the so-called colloidosomes.[26] Although such interlocking can fix the particles at the interface,[27] interstitial pores between particles remain and need to be dealt with when designing slow or controlled release systems.[28]

In this chapter, we explore the use of Pickering emulsions as templates for electrostatic LbL assemblies in order to make microcapsules. The high stability of the

Pickering emulsions would allow use of handling methods common for solid templates. Successive coatings with polyelectrolytes and charged nanoparticles may make it possible to cover the interstitial pores, resulting in microcapsules with tighter capsule walls.

6.2 Experimental Section

6.2.1 Materials

Ludox CL silica particle dispersion (CL particle dispersion, 30 wt % in H_2O), Ludox HS-30 silica particle dispersion (HS particle dispersion, 30 wt % in H_2O), xylenes (a mixture of *p*-, *m*-, and *o*-xylene), poly(sodium styrenesulfonate) (PSS, M_w ~200,000), poly(diallyldimethylammonium chloride) (PDADMAC, M_w ~ 400 000−500 000), trimethylolpropane triglycidyl ether (TTE), and 4,4′-methylenebis(2-methylcyclohexylamine) (MBMCA) were obtained from Aldrich. All chemicals were used as received. CL particles are silica core nanoparticles with a thin layer of alumina on surface, rendering the surface positively charged at pH values below 8.5. HS particles are silica nanoparticles with negatively charged surface. The average diameters of CL and HS particles were determined to be 15 ± 2 nm by Binks.[29]

6.2.2 Materials

Preparation of Particle/PSS Suspensions

PSS-modified CL particle suspensions were prepared by combining 1 mL of 4 wt % CL particle suspensions with equal volumes of PSS solutions of different

concentrations. The resulting suspensions were manually shaken for 30 s. The pH of each suspension was adjusted to ~4.5 using 30 wt % aqueous HCl. A semimicro Thermo Orion PerpHecT combination pH electrode combined with a Corning Model 440 Benchtop pH meter was used to determine solution pH values. Photographs of particle suspensions were taken using a Canon PowerShot S5 IS digital camera 7 days after their preparation. The extent of CL particle aggregations after PSS modification was evaluated using a Malvern Mastersizer.

Emulsion Preparation

1.40 mL of 2 wt % CL particle suspension was added into a 3 mL glass vial containing 0.21 mL of organic solvent. The mixtures were homogenized using a Dremel Moto-Tool equipped with a tungsten carbide cutter (catalog no. 9905) at ~16 000 rpm for 2 min. The spin rate was determined using an AMETEK model 1726 dual function digital tachometer. Micrographs of the emulsions were taken from a drop of the emulsions deposited on a glass slide without dilution, using an Olympus BX51 optical microscope fitted with a Q-Imaging Retiga EXi digital camera and ImagePro software. Photographs of emulsions were taken 7 days after their preparation.

Cleaning Primary Pickering Emulsions

Xylene-in-water emulsions made from a mixture containing 2 wt % CL particles and 0.25 wt % PSS were used as templates for subsequent LbL depositions. Emulsions from eight individual batches were combined in a 50 mL centrifuge tube and diluted to 45 mL with deionized water. The resulting emulsion was centrifuged at 1000 rpm for 5 min and then decanted from sedimented CL particles. The emulsion was again centrifuged to

facilitate creaming, and the excess liquid was removed from the bottom using a syringe to reduce the volume of the emulsion to ~2.5 mL. This dilution/sedimentation cycle was repeated two more times. The mean size of the clean emulsion droplets was obtained by averaging the sizes of over 200 emulsion droplets that were manually measured using the optical microscope.

Microcapsule Fabrication via Layer-by-Layer Assemblies

2.5 mL cleaned Pickering emulsions were placed in a 50 mL centrifuge tube. 40 mL of 0.2 wt % PDADMAC in 0.5 M NaCl was added, and the mixture was mounted on a rotator (Glas-Col) at 60 rpm for 30 min. The mixture was creamed by centrifugation at 1000 rpm for 5 min, and the excess liquid was removed from the bottom by syringe. The resulting concentrated emulsion was washed twice by addition of 40 mL of deionized water followed by centrifuge-assisted creaming. The resulting cleaned, PDADMAC-coated Pickering emulsion was then exposed to 40 mL of 0.2 wt % PSS in 0.5 M NaCl in a process as used for the PDADMAC coating, including two washing steps. This coating sequence was repeated until four double layers of polyelectrolytes had been deposited. In the case of nanoparticle coatings, the PSS solution was replaced by equal volumes of 2 wt % HS particle suspensions. For optical microscopy imaging, microcapsule suspension was manually shaken before an aliquot of sample was taken from the center of suspension. A drop of such suspension was placed on a microscope slide, and the slide was slightly tilted to briefly spread the drop right before imaging by a Olympus BX51 optical microscope. Dry state images of microcapsules were taken after the microcapsules were fully dried on the slide.

Mobility Tests

Electrophoretic mobilities of particles and microcapsules were measured on a ZetaPlus zeta-potential analyzer (Brookhaven Instruments Corp.). In the case of CL particle suspensions, suspensions with different PSS concentrations were tested directly without adding extra electrolytes. The error bars of the electrophoretic mobilities represent the standard error of the mean value of 10 runs (15 cycles per run). To measure the mobilities of microcapsules, clean capsules were resuspended in 2.5 mM KCl solution, and the error bars stand for the standard error of the mean value of three runs (15 cycles per run).

TEM Imaging of Microcapsule Wall Cross Sections

Microcapsules were washed by adding 10 mL of ethanol to 0.5 mL of concentrated microcapsule suspension and removing the supernatant after the microcapsules have settled. This washing process was repeated once, and the microcapsules were allowed to dry in the air. For embedding, the dried microcapsules were transferred into BEEM embedding molds, followed by the addition of a mixture of TTE and MBMCA (1:1 weight ratio). The mixture was cured at 70 °C for 3 days before the embedding blocks were taken out of the BEEM embedding molds. Thin (60−80 nm) sections of the embedding blocks were cut with a Leica Ultracut UCT ultramicrotome and picked up onto Cu Formvar-coated grids and viewed with a JEOL JEM 1200 EX TEMSCAN transmission electron microscope operated at an accelerating voltage of 80 kV. For cryo-microtoming, a drop of microcapsule suspension was added to a small drop of 2 M sucrose solution on a cryopin which was then plunge-frozen in liquid nitrogen.

The pin was placed in a precooled (−110 °C) cryochamber fitted onto a Reichert Ultracut E ultramicrotome and cut to form 100−200 nm thick frozen sections. The sections were transferred to formvar-coated TEM grids via a wire loop filled with frozen sucrose solution, and the grids were placed into water baths to remove the sucrose. The sections were air-dried prior to viewing by TEM.

6.3 Results and Discussion

6.3.1 Particle Surface Modification and Pickering Emulsion Preparation

The use of Pickering emulsions as templates for LbL assemblies of polyelectrolytes requires charged emulsion droplet surfaces. Inorganic particles are good candidates for such Pickering emulsifiers as they are often charged. There are many methods available for producing inorganic particles with controlled particle size and distribution[30] as well as methods for hydrophobizing these usually hydrophilic particles in order to make them surface active.[24] Covalently attaching hydrophobic modifiers onto particle surfaces[31] often requires significant effort and must be well controlled to keep it within the desirable range. Electrostatic deposition of charged surfactants to oppositely charged particles has been used successfully to modify inorganic particle surfaces,[32] though the subsequent emulsification was complicated by competitive adsorption of both surfactants and particles at the interface. Recently, we[33] and others[34] reported using small organic electrolytes that are not very surface active by themselves to modify inorganic particle surfaces in order to make Pickering emulsifiers. These modifiers can lower the

charge density on particle surfaces and introduce hydrophobic groups, which makes the particles surface active. At the same time, free modifiers do not compete with particles in adsorbing at the interface. Our approach involved a Pickering emulsion system based on potassium hydrogen phthalate (KHP) modified Ludox CL particles as emulsifiers.[33] In the current work, the same system was explored first and the resulting emulsion used to template LbL assembly of polyelectrolytes. However, significant emulsion coalescence was observed when the emulsions were diluted during washing, which was attributed to loss of KHP from the CL particle surfaces.[33]

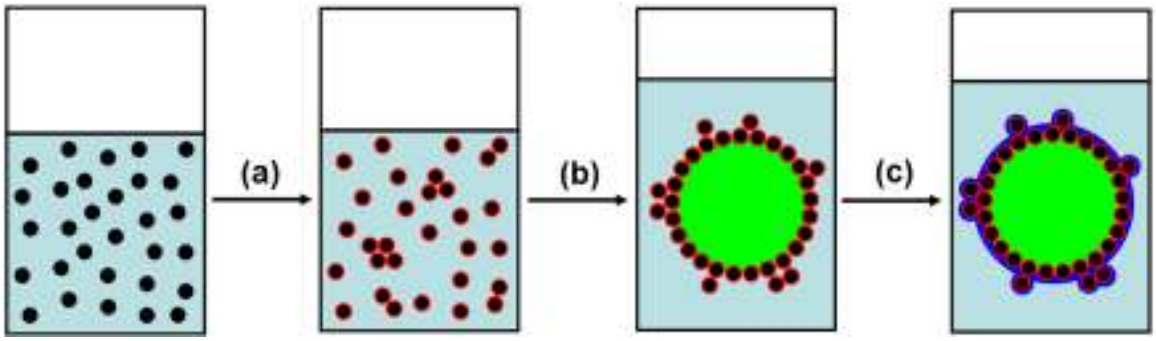

Scheme 6.1 Formation of microcapsules by LbL assembly on pickering emulsion surfaces: (a) CL particle surface modification using PSS; (b) emulsification to form oil-in-water pickering emulsions; (c) LbL assemblies of polyelectrolytes To form microcapsules. Note: particles and capsules are not drawn to scale.

To overcome this problem associated with small organic electrolytes as modifiers, we here explore the use of polymeric modifiers that should bind irreversibly with oppositely charged particle surfaces. The resulting polyelectrolyte-modified particles

should form stable Pickering emulsions that could serve as robust templates for LbL assembly of further polyelectrolytes, as shown in Scheme 1.

In this study, poly(sodium styrenesulfonate) (PSS) was selected as the polymeric modifier as it should complex with positively charged CL particle surface. CL particle suspensions were added to PSS, followed by vigorous manual shaking for 30 s and the pH of these particle suspensions were adjusted to ~4.5 using a concentrated HCl solution. The reason for the pH adjustment is that we previously observed that electrostatic modifications on charged particles could be modulated by pH, causing changes of stability of the corresponding emulsions.[33] Therefore, in this study, we kept the pH of suspensions constant in order to avoid the implications of pH change on the stability of resulting emulsions, and the pH at 4.5 ensures sufficient positive charge on CL particle surfaces to facilitate PSS binding.[33]

The net charges on the CL particles before and after PSS modifications were studied using electrophoretic mobility tests. As shown in Figure 6.1, the average charge on the CL particles changed from positive to negative with increasing PSS concentration, which suggests that the amount of PSS electrostatically adsorbed on CL particle surfaces increased with increasing PSS concentration. The isoelectric point was reached around 0.25 wt % of PSS, while above 0.5 wt % PSS the mobility leveled off, indicating saturation of PSS on CL particle surfaces.

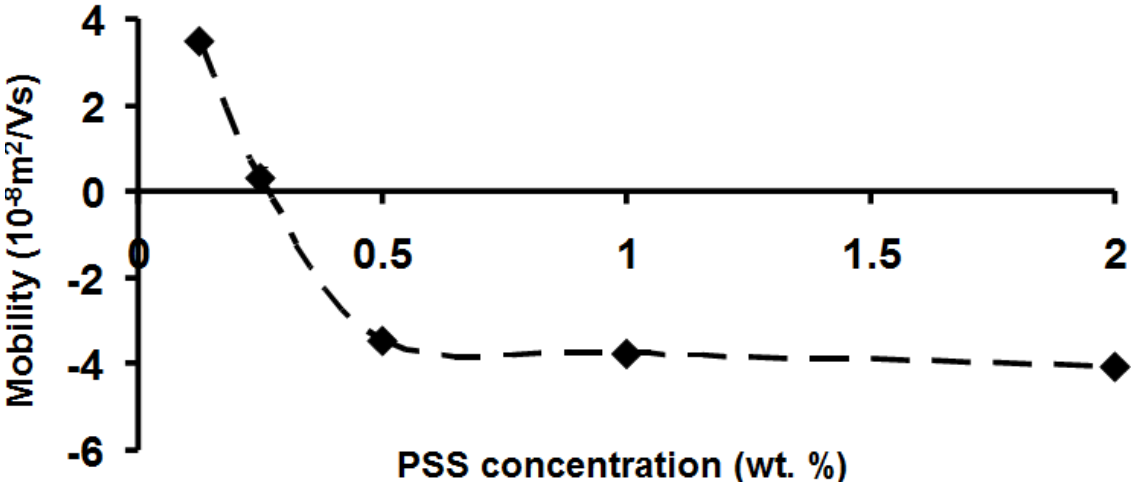

Figure 6.1 Plot of electrophoretic mobility of CL particles vs PSS concentration. The line is drawn to guide the eye.

Figure 6.2a shows 2.0 wt % CL particle suspensions modified with different amounts of PSS. The CL particle suspension without PSS was transparent with a bluish color. Upon mixing with PSS, particle suspensions turned cloudy due to particle aggregation, which led to particle sedimentation with time. The apparent volume of aggregates reaches a maximum at 0.25 wt % PSS (the volume average diameter of these aggregates in the absence of shearing is 15.8 μm, and the size distribution is shown in Appedix Figure 6A.1), near the isoelectric point, and then decreases upon addition of further PSS. Some aggregate persists even at high PSS concentrations. The fact that aggregates may not redisperse after passing through the isoelectric point during coating could be attributed to the bridging effect of the high molecular PSS or the depletion flocculation of particles in close proximity.[35]

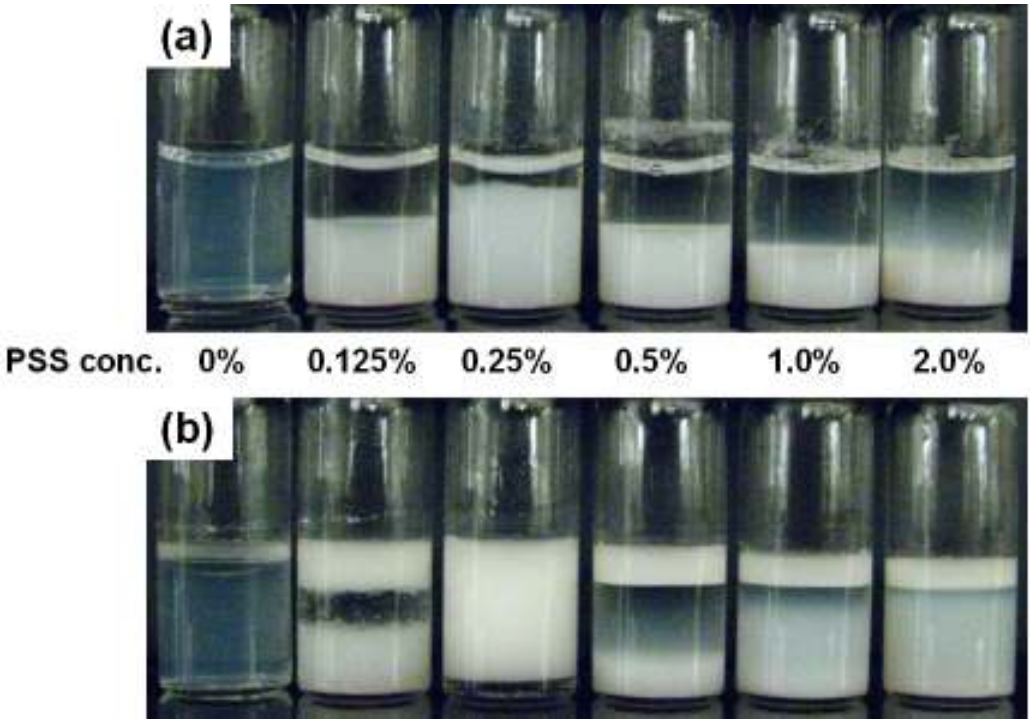

Figure 6.2 Photographs of (a) CL particle suspensions with different PSS concentrations. CL particle concentration was set to 2.0 wt %. (b) Attempted xylene-in-water emulsions made from corresponding particle suspensions. Volume ratio of xylene to aqueous particle suspension was 3:20.

CL particles with different levels of PSS modification were then used as Pickering emulsifiers to make xylene-in-water emulsions, using a volume ratio of xylene to aqueous phase of 3:20. As shown in Figure 6.2b, CL particles without PSS modification did not lead to emulsification. This is due to the hydrophilic nature of the CL particle surfaces and is consistent with previous studies.[32a] PSS modification increases the surface activity of the CL particles, leading to stable xylene-in-water emulsions at all PSS concentrations tested (from 0.125 to 2.0 wt %). However, PSS alone did not lead to stable emulsions. CL

particles coated with 0.25 wt % PSS resulted in the most stable emulsions, which is attributed to their near zero net charge, as was seen in other cases.[32a] Above and below 0.25 wt % PSS modification, CL particle surface charge increased significantly as shown by Figure 6.1, leading to more hydrophilic surfaces and thus less stable emulsions. Addition of sodium hydroxide to test the pH response showed that the emulsion made from 0.25 wt % PSS modified CL particles remained stable up to pH 9.5. In previous studies, we showed that KHP-modified CL particles were good Pickering emulsifiers only within pH 3.5 to 5.5, while in this study, the pH range for stable emulsions was extended to much more alkaline values. This is likely due to enhanced interaction between the polymeric modifier and particle surface, which made the emulsion less susceptible to the pH change.

Table 6.1 Solubility Parameters of Selected Solvents for Making Pickering Emulsions

Solvent	Perfluoro-heptane	Heptane	n-Butyl acetate	Xylene	Chloroform
Solubility parameter/ δ(cal/cm^3)$^{1/2}$ [36]	5.8	7.4	8.5	8.8	9.3
Density (g/mL)[37]	1.745	0.684	0.880	0.868	1.492

In addition to stabilizing xylene-in-water emulsions, the use of CL particles modified with 0.25 wt % PSS was also explored for the preparation of Pickering emulsions involving different organic phases. Solvents with a range of solubility

parameters (shown in Table 1) were chosen to represent fills with different polarity. In all cases, stable emulsions were obtained regardless of the polarity of the solvents, and the photograph of corresponding emulsions is shown in Appendix Figure 6A.2.

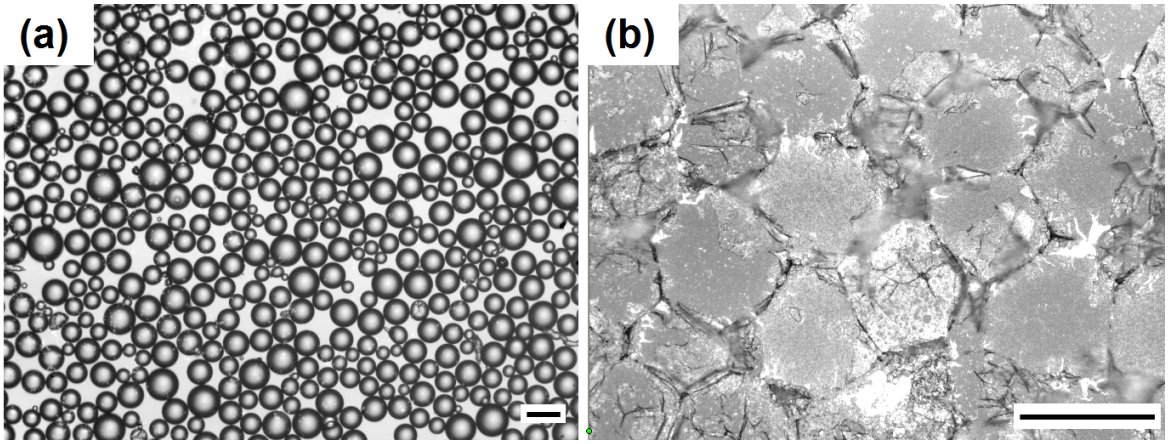

Figure 6.3 Optical micrographs of clean Pickering emulsions in the (a) wet state and (b) dry state. The scale bars denote 100 μm.

The xylene-in-water Pickering emulsion prepared by the mixture of 2.0 wt % CL particles with 0.25 wt % PSS modification was then adopted as the template for LbL assembly of polyelectrolytes in order to make microcapsules. To obtain a clean template for LbL assemblies, free of excess nanoparticles, the emulsion was cleaned by centrifuge-assisted creaming and replacement of supernatant for 2 times. Figure 6.3 shows optical microscope images of the emulsions after cleaning. The emulsion droplets were spherical and had an average droplet diameter of 70 μm. No significant coalescence was observed. When dried on a glass slide, emulsion droplets ruptured upon dehydration, leaving behind fragmented membranes composed of CL particles, shown in Figure 6.3b.

6.3.2 Polyelectrolyte Complex Shells by LbL Assembly

The LbL assembly was carried out by coating the clean emulsion templates in sequence with PDADMAC and PSS to prepare four double-layered microcapsules, CL/(PSS/PDADMAC)$_4$. Between each coating, centrifugation-accelerated creaming and washing were used to remove unbound polyelectrolytes.

Figure 6.4 shows the mobilities of washed microcapsules with different number of coating layers. It is interesting to see that the cleaned initial emulsion stabilized with PSS-modified CL particles was slightly positive but could still be coated with the polycation, PDADMAC, resulting in a large increase in cationic charge. This discrepancy may be explained by the existence of patches of different charges on the CL particle surface, caused by the rigid particle surface and high charge density of PSS (see Appendix Scheme 6A.1 for illustration). Mobility tests reflect the average charge on the particle surface, and the uneven distribution of charges on a particle surface would not be detected. When the clean emulsion was coated with PDADMAC, the polycation likely complexed with negatively charged patches on the CL particle surfaces, locking those particles into a polyelectrolyte complex at the interface. It is possible that the same template could also be coated with polyanions to form similar anionic colloidosomes, as polyanions could interact with positive patches on CL particle surfaces.

Further LbL assembly proceeded by alternately applying PSS and PDADMAC coatings until four double-layered coatings were reached. Figure 6.4 shows that the CL particle surface charge changed sign with each coating to give a typical zigzag-shaped plot (solid line),[38] suggesting successful coating with oppositely charged polyelectrolytes in each step.

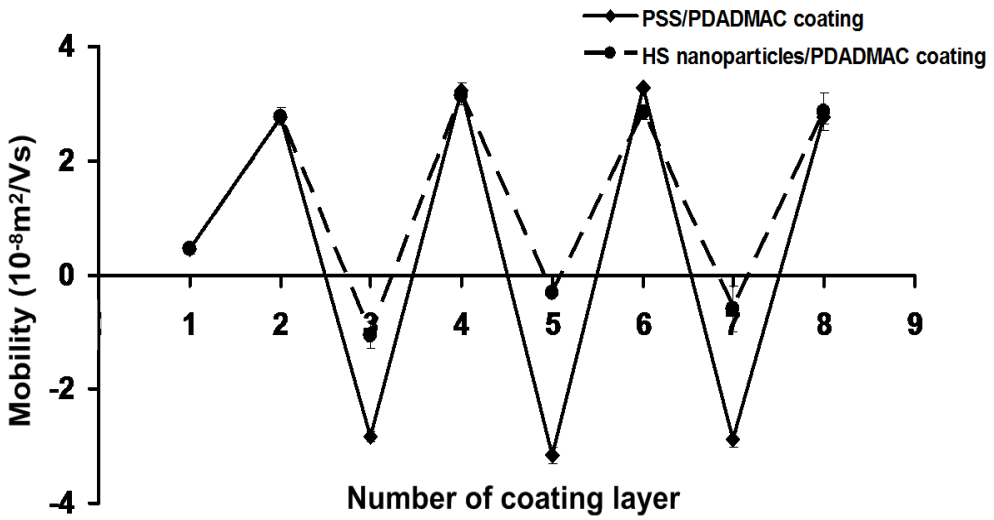

Figure 6.4 Plot of electrophoretic mobility of microcapsules vs number of coating layers.

CL/(PSS/PDADMAC)$_4$ microcapsules made by LbL coating are shown in Figure 6.5a−c. In the wet state, most microcapsules seemed partially collapsed with multiple dents on microcapsule surfaces, as shown in Figure 6.5a. The microcapsule deformation was likely caused by the loss of xylene from the core as xylene is slightly soluble in water.[39] In addition to microcapsules, significant amount of free xylene droplets (light areas) was observed, which were caused by manual shaking before sampling and tended to cream and coalesce over time in the capsule suspension. The release of core solvent was likely due to the breakage of some microcapsules during LbL coatings. When intact microcapsules were allowed to slowly dry on a glass slide, they tended to lose xylene immediately upon dehydration, followed by complete collapse of the microcapsules as shown in Figure 6.5b. Close examination of these collapsed microcapsules revealed small cracks on the microcapsule surfaces, as shown in Figure 6.5c. Compared to dried emulsion template (Figure 6.2b), the cracks on CL/(PSS/PDADMAC)$_4$ microcapsule

surfaces were much smaller, showing the increased resistance of microcapsules toward sudden rupture. This was expected as the coated polyelectrolyte layers strengthened microcapsule walls.

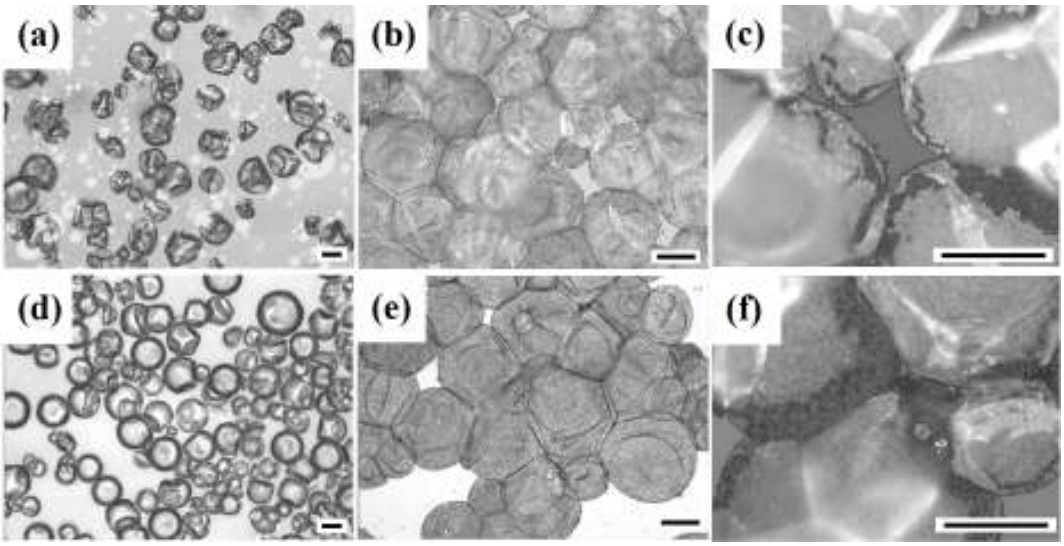

Figure 6.5 Optical micrographs of CL/(PSS/PDADMAC)$_4$ (a−c) and CL/PSS/PDADMAC/ (HS/PDADMAC)$_3$ (d−f) microcapsules. (a, d) are in wet state and (b, c, e, f) are in dry state. Scale bars denote 50 μm.

6.3.3 Composite Shells

In order to increase the encapsulation efficiency, negatively charged Ludox HS-30 silica particles were used to replace PSS as the anionic coating material to make composite microcapsules. One thought was that HS particles could fit into the interstices of CL particle aggregates at the interface to give tighter microcapsule walls since they have a similar size as CL particles. In addition, using nanoparticles as building blocks for LbL assemblies could render thicker walls with the same number of coating layers,

increasing the capsule strength. The same emulsion template based on 0.25 wt % PSS modification was used for these LbL coatings. After coating with one layer of PDADMAC, microcapsules were further coated with three double layers of (HS/PDADMAC) to make CL/PSS/PDADMAC/$(HS/PDADMAC)_3$ microcapsules. Mobility tests were used to monitor the LbL process, and results are shown in Figure 6.4 (dotted line), showing a similar zigzag shape as that in LbL assembly of PSS/PDADMAC, implying a successful coating in each step. However, unlike coating with PSS/PDADMAC where significant negative mobility values were obtained after each PSS coating, the corresponding values in (HS/PDADMAC) coating were close to zero. Since an excess of HS particles were used in each coating, we believe this limited development of negative charge is due to residual uncoated PDADMAC being exposed to the aqueous phase through HS particle interstices. The CL/PSS/PDADMAC/$(HS/PDADMAC)_3$ microcapsules are shown in Figure 6.5d−f. In the wet state, most microcapsules showed collapse on the surface, but the extent of deformation is less than that of CL/$(PSS/PDADMAC)_4$ microcapsules. Although small free xylene droplets were still observed in the CL/PSS/PDADMAC/$(HS/PDADMAC)_3$ microcapsule suspension, the amount was much less than that seen in CL/$(PSS/PDADMAC)_4$ microcapsule suspensions, indicating these microcapsules had improved resistance toward breakage and a higher encapsulation efficiency with HS nanoparticle coatings. The lower degree of wrinkling seen in the composite capsules (Figure 6.5d) compared to the polyelectrolyte capsules (Figure 6.5a) further suggests slower rates of diffusional release of xylene. Similar to CL/$(PSS/PDADMAC)_4$

microcapsules, dry CL/PSS/PDADMAC/$(HS/PDADMAC)_3$ microcapsules fully collapsed upon dehydration by releasing the fill, which was caused by the stress-induced cracking of microcapsule walls. This property could lead to applications that require dehydration-triggered release of the core contents like one-pot water-borne paints and adhesives.

The morphology of microcapsule wall cross sections was studied by transmission electron microscopy. Three types of microcapsules (CL/PSS/PDADMAC, $CL/(PSS/PDADMAC)_4$, and $CL/PSS/PDADMAC/(HS/PDADMAC)_3$) were treated with ethanol to remove the core solvent and then allowed to dry in air. Dry microcapsules were embedded in an epoxy resin consisting of a mixture of TTE and MBMCA. The resulting embeddings were ultramicrotomed to about 60−80 nm thickness. Figure 6.6 shows the TEM images of the wall cross sections of these three types of microcapsules. Figure 6.6a,b shows the wall cross section of a CL/PSS/PDADMAC microcapsule that shows a two-layer wall structure. The inner layer is less than 50 nm thick and compact with CL particles, while the thickness of the outer diffuse layer varies from several tens of nanometers to more than 1 μm and is very sparse of CL particles, indicating a porous structure of the outer layer. This two-layer structure suggests that the primary Pickering emulsion was stabilized by CL particle aggregates instead of a monolayer of nanoparticles, which is in line with our observations on the CL particle aggregation after PSS modification. These particle aggregates showed a loose structure, resulting in the formation of a porous outer diffuse layer. The formation of a dense inner layer can be attributed to the full coverage of the xylene/water interface by CL particle aggregates

which lowers the interfacial tension. Polyelectrolytes are not visible in the section due to the small number of coating layers. Figure 6.6c,d shows the wall cross section of CL/$(PSS/PDADMAC)_4$ microcapsules. It seems that the two-layer wall structure still holds with the outer layers being tightened by the LbL coatings. The bright areas in the wall cross section possibly denote PSS/PDADMAC coating layers, implying that CL particles were interconnected at the interface by these polyelectrolyte layers to transform the loose-structured particle aggregates into nanoparticles/polyelectrolytes composites. However, the wall was still porous, a quality inherited from the primary emulsion, making the microcapsule walls susceptible to breaking. This could be the reason that there was a large extent of release of the core solvent during the LbL coating. CL/PSS/PDADMAC/$(HS/PDADMAC)_3$ microcapsules were also embedded using the same procedure. However, separated capsule walls were not identified in the sections, and only big chunks of nanoparticles aggregates were observed, which was due to clumping of microcapsule walls. Attempts to better disperse these microcapsule walls in the same embedding matrix by gentle rotation also ended in clumped microcapsule walls, suggesting that this wall aggregation is due to the incompatibility of these capsule walls with the embedding matrix. The cross section of aggregated CL/PSS/PDADMAC/$(HS/PDADMAC)_3$ microcapsule walls embedded in the TTE/MBMCA resin is shown in Figure 6.6e. Although individual microcapsule walls could not be easily distinguished, these microcapsule wall aggregates show a dense structure, composed of tightly packed nanoparticles, much different from the porous wall structure observed in both CL/PSS/PDADMAC and CL/$(PSS/PDADMAC)_4$

microcapsules. The dense microcapsule wall was also confirmed by looking at the wall cross sections of well-dispersed microcapsules that were obtained by cryo-microtoming a drop of CL/PSS/PDADMAC/$(HS/PDADMAC)_3$ microcapsule suspension as shown in Figure 6.6f. The nonporous microcapsule walls suggest that the HS particle coating effectively filled the pores in the loose CL particle aggregates at interface to produce tight microcapsule walls. These dense microcapsule walls showed higher stability against rupture during the LbL coating process, resulting in a better surviving of these HS particles coating microcapsules.

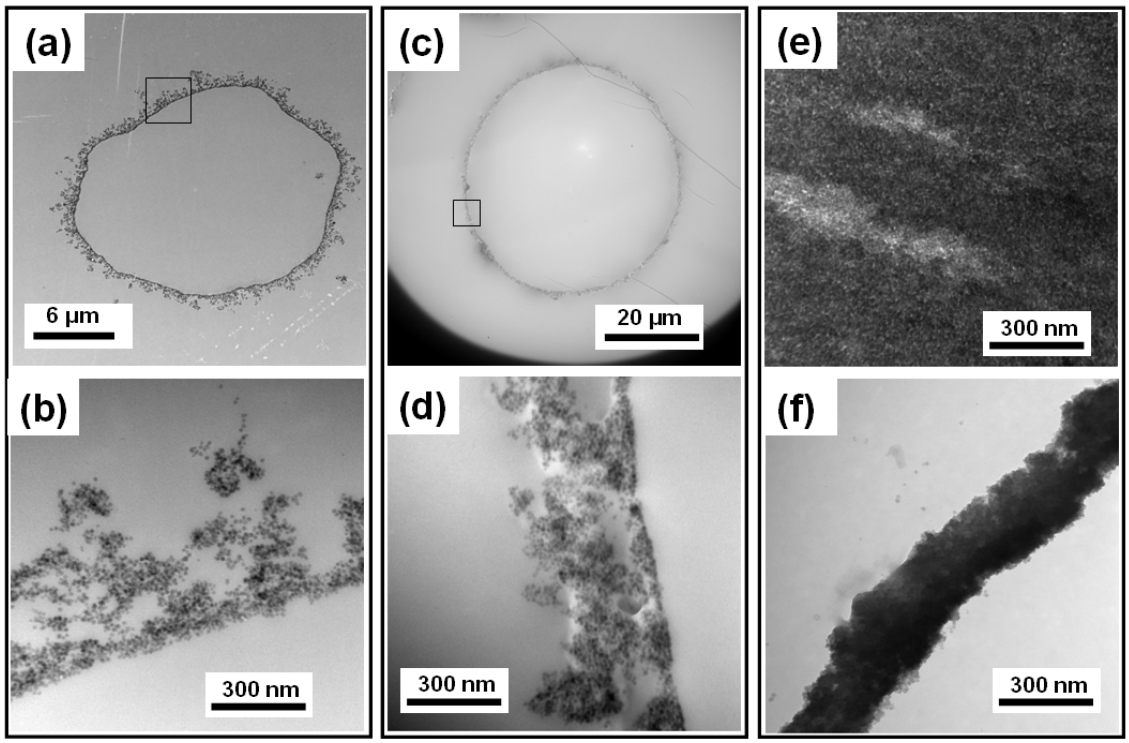

Figure 6.6 TEM micrographs of the wall cross sections of CL/PSS/PDADMAC (a, b), CL/$(PSS/PDADMAC)_4$ (c, d), and CL/PSS/PDADMAC/$(HS/PDADMAC)_3$ (e, f)

microcapsules. (a−e) were from TTE/MBMCA embedding, and (f) was from the cryo-sectioning of CL/PSS/PDADMAC/$(HS/PDADMAC)_3$ microcapsule dispersion in water.

6.4 Conclusions

Ludox CL particles were electrostatically modified on their surface with PSS to become surface active, and oil-in-water Pickering emulsions made by these particulate emulsifiers showed good stability against coalescence and creaming. Because of the residual charges on modified CL particle surfaces, the Pickering emulsions were used as templates to initiate the LbL coating of charged species from xylene/water interface for making microcapsules. Because of the high stability of Pickering emulsions, creaming by centrifugation and water washing could be carried out without noticeable emulsion coalescence, facilitating the handling of emulsions/capsules during LbL coating. Both polyelectrolytes and polyelectrolyte/nanoparticles were chosen to coat the Pickering emulsion templates to generate two types of microcapsules. The polyelectrolyte-coated microcapsules showed significant breakage during LbL coating process, which could be attributed to this polyelectrolyte complex microcapsule walls. In contrast, the polyelectrolyte/nanoparticle coated microcapsules showed higher stability as much less release of the core solvent was observed. This improved property was attributed to the dense microcapsule walls that were formed by filling the pores of CL particle aggregates with coating HS nanoparticles. We have shown that a range of core solvents with different polarity could be utilized to make oil-in-water emulsions using the same type of

particulate emulsifiers, which could be in turn be used as templates for making microcapsules with different fills. Therefore, this microencapsulation method supplements the CT-LbL assembly technique for making microcapsules and is suitable for encapsulating various hydrophobic materials with different polarities.

6.5 References

[1] Wang, W.; Liu, X. D.; Xie, Y. B.; Zhang, H.; Yu, W. T.; Xiong, Y.; Xie, W. Y.; Ma, X. J. *Journal of Materials Chemistry* **2006**, *16*, 3252-3267. (b) Tong, W. J.; Gao, C. Y. *Journal of Materials Chemistry* **2008**, *18*, 3799-3812.

[2] White, S. R.; Sottos, N. R.; Geubelle, P. H.; Moore, J. S.; Kessler, M. R.; Sriram, S. R.; Brown, E. N.; Viswanathan, S. *Nature* **2001**, *409*, 794-797.

[3] (a) Ramarao, C.; Ley, S. V.; Smith, S. C.; Shirley, I. M.; DeAlmeida, N. *Chemical Communications* **2002**, 1132-1133. (b) Ley, S. V.; Ramarao, C.; Gordon, R. S.; Holmes, A. B.; Morrison, A. J.; McConvey, I. F.; Shirley, I. M.; Smith, S. C.; Smith, M. D. *Chemical Communications* **2002**, 1134-1135. (c) Poe, S. L.; Kobaslija, M.; McQuade, D. T. *Journal of the American Chemical Society* **2007**, *129*, 9216-9221.

[4] (a) Tsuji, K. *Journal of Microencapsulation* **2001**, *18*, 137-147. (b) Shirley, I. M.; Scher, H. B.; Perrin, R. M.; Wege, P. J.; Rodson, M.; Chen, J. L.; Rehmke, A. W. *Pest Management Science* **2001**, *57*, 129-132.

[5] (a) Jacquemond, M.; Jeckelmann, N.; Ouali, L.; Haefliger, O. P. *Journal of Applied Polymer Science* **2009**, *114*, 3074-3080. (b) Hawlader, M. N. A.; Uddin, M. S.; Khin, M.

M. *Applied Energy* **2003**, *74*, 195-202. (c) Comiskey, B.; Albert, J. D.; Yoshizawa, H.; Jacobson, J. *Nature* **1998**, *394*, 253-255.

[6] Scher, H. B.; Rodson, M.; Lee, K. S. *Pesticide Science* **1998**, *54*, 394-400.

[7] (a) Ali, M. M.; Stöver, H. D. H. *Macromolecules* **2004**, *37*, 8812-8812. (b) Okubo, M.; Konishi, Y.; Minami, H. *Colloid and Polymer Science* **1998**, *276*, 638-642.

[8] (a) Loxley, A.; Vincent, B. *Journal of Colloid and Interface Science* **1998**, *208*, 49-62. (b) Atkin, R.; Davies, P.; Hardy, J.; Vincent, B. *Macromolecules* **2004**, *37*, 7979-7985.

[9] Arshady, R. *Polymer Engineering and Science* **1990**, *30*, 905-914.

[10] (a) Wang, Y.; Angelatos, A. S.; Caruso, F. *Chemistry of Materials* **2008**, *20*, 848-858. (b) Peyratout, C. S.; Dahne, L. *Angewandte Chemie-International Edition* **2004**, *43*, 3762-3783.

[11] (a) Donath, E.; Sukhorukov, G. B.; Caruso, F.; Davis, S. A.; Mohwald, H. *Angewandte Chemie-International Edition* **1998**, *37*, 2202-2205. (b) Sukhorukov, G. B., Donath, E.; Davis, S. A.; Lichtenfeld, H.; Caruso, F; Popov, V. I.; Möhwald, H. *Polym. Adv. Technol.* 1998, 34, 759-767. (c) Caruso, F.; Caruso, R. A.; Mohwald, H. *Science* **1998**, *282*, 1111-1114.

[12] (a) Schuler, C.; Caruso, F. *Biomacromolecules* **2001**, *2*, 921-926. (b) Shenoy, D. B.; Antipov, A. A.; Sukhorukov, G. B.; Mohwald, H. *Biomacromolecules* **2003**, *4*, 265-272. (c) Becker, A. L.; Zelikin, A. N.; Johnston, A. P. R.; Caruso, F. *Langmuir* **2009**, *25*,

14079-14085. (d) Schwiertz, J.; Meyer-Zaika, W.; Ruiz-Gonzalez, L.; Gonzalez-Calbet, J. M.; Vallet-Regi, M.; Epple, M. *Journal of Materials Chemistry* **2008**, *18*, 3831-3834.

[13] (a) Caruso, R. A.; Susha, A.; Caruso, F. *Chemistry of Materials* **2001**, *13*, 400-409. (b) Caruso, F.; Spasova, M.; Saigueirino-Maceira, V.; Liz-Marzan, L. M. *Advanced Materials* **2001**, *13*, 1090-1094. (c) Wang, C. Y.; Ye, S. Q.; Dai, L.; Liu, X. X.; Tong, Z. *Biomacromolecules* **2007**, *8*, 1739-1744. (d) Wiemann, L. O.; Buthe, A.; Klein, M.; van den Wittenboer, A.; Dahne, L.; Ansorge-Schumacher, M. B. *Langmuir* **2009**, *25*, 618-623. (e) Kinnane, C. R.; Such, G. K.; Antequera-Garcia, G.; Yan, Y.; Dodds, S. J.; Liz-Marzan, L. M.; Caruso, F. B*iomacromolecules* **2009**, *10*, 2839-2846.

[14] Bergbreiter, D. E.; Chance, B. S. *Macromolecules* **2007**, *40*, 5337-5343. (b) Wang, F.; Ma, N.; Chen, Q. X.; Wang, W. B.; Wang, L. Y. *Langmuir* **2007**, *23*, 9540-9542. (c) Huang, C. J.; Chang, F. C. *Macromolecules* **2009**, *42*, 5155-5166. (d) Beyer, S.; Mak, W. C.; Trau, D. *Langmuir* **2007**, *23*, 8827-8832. (e) Khapli, S.; Kim, J. R.; Montclare, J. K.; Levicky, R.; Porfiri, M.; Sofou, S. *Langmuir* **2009**, *25*, 9728-9733.

[15] Sukhishvili, S. A. Current Opinion in Colloid & Interface Science **2005**, 10, 37-44.

[16] (a) Dahne, L.; Leporatti, S.; Donath, E.; Mohwald, H. *Journal of the American Chemical Society* **2001**, *123*, 5431-5436. (b) Sukhorukov, G. B.; Antipov, A. A.; Voigt, A.; Donath, E.; Mohwald, H. *Macromolecular Rapid Communications* **2001**, *22*, 44-46. (c) Gaponik, N.; Radtchenko, I. L.; Sukhorukov, G. B.; Weller, H.; Rogach, A. L. *Advanced Materials* **2002**, *14*, 879-882.

[17] Ogawa, S.; Decker, E. A.; McClements, D. J. *Journal of Agricultural and Food Chemistry* **2004**, *52*, 3595-3600.

[18] (a) Mak, W. C.; Cheung, K. Y.; Trau, D. *Chemistry of Materials* **2008**, *20*, 5475-5484. (b) Mak, W. C.; Bai, J.; Chang, X. Y.; Trau, D. *Langmuir* **2009**, *25*, 769-775.

[19] Shchukin, D. G.; Kohler, K.; Mohvald, H.; Sukhorukov, G. B. *Angewandte Chemie-International Edition* **2005**, *44*, 3310-3314.

[20] Ogawa, S.; Decker, E. A.; McClements, D. J. *Journal of Agricultural and Food Chemistry* **2003**, *51*, 2806-2812.

[21] Tjipto, E.; Cadwell, K. D.; Quinn, J. F.; Johnston, A. P. R.; Abbott, N. L.; Caruso, F. *Nano Letters* **2006**, *6*, 2243-2248.

[22] Grigoriev, D. O.; Bukreeva, T.; Mohwald, H.; Shchukin, D. G. *Langmuir* **2008**, *24*, 999-1004.

[23] (a) Preetz, C.; Rube, A.; Reiche, I.; Hause, G.; Mader, K. *Nanomedicine-Nanotechnology Biology and Medicine* **2008**, *4*, 106-114. (b) Szczepanowicz, K.; Dronka-Gora, D.; Para, G.; Warszynski, P. *Journal of Microencapsulation* **2010**, *27*, 198-204.

[24] (a) Ramsden, W. *Proc. R. Soc. London* **1903**, *72*, 156-164. (b) Pickering, S. U. *J. Chem. Soc.* **1907**, *91*, 2001-2021

[25] Binks, B. P. Current Opinion in Colloid & Interface Science **2002**, 7, 21-41.

[26] Dinsmore, A. D.; Hsu, M. F.; Nikolaides, M. G.; Marquez, M.; Bausch, A. R.; Weitz, D. A. *Science* **2002**, *298*, 1006-1009.

[27] (a) Velev, O. D.; Furusawa, K.; Nagayama, K. *Langmuir* **1996**, *12*, 2374-2384. (b) Lawrence, D. B.; Cai, T.; Hu, Z.; Marquez, M.; Dinsmore, A. D. *Langmuir* **2007**, *23*, 395-398. (c) Akartuna, I.; Tervoort, E.; Studart, A. R.; Gauckler, L. J. *Langmuir* **2009**, *25*, 12419-12424.

[28] Yow, H. N.; Routh, A. F. *Langmuir* **2009**, *25*, 159-166.

[29] Binks, B. P.; Liu, W. H.; Rodrigues, J. A. *Langmuir* **2008**, *24*, 4443-4446.

[30] Cushing, B. L.; Kolesnichenko, V. L.; O'Connor, C. J. *Chemical Reviews* **2004**, *104*, 3893-3946.

[31] (a) Saleh, N.; Sarbu, T.; Sirk, K.; Lowry, G. V.; Matyjaszewski, K.; Tilton, R. D. *Langmuir* **2005**, *21*, 9873-9878. (b) Chen, Y. H.; Wang, C. Y.; Chen, J. X.; Liu, X. X.; Tong, Z. *Journal of Polymer Science Part a-Polymer Chemistry* **2009**, *47*, 1354-1367.

[32] (a) Binks, B. P.; Desforges, A.; Duff, D. G. *Langmuir* **2007**, *23*, 1098-1106. (b) Binks, B. P.; Rodrigues, J. A.; Frith, W. J. *Langmuir* **2007**, *23*, 3626-3636.

[33] Li, J.; Stöver, H. D. H. *Langmuir* **2008**, *24*, 13237-13240.

[34] Akartuna, I.; Studart, A. R.; Tervoort, E.; Gonzenbach, U. T.; Gauckler, L. J. *Langmuir* **2008**, *24*, 7161-7168.

[35] Furusawa, K.; Sato, A.; Shirai, J.; Nashima, T. *Journal of Colloid and Interface Science* **2002**, *253*, 273-278.

[36] Grulke E. A. In *Polymer Handbook*, 4th ed.; Brandup, J., Immergut, E. H., Grukle E. A., Eds.; Wiley: New York, 1999; p VII/675.

[37] *Aldrich Catalogue, Handbook of Fine Chemicals,* **2008-2009**

[38] Caruso, F. *Chemistry-a European Journal* **2000**, *6*, 413-419.

[39] Polak, J.; Lu, B. C. –Y. *Canadian Journal of Chemistry* **1973**, *51*, 4018-23

6.6 Appendix

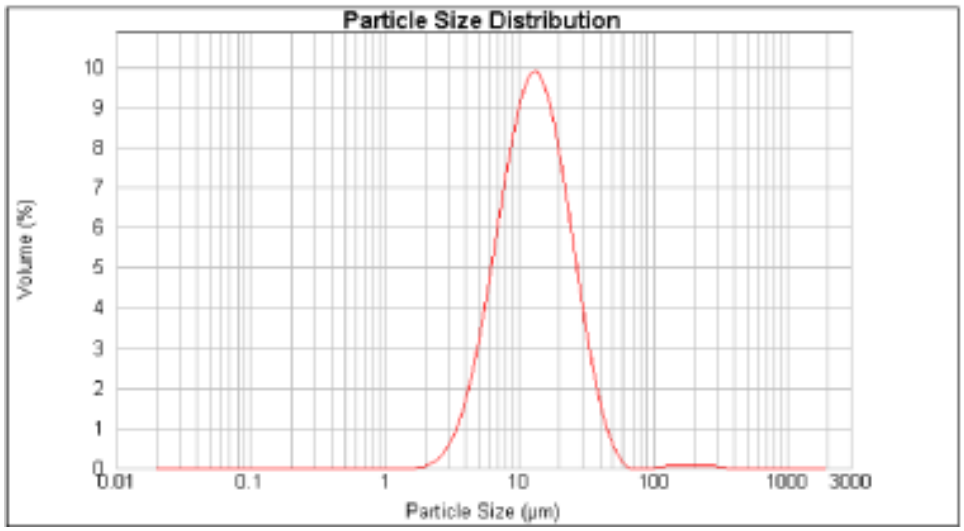

Figure 6A.1 Particle size distribution of CL particle aggregates after 0.25 wt % PSS modification measured using Malvern Mastersizer 2000.

Figure 6A.2 Photograph of oil-in-water Pickering emulsions made with different oil phase. From left to right: perfluoroheptane, heptane, xylene, butyl acetate, chloroform.

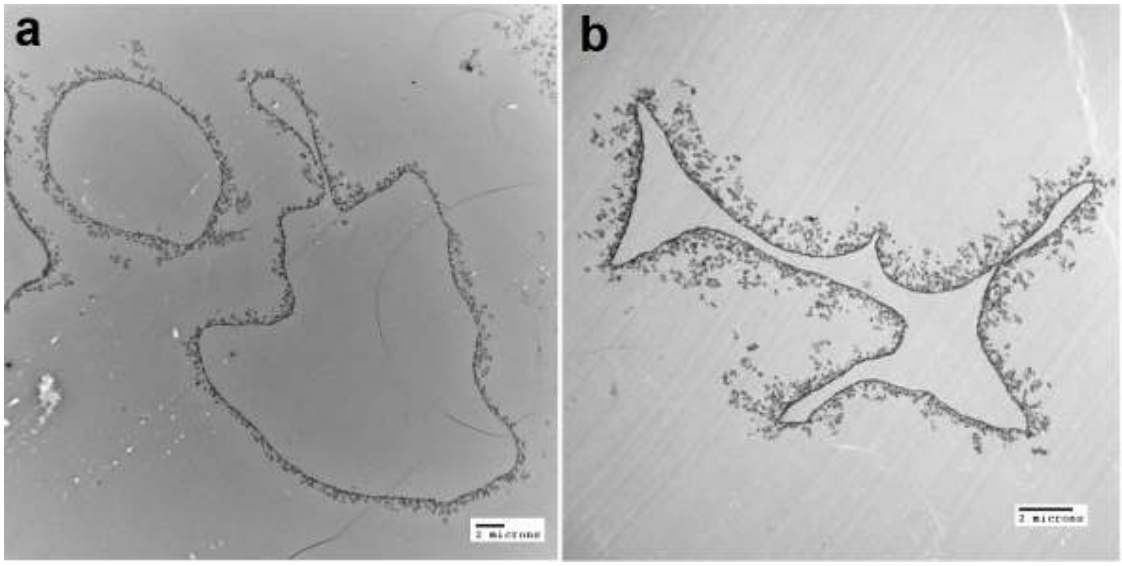

Figure 6A.3 TEM micrographs of the wall cross-sections of CL/PSS/PDADMAC microcapsules embedded in an epoxy matrix

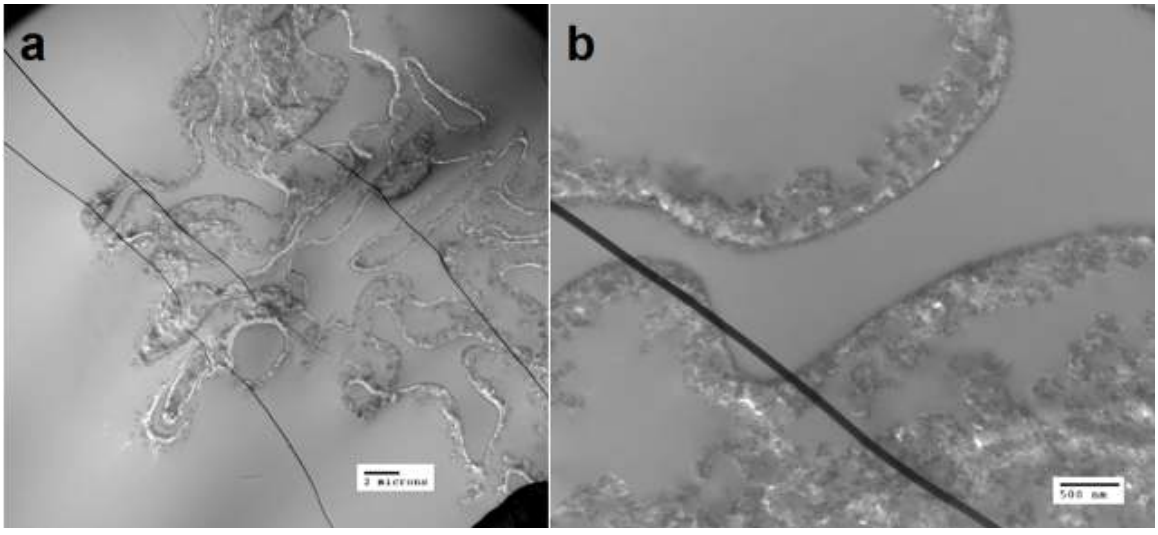

Figure 6A.4 TEM micrographs of the wall cross-sections of CL/$(PSS/PDADMAC)_4$ microcapsules embedded in an epoxy matrix

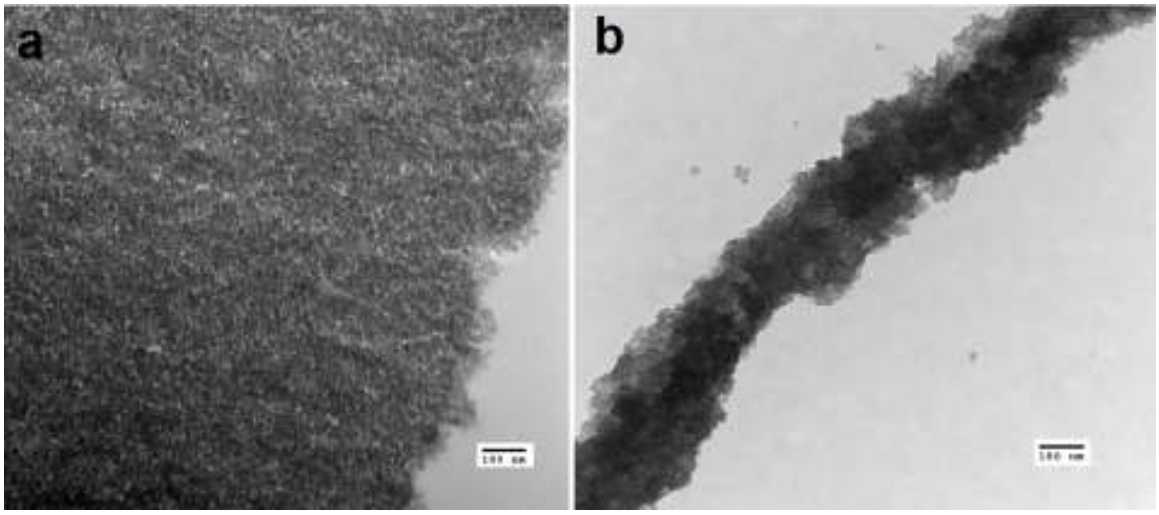

Figure 6A.5 TEM micrographs of the wall cross-sections of CL/PSS/PDADMAC/ $(HS/PDADMAC)_3$ microcapsules (a) from microtoming the capsule embedding in an epoxy matrix; (b) from cryo-microtoming a capsule suspension in water.

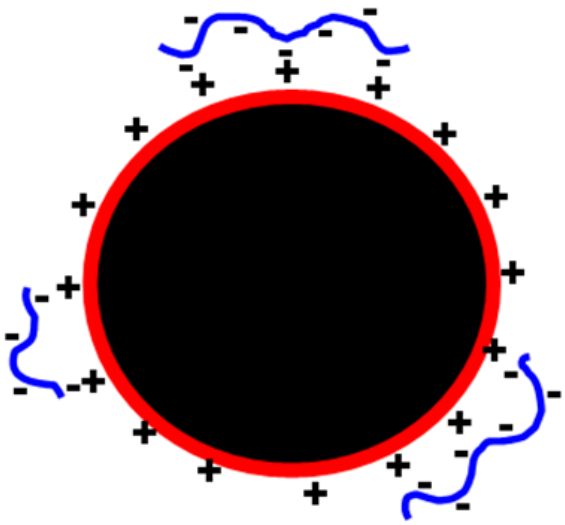

Scheme 6A.1 Schematic illustration of the patchy charge distribution on the surface of a PSS modified CL particle

CHAPTER 7 - PICKERING EMULSION TEMPLATED INTERFACIAL ATOM TRANSFER RADICAL POLYMERIZATION FOR MICROENCAPSULATION

7.1 Introduction

Polymeric microcapsules (MCs) are of great importance in industrial applications such as pesticide delivery[1], food science[2], imaging materials[3], catalyst design[4], and self-healing materials [5] . Many microencapsulation processes including in-*situ* radical polymerization [6] , interfacial polycondensation [7] , polymer phase separation [8] and coacervation[9] rely on emulsions as templates to form capsular structures. Developments in controlled radical polymerization[10] make it possible to achieve a high-level of control of the site of polymerization, making it ideal for designing microencapsulation processes.[11]

Recently, there has been an increasing interest in using emulsion-templated radical polymerization (ETRP) for preparing MCs due to the good compatibility of radical chemistry with most functional groups, and the availability of a vast number of vinyl monomers, allowing for encapsulation of a wide range of core materials. Dispersion radical polymerizations (DRP) where polymerization is confined to the dispersed phase has led to MC shell formation through in-*situ* phase separation. In Okubo's self-assembly of phase-separated polymer (SaPSeP) method[12], a homopolymer forming in the dispersed

phase phase-separates towards the interface to form a capsule shell. Similarly, copolymerization of hydrophilic with hydrophobic monomers in a dispersed phase can lead to amphiphilic copolymers that migrate to the oil-water interface and cross-link to form a permanently networked shell at the interface[13]. While capable of forming microcapsules, these methods tend to require restrictive matching of core liquids and monomers. In this regard, interfacial radical polymerization (IRP) is advantageous as polymerization and cross-linking can only occur at the oil-water interface to produce polymers that automatically serve as MC walls. This approach is also much less dependent on the properties of monomers and core materials, making it possible to encapsulate a wider range of materials and to design functional MCs by taking advantage of the diversity of vinyl monomers available.

The key to IRP then is to confine radical polymerization at oil-water interfaces, which can be realized by employing amphiphilic radical initiators or chain transfer reagents that could restrict the growing polymer to the interface. It is equally important to cross-link the growing polymer at the interface to form networked MC walls regardless of the polarity of the monomers. IRP has been implemented in oil-in-water mini-emulsion polymerizations, using amphiphilic RAFT agents as reactive surfactants to confine polymerization of styrene at oil-water interfaces to form oil-filled polystyrene nanocapsules.[14] This approach was extended to water-in-oil mini-emulsions to prepare water-filled poly(N-isopropylacrylamide) nanocapsules.[15] Similarly, Matyjaszewski used an amphiphilic block copolymer both as mini-emulsion stabilizer and as ATRP macroinitiator for an oil-in-water mini-emulsion polymerization of butyl methacrylate.

Cross-linking was incorporated to strengthen the shells, and the resulting nanocapsules could be well dispersed in different solvents.[16] Although the above methods could produce nanocapsules with different compositions, formation of MCs requires interfacial initiators less prone to micelle formation which could dominate particle generation. Additionally, in these methods, monomers are present in the dispersed phase and their polymerizations in the organic phase could potentially interfere with core materials. After polymerization, unreacted monomers may remain in the core and act as impurities, which would have a proportionally greater impact in case of the much larger MCs.

In addition to using reactive molecular surfactants to confine radical polymerization at the interface, IRP can also be achieved using reactive Pickering emulsifiers. Pickering emulsions are particle stabilized emulsions[17] that in comparison to surfactant stabilized emulsions often show high stability and less foaming, making them popular candidates for templating MC formation.[18] By modifying the surface of Pickering emulsifiers with radical initiators or chain transfer agents, radical polymerizations can be localized on the particle surface or at the oil-water interface. In the presence of cross-linking, particulate emulsifiers can be locked-in at the interface to produce colloidosomes or composite MCs. The absence of micellization in Pickering emulsions avoids competition from micellar nucleations. As a result, polymerizations can be exclusively confined to the oil-water interface, which makes Pickering emulsions a promising base for templating IRP in microemulsion systems to produce MCs. Wang et al.[19] reported the use of ATRP initiator modified silica nanoparticles as Pickering emulsifiers in a paraffin-in-water emulsion system to confine the ATRP of 2-hydroxyethyl methacrylate (HEMA)

at the interface. They covalently attached an ATRP initiator to silica nanoparticles by stepwise reactions.[19] Slight in-*situ* cross-linking between the polyHEMA chains was observed during polymerization, and led to the formation of cross-linked MC shells. Wang's approach involved polymerization of the water soluble monomer, HEMA, on the aqueous side of the interface, avoiding interference with core materials. However, this approach used a multi-step synthesis to covalently functionalize the silica nanoparticles with an ATRP initiator. The degree of functionalization had to be carefully controlled to make appropriate Pickering emulsifiers, and the encapsulation was limited to very specific solvents.

Here, we present a robust and general method to immobilize ATRP initiators on Pickering emulsifiers, which can be utilized to template IRP to form MCs with a broad range of sizes and properties. This method involves the electrostatic deposition of a polyanionic ATRP initiator on cationic nanoparticle surfaces. The resulting modified nanoparticles are shown to be good Pickering emulsifiers, and the resulting Pickering emulsions can template interfacial ATRP of different monomers for encapsulating core materials with different polarities.

7.2 Experimental Section

7.2.1 Materials

Diethyl ether, dimethyl sulfoxide (DMSO), dichloromethane (DCM), xylenes (a mixture of *para*, *meta* and *ortho*-xylene) were purchased from Caledon Laboratories Ltd.

Perfluoroheptane (mixed isomers) was acquired from PCR Research Chemicals. Sodium styrenesulfonate (>80%) was supplied by Fluka. Other chemicals were obtained from Aldrich. All chemicals were used as received.

7.2.2 Methods

Synthesis of 2-(2-Bromoisobutyryloxyethyl) Methacrylate (BIEM)

BIEM was prepared as described by Venkatesh.[20] 2-Hydroxyethyl methacrylate (HEMA, 8.8 g, 67.7 mmol), triethylamine (TEA, 13.7 g, 135.6 mmol) and DCM (86 g) were added into a 250 ml three-necked round bottom flask. The mixture was cooled to 0 ˚C in an ice bath and 2-bromoisobutyryl bromide (18.7 g, 81.3 mmol) was introduced into the flask under stirring over 1 hour through an addition funnel. The reaction mixture was stirred for another 4 hrs at 0 ˚C, and then filtered to remove salts. The filtrate was extracted with de-ionized water (100 mL x 2), 0.5 M aqueous Na_2CO_3 (100 mL x 2) and saturated NaCl solution (100 mL x 1). The resulting solution was dried over Na_2SO_4 and DCM was removed on a rotary evaporator. The crude product was further dried under vacuum for 24 hrs to afford a brown liquid 15.7 g (83% yield). ^{1}H-NMR ($CDCl_3$): δ = 6.124 (1H), 5.582 (1H), 4.406 (4H), 1.917 (9H).

Synthesis of Poly (Sodium styrenesulfonate-co-2-(2-bromoisobutyryloxy)-ethyl methacrylate) (PSB)

Sodium styrenesulfonate (7.0g, 34.1 mmol), 2-(2-bromoisobutyryloxyethyl) methacrylate (BIEM, 3.23 g, 11.6 mmol), DMSO (91 g) and AIBN (99.1 mg, 0.60 mmol)

were added to a 125 mL HDPP bottle. After dissolution, the mixture was bubbled with N_2 for 0.5 hrs. Polymerization was carried out at 70˚C for 24 hrs in a HB-1000 hybridizer at 15 rpm rotation. The polymer was precipitated in 1000 mL diethyl ether, washed on a vacuum filter with diethyl ether (100 mL x 3), and dissolved in 250 mL water. The solution was dialyzed against continuously running de-ionized water for 3 days in a MEMBRA-CEL® dialysis tubing (molecular weight cutoff 7 kDa) and freeze-dried to give 4.22 g white product (41.3% yield). The ^{1}H-NMR spectrum of the final product is shown in Appendix Figure 7A.1.

Preparation of Particle/PSB Suspensions

The PSB modified CL particle suspensions were prepared by mixing 4 wt % CL particle suspensions with equal amounts of PSB solutions with a range of PSB concentrations. The resulting suspensions were immediately manually shaken for 30 seconds, and allowed to settle for one week before photographs were taken.

Determination of Free PSB in CL Particle Suspensions

2.0 wt % CL particle suspensions with different PSB/CL ratios were ultra-centrifuged for 40 min at 50,000 rpm at 25 °C using a Beckman L7-55 Preparative Ultracentrifuge. The depletion of PSB in the supernatants was measured by UV-Vis spectroscopy, using the peak at ~296 nm.

Mobility Tests

Electrophoretic mobilities of CL particles and MCs were measured on a ZetaPlus zeta-potential analyzer (Brookhaven Instruments Corp.). The mobilities of 2.0 wt % CL particles with different PSB/CL ratios were tested directly without adding extra

electrolytes. The error bars of the electrophoretic mobilities represent the standard error of the mean value of 10 runs (15 cycles per run). The mobilities of MCs were measured by suspending clean MCs in 2.5 mM KCl. The error bars stand for the standard error of the mean value of 3 runs (15 cycles per run).

Preparation of Emulsions

To prepare an emulsion, 0.75 mL CL particle suspension was added into a 3 mL glass vial containing 0.75 mL xylenes. The mixture was homogenized using a Dremel Moto-Tool equipped with a tungsten carbide cutter (catalog No. 9905) at ~16,000 rpm for 2 min. Optical micrographs of the emulsions were taken from a drop of the emulsions deposited on a glass slide without dilution. Photographs of the emulsions were taken 7 days after their preparations. The mean size of the emulsion droplets was obtained by averaging the sizes of over 200 emulsion droplets that were manually measured using the optical microscope.

Preparation of Poly(N,N'-methylene bisacrylamide) Microcapsules with Different Fills

In an Aldrich Hands-in-bag polyethylene bag filled with N_2, 0.75 mL CL particle suspension containing 0.8 wt % CL particles and 0.2 wt % PSB (PSB/CL=0.25) was added into a 3 mL glass vial containing 0.75 mL core solvent. The mixture was then emulsified using the Dremel Moto-Tool at ~16,000 rpm for 2 min. Four batches of such emulsion were prepared and combined. Separately, 10 mL aqueous solution containing 0.20 g MBAAm (1.297 mmol) and 6.4 mg 1,1,4,7,10,10-hexamethyltriethylenetetramine (HMTETA, 0.046 mmol) was bubbled with N_2 for 30 min in a 20 mL glass vial and then transferred into the Hands-in-bag. 3 mg CuBr (0.046 mmol) was then added into this

solution, followed by the addition of the pre-prepared emulsion. The reaction mixture was sealed and placed on a set of horizontal rollers at room temperature or heated to 65 °C, and rotated for different amounts of time. After polymerization, the formed MCs were allowed to cream in a 50 mL centrifuge tube and the supernatant removed from the bottom using a syringe. 40 mL de-ionized water was added to dilute the MC suspension. This separation was repeated 3 times to remove unreacted monomer, catalyst and ligand. Optical micrographs of the MCs were taken from a drop of the MC suspension deposited on a glass slide. The mean size of MCs was obtained by averaging the sizes of 100 MCs. Different core solvents including xylenes, hexadecane and perfluoroheptane were encapsulated using the same procedure. Dry hexadecane filled polyMBAAm MCs were sputter-coated with a layer of gold before scanning electron microscope (SEM) measurements.

Preparation of Poly(sodium methacrylate-co-N,N'-methylene bisacrylamide) (poly(SM-MBAAm) Microcapsules with a Xylene Core

An aqueous solution containing 287.0 mg methacrylic acid (MA), 138.4 mg NaOH, 192.4 mg MBAAm and 9.39 mL H_2O was passed through a 10 cm long column (inner diameter ~6 mm) packed with inhibitor remover (Aldrich). After treatment, 5 g of such solution was mixed with 3.0 mg HMTETA (0.022 mmol) in a 20 mL glass vial and the pH of this solution was adjusted to 9.5 by addition of 0.1 N HCl solution. The solution was then bubbled with N_2 for 30 min before being transferred into a N_2 filled Hands-in-bag and mixed with 1.5 mg CuBr (0.023 mmol). The emulsion preparation was the same as that of polyMBAAm MCs aforementioned. Two batches of freshly prepared xylene-in-

water emulsion were added to the abovementioned solution. The resulting solution was then sealed in a vial and placed into the roller reactor at 65 ˚C for 1 hour. After polymerization, MCs were purified using a procedure similar to that used for polyMBAAm MCs.

Preparation of Poly([3-(methacrylamino)propyl]trimethylammonium chloride-co-N,N'-methylene biscrylamide) (poly(MAPTAC-MBAAm)) Microcapsules with a Xylene Core

575.8 mg 3-(methacrylamino)propyl]trimethylammonium chloride (MAPTAC) solution (50 wt %), 190.2 mg MBAAm and 9.24 mL H_2O were mixed and the resulting solution passed through a 10 cm column (inner diameter ~6 mm) packed with inhibitor remover particles. After treatment, 5 g of such solution was mixed with 3.7 mg HMTETA (0.027 mmol), 1.95 mg CuBr (0.030 mmol) in a 20 mL glass vial and the pH of this solution was adjusted to 9.6 by addition of 0.1 N NaOH solution. The solution was then bubbled with N_2 for 30 min before being transferred into a N_2 filled Hands-in-bag. Two batches of freshly prepared xylene-in-water emulsion were then mixed with the solution. The resulting solution was then sealed in a vial and put into the roller reactor at 65 ˚C with for 1 hour. After polymerization, MCs were purified using a procedure similar to that used for polyMBAAm MCs.

Preparation of Double-walled Microcapsules

An aqueous phase containing 16 mg CuBr (0.25 mmol), 25.7 mg HMTETA (0.18 mmol), and 330 mg MBAAm (2.14 mmol) in 18.2 g water was bubbled with N_2 in a 20 mL vial for 30 min and then transferred into a N_2 filled Hands-in-a-bag. In the same Hands-in-a-bag, 0.75 mL organic phase containing 15 % (v/v) styrene, 1.0 wt % AIBN in

hexadecane was emulsified with 0.75 mL PSB modified CL particle suspension (0.8 wt % CL particles and 0.2 wt % PSB) at ~13,000 rpm for 2 min. The freshly prepared emulsion was then mixed with the aqueous solution in the vial. The vial was promptly sealed and placed on a rotator (Glas-Col®) at a rate ~60 rpm for 5 hrs at room temperature. The vial was then transferred into the roller reactor and rotated there at 60 ˚C for 22 hrs. After polymerization, MCs were purified using a procedure similar to that used for polyMBAAm MCs.

Microcapsule Wall Permeability Tests

The permeability tests were based on xylene-filled polyMBAAm MCs that were prepared using polymerization at 65 ˚C for 1 hour. The aqueous MC suspension was placed on a rotary evaporator under vacuum at 60 ˚C for 30 min to replace the xylene fill with aqueous phase. 0.2 mL of the resulting water-filled MC suspension was then mixed with 0.2 mL 0.1 wt % fluorescein-labeled dextran solutions with different molecular weights. After incubation for 72 hrs, one drop of MC suspension was placed on a microscope glass slide and covered with a glass coverslip to flatten and seal the top and bottom surfaces of the MCs, which permitted the observation of dextran-*f* in the capsules by fluorescence microscopy.

Preparation of Dry Microcapsule Wall Fragments

3 mL concentrated MC suspension was diluted in 40 mL ethanol. The MCs were allowed to sediment, and the supernatant was decanted. This washing procedure was repeated another three times to ensure complete removal of water and the core solvent.

The final sedimented MCs were then dried under vacuum for 48 hrs to yield powder-like MC wall fragments.

Thermogravimetric Analysis (TGA) of Microcapsule Walls

Thermogravimetric analysis (TGA) of MC fragments was performed using a NETZSCH STA 409 PC/PG. TGA measurements were carried out by heating 20-30 mg of dry MC wall fragments at a rate of 5.00˚C /min until 800 ˚C in the air. The percentage of polymer ($P_{polymer}$) in the MC walls was calculated by the measured weight loss from 200 to 800 ˚C. The remaining percentage was assigned to CL particles (P_{CL}). The percentage of PSB was estimated to be ¼ that of P_{CL}. Therefore, polyMBAAm/CL ratios were determined by the equation below:

$$r_{polyMBAAm/CL}=(P_{polymer} - ¼ P_{CL}) / P_{CL}.$$

The conversion of MBAAm (C_{MBAAm}) was calculated using the following equation: $C_{MBAAm}=(m_{CL} \times r_{polyMBAAm/CL} /m_{MBAAm}) \times 100\%$, where m_{MBAAm} is the total mass of MBAAm added.

Sample Preparation for Transmission Electron Microscopy and Scanning Transmission X-ray Microscopy

Dry MC wall fragments were embedded in an epoxy resin prepared by mixing trimethylolpropane triglycidyl ether and 4,4′-methylenebis(2-methylcyclohexylamine) in a 1:1 weight ratio and curing at 70 °C for 3 days. Thin sections were cut using a Leica Ultracut UCT ultramicrotome and deposited onto Formvar-coated Cu grids.

Characterization

^{1}H-NMR was recorded using a Bruker 200MHz NMR spectrometer. The carbon and hydrogen content in PSB was determined by combustion analysis using an EA 1108 CHN Analyzer. The bromide content of PSB was determined by oxygen flask combustion method and analyzed using the Ion Chromatography technique. Photographs of particle suspension and emulsions were taken using a Canon PowerShot S5 IS digital camera. UV measurements were carried out on a Cary 50 UV/Vis spectrophotometer. The spin rates of the Dremel Moto-Tool for emulsification were determined using an AMETEK® Model 1726 dual function tachometer. The optical micrographs of emulsions and MCs were obtained using an Olympus BX51 optical microscope fitted with a Q-Imaging Retiga EXi digital camera, ImagePro software and fluorescence optics for fluorescein and rhodamine. Fourier Transform Infra-red (FTIR) analyses were carried out on a Bio-Rad infrared spectrometer (FTS-40) in transmission mode. TEM images were recorded using a JEOL JEM 1200 EX TEMSCAN transmission electron microscope (JEOL, Peabody, MA, USA) operated at an accelerating voltage of 80 kV. Scanning electron microscopy images were obtained using a TESCAN VEGA 3 XM SEM. Scanning transmission X-ray microscopy (STXM) measurements on ultramicrotomed cross-section samples of the double-walled MCs were performed at the polymer STXM beamline 5.3.2 of the Advanced Light Source (ALS).[21]

7.3 Results and Discussion

7.3.1 Synthesis of Particle Surface Modifier

Recently, we and others have shown that the surface of charged inorganic particles can be easily modified by electrostatic interaction using oppositely charged organic electrolytes, turning these hydrophilic particles into Pickering emulsifiers for oil-in-water emulsions.[22] The modification decreases the charge density on the particle surface and introduces hydrophobic groups, which both help make the particle surface active. This method of particle modification seems quite general, and has been used to turn various types of particles into effective Pickering emulsifiers.[22] We recently showed that nano particles coated electrostatically with polyelectrolytes can be used to form Pickering emulsions less sensitive to pH changes, and capable of forming multi-layer shells by further layer-by-layer deposition of polyelectrolytes and charged nanoparticles.[23]

In the present work, a polyanion containing ATRP initiator groups, poly (sodium styrenesulfonate-*co*-2-(2-bromoisobutyryloxy)ethyl methacrylate) (PSB), was used as a surface modifier to make Ludox CL particles surface active. These positively charged nanoparticles are narrow-disperse and have been studied as emulsifier precursors before[24]. Their small size makes it possible to produce small emulsion sizes and in turn relatively small sized MCs. The sodium styrenesulfonate unit in PSB can bind to the positively charged CL particle surface between pH 2.0 to 8.5 while the 2-(2-bromoisobutyryloxy)ethyl methacrylate unit was designed to function as an ATRP initiator to confine radical polymerization at the oil-water interface, promoting the formation of MCs (Scheme 7.1).

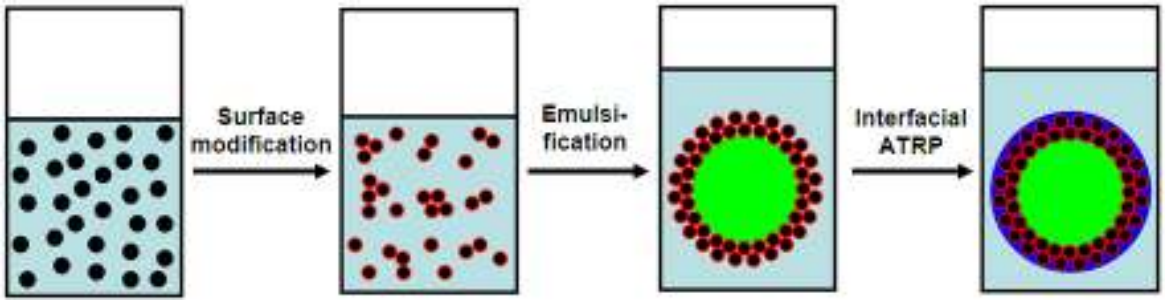

Scheme 7.1 Illustration of the microencapsulation process using PETI-ATRP. Note: particles and capsules are not drawn to scale.

PSB was prepared by copolymerization of sodium styrenesulfonate (SS) with 2-(2-bromoisobutyryloxy)-ethyl methacrylate (BIEM) in DMSO using AIBN as the radical initiator (Scheme 7.2). The SS to BIEM ratio in the copolymer was determined to be 68:32 by ^{1}H-NMR (See Appendix Figure 7A.1), close to the comonomer feed ratio of 70:30, in agreement with the tendency of such comonomers to form random copolymers with a slight tendency towards alternation.[25] In contrast, elemental analysis for bromine gave an SS to BIEM ratio of 86:14. The discrepancy between the NMR and elemental analysis results is attributed to partial loss of bromine from the tertiary site during dialysis. The syntheses of similar polyelectrolyte macro-initiators bearing 2-bromoisobutyrate moieties through ATRP and post-esterification have recently been reported by Armes' group.[26] Our copolymerization approach is shorter but may lead to more hydrolysis during work-up.

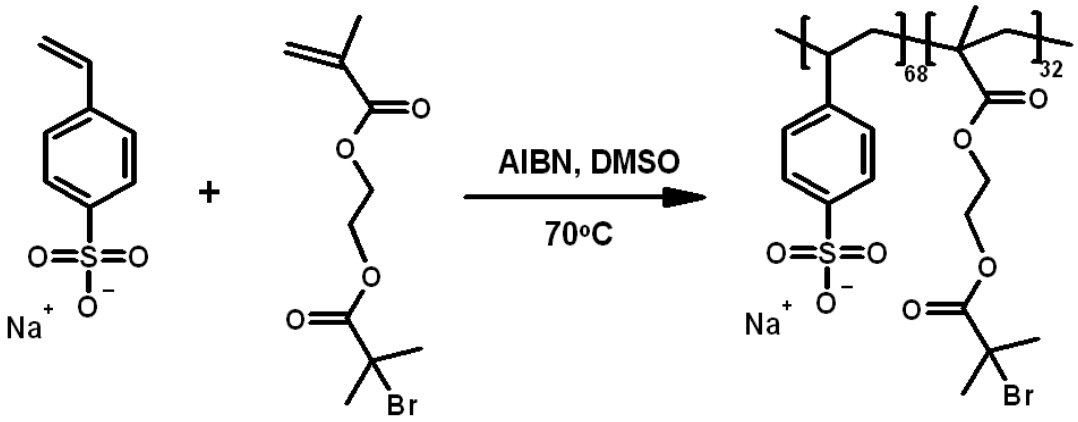

Scheme 7.2 Synthesis of poly (sodium styrenesulfonate-co-2-(2-bromoisobutyryloxy)ethyl methacrylate) (PSB)

7.3.2 CL Particle Surface Modification

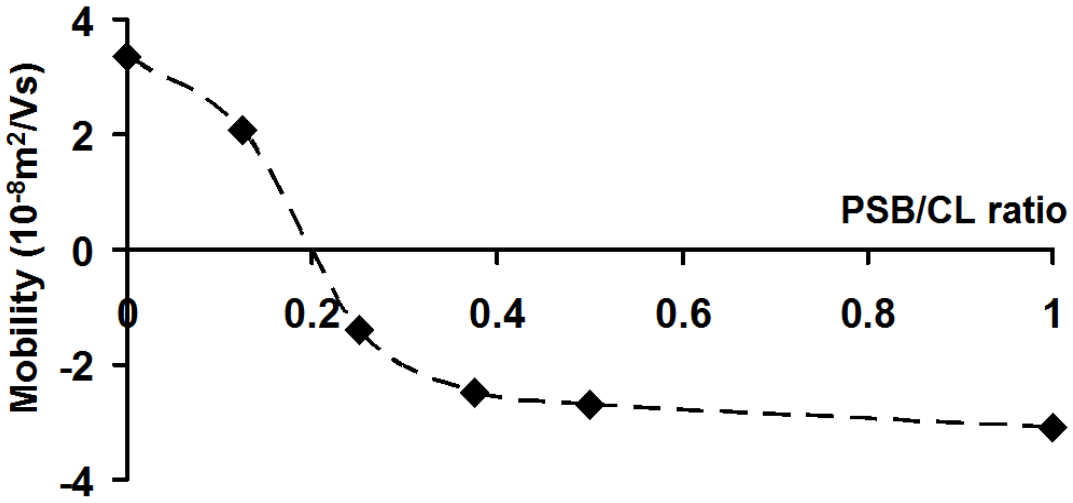

Figure 7.1 Electrophoretic mobility of PSB modified CL particles in suspensions as a function of PSB/CL ratio. The line is drawn to guide the eye.

CL particles were coated by mixing 4.0 wt % CL particle suspensions with equal volumes of PSB solutions of different concentrations. CL particles are positively charged

at pH values below 8.5 due to a thin alumina layer on their outer surface.[27] Negatively charged PSB will thus electrostatically bind to the particle surfaces and render the CL particles surface active. Electrophoretic mobility tests (Figure 7.1) showed that the direction of motion, and hence the surface charge, reverses with increasing PSB/CL ratio used in the coating process, with a minimum near a PSB/CL ratio of about 0.2 indicating the isoelectric point. Beyond a PSB/CL ratio of about 0.4, the mobility levels off again, presumably reflecting surface saturation with PSB. The negative charge on CL particle surfaces at PSB/CL ratios above 0.25 is attributed to the free tails and loops of excess PSB chains bound to the particle surface.

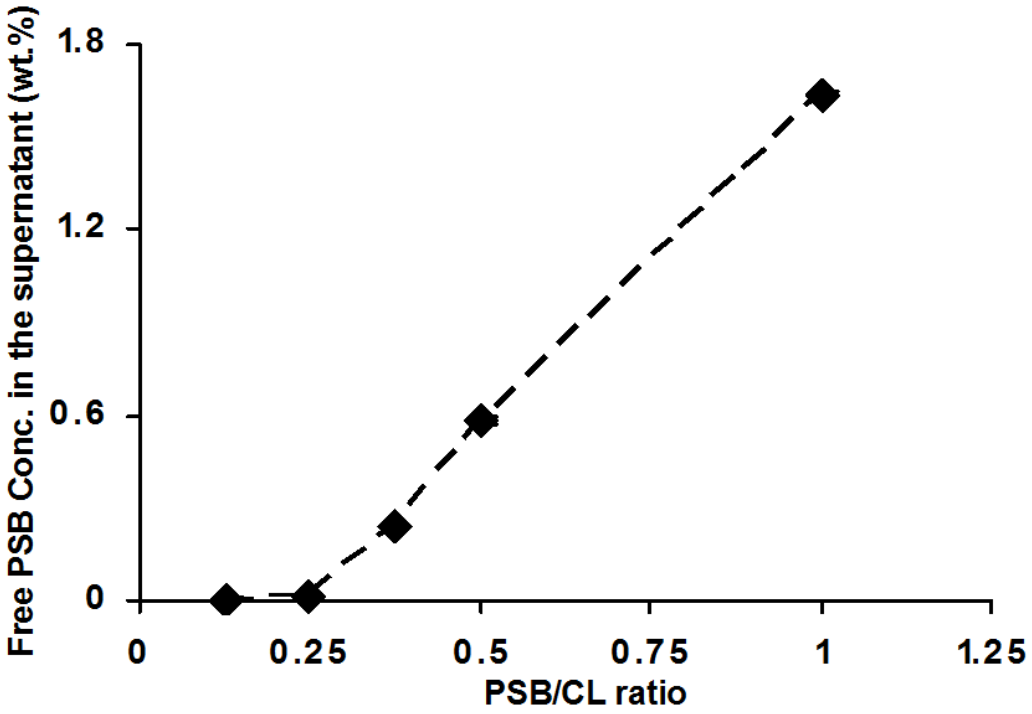

Figure 7.2 The plot of weight concentration of free PSB in supernatant vs. PSB/CL ratio. The line is drawn to guide the eye.

The residual amounts of PSB present in the supernatants following CL particle coating with different PSB/CL ratios were determined by UV/Vis. Figure 7.2 shows that for PSB/CL ratios up to and including 0.25, all PSB added was adsorbed onto the particles, while above that value the amount of free PSB in the supernatant increased linearly with increasing PSB/CL ratio, indicating that the surfaces of CL particles are saturated with PSB.

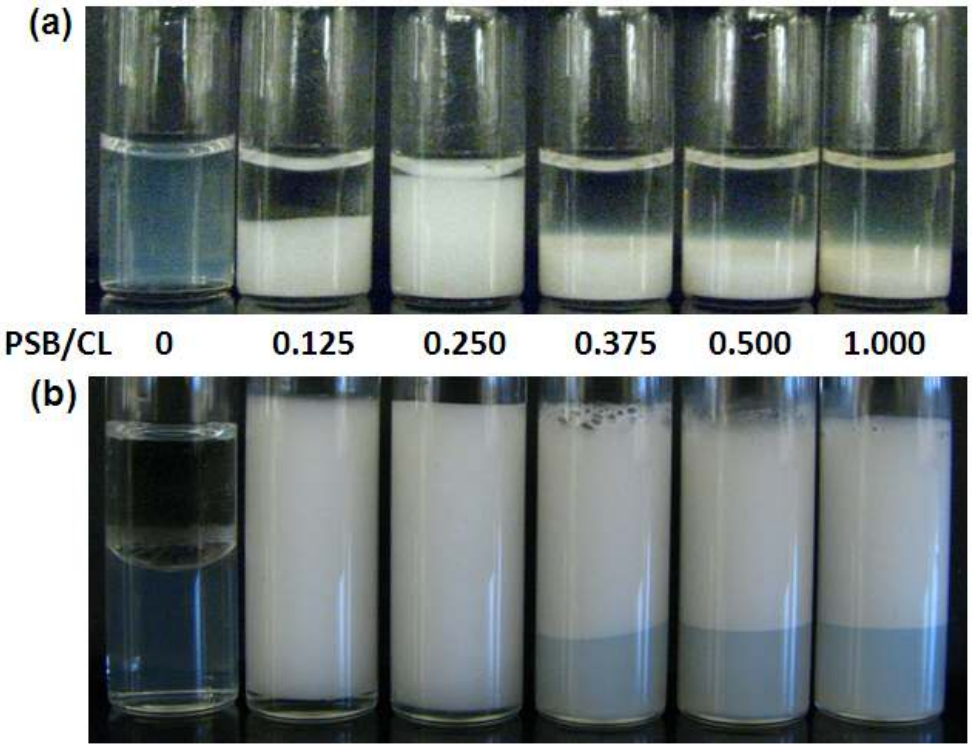

Figure 7.3 Photographs of (a) CL particle suspensions with different levels of PSB modification and (b) attempted xylene-in-water Pickering emulsions made with corresponding particle suspensions from (a).

The visual appearance of CL particle suspensions modified with different PSB/CL ratios is shown in Figure 7.3a. The concentration of CL particles was set to 2 wt % in all

suspensions. The CL particle suspension without PSB addition is almost clear with a bluish tint. The addition of PSB caused immediate cloudiness and increased viscosity due to particle flocculation, which then led to precipitation with time. The volume of precipitate showed a maximum at the PSB/CL ratio of 0.25, which is attributed to charge neutralization at the CL particle surface at this PSB/CL ratio, indicated by the minimum in mobility shown in Figure 7.1. At higher PSB/CL ratios, CL particles carry net negative charges, increasing their colloidal stability.

7.3.3 Xylene-in-water Emulsions Made by PSB Modified CL Particle Suspensions

CL particle suspensions with different PS/CL ratios were used to emulsify xylenes in a 1/1 v/v ratio (Figure 7.3b). CL particles without PSB are unable to stabilize these emulsions, and within seconds reform two layers. In contrast, CL particles modified with PSB formed stable xylene-in-water emulsions at PSB/CL ratios from 0.125 to 1.000. In particular, emulsions prepared with a PSB/CL ratio of 0.250 combine excellent resistance against coalescence and creaming and a high loading of initiator groups, with an absence of free PSB in the continuous phase. Emulsions from higher PSB/CL ratios could also be used for ATRP coating, following removal of excess free PSB in the supernatant to prevent solution initiation.

7.3.4 Preparation of Xylene-filled Poly(N, N'-methylenebisacrylamide) Microcapsules

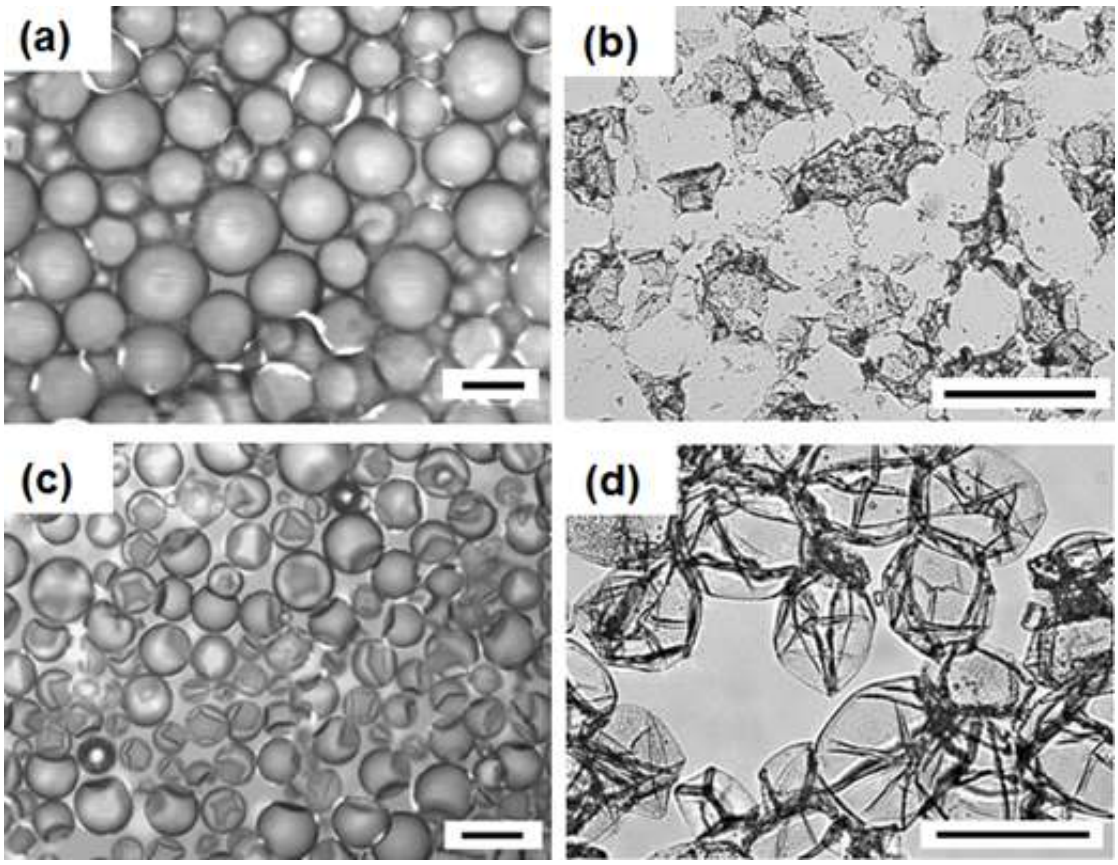

Figure 7.4 Optical micrographs of Pickering emulsions (a, b) and polyMBAAm microcapsules (c, d) in both wet (a, c) and dry (b, d) states. The scale bars are 50 μm.

Xylene-in-water emulsions with a PSB/CL ratio of 0.250 were used as template for the interfacial atom transfer radical polymerization of methylenebisacrylamide (MBAAm). MBAAm was chosen as it has sufficient solubility in water to restrict the polymerization to the aqueous side of the capsules. As a divinyl monomer it further has the ability to form a cross-linked network, required to form stable shell. Emulsions made

using 2.0 wt % CL particle suspension showed a large number of free particles in the supernatant of the emulsion. These PSB-coated, free CL particles could initiate polymerization of MBAAm in the supernatant, competing with the interfacial polymerization for MC wall formation and causing bulk precipitation of polyMBAAm. To minimize the polymerization in the supernatant, we reduced the CL particle loading to 0.8 wt % where the emulsions showed nearly no free particles in the emulsions. The optical micrographs of the resulting Pickering emulsion are shown in Figure 7.4a (wet) and 7.4b (dry). The emulsion showed a fairly wide size distribution with an average diameter around 44 μm. When allowed to dry on a glass slide, the membrane at the xylene/water interface ruptured instantly to release xylene from the core, resulting in shattered fragments on the glass slide (Figure 7.4b).

The Pickering emulsion was then exposed to an aqueous solution containing MBAAm, HMTETA and CuBr to carry out the interfacial ATRP. HMTETA was selected as the ligand as it provides tetradentate coordination to Cu(I), which could suppress the disproportionation of Cu(I) and provide sufficient catalytic activity.[28] Due to the hydrophilic nature of HMTETA, its complexes with Cu(I) and Cu(II) reside primarily in the aqueous phase. As a result, the polymerization happened mainly on the aqueous side of the interface, having minimum impact on the core materials.

Figures 7.4c and 7.4d show the polyMBAAm MCs after polymerization at 65 ˚C for 1 hour. The MCs were well dispersed in the suspension. These MCs showed an average diameter of 33 μm, slightly smaller than that of the primary emulsion. Bulk precipitation of polymers was not observed in the MC suspension, indicating

polymerization mainly occurred at the xylene-water interface. These MCs rapidly lost xylene and collapsed when dried on a glass slide, reflecting their permeable shell. Compared to the primary Pickering emulsion, the MC wall showed improved resistance to rupture as almost intact MC walls remained after loss of the core, indicating that the CL particles at the interface had been interconnected by polyMBAAm to form a coherent MC shell.

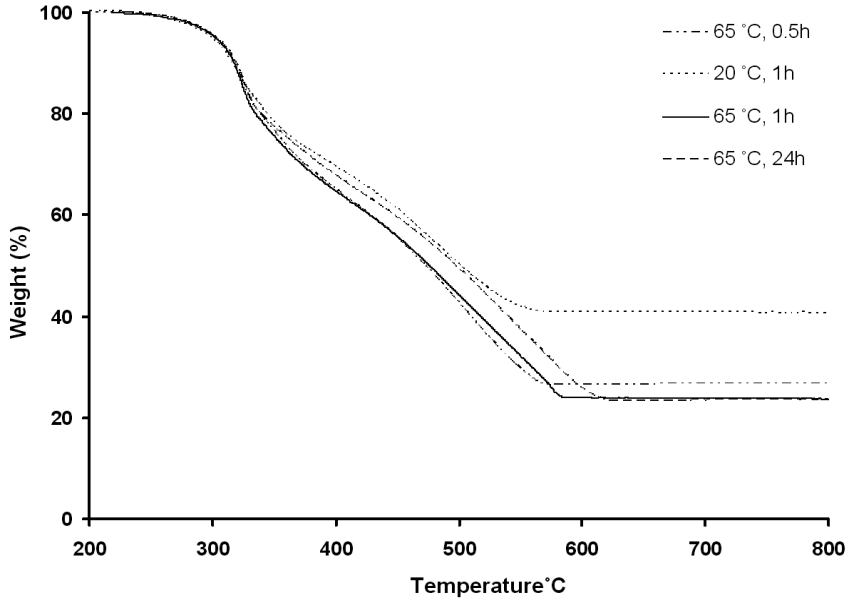

Figure 7.5 TGA plots of polyMBAAm microcapsules synthesized using different reaction conditions.

MC walls made with different polymerization time and temperature were subjected to thermogravimetric analysis (TGA) (Figure 7.5). The conversion of MBAAm in each run was calculated based on the TGA results, and is given in Table 7.1. The weight loss from room temperature to 200 ˚C was attributed to loss of moisture and other low molecular weight substances in the MC walls. The thermal degradation of polymers

was observed from 230 ˚C to 650 ˚C, with weight remaining above 650 ˚C assigned to the inorganic CL particles. As shown in Table 7.1, MBAAm conversion increased with temperature, and with reaction time up to one hour. The relatively low conversion of the monomer in all runs can be attributed to the disproportionation of CuBr to form Cu and $CuBr_2$ and to the slow oxidation of CuBr to $CuBr_2$ during polymerization.

Table 7.1 The Influences of Reaction Temperature and Time on the Composition of Microcapsule Walls

Run	Temperature/˚C	Time/h	PolyMBAAm/CL	Conversion/%*
1	20	1	1.21	14.5
2	65	0.5	2.49	29.9
3	65	1	2.97	35.7
4	65	24	2.98	35.7

* The calculations are based on TGA results. Only the polymers in the MC walls were considered for calculation. The conversion of MBAAm to free polymer in solution was considered negligible.

The composition of the PSB-modified CL particles and the resulting MC walls was studied using FTIR. The FTIR spectrum of CL particles (Figure 7.6b) shows the typical IR adsorption signal from silica at wavenumbers of 798.8 cm^{-1} and 1110.6 cm^{-1},

which are assigned to the symmetrical and asymmetrical stretching vibrations of Si-O-Si bonds. The PSB modification led to a small peak at 1734.1 cm^{-1} (Figure 7.6c) attributed to the C=O stretching vibration of PSB. The FTIR spectrum of the MC wall (Figure 7.6d) is similar to that of SiO_2/polyMBAAm core-shell composite materials reported by Yang et al[29]. In addition to a strong silica signature at 1110.6 cm^{-1}, the spectrum shows strong absorptions at 1525.0 cm^{-1} and 1661.8 cm^{-1}, which are characteristic of an amide group. This confirms that the MC wall was a composite of polyMBAAm and CL particles. The absorption of vinyl group was not observed in the spectrum of polyMBAAm MC walls, which, we believe, could be hidden in the broad peak at 1661.8 cm^{-1}.

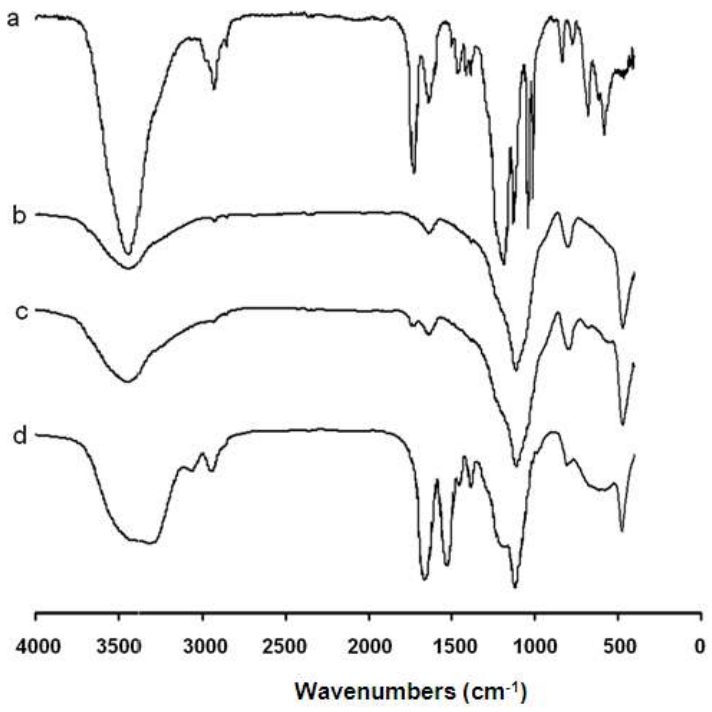

Figure 7.6 Transmission FITR spectra of (a) PSB, (b) CL particles, (c) PSB modified CL particles (PSB/CL=0.25) and (d) polyMBAAm MC walls (65 ˚C, 1 h)

Cross-sections of the wall of polyMBAAm MCs were studied by TEM. Dry polyMBAAm MCs from run 3 in Table 7.1 were embedded in an epoxy resin consisting of trimethylolpropane triglycidyl ether and 4,4′-methylenebis(2-methylcyclohexylamine), an embedding resin we developed that has proven to be very radiation resistant, due to the absence of ester and polyether groups.[30] Figure 7.7 shows that the MC walls contained an ~80 nm thick layer of CL nanoparticle aggregates that were likely originally formed during PSB modification of the CL nanoparticles. After serving as Pickering emulsifiers and initiators for interfacial ATRP, these nanoparticle aggregates are now covalently interconnected at the xylene-water interface to form a MC wall. The polyMBAAm in the MC walls was not visible in these TEM micrographs, likely due to its low contrast relative to the embedding resin.

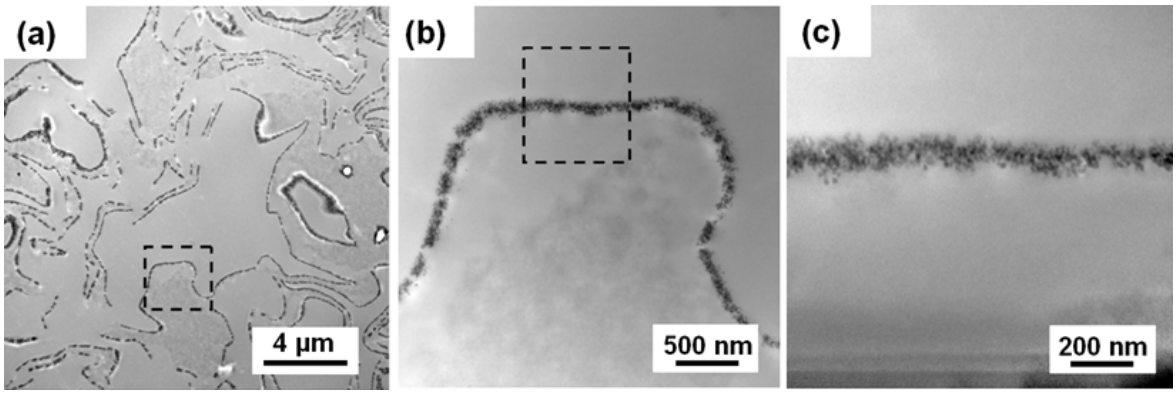

Figure 7.7 TEM micrographs of wall cross-sections of polyMBAAm microcapsules with different magnifications. b shows the boxed area in a and c shows the boxed area in b.

The permeability of polyMBAAm MC walls was studied using fluorescently labeled dextran. A MC suspension from run 3 in Table 7.1 was placed on a rotary

evaporator under vacuum at 60 ˚C for 30 min to replace the xylene fill of MCs with water. Some MC aggregation was observed during this process. The resulting water-filled MCs were mixed with dextran-*f* solutions having molecular weights ranging from 70 kDa to 500 kDa. After incubation for 72 hrs, fluorescence microscopy was used to test for the presence of dextran-*f* within the MC interior. As shown in Figure 7.8, the 70 kDa dextran-*f* entered the majority of MCs. The fraction of permeable MCs decreased with increasing molecular weight of dextran-*f*, such that 500 kDa dextran-f was unable to diffuse into any MCs.

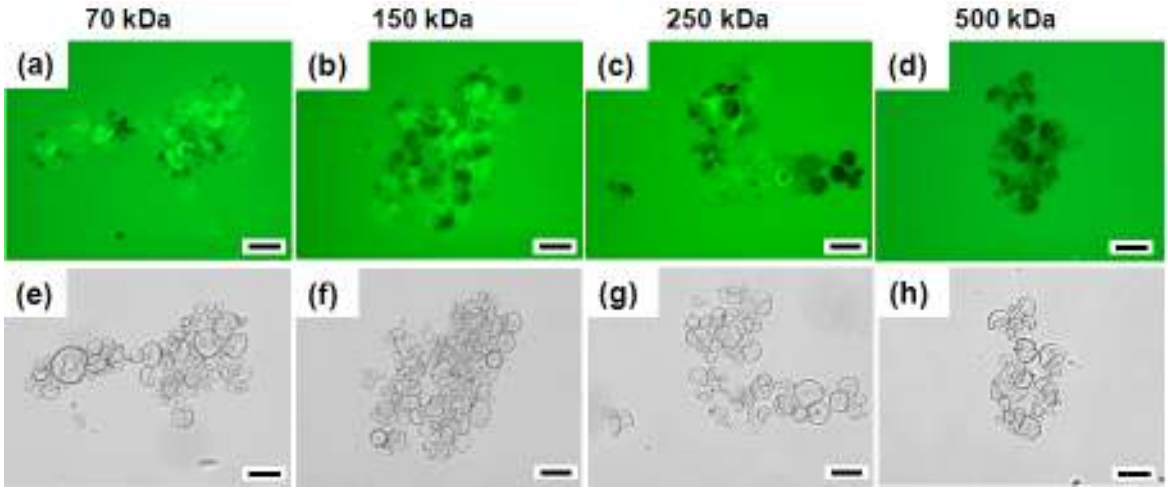

Figure 7.8 Fluorescence microscope images (a, b, c, d) and the corresponding optical microscope images (e, f, g, h) of polyMBAAm microcapsules incubated with dextran-*f* of different molecular weights (70 kDa, 150 kDa, 250 kDa and 500 kDa) for 72 hrs. The scale bars are 50 μm.

7.3.5 Preparation of PolyMBAAm Microcapsules with Different Core Solvents

Table 7.2 Some Physical Properties of Selected Solvents for Microencapsulation

Solvent	Perfluoroheptane	Hexadecane	Xylene
Solubility parameter/δ($MPa^{1/2}$)[31]	12.5	16.4	18
Density (g/mL)[32]	1.745	0.773	0.868
Boiling point (°C)[32]	82-84	287	137-140

Polyelectrolyte-coated nano particles can serve as Pickering emulsifiers for a wide range of core solvents.[23] Therefore, the PETI-ATRP described here was also used to encapsulate the more hydrophobic solvents, hexadecane and perfluoroheptane. Table 7.2 shows the solubility parameters, densities and boiling points of perfluoroheptane, hexadecane and xylene. Microencapsulated perfluorocarbons may be used as blood substitutes.[33] However, encapsulation of perfluorocarbons has proven to be challenging for traditional microencapsulation methods due to their non-polar character. Perfluoroheptane-in-water emulsions were successfully prepared using PSB modified CL particles (PSB/CL=0.25), and used as the template for interfacial ATRP of MBAAm. Figures 7.9a and 7.9b show the optical micrographs of perfluoroheptane containing MCs in both wet and dry states. These MCs resemble the xylene-filled MCs (Figure 7.4c), with

dimpled surfaces. Upon drying, the MCs collapsed completely by losing perfluoroheptane core, leaving behind ruptured MC walls. This fast rupture of the Mc walls is similar to what we observed for xylene cored MCs, which could be attributed to the capillary forces during drying and the thin MC walls.[34]

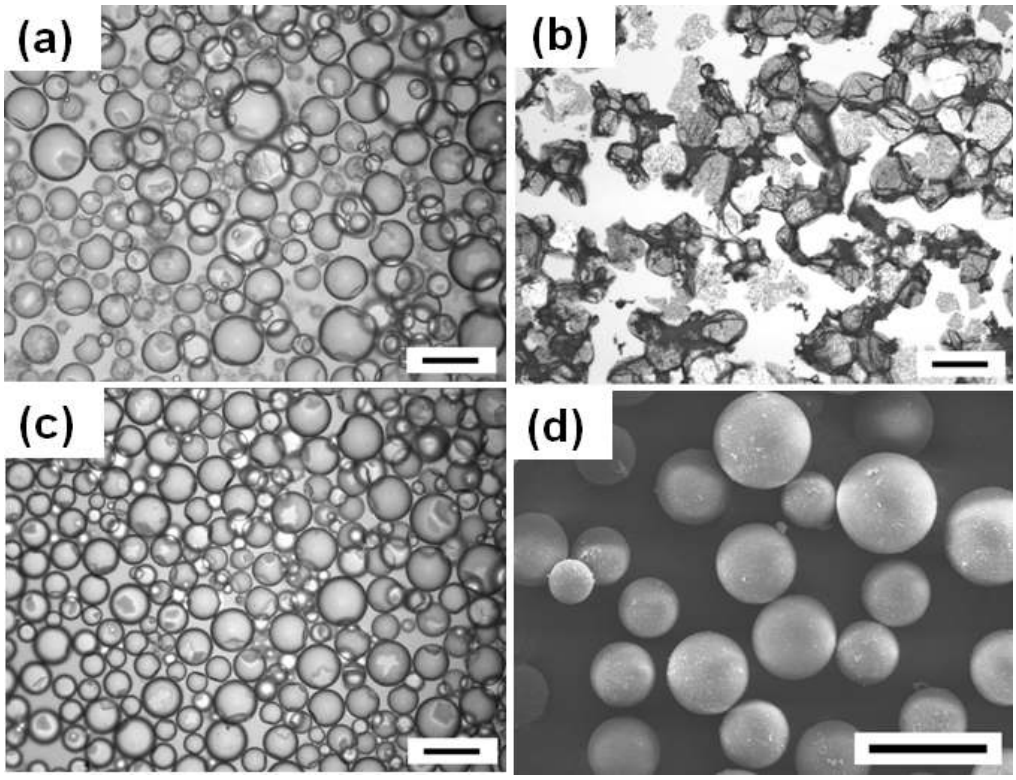

Figure 7.9 Optical micrographs of perfluoroheptane filled (a, b) and hexadecane filled (c) microcapsules in both wet (a, c) and dry (b) states. (d) is a SEM image of hexadecane filled MCs in a dry state. The scale bars are 100 μm.

The analogous hexadecane-filled MCs stayed inflated upon drying, likely because the high-boiling hexadecane did not evaporate at a significant rate from their surfaces (Figure 7.9d). MCs containing hexadecane and other hydrocarbons are of interest as

thermal storage materials.[35] Traditional methods for preparing hexadecane filled MCs include in-*situ* polymerization [36], polymer phase separation[9a], coacervation [37] and interfacial polycondensation[38]. The current method supplements these existing methods by providing a higher core-to-shell ratio and minimum interference with the core by both the encapsulation process and wall forming materials.

7.3.6 Preparation of Xylene Core Microcapsules with Different Wall Materials

Table 7.3 Electrophoretic Mobilities of Different Microcapsules

MCs	PolyMBAAm	Poly(SM-co-MBAAm)	Poly(MAPTAC-co-MBAAm)
Mobility ($10^{-8}m^2/Vs$)	-0.58±0.25	-2.50± 0.25	+2.51±0.09

An advantage of interfacially confined polymerization is its decreased dependence on the polarity of wall-forming materials, making it possible to prepare MC walls with an array of different functionalities. To demonstrate this, both positively and negatively charged vinyl monomers were used as co-monomers with MBAAm to form charged MC walls. In both cases, a feed ratio of ionic monomer to MBAAm of 7:3 was used in order to ensure sufficient cross-linking in the formed MC walls. Sodium methacrylate (SM) and [3-(methacrylamino)-propyl]trimethylammonium chloride (MAPTAC) were chosen as

the charged monomers. The resulting MCs are shown in Figures 7.10b, 7.10c, 7.10e and 7.10f. In the wet state, both MCs resembled the original polyMBAAm MCs. The poly(SM-MBAAm) MCs released xylene fill rapidly when they dried on a glass slide, similar to what we observed for polyMBAAm MCs. In contrast, a portion of the poly(MAPTAC-MBAAm) MCs retained their fill under the same conditions, apparently due to the lower swellability of the polycationic shells in xylene. The electrophoretic mobility measurements of the resulting MCs reveal the strongly negative and positive surface charges of these MCs (Table 7.3). The corresponding measurement of the original polyMBAAm MCs indicate only slightly negative surface charges, attributed to the negatively charged PSB modifiers.

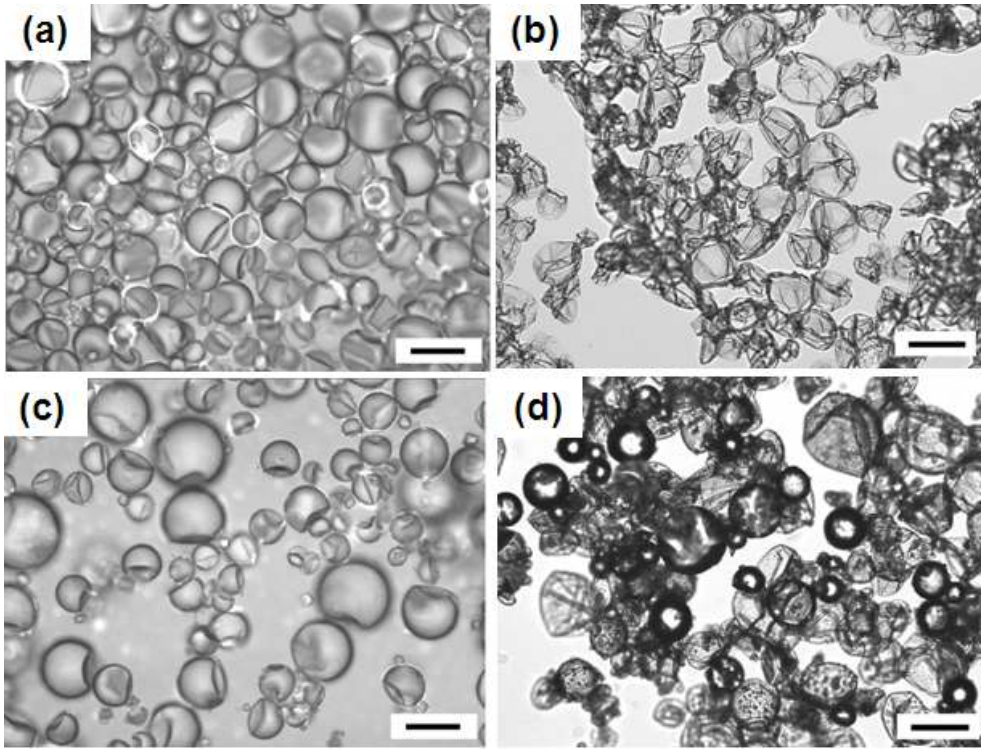

Figure 7.10 Optical micrographs of poly(SM-MBAAm) microcapsules (a, b) and poly(MAPTAC-MBAAm) microcapsules (c, d) in both wet (a, c) and dry (b, d) states. The scale bars are 50 μm.

7.3.7 Synthesis and Characterization of Double-walled Microcapsules

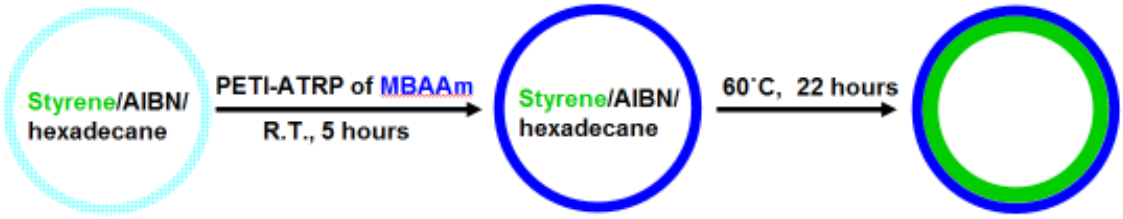

Scheme 7.3 Two-step synthesis of double-walled microcapsules

Recently, double-walled MCs have attracted much attention due to their potential in designing multi-functional MCs. Common approaches for preparing this type of MCs include the sequential execution of two separate microencapsulation processes,[39] and sequential polymerization of two monomers with different reactivities using the same mechanism[40]. In this study, we combined interfacial PETI-ATRP with a subsequent internal styrene free radical polymerization to prepare double-walled MCs. PSB modified CL particles (PSB/CL=0.25) were used to stabilize an oil phase consisting of styrene, AIBN and hexadecane. The PETI-ATRP of MBAAm was carried out at room temperature for 5 hrs to form the outer layer composed of a polyMBAAm/CL particle composite shell. The MC suspension was then heated to 60 ˚C for 22 hrs to induce the polymerization of styrene in the oil phase. The resulting polystyrene precipitated from the non-solvent hexadecane at the interface to form the second, interior shell layer, as illustrated in Scheme 7.3. The optical micrographs of the resulting double-walled MCs are shown in Figures 7.11a and 7.11b. These MCs were stable and retained their core after they were dried on a glass slide. The double-walled structure was verified by TEM imaging of shell cross-sections. Figures 7.11c and 7.11d clearly show a two-layer structure of the MC shell, consisting of an outer nanoparticle layer and an inner polymer layer.

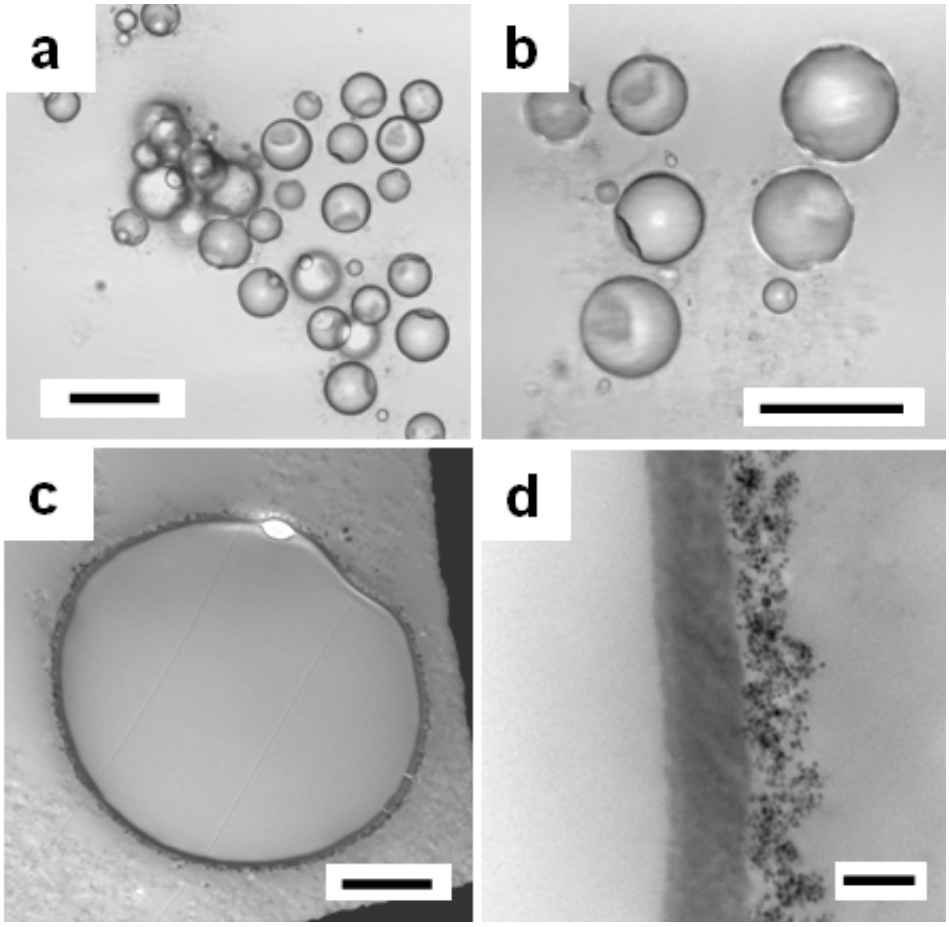

Figure 7.11 Optical micrographs (a, b) of double-walled microcapsules and TEM micrographs (c, d) of the wall cross-section of a double-walled microcapsules. The scale bars in a, b, c, d are 100 μm, 100 μm, 4 μm and 200 nm, respectively.

The polyMBAAm formed in the first stage of the process should be associated with the nanoparticles in the outer layer but could not be resolved by TEM due to its low contrast against the embedding matrix. The dense inner layer is expected to consist of polystyrene formed in the second stage. We used scanning transmission X-ray microscopy (STXM) to positively identify and quantitatively map these shell components.

STXM is a synchrotron based X-ray spectromicroscopy technique that combines good spatial resolution with excellent spectral resolution, making it a very useful tool for mapping the composition of polymeric microspheres[41] and microcapsules[42]. Figure 7.12a shows a STXM optical density image of the cross-section of a double-walled MC imaged at 285.1 eV, the energy of highest contrast of the MC wall against the embedding material. The white ribbon in the image is assigned to the polystyrene layer in the MC wall, which has a significant X-ray absorption at 285.1 eV due to the C 1s $\rightarrow \pi^*$ transition of phenyl rings. A small wall area on the bottom (yellow box in Figure 7.12a) was further studied by recording an image sequence at selected energies through the carbon 1s region between 280 eV to 315 eV. For quantitative analysis, near edge X-ray absorption fine structure (NEXAFS) spectra for the embedding matrix, polystyrene and polyMBAAm were obtained[43] and normalized at both 280 eV and 315 eV to a scale that is set by the known elemental composition and atomic absorption coefficients for 1 nm thick samples.[44] Figure 7.13 shows the normalized reference NEXAFS spectra of embedding matrix, polystyrene and polyMBAAm. Polystyrene shows the strong C 1s $\rightarrow \pi^*_{C=C}$ absorption at 285.1 eV, while polyMBAAm has a strong peak at 288.2 eV due to the C 1s $\rightarrow \pi^*_{C=O}$ transition of the amide groups. The energy separation of 3.1 eV between the signals of these two polymers ensures accurate differentiation of polystyrene and polyMBAAm. The embedding matrix, which consists of aliphatic polyetheramines, has no sharp spectral features that could interfere with these two major components in the MC wall. It is noteworthy that the CL particles, which are primarily silica, do not have any

spectral features in the C 1s region. The image sequence was then fitted with reference spectra using singular value decomposition to yield the component maps shown in Figure 7.12b. The greyscale of each map indicates the spatial distribution of the thickness of that component. The component maps show that the section has an average thickness of ~220 nm. The polystyrene layer has a thickness of around 230 nm and is fairly dense with little penetration of the embedding material. The polyMBAAm layer was identified using this polyMBAAm map as fairly thin (150-200 nm thick) and either porous or swellable, allowing the embedding resin to diffuse into it during the embedding process, making its visualization in TEM more challenging. Based on these component maps, a rescaled color-coded composite map (Figure 7.12c) was then constructed to reflect the relative spatial arrangement of each component. Red, green and blue colors were assigned to the embedding matrix, polystyrene and polyMBAAm respectively in the map. This color-coded map confirmed the double-walled structure with polystyrene in the inner wall and polyMBAAm in the outer wall. The swelling of the polyMBAAm layer by the aliphatic embedding resin reflects the apparent low cross-link density of the grafted layer, and is in accordance with the high permeability seen, especially in absence of the polystyrene inner shells. This suggests that in future studies STXM can be used to monitor layer porosity/swellability, a useful feature in the design of capsules containing fugitive fills.

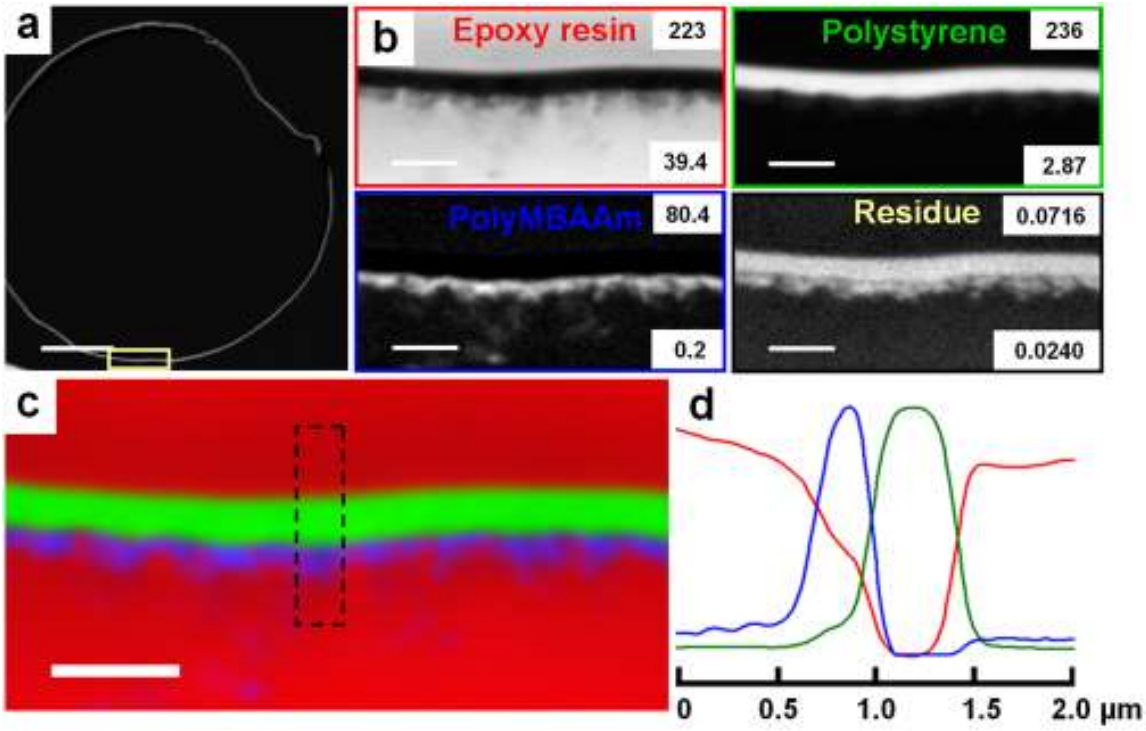

Figure 7.12 STXM analyses of the cross-section of a double-walled microcapsules. (a) a STXM optical density image recorded at 285.1 eV.; (b) Individual component maps of epoxy resin, polystyrene, polyMBAAm and residue; (c) Color-coded composite map of the three components; (d) Component profiles across the microcapsule wall (dashed box in c). The scale bar in a denotes 10 μm and the rest scale bars are 1 μm.

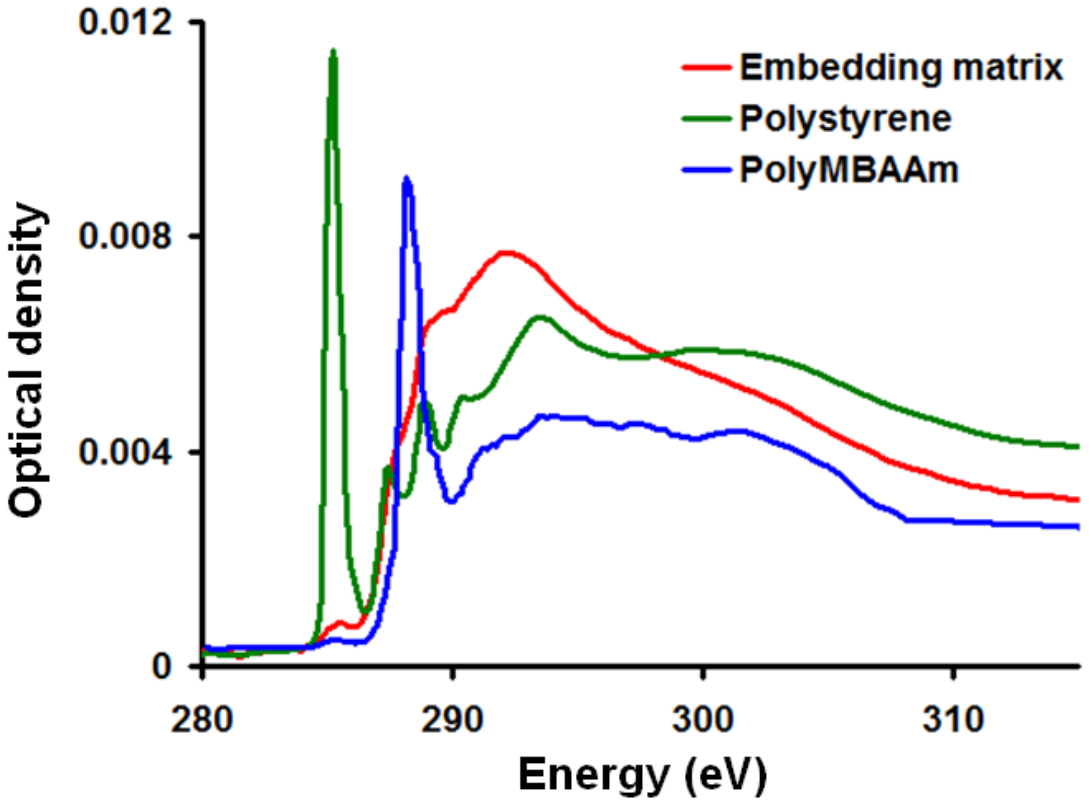

Figure 7.13 NEXAFS reference spectra of the embedding matrix, polystyrene and polyMBAAm that correspond to 1 nm thickness of each component.

7.4 Conclusions

Ludox CL particles were surface modified with PSB by electrostatic interaction, and the modified, surface active particles were used to stabilize xylene-in-water Pickering emulsions. The ratio of PSB/CL of 0.25 was found to result in stable emulsions with very little free PSB. Such Pickering emulsions were then used as templates to confine interfacial ATRP of MBAAm at the oil-water interface to form composite polyMBAAm/CL MC walls. Studies of the MC walls using transmission electron

microscopy (TEM) and Fourier transform infrared (FTIR) spectroscopy confirmed their composite nature, with a total wall thickness about 80 nm. The permeability of the MC walls was investigated using fluorescently labelled dextran with different molecular weights, which suggested that the molecular weight cut-off for the MC walls was below 500 kDa.

The same method was successfully applied to encapsulate fills of different polarities and viscosities such as hexadecane and perfluoroheptane. The wall chemistry was also varied by incorporating monomers with different charges to tune the charge character of the MC walls.

Finally, double-walled MCs were synthesized by sequentially performing an interfacial ATRP of MBAAm to form the outer layer, followed by an internal free radical polymerization of encapsulated styrene to form the inner layer. The resulting double-walled shell structure was confirmed using both TEM and STXM.

7.5 References

[1] (a) Tsuji, K. *Journal of Microencapsulation* **2001**, *18*, 137-147. (b) Shirley, I. M.; Scher, H. B.; Perrin, R. M.; Wege, P. J.; Rodson, M.; Chen, J. L.; Rehmke, A. W. *Pest Management Science* **2001**, *57*, 129-132.

[2] Madene, A.; Jacquot, M.; Scher, J.; Desobry, S. *International Journal of Food Science and Technology* **2006**, *41*, 1-21.

[3] Comiskey, B.; Albert, J. D.; Yoshizawa, H.; Jacobson, J. *Nature* **1998**, *394*, 253-255.

[4] (a) Ramarao, C.; Ley, S. V.; Smith, S. C.; Shirley, I. M.; DeAlmeida, N. *Chemical Communications* **2002**, 1132-1133. (b) Ley, S. V.; Ramarao, C.; Gordon, R. S.; Holmes, A. B.; Morrison, A. J.; McConvey, I. F.; Shirley, I. M.; Smith, S. C.; Smith, M. D. *Chemical Communications* **2002**, 1134-1135. (c) Poe, S. L.; Kobaslija, M.; McQuade, D. T. *Journal of the American Chemical Society* **2007**, *129*, 9216-9221.

[5] White, S. R.; Sottos, N. R.; Geubelle, P. H.; Moore, J. S.; Kessler, M. R.; Sriram, S. R.; Brown, E. N.; Viswanathan, S. *Nature* **2001**, *409*, 794-797.

[6] Berg, J.; Sundberg, D.; Kronberg, B. *Journal of Microencapsulation* **1989**, *6*, 327-337.

[7] (a) D. F. Klassen; D. J. Muir, *U.S. Patent 6540991,* April 1, **2003** (b) Vassiliades, A. E.; Vincent, D. N.; Powell, M. P. *U.S. Patent 3,875,074*, April 1, **1975**

[8] (a) Loxley, A.; Vincent, B. *Journal of Colloid and Interface Science* **1998**, *208*, 49-62. (b) Atkin, R.; Davies, P.; Hardy, J.; Vincent, B. *Macromolecules* **2004**, *37*, 7979-7985.

[9] (a) Bakan, J. A. U.S. patent 3,567,650, March 2, **1971**. (b) Arshady, R. *Polymer Engineering and Science* **1990**, *30*, 905-914.

[10] (a) Matyjaszewski, K.; Xia, J. H. *Chemical Reviews* **2001**, *101*, 2921-2990. (b) Moad, G.; Rizzardo, E.; Thang, S. H. *Australian Journal of Chemistry* **2005**, *58*, 379-410. (c) Hawker, C. J.; Bosman, A. W.; Harth, E. *Chemical Reviews* **2001**, *101*, 3661-3688.

[11] Zetterlund, P. B.; Kagawa, Y.; Okubo, M. *Chemical Reviews* **2008**, *108*, 3747-3794.

[12] Minami, H.; Okubo, M.; Oshima, Y. *Polymer* **2005**, *46*, 1051-1056.

[13] (a) Ali, M. M.; Stöver, H. D. H. *Journal of Polymer Science Part a-Polymer Chemistry* **2006**, *44*, 156-171. (b) Scott, C.; Wu, D.; Ho, C. C.; Co, C. C. *Journal of the American Chemical Society* **2005**, *127*, 4160-4161. (c) Wu, D.; Scott, C.; Ho, C. C.; Co, C. C. *Macromolecules* **2006**, *39*, 5848-5853.

[14] Luo, Y. W.; Gu, H. Y. *Macromolecular Rapid Communications* **2006**, *27*, 21-25.

[15] Lu, F. J.; Luo, Y. W.; Li, B. G.; Zhao, Q.; Schork, F. J. *Macromolecules*, *43*, 568-571

[16] Li, W. W.; Matyjaszewski, K.; Albrecht, K.; Moller, M. *Macromolecules* **2009**, *42*, 8228-8233.

[17] (a) Pickering S. U. *J Chem Soc* **1907**, *91*, 2001-2021. (b) Ramsden W. *Proc R Soc* **1903**, *72*, 156-164.

[18] (a) Chen, T.; Colver, P. J.; Bon, S. A. F. *Advanced Materials* **2007**, *19*, 2286-+. (b) Ao, Z.; Yang, Z.; Wang, J. F.; Zhang, G. Z.; Ngai, T. *Langmuir* **2009**, *25*, 2572-2574. (c) Gao, Q. X.; Wang, C. Y.; Liu, H. X.; Wang, C. H.; Liu, X. X.; Tong, Z. *Polymer* **2009**, *50*, 2587-2594. (d) Yow, H. N.; Routh, A. F. *Soft Matter* **2006**, *2*, 940-949. (e) Laib, S.; Routh, A. F. *Journal of Colloid and Interface Science* **2008**, *317*, 121-129. (f) Yow, H. N.; Routh, A. F. *Langmuir* **2009**, *25*, 159-166.

[19] Chen, Y. H.; Wang, C. Y.; Chen, J. X.; Liu, X. X.; Tong, Z. *Journal of Polymer Science Part a-Polymer Chemistry* **2009**, *47*, 1354-1367.

[20] Venkatesh, R.; Yajjou, L.; Koning, C. E.; Klumperman, B. *Macromolecular Chemistry and Physics* **2004**, *205*, 2161-2168.

[21] Kilcoyne, A. L. D.; Tyliszczak, T.; Steele, W. F.; Fakra, S.; Hitchcock, P.; Franck, K.; Anderson, E.; Harteneck, B.; Rightor, E. G.; Mitchell, G. E.; Hitchcock, A. P.; Yang, L.; Warwick, T.; Ade, H. *Journal of Synchrotron Radiation* **2003**, *10*, 125-136.

[22] (a) Li, J.; Stöver, H. D. H. *Langmuir* **2008**, *24*, 13237-13240. (b) Akartuna, I.; Studart, A. R.; Tervoort, E.; Gonzenbach, U. T.; Gauckler, L. J. *Langmuir* **2008**, *24*, 7161-7168.

[23] Li, J.; Stöver, H. D. H. *Langmuir*, submitted, **2010**

[24] (a) Binks, B. P.; Rodrigues, J. A. *Langmuir* **2007**, *23*, 7436-7439. (b) Binks, B. P.; Liu, W. H.; Rodrigues, J. A. *Langmuir* **2008**, *24*, 4443-4446.

[25] Belleney, J.; Helary, G.; Migonney, V. *European Polymer Journal* **2002**, *38*, 439-444.

[26] (a) Vo, C. D.; Schmid, A.; Armes, S. P.; Sakai, K.; Biggs, S. *Langmuir* **2007**, *23*, 408-413. (b) **DOI:** 10.1021/la904346j

[27] Van der Meeren, P.; Saveyn, H.; Kassa, S. B.; Doyen, W.; Leysen, R. *Physical Chemistry Chemical Physics* **2004**, *6*, 1408-1412.

[28] Tsarevsky, N. V.; Braunecker, W. A.; Matyjaszewski, K. *Journal of Organometallic Chemistry* **2007**, *692*, 3212-3222.

[29] Liu, G. Y.; Yang, X. L.; Wang, Y. M. *Polymer* **2007**, *48*, 4385-4392.

[30] (a) Takekoh, R.; Okubo, M.; Araki, T.; Stöver, H. D. H.; Hitchcock, A. P. *Macromolecules* **2005**, *38*, 542-551. (b) Rousseau, M. E.; Cruz, D. H.; West, M. M.; Hitchcock, A. P.; Pezolet, M. *Journal of the American Chemical Society* **2007**, *129*, 3897-3905.

[31] Grulke E. A. In *Polymer Handbook*, 4th ed.; Brandup, J., Immergut, E. H., Grukle E. A., Eds.; Wiley: New York, 1999; p VII/675.

[32] *Aldrich Catalogue, Handbook of Fine Chemicals,* **2008-2009**

[33] Speaker T. J. *U.S. Patent 5,284,663*, Feb. 8, **1994**

[34] Akartuna, I.; Tervoort, E.; Studart, A. R.; Gauckler, L. J. *Langmuir* **2009**, *25*, 12419-12424.

[35] Zalba, B.; Marin, J. M.; Cabeza, L. F.; Mehling, H. *Applied Thermal Engineering* **2003**, *23*, 251-283.

[36] (a) Chaiyasat, P.; Ogino, Y.; Suzuki, T.; Okubo, M. *Colloid and Polymer Science* **2008**, *286*, 753-759. (b) Chaiyasat, P.; Suzuki, T.; Minami, H.; Okubo, M. *Journal of Applied Polymer Science* **2009**, *112*, 3257-3266.

[37] Mauguet, M. C.; Legrand, J.; Brujes, L.; Carnelle, G.; Larre, C.; Popineau, Y. *Journal of Microencapsulation* **2002**, *19*, 377-384.

[38] Zou, G. L.; Lan, X. Z.; Tan, Z. C.; Sun, L. X.; Zhang, T. *Acta Physico-Chimica Sinica* **2004**, *20*, 90-93.

[39] (a) Li, G.; Feng, Y. Q.; Gao, P.; Li, X. G. *Polymer Bulletin* **2008**, *60*, 725-731. (b) Long, Y.; Vincent, B.; York, D.; Zhang, Z. B.; Preece, J. A. *Chemical Communications* **2010**, *46*, 1718-1720. (c) Caruso, M. M.; Blaiszik, B. J.; Jin, H. H.; Schelkopf, S. R.; Stradley, D. S.; Sottos, N. R.; White, S. R.; Moore, J. S. *ACS Applied Materials & Interfaces* **2010**, *2*, 1195-1199.

[40] Li, J.; Hitchcock, A. P.; Stöver, H. D. H.; Shirley, I. *Macromolecules* **2009**, *42*, 2428-2432.

[41] Koprinarov, I.; Hitchcock, A. P.; Li, W. H.; Heng, Y. M.; Stöver, H. D. H. *Macromolecules* **2001**, *34*, 4424-4429.

[42] (a) Croll, L. M.; Stöver, H. D. H.; Hitchcock, A. P. *Macromolecules* **2005**, *38*, 2903-2910. (b) Hitchcock, A. P.; Li, J.; Reijerkerk, S. R.; Foley, P.; Stöver, H. D. H.; Shirley, I. *Journal of Electron Spectroscopy and Related Phenomena* **2007**, *156*, 467-471. (c) Tzvetkov, G.; Graf, B.; Wiegner, R.; Raabe, J.; Quitmann, C.; Fink, R. *Micron* **2008**, *39*, 275-279.

[43] The reference spectrum of polystyrene was measured using pure polystyrene sections. The reference spectrum of the embedding matrix was extracted from the image sequence. The NEXAFS spectrum of polyalanine was used as the reference spectrum for polyMBAAm due to the structural similarity between these two polymers.

[44] Henke, B. L.; Gullikson, E. M.; Davis, J. C. *Atomic Data and Nuclear Data Tables* **1993**, *54*, 181-342.

7.6 Appendix

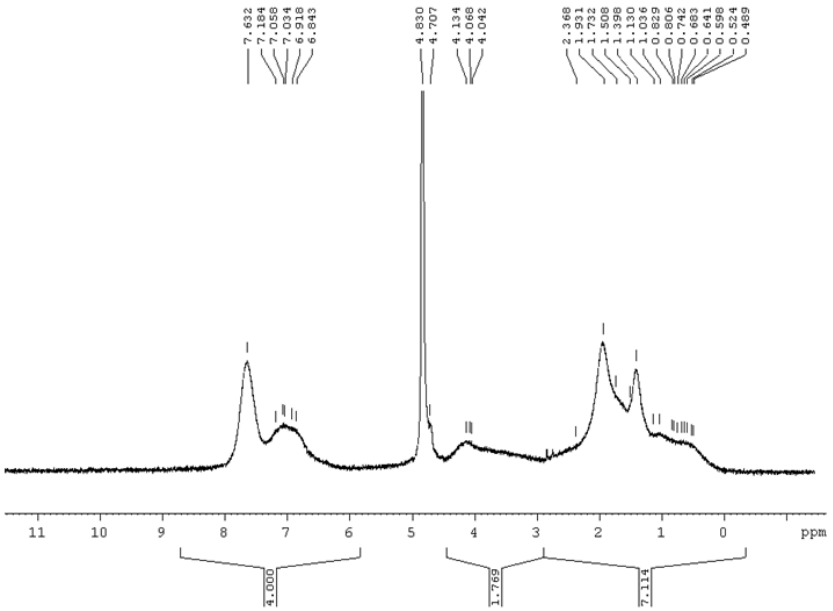

Figure 7A.1 ^{1}H-NMR spectrum of poly (sodium styrenesulfonate-*co*-2-(2-bromoisobutyryloxy)ethyl methacrylate) (PSB) measured in D_2O using a Bruker 200MHz NMR spectrometer.

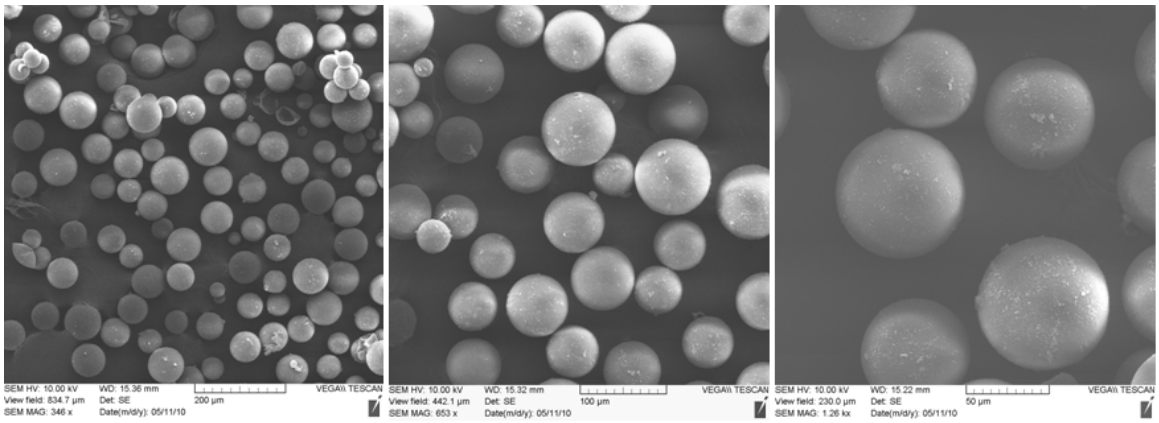

Figure 7A.2 SEM images of hexadecane filled polyMBAAm microcapsules acquired using a TESCAN VEGA 3 XM SEM.

CHAPTER 8 – SUMMARY AND FUTURE WORK

8.1 Summary

Microencapsulation has been proven to be a powerful technique to render materials with new properties and functions. The use of MCs in product designs has greatly fostered the development of new consumer and industrial products that are high-performance, easy-to-use, safe, stimuli-responsive, intelligent and durable, which greatly improves the quality of human life. The ever-emerging applications have been the main driving force for the advancement of microencapsulation technology. Over the last 60 years, many different microencapsulation methods have been developed that are capable of producing MCs with a wide range of morphologies and properties. Even though, the properties and functions of the MCs generated using these methods are still not sufficient to completely satisfy the requirements of many applications. This thesis focuses on the characterization, modification and synthesis of MCs, exploring the structures and properties of MCs using advanced analytical tools, modifying microencapsulation processes and MCs to maximize MC's properties, and developing new microencapsulation methods with new features, which allow the access of MCs with diverse properties that may be desirable for a wide range of applications. The contributions in this thesis to MC studies can be summarized as follows:

1. STXM has been successfully applied to study both composite polyurea and base-triggerable aminoplast MCs. STXM's unique characteristic of good chemical sensitivity

with a high spatial resolution enables the chemical mappings of different components in MC walls. The studies on polyurea MCs suggest that MC wall formation may follow different mechanisms, e.g. moving boundary mechanism and stationary boundary mechanism, which could be the result of using different monomers. Investigations on base-triggerable aminoplast MCs using STXM revealed that, in the microencapsulation process, a polymer phase separation mechanism might prevail over the interfacial polycondensation mechanism that is widely assumed for aminoplast MC formation. It is also found that the condensation reaction between the pendant methylol groups in the aminoplast resin and the cross-linker (thioester) might be primarily responsible for the wall formation, while the reaction between the pendant butoxymethyl groups and the thioester only played a minor role in the process. Such information is important as it provides in-depth understanding of the microencapsulation processes and enables optimization of MC properties in future.

2. A post-modification method for polyurea MC surfaces was developed. It was suggested by fluorescently labelling and CLSM studies that there exist residual amines on polyurea MC surfaces that could be utilized for surface modification. An amine-reactive polyelectrolyte was designed to attach to polyurea MC surfaces through both electrostatic and covalent interactions. The modification was confirmed by both CLSM and fluorescence microscopy to be restricted to the outermost part of MC walls, showing its minimum interference with other wall properties.

3. A microfluidic device based on commercially available MicroTEEs was designed that is capable of making monodisperse oil-in-water emulsions. Narrow-disperse polyurea

MCs were produced based on these emulsions and the size of MCs could be easily modulated by controlling the flow rates. This device features low cost, simplicity and robustness, making it a useful tool for preparing narroe-disperse MCs and for studying size-dependent MC properties.

4. A new method was discovered for modifying charged nanoparticle surfaces to make Pickering emulsifiers. This method used a negatively charged organic electrolyte (potassium hydrogen phthalate, KHP) to bind to positive nanoparticle surfaces (Ludox CL silica particles) electrostatically, which caused nanoparticles to become surface active. Due to the reversible nature of this modification, the resulting Pickering emulsions exhibited pH-responsiveness, with stable emulsions only obtained at intermediate pHs (3.5-5.5), while at high or low pH values the system demulsified, resulting in a reversible Pickering emulsion having two pH-controlled, reversible transitions. This type of Pickering emulsion may find applications in heavy oil transportation, oil recovery and emulsion polymerization.

5. A microencapsulation method based on Pickering emulsion templated layer-by-layer assembly was developed. This study features the use of a polyelectrolyte to modify charged nanoparticle surfaces via electrostatic interaction for making Pickering emulsifiers. The resulting oil-in-water Pickering emulsions with residual charges on surface were shown to be suitable templates for LbL assemblies of polyelectrolytes and charged nanoparticles, resulting in composite MC wall formation. The LbL coatings using only polyelectrolytes produced porous MC walls with relatively low encapsulation efficiency, while the alternate coatings on the same emulsion templates with nanoparticles

and polyelectrolyte resulted in dense and strong MC walls. This new microencapsulation method eliminates the need for using sacrificial templates in CT-LbL assembly and is useful for encapsulating a wide range of hydrophobic materials.

6. A functional polyelectrolyte bearing initiators for atom transfer radical polymerization was designed and used to modify nanoparticle surfaces to make Pickering emulsifiers via the electrostatic interaction. The oil-in-water Pickering emulsions based on these emulsifiers were used to confine the ATRPs of different monomers at oil-water interface, rendering the formation of composite MC walls. This microencapsulation method can be used to encase various core materials and different MC wall properties can be achieved by choosing different monomers, demonstrating the versatility of this method. Double-layered composite MCs were also synthesized by coupling this new method with a conventional in *situ* polymerization method.

8.2 Future work

A large portion of this thesis is devoted to the development of Pickering emulsion templated microencapsulation methods that are based on the electrostatic modification of charged nanoparticles for making suitable Pickering emulsifiers. The progress made to date includes the demonstration of the effectiveness of the electrostatic modification method and devising two new microencapsulation methods templated by the resulting Pickering emulsions. Further development of this research requires better understanding the nature of this electrostatic modification method and testing the generality of the

developed microencapsulation methods in order to make them more practical for industrial applications.

8.2.1 Contact Angle Measurements on Electrostatically Modified Pickering Emulsifiers

Our previous studies have shown that positively charged Ludox CL particles can be electrostatically modified on their surface using either simple organic electrolyte like KHP or polyeletrolytes such as PSS and PSB, and the surface modified CL particles show sufficient surface activeness for making stable oil-in-water emulsions with various organic solvents. Negatively charged Ludox HS particles were also tested as the Pickering emulsifier precursors with the electrostatic modification using aniline hydrochloride. Xylene-in-water emulsions were attempted using HS particles, aniline hydrochloride and aniline hydrochloride modified HS particles as emulsifiers, respectively. The results show that HS particles and aniline hydrochloride are not good emulsifiers by themselves to produce stable emulsions, while the modified HS particles are surface active to effectively stabilize xylene-in-water emulsions (Figure 8.1). This result is similar to what we observed for modified CL particles, implying that this electrostatic modification method could be general and it could be applied to a wide range of charged particles and modifiers to make effective Pickering emulsifiers.

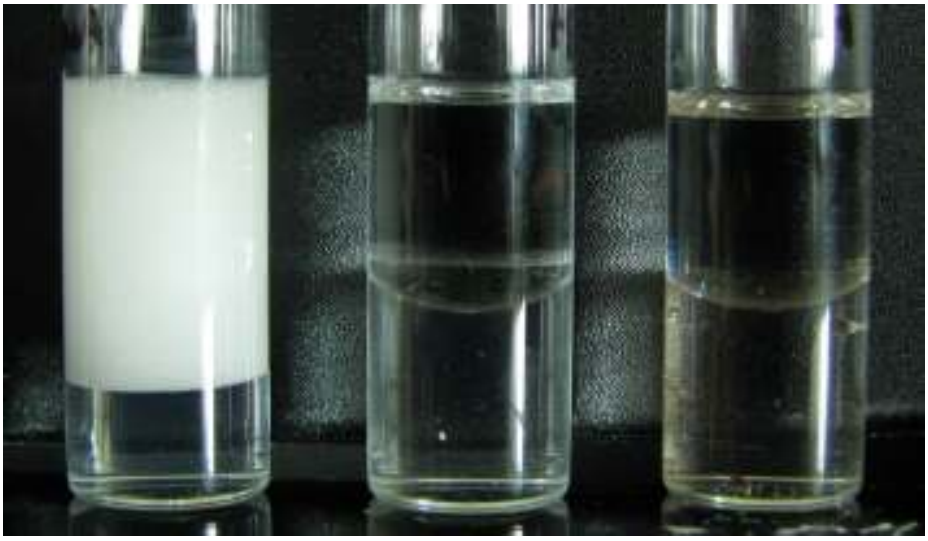

Figure 8.1 Photograph of attempted xylene-in-water emulsions using aniline hydrochloride modified HS particles (left), HS particles (middle) and aniline hydrochloride (right) as emulsifiers. The pH was 4.0 in each vial and the photograph was taken 7 days after the emulsion preparations.

In order to estimate the stability of the Pickering emulsions based on electrostatically modified particles, to gain more insight of this modification and also to quantitatively compare the effectiveness of this modification to other modification methods, it is important to measure the contact angles of the particles before and after electrostatic modifications.

Direct measurement of the contact angles of nano-sized particles with oil-water interfaces is challenging due to the difficulties in visualizing these particles at interfaces. Aveyard et al. suggested that particle contact angles with planar liquid-liquid interfaces were close to contact angles between one liquid and a planar surface immersed in the other liquid, provided the chemistry of the planar substrate surface is similar to that of

particle surface.[1] As a result, the contact angles of one liquid drop under the other liquid on a planar surface are often measured to estimate the contact angles of particles with oil-water interfaces.[2] The method can be directly adopted to estimate the contact angles of CL particles with oil-water interfaces before and after electrostatic modifications using different modifiers. In detail, a silicon wafer may be used as the coating substrate. After nitric acid treatment and water washing, the substrate may be coated with 3 double-layers of PDADMAC/PSS. The CL particle coating can then be established by immersing the polyelectrolytes coated silicon wafer in a CL particle suspension to allow absorption of CL particles onto the silicon wafer surface. The unbound particles can be removed by rinsing with water and the silicon wafer be dried before measurement. The contact angles can be measured using contact angle goniometers. The silicon wafer may be placed in the oil phase and then a sessile drop of aqueous modifier solution is placed on the silicon wafer surface to measure the advancing and receding contact angles of the droplet (Scheme 8.2). The influences of oil phase, type of modifier, modifier concentration, pH, salt concentration, etc. on the contact angle can be investigated using this method, which will allow us to better understand the nature of this modification and help us find ways to further improve it.

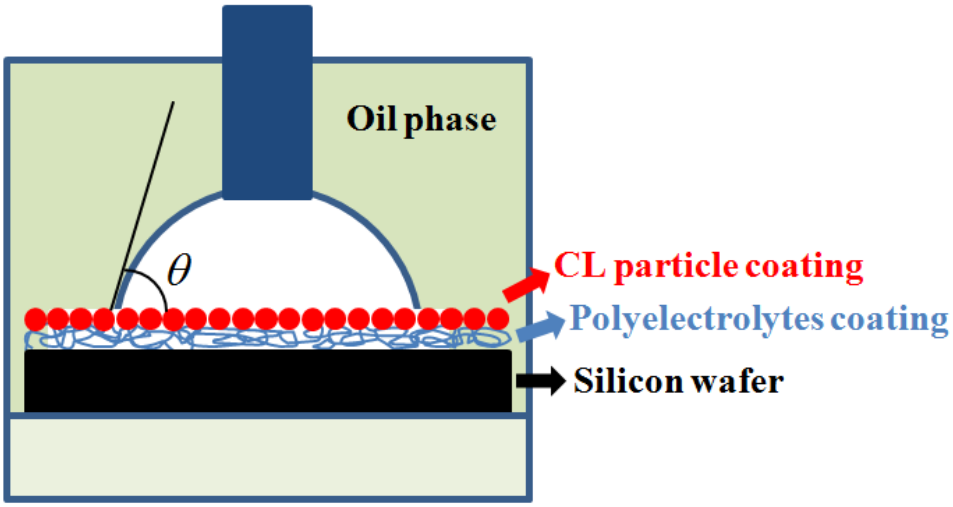

Scheme 8.1 Schematic illustration of the setup for contact angle measurements

8.2.2 Synthesis of Functional Microcapsules Templated by Pickering Emulsions

After establishing the Pickering emulsion templated microencapsulation methods, the next phase of research should focus on the application of these methods for making functional MCs that are not easily prepared using other microencapsulation methods, as Pickering emulsions based methods have good chemical compatibility with a wide range of core and wall-forming materials.

Although, so far, this thesis has focused on CL particles to make MCs, the methods developed could be extended to using other charged particles that could provide additional functionalities for MCs. Therefore, different charged particles could be surface modified using oppositely charged functional polyelectrolytes to render them surface active and the corresponding Pickering emulsions could then be utilized to template MC wall formation using either LbL assembly or interfacial ATRP. One example is to use

magnetic nanoparticles as the precursors for making Pickering emulsifiers. MCs templated by these emulsions would respond to external magnetic field, making them easy to be separated from other non-magnetic materials. This type of MCs may find applications such as in agriculture, catalysis and controlled drug delivery. Another example is to incorporate gold nanoparticles or carbon nanotubes into MC walls using Pickering emulsion templated microencapsulation methods. The walls of such MCs may be heated through remote radiation to cause abrupt increase of local temperature, which would result in either mechanical rupture of MCs or increased diffusion rate of core materials through capsule walls.

In addition to nanoparticles, new properties of MCs could also be achieved by using other functional wall formers. For instance, N-isopropylacrylamide (NIPAM) could be utilized in PETI-ATRP for making thermo-sensitive MCs, while the use of weak acids or bases as wall-forming materials could render MCs pH sensitivity.

8.3 References

---

[1] Aveyard, R.; Binks, B. P.; Fletcher, P. D. I.; Rutherford, C. E. *Colloids Surf., A* **1994**, *83*, 89.

[2] (1) Binks, B. P.; Desforges, A.; Duff, D. G. *Langmuir* **2007**, *23*, 1098-1106. (2) Binks, B. P.; Liu, W. H.; Rodrigues, J. A. *Langmuir* **2008**, *24*, 4443-4446.